

UNCLASSIFIED

AD NUMBER

AD368048

CLASSIFICATION CHANGES

TO: **unclassified**

FROM: **confidential**

LIMITATION CHANGES

TO:
**Approved for public release, distribution
unlimited**

FROM:
Distribution: DoD only.

AUTHORITY

**May 1980, Group-4, DoDD 5200.10, 26 July
1962; NRL ltr, 26 Feb 2001.**

THIS PAGE IS UNCLASSIFIED

CONFIDENTIAL

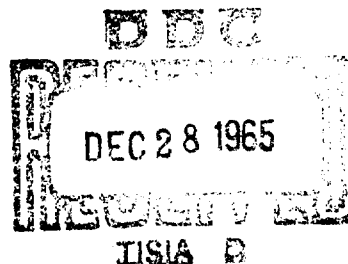
NRL Memorandum Report 754

**SUMMARY OF NAVY STUDY PROGRAM
FOR
F4H-1 and F8U-3 WEAPON SYSTEMS
VOLUME III**

C. M. Loughmiller, J. C. Ryon,
I. N. Bellavin, and R. L. Lister

RADAR DIVISION

May 1958



DDC AVAILABILITY NOTICE
4. U.S. Military agencies may obtain copies of this report directly from DDC. Other qualified users shall request through Director, U.S. Naval Research Laboratory, Washington, D. C., 20390.

**NAVAL RESEARCH LABORATORY
Washington, D.C.**

CONFIDENTIAL

~~Further distribution of this report, or of an abstract, or reproduction thereof may be made only with the approval of the Director, Naval Research Laboratory, Washington 25, D. C., or of the activity sponsoring the research reported therein, as appropriate.~~

SECURITY

This document contains information affecting the national defense of the United States within the meaning of the Espionage Laws, Title 18, U.S.C., Sections 793 and 794. The transmission or revelation of its contents in any manner to an unauthorized person is prohibited by law.

CONFIDENTIAL

NRL Memorandum Report 754

SUMMARY OF NAVY STUDY PROGRAM
FOR
F4H-1 and F8U-3 WEAPON SYSTEMS

by

C. M. Loughmiller J. C. Ryon
I. N. Bellavin R. L. Lister

VOLUME III

MAY 1958

CONFIDENTIAL

TABLE OF CONTENTS

INTRODUCTION	1
STUDY PROCEDURE	2
F4H-1 and F8U-3 WEAPON SYSTEMS PERFORMANCE UNDER IDEAL CONDITIONS - INPUT DATA	6
Radar Analyses	6
Aircraft Analyses	7
Missile Analyses	7
PHASE I - SYSTEM PERFORMANCE UNDER IDEAL CONDITIONS - HORIZONTAL ATTACKS.....	8
Attack Zones	8
Remaining Study	14
PHASE II - SYSTEM CAPABILITIES FOR PULL-UP UNDER IDEAL CONDITIONS	14
Conditions	14
Attack Zones	16
Comparison of F8U-3 and F4H-1 Pull-Up Capability	19
Remaining Study	21
PHASE III - F4H-1-F8U-3 WEAPON SYSTEMS PERFORMANCE UNDER EXPECTED TACTICAL CONDITIONS	21
Degradation Caused by Vectoring Inaccuracy	22
Settling Time Study	23
Allowable Launch Errors	25

CONFIDENTIAL

Probability of Successful Arrival to Missile Launch - Co-Altitude Attacks	28
Probability of Successful Arrival to Missile Launch - Pull-Up Attacks	31
Degradation of Probability of Successful Arrival to Missile Launch Due to Target Maneuvers	34
Weather Degradation of System Performance	36
Early Warning Detection Requirements	37
Degradation Caused by Countermeasures	42
Remaining Study	42
PHASE IV - SYSTEM PERFORMANCE UNDER EXPECTED TACTICAL CONDITIONS WITH ADDITION OF CURRENTLY PROPOSED IMPROVEMENTS..	43
AN/APQ-72 and 74 Improvements in Fair Weather	43
Probability of Successful Arrival to Missile Launch - Improved Radar	43
Probability of Successful Arrival to Missile Launch - Improved Radar - Maneuvering Target	45
Probability of Successful Arrival to Missile Launch - Improved Radar - Pull-Up Attacks	47
System Performance Resulting From the Use of Advanced Interceptor Performance	50
Remaining Study	53
PHASE V - STUDY TO DETERMINE AND ASSESS REALIZABLE IMPROVE- MENTS	54
PHASE VI - STUDY OF IR TIE-IN FOR AI FIRE CONTROL SYSTEMS ...	55
PHASE VII - REPEAT STUDY PHASES I-VI FOR SPARROW III WITH IR SEEKER	56

CONFIDENTIAL

PHASE VIII - REPEAT STUDY PHASES I - VI FOR SIDEWINDER	56
CONCLUSIONS AND RECOMMENDATIONS	59
ACKNOWLEDGEMENTS	68
LIST OF REFERENCES	69

CONFIDENTIAL

INTRODUCTION

The Bureau of Aeronautics has contracted with Westinghouse, Air Arm Division, for analytical services to be used in a study to establish the tactical use capability of the F4M-1 and F8U-3 Weapon Systems. This study is conducted under the technical direction of the Naval Research Laboratory with all inputs derived from Navy sources. Westinghouse, using these inputs, will submit analytical results to the Navy. Recommendations and conclusions to be drawn from analytical results are assumed to be a Navy responsibility and in particular the responsibility of the technical directors (NRL). This report is the third in a series devoted toward carrying out this responsibility.

In Volumes I & II of this series, the results of the first half of the study effort covered by the current contract were presented. The data presented in this report, along with supporting material presented in Volumes IV through VIII represents the remaining study effort for the current contract.

As the current study program progressed, it became obvious that many of the critical areas of the weapon systems could not be analyzed in detail. Among the reasons are: 1) emergence of sensitive areas as a result of the study to date, 2) lack of input data required for investigation of sensitive areas, 3) time required to investigate additional sensitive areas, and 4) increased financial support required. Much work remains to be done. Because of this, negotiations are currently underway to extend the study contract for an additional year. NRL believes that it is imperative that this extension be approved. The study results to date have and are being used by the Bureau in making decisions on hardware development. They are being used as inputs for design and development of long lead time items. The contractors involved in system development are using these study results as guide lines for their own study efforts. Last, but most important of all, is the fact that for the first time in the history of air-to-air weapon systems, the Bureau of Aeronautics and their associates have an estimate, based on Navy inputs, of the tactical use capability of a proposed system prior to the time of military tests.

The Navy study has and will continue to be a cooperative effort. Wherever possible, duplication has been avoided. Input data for the study has been obtained from the government facilities which most logically would cover the particular field. For example, radar test data was obtained from NATC, Patuxent, Sidewinder performance data has been obtained from NOTS, Inyokern, and seeker performance data was obtained from NAMTC, Pt. Mugu. In addition, the facilities of the various activities have been, in effect,

pooled in order that special talents and equipments can be employed. The results of NAMTC, Pt. Mugu simulator studies to ascertain the allowable launch error for Sparrow III and the effects of hydraulic oil limits have been incorporated in the overall study. In addition, Pt. Mugu is currently conducting flight tests to determine tactical doctrine to be employed during the vectoring phase. This work will be incorporated in the extended phase of the Navy's study. The results of NOTS, Inyokern studies on Sidewinder have been utilized. It is very important that everyone concerned recognize that a study such as this must be a team effort. It is every bit as important to continue this team effort in the extended study program.

The material contained in this memorandum is intended primarily for Bureau information. As agreed during the contract negotiation phase, except for government activities all distribution will be handled through the Bureau channels.

STUDY PROCEDURE

The basic outline for the Navy's study was given in Volume I. It will be repeated here for quick reference and for clarification of changes which have occurred during the program. Table I gives this outline of the Navy's air-to-air missile study program. As originally planned, the outline was intended to be a general guide having flexible elements in order that additionally needed study areas which developed as the study progressed, could be included if desired. A second investigation, considered separate for contractual reasons, was planned to be essentially a repeat for the Sparrow II missile of Phases I to V of the basic study. The Sparrow II study and Phase VIII of Table I were postponed in order that more pressing problems could be investigated. It is proposed that the tactical use capability of alternate guidance techniques be investigated in the extended study program.

TABLE I

OUTLINE OF NAVY AIR-TO-AIR MISSILE SYSTEM STUDY PROGRAM

- PHASE I System Performance Under Ideal Conditions
- A. Aircraft Characteristics
1. F4H-1
 2. F8U-3
- B. Altitudes (co-altitude case)
1. 1000 feet or less
 2. 30,000 feet
 3. 50,000 feet
- C. Interceptor Velocity
1. F4H-1 at altitude $\{V_{max} \text{ \& } V_{cruise}\}$
 2. F8U-3 at altitude $\{V_{max} \text{ \& } V_{cruise}\}$
- D. Target to interceptor speed ratio for interceptor at V_{max}
1. 0.45
 2. 0.8
 3. 1.0
- } Some cases may be trivial and will not be used
- Target speed resulting from above will be used for interceptor at V_{cruise}
- E. Conditions
1. Perfect vectoring
 2. Straight line flight path
 3. Current AI detection capability
 4. B-47 size target
 5. Preparation time - two cases determined by study
 6. Sparrow III - capability of current seeker is to be used
 7. Sparrow III - aerodynamic capability of current missile is to be used
 8. Gimbal angle limits in F4H-1 and F8U-3 aircraft
 - a. AFQ-72
 - b. Seeker

9. Illumination consideration - Geometry of keeping both target and missile illuminated. Illumination requirements to be determined by study.

PHASE II System Snap-up Performance Under Ideal Conditions

A. A, C, D, and E - same as Phase I

B. Altitudes (snap-up case)

1. Target

- a. 30,000 feet
- b. 50,000 feet
- c. 65,000 feet

2. Interceptor Altitude - To be determined by study of system capability.

PHASE III System Performance Under Expected Tactical Conditions

A. Target maneuver

B. Vectoring accuracy

C. Weather

D. Limits imposed by interceptor tactics

1. Climb capability
2. Endurance
3. Dead time

E. Countermeasures

1. Airborne weapons system

PHASE IV System Performance Under Expected Tactical Conditions With Addition of Currently Proposed Improvements

A. Improvements proposed:

1. Search volume optimization

2. Triangle system vectoring
3. Automatic alarm
4. Improved receiver noise figure
5. Back-biased range and display IF amplifier with broad-band switching
6. Gated narrowband angle track IF amplifier (home on jam)
7. Bright display
8. Provision for switching polarization (circular and vertical)
9. Broad banding of the plumbing
10. Jittered PRF
11. Antenna with high altitude feed
12. Improved two-speed AFC
13. Relocation of CW injection plumbing to increase gimbal angle in elevation
14. Nonsaturating AGC

PHASE V Study to determine and assess realizable system improvements

- A. AI Radar
- B. Missile
- C. Vectoring
- D. Tactics

PHASE VI Study of IR tie-in with the fire control system

PHASE VII Performance capability of Sparrow III with an IR seeker

PHASE VIII Sparrow X performance capability

PHASE IX Repeat study Phase I through Phase VI for the Sidewinder 1-B and 1-C

As listed in Volume I, a working framework for the study, which consists of six parts, has been constructed against which the performance of each system combination is analyzed. This framework is repeated here:

- Part 1: Development of effective theoretical co-altitude attack zones under ideal conditions.
- Part 2: Development of effective theoretical non co-altitude attack zones under ideal conditions.
- Part 3: Development of effective theoretical attack zones in the presence of the degradation of expected tactical conditions.
- Part 4: Repeat Part 3 for possible improvements to the systems which are being considered by the Navy.
- Part 5: Study to determine and assess realizable improvements.
- Part 6: Study of infrared (IR) tie-in for AI fire control systems.

The material presented in Volume I of this memorandum was grouped to fit this framework. Most of this material will not be presented here. However, new results will be fitted into the appropriate phase in the framework.

F4H-1 and F8U-3 WEAPON SYSTEMS PERFORMANCE UNDER IDEAL CONDITIONS - INPUT DATA

The system analysis under "ideal" conditions, which was started in Volume I, is continued here. As stated in Volume I, the resulting performance will indicate a capability representative of the best that can be achieved with high probability. The target is nonmaneuvering and the vectoring is perfect. However "ideal" should be interpreted in a limited sense, since the performance of the weapon system subelements is defined by realizable rather than infinite quantities.

Radar Analyses

In Volume I, the parameters of the 62 lot AN/APQ-72 radar were given. Attack zones resulting from the use of this radar were presented for high altitude targets. Analysis of the low altitude case was not presented because of the lack of data. Limited data is now available

On the low altitude performance of the AN/APQ-50 (same as radar of 62 lot AN/APQ-72). Figure 1 gives the results of low altitude tests¹ conducted by NATC, Patuxent using the AN/APQ-50 against an F2H-2 target, head-on aspect. The 85% probability of detection range (7.2 n.mi.) will be extrapolated to a B-47 size target and used to develop the effective attack zones presented later in the report. Figure 2 is a copy from Volume I of theoretical range calculations on the low altitude performance of the 62 lot AN/APQ-72 radar. A discussion of the correlation between these two curves will be given later in the report.

To date, differences in radar performance in a two-seat aircraft (F4H-1) and a single-seat aircraft (F8U-3) has not been included in this study. To date only educated guesses exist on this difference. The general opinion is that there will be about 12% range improvement in the two-seat system. This is not supported by test data and for this reason has not been considered in detail. As far as the improved systems are concerned, there are many who feel that an optimized system for the single-seat application will yield as good performance as one for the two-seat application.

Aircraft Analyses

In Volume I all attack zones were generated using F4H-1 characteristics. Since the preparation of Volume I, complete data has become available on the F8U-3. While the F8U-3 has a power plant which yields a maximum speed capability greater than that of the F4H-1, the aircraft and its auxiliaries are only guaranteed for M 2.0 operation. Using a constant power setting equivalent to M 2.0 the results obtained for the F8U-3 are essentially the same as for the F4H-1 (within the limits of this study) for the co-altitude attacks. As shown in Volume V, the advantages gained by the F4H-1 through higher performance in acceleration is offset by the greater maneuverability of the F8U-3. However, there will be a significant difference in snap-up capability due to the greater altitude capability of the F8U-3. Effective attack zones demonstrating these facts are presented later in this report. As stated previously, a detailed study of system performance due to differences in radar performance in a two-seat aircraft versus a single-seat aircraft has not been included in the study to date. The performance data for the F8U-3 is given in Appendix I, Volume IV of the report. A comparison of the characteristics of these two aircraft are given in Volume V of this report.

Missile Analyses

Data describing the performance of the Sparrow III missile was given in Volumes I and II of this report. Additional data required at that time

consisted of contours outlining the hydraulic oil limits of the current missile. Figures 3 and 4 give overlays developed by NAMTC² which depict the effect of the hydraulic wing servo system performance on this missile. These curves indicate that against a nonmaneuvering target, the hydraulics available should not limit the Sparrow III performance when used in co-altitude attacks. On these figures, curve C represents the maximum interlock range, curve H the hydraulics oil limit range, and curve M the range for M 2.0 missile velocity at intercept. The maximum range interlock curve given here is actually a combination of mechanized maximum interlock and the 6.5 n.mi. interlock. Examination of these curves show that if the maximum interlock range was increased to more closely approximate the maximum range curve (M), hydraulic oil consumption might become a problem, especially at 50,000 feet altitude.

PHASE I - SYSTEM PERFORMANCE UNDER IDEAL CONDITIONS - HORIZONTAL ATTACKS

In Volume I of this report the results of investigations conducted to determine the effective attack zones for the F4H-1 Weapon System in horizontal attacks under "ideal" conditions were presented. As stated previously, when the F8U-3 is limited to a power setting equivalent to M 2.0, the results using both aircraft are essentially identical (see Volume V). Therefore all curves of Volume I relating to co-altitude attacks should now be considered representative of the results which would be obtained with either aircraft.

At the time Volume I was written the work remaining was,

- (a) investigation of the effective attack zones under low altitude conditions,
- (b) investigation of the hydraulic oil limit effects on system performance, and
- (c) investigation of the effect of accelerating the interceptor toward V_{max} in those cases where the attack began at V_{cruise} .

Item (b) above was discussed in the preceding section. The result is that hydraulics do not represent a limit against a nonmaneuvering co-altitude target.

Attack Zones

Figures 5 thru 7 give the resulting effective attack zones for 1000 feet altitude attacks. The AI radar detection data was obtained by scaling

the 85% detection capability of the AN/APQ-50 (Fig. 1) to a B-47 size target and degrading it 10 db for field degradation. While the data represented by Fig. 1 is very limited (very little known about the clutter conditions) and represents a non-co-altitude attack, it is the best data available at the present time. The Bureau of Aeronautics is currently planning a series of tests at NATC against the actual target of interest. As soon as this data is available it will be incorporated in these results.

Referring to Fig. 5, it is seen that against a B-47 size target, the head-on detection range is 6.1 n.mi. Comparing this to the theoretical calculations of Fig. 2, it is seen that this corresponds to a co-altitude attack occurring at 5000 feet. Here again, the results of Fig. 2 are questionable since little is known about the correct value to use for the surface reflective coefficient. Because of the nature of the original tests, it is believed that the AI radar data used for these low altitude cases is optimistic.

The contours describing the effective attack zones of Figs. 5 thru 7 are curve A (85% probability of AI detection range), curve B (AI lock-on range), curve C (Sparrow III maximum aerodynamic range), curve D (Sparrow III minimum aerodynamic range), curve E (constant load factor loci $N_z = 3$), curve F (90% Sparrow III seeker lock-on range), and curve G (6.5 n.mi. interlock range).

Referring to Fig. 5, it is seen that for the conditions of $V_T/V_F = 1$ and $V_T = V_{max}$, there is essentially no forward hemisphere capability even for this "ideal" situation when 85% to 90% probability of success is assigned to each barrier. If a 10 second lock-on time is used, the zone forward of 60° off the target's nose is virtually eliminated. The usable zone is thus restricted to 60° off the target's nose and aft. The usable approach courses are those between 30° off the target's nose and 70° off the target's nose. The resulting attack zone is that bound by the heavy line. The limits from which this line results are AI lock-on range, Sparrow III maximum aerodynamic range, Sparrow III minimum aerodynamic range and the range at which the load factor (N_z) on the interceptor equals 3. It should be noted that the same seeker lock-on contour presented in the overlays for 50,000 feet and 30,000 feet altitude is presented on these overlays for 1000 feet altitude. Lack of seeker performance data at this altitude precludes the use of a more realistic seeker lock-on contour.

One very important factor should not be overlooked at this point. While under the "ideal" situation no errors exist, additional time over the 10 seconds used will be required to settle out errors in the actual tactical situation. The magnitude of this time is variable and depends

upon closing rate, aspect angle, etc. As was shown in Volume I, for forward hemisphere attacks, this time varies between 10 and 20 seconds. If a curve is drawn through the 27 second points (selected as a mean value) on the overlay of Fig. 5, it is seen that except for a very small zone aft of the beam, the effective zone is eliminated. It is very interesting to note that the small remaining zone can be entered only through a corridor 10° wide or from angles off the nose of the target between 60° and 70° .

Figure 6 gives the effective attack zone for the case of $V_T/V_F = 0.8$ and $V_F = V_{max}$. Since there is a speed advantage, around-the-clock approach courses can be used. In addition, the usable effective attack zone has been increased in the forward hemisphere due to the reduced closure rate. The effect of the reduced closure rate is to increase AI detection thus increase the range at which lock-on occurs and to reduce the minimum aerodynamic range (R_{min}). The limiting parameters are the same as those of Fig. 5 except that the $N_z = 3$ curve does not result in a limit.

The effective attack zones for the 1000 feet co-altitude attack where $V_T/V_F = 0.45$ and $V_F = V_{max}$ is given by Fig. 7. As in the case given by Fig. 6, around-the-clock attacks are possible. Essentially all of the maximum aerodynamic range is now utilized. Except for a very small region around 20° off the target's nose, the lock-on range does not represent a limit. The 3 g contour is now reduced to the point where it is no longer a limit.

Comparison of the three polar plots given in Figs. 5 thru 7 illustrate that;

- (1) Even under "ideal" conditions and using optimistic detection ranges, high speed engagements result in essentially no attack capability for high probability of success.
- (2) When additional time is added to reduce vectoring errors, even the use of $V_T/V_F = 0.8$ will be extremely marginal. No forward hemisphere capability exists.
- (3) As the relative closure rate is reduced to the case of $V_T/V_F = 0.45$, the effect of the delay required to lock-on is reduced. However, when the preparation time comparable to that required in the tactical situation is employed, the forward hemisphere capability is wiped out.

In addition to the attack zones described above, much additional valuable information relating to parameter variation can be obtained from the computer generated courses. Samples of the parameter variations are given in Volume I. Figures 6a thru 6m of this report give additional plots of the parameters involved. Two new plots different from those of Volume I are given here (λ'_a and λ'_e). These quantities represent the antenna rates in airframe coordinates while ω_k and ω_j values given in Volume I and here in this volume are antenna rates in space coordinates. Parameter plots for all courses investigated in the study to date are given in Volumes VII and VIII.

The parameter plots of Figs. 6a thru 6m give the results obtained for 1000 feet. co-altitude attacks where $V_T/V_F = 0.8$. The parameters are defined as follows:

- λ_a = lead angle in azimuth
- λ_e = lead angle in elevation
- λ = total lead angle in the plane of action
- τ = angle between target velocity vector and the line of sight measured from the nose of the target
- ψ = angle between the target velocity vector and the interceptor velocity vector measured from the nose of the target
- ω_j = angular rate of the line of sight in the elevation plane of the antenna system (space coordinates)
- ω_k = angular rate of the line of sight in the azimuth plane of the antenna system (space coordinates)
- L/W = load factor
- ϕ = roll angle
- V_F = speed of the interceptor
- α = angle of attack
- λ'_a = azimuth antenna rates in airframe coordinates
- λ'_e = elevation antenna rates in airframe coordinates

On the courses presented, A, B, C and D correspond to the maximum aerodynamic range of the missile (P_{max}), the minimum aerodynamic range of the missile (R_{min}), load factor $L/W = 3$, and impact for a missile fired at R_{min} respectively. Figure 6a gives plots of λ_a versus range for the runs corresponding to those of Fig. 6. For all courses, conversion to successful attacks could be made. λ_a varies between -26 degrees at the beginning of the runs and 0 to -10° in the vicinity of minimum aerodynamic range.

Figure 6b gives plots of elevation lead angle (λ_e) versus range. The case of $\tau = 60^\circ$ gives the largest elevation gimbal angle during the portion of the run that is of interest. As shown on the figure, the elevation gimbal angle for this case varies from -6.5° to 24°. Of course the situation will deteriorate as one deviates from the perfectly vectored situation to one representative of the tactical situation.

Total lead angle (λ) versus range is plotted on Fig. 6c. These curves show the combined effects of Figs. 6a and 6b. Figure 6d gives the angle off the target's nose (γ) as a function of range for the various approach courses. Figure 6e shows the herding angle (ψ) versus range.

The azimuth antenna rates in space coordinates (ω_a) for the courses of Fig. 6 are shown on Fig. 6f. Here again, the rate gets largest for the case of $\tau = 60^\circ$. For this case ω_a varies from 0.5 deg/sec at the start of the run to 1.5 deg/sec in the vicinity of R_{min} . The elevation antenna rates in space coordinates (ω_e) are shown on Fig. 6g. Again the highest rates are encountered on the $\tau = 60^\circ$ case. Here the elevation antenna rate varies from zero deg/sec to 7.5 deg/sec in the region of interest. The corresponding antenna rates in airframe coordinates are shown on Figs. 6i thru 6o.

The load factor (L/W) variation is shown on Fig. 6h. On the attack zone overlays of Figs. 5, 6 and 7 one of the limiting conditions is that resulting from $L/W = 3$. As seen on Fig. 6h, $L/W = 3$ is encountered on the course originating at $\tau = 30^\circ$ and $\tau = 60^\circ$ and occurs at approximately 5000 feet on the runs. Figure 6i gives the roll angle (ϕ) versus range. As can be seen from this figure, even in the perfect situation roll angles as high as 75° are encountered during the approach course. Figure 6j shows the fighter velocity (V_F) during the runs. These curves illustrate the slow-down resulting from a lead pursuit run. The curves of Fig. 6k give the angle of attack (α) versus time. For the $\tau = 30^\circ$ and 60° cases, the angle of attack builds up quite rapidly.

In Volume I polar plots were given for attacks started with the interceptor operating under V_{cruise} conditions. The lower interceptor speeds were chosen to study the possible system improvement as a result of lower closing velocity. Figures 8 thru 10 are a continuation of this investigation. The attack occurs at 1000 feet altitude. The interceptor is assumed to be at V_{cruise} at detection and continues at V_{cruise} throughout the engagement. The result is greater detection ranges and reduced effects of preparation time in the forward hemisphere. These factors are illustrated by Fig. 8 where $V_F = V_{cruise}$ and $V_T = 1189$ ft/sec. Comparing the overlays of this figure to those of Fig. 5, it is seen that the head-on detection range for 85% probability has been increased from 6.1 n.mi. to 6.6 n.mi. and the 10 second lock-on point has moved out in range from 2 n.mi. to 3.75 n.mi. In Fig. 5 it is seen that the zone forward of 60° is unusable because of lock-on time. This restriction is no longer present for the conditions of Fig. 8. However, attacks must originate forward of 42° off the target's nose. Figures 9 and 10 give polar plots for reduced target speeds.

The study of the case of an interceptor beginning an attack under V_{cruise} conditions is not complete at this point. The overlays given in Volume I and by Figs. 8 thru 10 assume that the interceptor starts the run at V_{cruise} and continues through the engagement under V_{cruise} conditions. The obvious question is, "What happens when the interceptor is allowed to accelerate after detection occurs?" The answer is, "The acceleration times involved are such that very little improvement is obtained especially when a high speed target is involved." Figure 11 gives the case of a lead pursuit co-altitude attack occurring at 50,000 ft. The fighter begins the runs at V_{cruise} (873 ft/sec) and accelerates toward V_{max} after detection. The target speed is 1940 ft/sec. The improvement realized can be seen by comparing this figure to Fig. 2 of Volume I. As would be expected a slight increase in allowable approach aspect occurs (from 45° off the target's nose to 50° off the target's nose). The effective attack zone is essentially unchanged. Figure 12 gives the results of attacks made by the same accelerating fighter against a slower target (1552 ft/sec). Again there is a minor improvement in allowable approach angle.

The curve overlays of Fig. 13 show the results of the accelerating interceptor attacking a target having a speed equivalent to the interceptor's V_{cruise} condition. Comparing this to Fig. 30 of Volume I, it is seen that a major improvement in allowable approach course is realized (from 70° off the target's nose to 180° off the target's nose). However, the times required to close range to R_{max} on courses originating from 90° off the target's nose are very high (250 seconds and higher).

The curve overlays of Figs. 14 thru 16 are a repeat of this investigation described above but for attacks occurring at 30,000 feet. The results are essentially the same as given above.

Remaining Study

The remaining study effort required for the completion of the co-altitude attack under "ideal" conditions involves further analyses of the 1000 feet altitude case. The data presented in this report is believed to be optimistic for current radars. As soon as sufficient test data becomes available, the attack zone overlays should be modified.

Throughout the co-altitude analyses to date, equal radar performance is considered to exist for either the XIA and XIB systems. If tests do prove that there is a significant improvement in performance of the radar in one application versus the other, the results of this study should be modified to include this improvement. However, if the improvement of AI radar performance is only 12% as is currently estimated, the difference in tactical use capability will be minor. This will be discussed later in the section on probability of successful arrival to missile launch.

PHASE II - SYSTEM CAPABILITIES FOR PULL-UP ATTACK UNDER IDEAL CONDITIONS

In Volume I of this study the pull-up capabilities of the system under "ideal" conditions were described. The curves presented were labeled F4H-1. As will be shown later, if the F8U-3 is restricted to M 2.0 top sustained speed, the system using this aircraft will yield performance which for all practical purposes is identical except for a difference in altitude capability. Thus these curves with slight modification should be interpreted to apply to either system.

At the time of publication of Volume I, parameter variations for the courses investigated were not available. Since this time these parameter variations have been developed and are presented here.

Conditions

The conditions of this investigation are as follows:

- (a) Aircraft characteristics - F4H-1, F8U-3
- (b) Target altitudes - 30,000 feet, 50,000 feet, and 65,000 feet

- (c) Interceptor altitudes - as capable from below
- (d) Reflective area - B-47 size target, assumed the same as for co-altitude case.
- (e) Velocities - interceptor velocity at altitude, V_{max} and V_{cruise}
- (f) Target to interceptor speed ratios for interceptor at V_{max} - 0.45, 0.8, 1.0. Resulting target speeds from above also used for interceptor at V_{cruise} .
- (g) Perfect vectoring
- (h) Straight line flight path (target)
- (i) Current AI detection capability - 85% probability
- (j) Time from detection to lock-on - 10 seconds
- (k) Seeker capability - current Sparrow III
- (l) Missile aerodynamics - current Sparrow III
- (m) Gimbal angle limitations of current AN/APQ-72 radar - $\pm 41^\circ$ azimuth, $+ 47^\circ$, $- 38^\circ$ elevation.
- (n) Interceptor restricted to 3 g pull-up or C_{Imax} during tracking portion of the run
- (o) Allowable heading error for launching Sparrow III - 10° .

A lead pursuit course is maintained by the interceptor after launch to provide illumination of the target. If the acceleration requirements of the course exceed the capability of the interceptor a C_{Imax} course is flown. At impact it is assumed that the interceptor is maneuvered so that the lift vector and the gravity vector are working together (rapidly redirecting the interceptor downward). To date the recovery problem has received only superficial coverage. The investigation of recovery was done separately from the actual computer runs as explained above and detailed in Appendix II of Volume IV. On the computer runs the interceptor was allowed to follow a lead pursuit run as restricted by C_{Imax} after impact.

This is shown on the parameter plots of Figs. 17a thru 19i. During this portion of the run the 3 g limitation is removed because it is possible for the pilot to pull more g's when he is not trying to solve a fire control problem. If during the breakaway portion of the run, a minimum L/W of 0.5 is maintained, the run is considered successful. During this portion of the run the acceleration conditions must also be such that C_{Lmax} is not exceeded. Details of the method used in the study are given in Appendix II of Volume IV. Two major simplifying assumptions are made. The first is that the pilot can fly a perfect C_{Lmax} course. This will yield optimistic results as far as recovery problems are concerned. The second simplification is that during the critical part of the recovery maneuver, thrust is assumed equal to drag. The inaccuracies resulting from these simplifications can be resolved only by more exact investigation. However, the method used represents a good first look at the problem.

Attack Zones

Figures 17 through 19 are selected samples of the resulting usable attack zones described in Volume I. They are repeated here for ready reference. Parameter plots for selected runs from these cases will be described. Parameter plots for all runs are included in Volumes VII and VIII. The points chosen for presentation here are:

- (a) From Fig. 17, the run that originates at 30,000 feet fighter altitude and 10 seconds delay. This illustrates the case where the error was never reduced to the point required for successful launching.
- (b) From Fig. 18, the run that originates at 10,000 feet fighter altitude and 10 seconds delay. This illustrates the run where recovery becomes a problem.
- (c) From Fig. 19, the run that originates at sea level and zero delay. This illustrates the case where gimbal angle becomes a problem.

It should not be interpreted that the authors are presenting these runs as representative of the expected tactical situation. This is not the case. They were merely chosen to show the parameter variations on runs where specific problems are encountered. On these parameter plots the points where the interceptor encounters various barriers are labeled as follows:

⊙ = R_{max}

+ = Start of Pull-up

▷ = Start of Lead Pursuit

X = Impact

⊗ = R_{min}

.... C_L = C_{Lmax}

On Figs. 17 and 18 the velocity of the fighter is labeled as M 0.9. Actually the velocity used corresponds to M 0.9 at 50,000 feet and was maintained constant for the other runs.

Figures 17a thru 17i give plots of parameter variation for the run shown on Fig. 17 which originates at 30,000 feet altitude and 10 seconds delay ($\phi = 17^\circ$). On these runs the target's altitude was 50,000 feet and its velocity was M 2.0. The interceptor starts his run at M 0.9 and accelerates toward V_{max} . Figure 17a shows the range versus time variation. For this particular run R_{max} occurred at 15.5 seconds after detection. C_{Lmax} was encountered 17.5 seconds after detection or 7.5 seconds after pull-up was started. On this run the interceptor was never able to reach a lead pursuit course nor was it able to close the range to R_{min} . The impact point is not labeled because the interceptor was unable to reduce the error to 10° or less between the R_{max} and R_{min} ranges.

The curve of Fig. 17b shows the variation of elevation gimbal angle (λ_e) in degrees as a function of range. As shown, λ_e varies between the extremes of -33° and $+22^\circ$ during the run. The hook in the curve at the end of the run indicates that range is beginning to increase again. Figure 17c gives the elevation antenna rate in space coordinates (ω_j) versus range. ω_j varies between 1 deg/sec at the time of pull-up to 11.6 deg/sec at the end of the run.

The angle between the target velocity vector and the interceptor velocity vector measured from the nose of the target (ψ) is shown on Fig. 17d. It is interesting to note that at the end of the run the interceptor velocity vector is 104° with respect to the target's vector. This means that the interceptor is beginning to fall over on its back. Load factor (L/W) as a function of range is shown on Fig. 17e.

As shown the load factor decreases rapidly toward zero. In the region where the interceptor is falling over on its back, the load factor is reduced to a point, $L/w < 0.5$, where recovery will become a problem. The method of recovery analysis is detailed in Appendix II of Volume IV.

The angle of attack (α) as a function of time is shown by Fig. 17f. α at the start of the pull-up (10 seconds) is 7° and increases rapidly to 16° . Figure 17g shows the rapid slow down of the interceptor during the run. V_p at the start of the run is 894 ft/sec. Between detection and lock-on (10 seconds), the interceptor accelerates to 975 ft/sec. From this point on the slow down is rapid. At the end of the run, the velocity is down to 340 ft/sec. During the run, the interceptor climbs from 30,000 feet to approximately 42,000 feet. This variation is shown by Fig. 17h. The elevation antenna rate in airframe coordinates ($\dot{\lambda}_e$) is shown on Fig. 17i.

The curves of 18a through 18i give the parameter variation for an interceptor starting a pull-up run from 10,000 feet altitude at 10 secs. after detection against a target flying at 50,000 feet. The target's velocity is 873 ft/sec. The interceptor starts its run at 873 ft/sec. and attempts to accelerate toward V_{max} . This run corresponds to a point on Fig. 18. Figure 18a shows range variation as a function of time. As shown, the interceptor is able to get on a lead pursuit course 12 seconds after start of pull-up. R_{max} is encountered 32 seconds after start of pull-up. The impact point for a missile launched at R_{max} occurs 44 secs. after pull-up.

Figure 18b shows the variation of elevation gimbal angle as a function of range and is seen to vary from $+28^\circ$ at pull-up to -32° at impact. ω_j is shown on Fig. 18c. As shown ω_j varies from -0.25 deg/sec to -1.75 deg/sec at impact.

The heading angle of the interceptor is shown on Fig. 18d. It is interesting to note that during the later part of the run (at impact where recovery starts) the interceptor is flying nearly vertically (80°). Referring to Fig. 18e it is seen that at the time of impact of the missile, the load factor is dropping rapidly. The recovery will be a problem. Also, as shown on Fig. 18f, it is in this same region that α builds up rapidly. For this case the angle of attack reaches 17° during the run.

Figure 18g shows the interceptor slow down during the run. As shown the interceptor attempts to accelerate toward V_{max} at the beginning of the run and is able to get up to 1070 ft/sec. However the deceleration is quite rapid. At impact the interceptor velocity has fallen to 500 ft/sec.

Figure 18h shows the interceptor altitude versus range. The interceptor reaches a maximum altitude of 36,500 feet at impact. λ_e is shown on Fig. 18i.

Figures 19a thru 19i give corresponding parameter plots for the run originating at sea level with pull-up occurring at detection. For this case, the initial interceptor velocity is 1,212 ft/sec. The target is flying at 30,000 feet at a velocity of 1,980 ft/sec. The significant point brought out by these plots is shown on Fig. 19b. It is seen that elevation gimbal angle available (-38°) is exceeded at 25,000 feet range. Therefore, for a system incorporating the unimproved radar the rest of the run is meaningless. Referring to Fig. 19e, it is seen that if more gimbal angle were available such that the run could proceed, $L/W = 3$ would occur at 15,000 feet range. Since the run failed both from the gimbal angle and L/W standpoint, the run is obviously a failure. The portion of the run from 15,000 feet range to the end of the run for this particular family of parameter plots is meaningless in the tactical situation, since the computer was not restrained to $L/W = 3$.

Comparison of F8U-3 and F4H-1 Pull-up Capability

As stated previously in the report, the F8U-3 is guaranteed to operate at V_{max} or M 2.0. As is shown in Volume V, the co-altitude performance of the two systems are essentially the same (neglecting differences in radar performance). The difference in altitude capability should be reflected in the ability to attack high altitude, high speed targets in the pull-up mode of operation. Pull-up attacks against 65,000 feet altitude targets were chosen as the area in which the system performance is most affected by aircraft limitations. The principal reasons are that this is the region where the maximum L/W capability of both interceptors falls below 3, ceiling problems are encountered for both aircraft, and aircraft acceleration limits are encountered. A few selected cases are presented in the following sections. The major difference between the two systems should occur due to the difference in altitude capability of the two aircraft. The specific intent of the following figures is to compare these two aircraft under pull-up attack conditions.

Figure 20 shows the results of attacking a M 2.0 target at 65,000 feet with the F4H-1 operating at M 2.0 or V_{max} and the F8U-3 restrained to a power setting equivalent to M2.0 in level flight. It is seen that the F4H-1 has an altitude ceiling of 58,000 feet while the F8U-3 has an altitude ceiling of 62,000 feet. For these curves initial detection range is that resulting from 50% probability of detection instead of the 85% probability of detection used in the preceding investigation. This is done

in order that there would be attack zones available to compare. Comparing the zones it is seen that except for the altitude capability difference the attack zones are essentially the same. For the case of the F4H-1, successful pull-up attacks could occur from a differential altitude of 6,000 feet while for the F8U-3 successful attacks could occur from a differential altitude of 10,000 feet. This is a significant improvement and should not be overlooked.

Figure 21 gives the resulting performance of the F8U-3 and F4H-1 pull-up runs starting with $V_f = M 0.9$ against a M 2.0 target at 65,000 feet. Again the runs originate at the 50% probability of detection point. Although these charts are not complete (full altitude range not investigated) they will suffice for comparison purposes. For example, a run originating at 45,000 feet and zero time delay results in a minimum error of 25.2° for the F4H-1 and 26° for the F8U-3. A run originating at 35,000 feet and 10 seconds delay results in a minimum of 14° error for the F4H-1 and 11° error for the F8U-3. The close comparison of results is obvious.

The graphs of Fig. 22 show the pull-up capability of the F4H-1 and the F8U-3 flying at M 2.0 or V_{max} when attacking a M 0.9 target at 65,000 feet. Comparison of the results shows that the major difference in capability is again due to the greater altitude capability of the F8U-3. Comparison of some of the points shows the minor differences in performance.

Figure 23 gives graphs which compare the F4H-1 and F8U-3 when attacking a M 0.9 target at 65,000 feet. Here the interceptor started out at V_{cruise} and accelerated toward V_{max} . Here again the F8U-3 was restrained to a maximum speed of M 2.0. These charts, although not complete (complete altitude range not investigated) do serve to illustrate the minor differences (neglecting difference in maximum altitude capability) that exist between these two interceptors. The failures shown occur after severe slowdown of the interceptor. In early pull-ups, lead pursuit is soon achieved, but loss in velocity results in negative flight path angle rates and larger errors before arrival at launching range. Although the greater maneuverability of the F8U-3 allows a higher initial pull-up rate and an earlier achievement of lead pursuit, its greater slowdown causes an earlier loss of pull-up capability. The error at launch range is thus greater for the F8U-3 than for the F4H-1 as indicated on Fig. 23 at the zero delay pull-up points. For long delayed pull-ups, such as the one shown on Fig. 23 at 45,000 feet and 30 seconds after detection, the attack duration is short, so that the difference in slowdown is minimized. The more maneuverable F8U-3 reaches launch range with an error of 8° as compared to 11° for the F4H-1.

From the above comparison it is obvious that if (1) the F8U-3 is restricted to M 2.0 operation and (2) if the AI detection capability is assumed the same for both the F4H-1 and the F8U-3 installations, the only important difference resulting from the pull-up investigation is that due to the greater altitude ceiling of the F8U-3. This is shown on the figures described above.

Remaining Study

The preceding section described the results of the pull-up studies for the "ideal" situation. Additional study effort is needed to reveal the sensitivity of pull-up attacks to approach aspect angle. For this reason, the extended phase of the study program will include investigation of several aspect angles other than head-on.

As stated previously, when data becomes available on differences in AI radar performance between the two systems, these differences should be included in the study. If the improvement for the two seat system is only 12%, as is estimated, the difference in the study results will be minor. . This will be illustrated later in the section on probability of successful arrival to missile launch.

The effects of hydraulic oil limits on system pull-up capability has not been investigated. As stated previously, hydraulics do not represent a limit on co-altitude attacks. This is not necessarily the case for pull-up attacks. Studies conducted by NADC, Johnsville (different input conditions) indicate that hydraulics are a severe limitation in pull-up attacks.

PHASE III - F4H-1 - F8U-3 WEAPON SYSTEMS PERFORMANCE UNDER EXPECTED TACTICAL CONDITIONS

The preceding sections have extended the description of results for the "ideal" situation given previously. in Volume I of this report. The results given represent the best that one would hope to achieve, with a high probability of success, when certain sources of error are neglected. It is now of interest to look at the degradation resulting from a more realistic tactical situation. The degrading factors considered in the current study program are:

1. Vectoring accuracy
2. Target maneuver
3. Weather
4. Countermeasures against the airborne weapon systems
5. Limits imposed by interceptor tactics
 - (a) climb capability
 - (b) endurance
 - (c) dead time

Degradation Caused by Vectoring Accuracy

One important effect of vectoring inaccuracy on system performance is the settling time that results. A preliminary investigation of this required settling time was presented in Volume I of the study. However at that time sufficient AI detection range intervals had not been investigated nor had the pilot been restricted to 3 g's during the run. This preliminary data can now be supplemented.

The input conditions are the same as those of Volume I except for the two parameters mentioned above. The vectoring accuracy used (now verified by simulation studies conducted by NOTS, INYOKERN) are ± 3 n.mi. in azimuth, ± 3 n.mi. in range and ± 1 n.mi. in altitude. A number of range intervals were investigated in order that the 85% AI detection contour could be approximated. The pilot was restricted to 3 g's by a positive indication (buzzer).

As shown on the polar plots for the "ideal" co-altitude attacks, 10 seconds was allowed for converting from detection to lock-on. If errors exist at lock-on (and they will in the tactical problem), additional time will be required to reduce these errors to those acceptable for Sparrow III missile launching. The same statements of course apply to the pull-up attacks. The problem then is to resolve this settling time to a value which can be used in the study.

For purposes of this study the work was actually divided into three parts: (1) establishment of allowable launch error for Sparrow III -- This work was done by NAMTC, Ft. Mugu and will be discussed in detail later. (2) conversion of vectoring inaccuracy at detection to a heading inaccuracy at lock-on and (3) investigation of events occurring after lock-on.

Settling Time Study

A complete description of the investigation is given in Appendix VI of Volume II and Appendix IV of Volume IV. Samples of the results are included here. It is important to recognize that the purpose of this part of the study is not to derive an exact value of settling time. Rather, it is to demonstrate to the many doubters that a finite and, in general, large value of settling time is required. Many people have argued that the conversion from AI detection to missile launch can be accomplished in 3 or 4 seconds, repeatedly. This is not the case in the tactical situation as is shown by the following examples. The exact value of the settling time for each examined run is automatically included in the sections later in the report which describe successful arrival to missile launch.

Figures 24 thru 27 show the results of investigation to convert vectoring inaccuracy at detection to heading error at lock-on. The altitude of the engagement is 30,000 feet. The interceptor velocity is 1,897 ft/sec. The interceptor is vectored on a pure collision course and continues on this pure collision course to lock-on (believed to be realistic for present operational conditions). The vectoring errors are normally distributed about this pure collision course (constant relative bearing line) with a 1 sigma value of - 3 n.mi. Courses are generated from this normal distribution and straight lines are flown to lock-on. The results are given on Table II. These results give us the heading errors which can be used in investigating events after lock-on.

TABLE II

CONVERSION OF VECTORING INACCURACY AT DETECTION
TO HEADING ERROR AT LOCK-ON
(Altitude - 30,000 feet)

Approach Aspect Angle (Degrees)	Heading Error at AI Radar Lock-on To Include 85-90% of Cases for the Follow- ing Speed Ratios		
	$V_T/V_F = 1.0$	$V_T/V_F = 0.8$	$V_T/V_F = 0.45$
20	30°	27°	23°
30	33°	31°	25°
40	37°	32°	25°
60	47°	37°	26°

Samples of the results of the investigation of the settling time required after lock-on are shown on Figs. 28 thru 30. The criteria for success is that the error can be held within a specified value for 3 seconds. All runs shown were made at 30,000 feet altitude. The interceptor velocity is V_{max} (1,897 ft/sec). The range at which the runs started (AI lock-on range) is 10 n.mi. Table III summarizes the results.

TABLE III

SYSTEM SETTLING TIME REQUIRED AFTER AI RADAR LOCK-ON
(30,000 Feet Altitude- $V_p = 1,397$ Ft/Sec)

Speed Ratio V_T/V_F	Aspect Angle θ	Heading Error at Lock-on ϕ	Cumulative Probability of Heading Error Occurrence (%)	Status of Run		
				85% Settling Time (REAC)	50% Settling Time (REAC)	IBM Settling Time
1.0	20	20	70	Could not reduce error		Error reduced to 10° in 7 seconds
1.0	20	30	87	Could not reduce error		Could not reduce error below 27°
1.0	40	20	56	Could not reduce error		Error reduced to 10° in 11 seconds
1.0	40	30	77	Could not reduce error		Could not reduce error below 27°
0.45	40	20	80	Error reduced to 10° in 7 seconds	Error reduced to 10° in 6 seconds	Error reduced to 10° in 6 seconds
0.45	40	30	94	Error could only be reduced to 14°	Error reduced to 10° in 17 seconds	Error reduced to 10° in 15 seconds

Referring to the upper left hand curve of Fig. 28 (row 1 of Table III) it is seen that if the requirement is that 85% of the time we must reduce the error to something less than the original error, we would fail. Thus if in the barrier analysis presented by the preceding polar plots, we require a barrier representative of 85% settling time, we would have a failure. The upper right hand curve of this figure shows the results of an IBM run. This is an exact solution since on the IBM runs there is no pilot in the loop. Thus the 50% probability label does not apply. It is on the drawing because on later figures it is used for comparative purposes.

Referring to Fig. 30, it is seen that the settling time problem is somewhat relieved because of the slower target involved. These results are shown by rows 5 and 6 of Table III. The right hand curves of Fig. 30 compare the 50% probability results of runs conducted using a cockpit simulator - REAC combination (pilot in the loop). and IBM runs. It is interesting to note the close correlation of results. This is to be expected, since the human error should be distributed normally about the correct solution (50% probability).

Allowable Launch Error

The next step in the investigation of system settling time is to determine the allowable launch errors which can be tolerated with the Sparrow III and still achieve a satisfactory miss distance. This work was done by NAMTC, Ft. Mugu and Figs. 31 thru 42 were taken from their results³. The maximum and minimum ranges on these figures were obtained from the polar plots presented in Volume I and are determined by AI radar lock-on, maximum aerodynamic range and minimum aerodynamic range. These figures have been modified to include limits of the seeker and 3 g maneuver. The gimbal angle limits of the current AI radar were used. The criteria for successful runs were that the miss distance be 25 feet or less, the missile velocity must be greater than M 0.8 and the missile target closing rate must be greater than 150 ft/sec. Fig. 31 shows the resulting allowable launch error for Sparrow III launched from a M 2.0 interceptor against a M 2.0 target, co-altitude attack at 50,000 feet, on a run originating from 20° off the target's nose at arrival to the launch zone. The angular limits are those imposed by maneuver capability of the missile. The range limits are those obtained from the polar plots (see Fig. 22, Volume I), and result from AI radar lock-on range and minimum aerodynamic range. As detailed in Reference³ random noise results in a 16 value of guidance system errors of 2°. This is included on the figure as a questionable region. Thus the allowable launch error for this condition is + 4° to - 5°.

neglecting noise effects. Considering noise, the allowable launch error is $+1^\circ$ to -3° (65% probability). For this particular case AI lock-on range and seeker lock-on coincide. It is interesting to note that for this case to be of tactical utility, the AI radar detection range would have to be increased to the point where the range at the end of total system settling time would occur at a range equivalent to that labeled lock-on range on the polar plot of Volume I.

Figure 32 gives the results of the high-speed interceptor attacking a high-speed target from an aspect angle of 80° off the target's nose at the time of entering the launch zone. This would actually be a course originating from approximately 65° at detection. The range limits correspond to the maximum interlock range and minimum interlock range limits shown on the polar plot of Fig. 22, Volume I. Thus it is seen that the allowable launch error is $+2.4^\circ$ to -19° (neglecting noise effects) at the extreme launch range. However, these allowable errors decrease as we decrease the range of launch. An important point brought out by Fig. 32 is that it is very important to increase the gimbal limits from the current $\pm 41^\circ$. Here again the questionable area due to noise is shown by the double cross-hatched area. As shown on the figure, a zone of interest is labeled which differs from the overall zone. This is due to the 3 g maneuver limit imposed on the interceptor. The zone inward from that of interest to the minimum range is questionable.

The results of runs entering the attack zone from 140° off the target's nose (course starting from 70° off the target's nose at detection) on an attack at 50,000 feet for $V_T = M 2.0$ and $V_T/V_F = 1.0$ are shown on Fig. 33. Here it is seen that the allowable launch error is restricted by maximum and minimum ranges (actual interlock ranges mechanized). The zone resulting from positive errors is primarily limited by AI gimbal limits. It is seen that at the extreme ranges, the allowable negative launch error has increased. However, it decreases rapidly as range decreases because of missile maneuver limits.

The graphs of Fig. 34 thru 36 show the results for attacks occurring at 50,000 feet for a slower target ($V_T = M 1.6$). Figure 34 shows the results of runs starting at 20° off the target's nose. For this case, the range limits are those resulting from AI radar lock-on range and minimum aerodynamic range as shown on the polar plots (see Fig. 23 of Volume I). This would correspond approximately to the seeker lock-on range plus a range equivalent to 2 seconds time of flight (seeker limit). The angular limits are due to missile maneuver limitations. The allowable launch error is from $+6^\circ$ to -8° as limited by noise.

The graph of Fig. 35 shows the results of runs which entered the launch zone at 80° off the target's nose. For this case, the maximum and minimum launch ranges shown are those resulting from maximum and minimum interlock ranges of the missile. Again, the angular limits result from AI gimbal limits and missile maneuver limits. The allowable launch error varies between $+10.8^\circ$ and -16° at the extreme ranges and $+2^\circ$ and -7° at the minimum range. Figure 36 illustrates the corresponding case for attack at 140° off the target's nose.

Figures 37 thru 39 illustrate the case of attacks occurring at 30,000 feet and $V_T/V_F = 1.0$ where $V_F = M 1.91$. The graphs of Fig. 37 show the results of runs originating from 20° off the target's nose. The maximum and minimum ranges result from AI lock-on range and missile minimum interlock range. The angular limits are again due to missile maneuver limitations. The allowable launch error varies from $+11^\circ$ to -12° at the extreme range and from $+3^\circ$ to -6° at the minimum range. Referring to the polar plot (see Fig. 19 of Volume I), it is seen that a large increase in AI radar detection capability must result before all of the envelope shown on Fig. 37 can be used.

When the angle of approach is changed to 80° off the target's nose, the results of Fig. 38 are achieved. The AI gimbal limit again represents a major limit. The range limits shown result from missile interlock ranges. A zone of interest different from the overall zone is labeled. The lower restriction is due to 3 g interceptor limit. Ranges outside of this zone of interest are questionable. Outside the zone of interest the system usefulness can only be determined by investigating how rapidly the error builds up when the interceptor flies a 3 g restricted course instead of a lead pursuit course. The allowable launch error is from $+2.2^\circ$ to -25° at maximum range and from $+2.2^\circ$ to -20° at the minimum range of the zone of interest.

Figure 39 shows the results of runs entering the launch zone at an aspect angle of 140° . The altitude and speed conditions are the same. The maximum and minimum missile interlock ranges represent the launch zone limits in range. Positive errors are limited by missile maneuver capability and AI gimbal limits. Negative errors are limited by missile maneuver limits. The allowable launch error varies between $+16.4^\circ$ and -25° at maximum range and $+1^\circ$ and -8° at minimum range.

The graph of Fig. 40 shows the resulting allowable launch errors for attacks at 30,000 feet. For this case $V_T/V_F = 0.8$ and $V_F = M 1.91$.

The runs enter the launch zone at 20° off the target's nose. The maximum launch range corresponds to AI radar lock-on range given on the corresponding polar plot (see Fig. 20 of Volume I). The minimum launch range corresponds to the missile minimum interlock range. The angular limits result from missile maneuver limits. Again a zone of interest different from the overall zone is shown. The outer limit on this new zone represents seeker lock-on ranges plus two seconds time of flight. Referring to the polar plot of Volume I, it is seen that the AI detection range must be increased to allow full use of the entire zone of interest (if overall system settling time is considered).

When the runs enter the allowable launch area at 80° off the target's nose, the results of Fig. 41 are obtained. These runs correspond to runs originating from approximately 60° off the target's nose at AI detection. Here the range limitations are those resulting from maximum and minimum missile interlock ranges. Positive errors are limited by AI gimbal angle limits and negative errors are limited by the maneuver capability of the missile. The zone of interest is limited due to the 3 g limit on the interceptor. Again the extent of the zone in range depends upon how fast the errors build up when the interceptor files a 3 g limited course as opposed to a lead pursuit course. Within the zone of interest, the allowable launch error varies between $+10.5^\circ$ and -28° at maximum range and $+10.5^\circ$ and -14° at the lower range of the zone of interest.

When the angle at which the interceptor enters the launch zone is changed to 140° the results shown on Fig. 42 are obtained. Again the maximum and minimum ranges result from the missile interlock ranges. The allowable launch errors vary from $+21.5^\circ$ (AI gimbal limited) to -32° (missile maneuver limited) at maximum range and from $+2^\circ$ to -6° at minimum range (missile maneuver limited).

Probability of Successful Arrival to Missile Launch-Co-Altitude Attacks

In Volume I, preliminary work on the probability of successful arrival to missile launch was presented. This work has been extended and the results are included in this report. In the model, the interceptor is assumed to be directed on a pure collision course. A normal distribution of AI radar lock-on probability is assumed with the 85% probability point consistent with the values given previously. A normal distribution of vectoring inaccuracy ($1\sigma = 3$ n.mi.) is assumed to occur along a line perpendicular to the pure collision course (relative bearing line).

Courses are then generated through the resulting probability zone with the interceptor flying straight lines parallel to the correct pure collision courses at the center of the distribution (see model sketch on Fig. 55 of Volume I). At lock-on the interceptor is placed on a constant $L/w = 3$ turn. This maneuver is optimistic since it allows for no reaction or evaluation time on the part of the pilot as is encountered on the REAC settling time runs presented previously. The criteria for success are that the launching error can be reduced to 10° before R_{min} is reached and that the gimbal angle required does not exceed that available during the lock-on to R_{min} interval. Thus we are in a position to evaluate the probability of successful arrival to missile launch for a system which uses currently available equipments. The ranges used are those obtainable with the 62 lot Q-72 radar. The gimbal angles used are those of the 62 lot Q-72 ($\pm 41^\circ$ in azimuth and $+ 47, - 38^\circ$ in elevation) and the settling times employed are those resulting from these current equipments installed in the F4H-1 or the F8U-3. The remaining question is whether the assigned allowable launch error for the Sparrow III (10°) is realistic. Referring to the graphs given in the preceding section and in Ref 3, it is seen that the allowable launch error is a function of altitude, aspect angle at the time of entry into the launch zone, gimbal angle (which is accounted for separately) and the point in the launch zone where the interceptor is in a position to launch the weapon. It is seen that for attacks entering the launch zone close to head-on the allowable launch error is extremely small (see Figs. 31 and 37). As we progress around toward the beam, the allowable launch error increases (see Figs. 32 and 38). However, as we come in-range the allowable launch error decreases. Thus the ideal solution would appear to be a mechanization which presents an allowable launch indication which is a function of altitude, aspect angle (closing rate), and range. Without this mechanization it will be necessary to assign a value of allowable launch error which will include a high percentage of the cases. For purposes of this study 10° has been assigned. If 25 values for noise uncertainty are considered, the allowable launch errors will be much less than 10° for many of the situations described previously.

Figure 43 through 45 gives the probability of successful arrival to missile launch versus vectoring angle for three altitudes. The attacks occur under co-altitude conditions. The results are summarized on Table IV.

TABLE IV

PROBABILITY OF SUCCESSFUL ARRIVAL TO MISSILE LAUNCH
(Co-Altitude Attacks - Unimproved Radar)

Interceptor Velocity V_F (ft/sec)	Speed Ratio V_T/V_F	Altitude (ft x 10^3)	Probability of Success (%)		
			For Aspect Angle (τ) = 0°	For Aspect Angle (τ) = 30°	For Aspect Angle (τ) = 60°
1940	1.0	50	46	52	0
1940	0.8	50	48	73	44
1940	0.45	50	69	86	85
1897	1.0	30	45	53	0
1897	0.8	30	52	75	44
1897	0.45	30	79	90	89
1189	0.8	1	52	60	47

The results presented on Fig. 43 (rows 1 thru 3 of Table IV), were presented in Volume I but there were two errors. First, the curves were incorrectly described as attacks occurring at 30,000 feet. Second, the probability curve for $V_T/V_F = 0.8$ was incorrectly plotted (too high).

Referring to Table IV and Figs. 43 thru 45, the following significant factors apply:

- (1) When $V_T/V_F = 1.0$ and $\tau = 60^\circ$, the probability of successful arrival to missile launch is zero because the gimbal angle required exceeds the capability of the radar, and the interceptor will be in a position, determined by vectoring inaccuracy, from which he cannot correct to a successful attack since he has no speed advantage.

- (2) When $V_T/V_F = 0.8$, the primary reason for reduction in probability as angle off increases toward 60° is gimbal angle limitations.
- (3) When $V_T/V_F = 0.45$, the resulting probabilities are uniformly high. Unfortunately this case represents today's target.
- (4) As stated previously, in the section on radar analysis, it is believed that the range values used in the 1000 feet altitude case (row 7 of Table IV and Fig. 45) are optimistic. These results will be modified as more firm data becomes available.

As stated previously, it is currently estimated that a 12% improvement in AI detection range will result from the use of a separate operator (F4H-1 vs F8U-3). The resulting improvement on probability of successful arrival to missile launch is shown by Fig. 43a. The conditions are the same as those of Fig. 43. The unimproved radar was used. This figure is copied from Volume I, and corrected as discussed previously. It is seen that a 12% improvement (1.5 n.mi.) results in an 8% improvement in probability of successful arrival to missile launch for the case of $V_T/V_F = 1$ and $\tau = 0^\circ$ and 30° . When $V_T/V_F = 0.8$ the resulting improvement in probability of successful arrival to missile launch is 18% for $\tau = 0^\circ$ and 6% for $\tau = 30^\circ$.

Probability of Successful Arrival to Missile Launch - Pull-up Attacks

The next problem to be investigated is that of probability of successful arrival to missile launch for pull-up attacks considering vectoring inaccuracies. The model and analytical approach is detailed in Appendix V of Volume IV. In brief, the model assumes a head-on attack with an azimuth distribution about this head-on attack of $1 \sigma = \pm 3$ n.mi. The 85% probability of detection on the range distribution is that of the unimproved radar (12-13 n.mi.). The gimbal limits are those of the unimproved radar. No corrections in altitude or azimuth were made until lock-on (10 seconds after detection). Upon lock-on the interceptor starts an immediate 3 g pull-up until it is on a lead pursuit course. The criteria for success is that the error can be reduced to 10° or less between the R_{max} and R_{min} interval without

- (1) load factors exceeding 3
- (2) coefficient of lift exceeding C_{Lmax}

(3) gimbal limits exceeding AI radar gimbal limits, and

(4) a minimum recovery of $L/W \leq 0.5$.

The interceptor parameters used are those of the F4H-1. As stated previously the results would be extended in altitude due to greater F8U-3 capability. The results of the investigation are shown on Figs. 46 thru 49 and are summarized on Table V.

TABLE V
PROBABILITY OF SUCCESSFUL ARRIVAL TO MISSILE LAUNCH
(Pull-up Attacks - Unimproved Radar)

Target Altitude (ftx10 ³)	Target Velocity (Mach)	Interceptor Altitude at Start of Pull-up (ftx10 ³)	Interceptor Velocity at Start of Pull-up	Probability of Successful Arrival to Missile Launch (%)	Primary Reasons for Failures
65	2.0	38	V _{Fmax}	0	
65	2.0	45	M 2.0	6	Excessive launch error
65	2.0	55	M 2.0	13	Excessive gimbal angle
65	0.9	15	V _{Fmax}	11	Excessive gimbal angle and recovery problems
65	0.9	25	V _{Fmax}	49	Excessive gimbal angle - Excessive launch error and $L/W < 0.5$
65	0.9	35	M 2.0	35	Excessive launch error
65	0.9	55	M 2.0	65	Excessive gimbal angle
50	2.0	30	V _{Fmax}	6	Excessive launch error

TABLE V (Cont'd)

PROBABILITY OF SUCCESSFUL ARRIVAL TO MISSILE LAUNCH
(Pull-Up Attacks - Unimproved Radar)

Target Alti- tude (ftx10 ³)	Target Velo- city (Mach)	Inter- ceptor Alti- tude at Start of Pull-up (ftx10 ³)	Interceptor Velocity at Start of Pull-up	Probability of Success- ful Arrival to Missile Launch (%)	Primary Reasons For Failures
50	2.0	40	M 2.0	12	Excessive launch error
50	2.0	50	M 2.0	46	Excessive launch error
50	0.9	10	V _{Fmax}	91	Excessive launch error - Excessive gimbal angle
50	0.9	20	V _{Fmax}	60	Excessive launch error -
50	0.9	30	V _{Fmax}	55	Excessive launch error - Excessive gimbal angle
50	0.9	40	M 2.0	65	Excessive launch error - Excessive gimbal angle
50	0.9	50	M 2.0	69	Excessive launch error - Excessive gimbal angle

Referring to Fig. 47, the hook in the curve, though unusual in appearance, has a very logical explanation. Between 50,000 feet and 35,000 feet the interceptor velocity is constant at M 2.0 and the pull-up rate is limited by the $L/W = 3$ requirement. Below 35,000 feet, the decrease in interceptor maximum velocity results in a great angular pull-up rate for a 3 g course.

Degradation of Probability of Successful Arrival to Missile
Launch Due to Target Maneuvers

Up to this point in the study, the degrading effect of vectoring accuracy has been presented. In addition, a cursory look at the degrading effect of clutter and weather has been made. Another important possible degrading factor is that resulting from target maneuvers. In this study, it is assumed that the primary job of the target is that of delivering a weapon against its target of interest. Thus the maneuver studied is one which can easily be accomplished by the target and which will not detract markedly from his ability to deliver his own weapon.

The model assumed is described in detail in Appendix VI of Volume IV. The same limitations were imposed as used in the preceding analysis of probability of success. The radar 85% detection range was 12 - 13 n.mi. The gimbal limits used were $\lambda_a = \pm 41^\circ$, $\lambda_c = + 47^\circ, - 38^\circ$. The vectoring accuracy used was 1.5 - 3 n.mi. Only one plane was investigated (no errors assumed in elevation). The target maneuver was assumed to start at AI radar lock-on and consisted of a 1 g lateral turn which criss-crossed the desired flight path having a maximum deviation of target heading from this path of 30° . The interceptor was vectored on a pure collision course and did not deviate from this until lock-on at which time a 3 g turn is used until the lead pursuit course is reached. The error must be reduced to 10° or less between R_{max} and R_{min} .

The results of target maneuver are shown on Figs. 50 thru 52. Figures 50 and 51 show polar plots along with typical trajectories of the interceptor. These figures are plotted in target coordinates (target fixed). Figure 50 shows the results of target maneuvers initially to the right (initial turn toward the interceptor). For these samples the maneuver started at AI detection. Figure 51 shows the results of target maneuvers initially to the left (initial turn away from the interceptor). Figure 52 compares the probability of success resulting from these two types of target maneuvers. The dashed line shows the result of an initial target maneuver to the left and the solid line shows the result of an initial target maneuver to the right. The investigation was restricted to co-altitude attacks at 30,000 feet. The results of this investigation are summarized on Table VI and a comparison of probability of successful arrival to missile launch for maneuvering and non-maneuvering targets are made.

TABLE VI

COMPARISON OF PROBABILITY OF SUCCESSFUL ARRIVAL TO MISSILE
LAUNCH FOR MANEUVERING AND NON-MANEUVERING TARGETS
(Co-Altitude Attacks -30,000 ft -Unimproved Radar)

Speed Ratio V_T/V_F	Aspect Angle τ (Deg)	Probability of Successful Arrival to Missile Launch (%)		
		Initial Maneuver Toward Inter- ceptor (Right Turn)	Initial Maneuver Away From Inter- ceptor (Left Turn)	Nonmaneuvering
1.0	0	42.5	42.5	45
1.0	30	51	56	53
1.0	60	0	0	0
0.8	0	53	53	52
0.8	30	62	77	75
0.8	60	44	44	44
0.45	0	77	77	79
0.45	30	84	92	90
0.45	60	89	89	89

Referring to Fig. 42 and to Table VI, it is seen that as could be expected, an initial target maneuver right or left yields the same results for the head-on case. For the case of $\tau = 30^\circ$, an initial maneuver to the right (toward the interceptor) always reduces the probability of success from that realized for the nonmaneuvering case. This is as expected since this initial right turn reduces the time that the interceptor has to solve the problem. Also, as was expected, an initial maneuver to the left (away from the interceptor) always results in an increased probability since there is more time for the interceptor to solve the problem. If the target always maneuvers toward the interceptor the lowest probability will result. However, as shown in Table VI, the reduction in probability over that realized for a nonmaneuvering target is not great.

It is seen from Table VI that for $\tau = 60^\circ$ the probability of successful arrival to missile launch is the same for each of the target maneuvers investigated and for the nonmaneuvering target. This is due to the limits of the assumed model. Since the model assumes that the interceptor makes no maneuver prior to lock-on and that the target makes no maneuver prior to lock-on, gimbal angle limits are the dominating factors. The model should be refined (pilot in the loop) to include maneuvers by the interceptor prior to lock-on which will, in some cases, reduce the gimbal angle problem. However, it is expected that under some conditions the pilot will make the wrong maneuver thus reducing further the probability of success. The adequacy of the model can be determined only by including the pilot in the loop. This will be done in the extended phase of the study. Figure 53 shows the results on probability of successful arrival to missile launch of using a combination of worst possible target maneuvers. This is assuming that the target has a vast amount of intelligence relating to the tactical problem. It assumes the target knows the exact angle of approach, the exact range between interceptor and target and the exact speed conditions at the time of initial maneuver. The dashed lines of Fig. 53 show the results for a non-maneuvering target. The solid line represents the results for a combination of worst target maneuvers. For the case of $V_T/V_F = 1$, the resulting probabilities are 33% at $\tau = 0^\circ$, 51% at $\tau = 30^\circ$, and 0% at $\tau = 60^\circ$ for the worst possible maneuvers. This compares to probabilities of 45%, 53% and 0% for the nonmaneuvering target situation. When the speed ratio is decreased to $V_T/V_F = 0.8$ the probabilities for the situation of worst target maneuvers are 46% at $\tau = 0^\circ$, 62% at $\tau = 30^\circ$ and 44% at $\tau = 60^\circ$. For the nonmaneuvering target the corresponding probabilities are 52%, 75% and 44%. When the speed ratio is decreased still further to 0.45, the resulting probabilities are 73% at $\tau = 0^\circ$, 85% at $\tau = 30^\circ$ and 89% at $\tau = 60^\circ$. For the nonmaneuvering situation the probabilities were 79%, 90% and 89%. The reason that the probabilities are the same at $\tau = 60^\circ$ for the maneuvering and nonmaneuvering cases is the same as given before.

Weather Degradation of System Performance

The low altitude performance of the AI radar has been presented in an earlier section of this report. Figure 54 shows theoretical degradation curves for performance of the 62 lot Q-72 radar in the presence of rain. These calculations consider the effects of humidity attenuation, attenuation from scattering by the rain particles in the two-way path and back scattering at the target due to rain. These curves were obtained from Ref 4.

Referring to Fig. 54, it is seen that if the performance of the 62 lot Q-72 is 12-13 n.mi. under fair weather conditions, the performance will be approximately 2.8 n.mi. in the presence of a light rain. Figure 55 gives the results of theoretical calculations (done separately from those of Fig. 54) of performance in rain which was presented in Volume I. It is important to note the close agreement of the two curves for the results of light rain degradation for nose-on aspect. The current 62 lot Q-72 radar yields 12 - 13 n.mi. detection range (see earlier polar plots) against the nose aspect. This would be reduced to 2.8 n.mi. if the degradation figures of Fig. 55 are used. At 70° off the B-47 target's nose the clear weather detection range is 18.5 n.mi. (high speed conditions). Using NAMTC calculations, this would be reduced to 5.5 n.mi. in the presence of light rain. This compares with 5.8 n.mi. from the results shown by Fig. 55.

Early Warning Detection Requirements

In addition to the degradation factors described in the preceding sections, it is necessary to consider the effects of early warning capability, interceptor climb capability and interceptor endurance capability. A preliminary study of these factors has been made and is shown by Figs. 56 thru 77. The models used and analyses methods are shown in Appendix IX of Volume IV.

Figure 56 shows early warning detection requirements. The assumptions made are:

- (1) the early warning equipment is located 100 n.mi. from fleet center,
- (2) the target(s) are flying at 30,000 feet, and
- (3) the targets are employing a 100 n.mi. air-to-surface missile (kill must be recorded 100 n.mi. from fleet center)

In the development of the graph of Fig. 56, the climb and speed characteristics of the F4H-1 were used. Two target speeds were used ($V_T = 10$ n.mi. per minute and $V_T = 20$ n.mi. per minute). Referring to Fig. 56, a typical game can be played. For example, if

- (1) 40 targets are attacking the fleet center,
- (2) the initial system dead time (T), which is the time between initial detection of the target and launching the first interceptor, is 3 minutes

- (3) the targets are flying at 30,000 feet at a speed of 10 n.mi. per minute (approximately M 1.0)
- (4) one interceptor per target is required and 40 interceptors can be launched in 20 minutes ($nk = 20$), where n = number of interceptors and k = interval between launchings in minutes,

then the early warning detection requirement is 300 n.mi. This means that if the requirement is that all targets must be intercepted before they reach a point 100 n. mi. from the fleet center, the initial detection of these targets must occur 300 n. mi. from the early warning location (in this example 400 n.mi. from fleet center).

If the target speed is changed to 20 n.mi. per minute (approximately M 2.0) and all other parameters are held constant, the early warning detection requirement is 600 n.mi. from the early warning location (for this example 700 n.mi. from fleet center). If the system dead time is changed to 6 minutes the requirement, of course, increases to 660 n.mi. These curves are optimistic since factors such as combat time and human factors are neglected. Later curves will show available combat time for one interceptor attacking one target.

Figures 57 thru 63 show the available combat time for co-altitude attacks (30,000 feet). It is assumed that the interceptor is in CAP at 30,000 feet under cruise conditions 100 n.mi. from fleet center. The allowable target penetration is to 100 n.mi. from fleet center. The interceptor accelerates as rapidly as possible to V_{max} (M 1.91). The early warning detection range (range from fleet center) and system dead time (time between early warning detection and initiating the first attack) are varied. The resulting combat times (time between first contact between interceptor and target and the time that the target passes the 100 n.mi. penetration barrier) are summarized on Table VII.

TABLE VII

EARLY WARNING DETECTION REQUIREMENTS
(Co-Altitude Attacks at 30,000 Feet - Interceptor
In CAP at 30,000 Feet)

Target Velocity V_T (Ft/Sec)	Early Warning Detection Range (Distance from Fleet Center) (n.mi.)	System Dead Time (Minutes)	Available Combat Time (Minutes)
854	300	3	13.93
1,518	300	3	5.42
1,897	300	3	3.53
1,897	300	6	2.05
1,897	200	3	1.15
1,518	300	6	3.67
1,518	200	3	1.67
854	300	6	11.67
854	200	3	5.59

The second case investigated is that of an interceptor at 30,000 feet attacking a target at 50,000 feet. For this investigation the interceptor is in CAP at 100 n.mi. from the fleet center. When the run starts, the interceptor accelerates to V_{max} and then climbs supersonically to 50,000 feet. The combat times given would be those available for a horizontal attack (snap-up not considered).

Figures 64 thru 70 show the available combat times. These results are summarized on Table VIII.

TABLE VIII

EARLY WARNING DETECTION REQUIREMENTS
(Co-Altitude Attacks at 50,000 Ft. -
Interceptor in CAP at 30,000 Ft.)

Target Velocity V_T (ft/sec)	Early Warning Detection Range (Distance From Fleet Center) (n.mi.)	System Dead Time (Minutes)	Available Combat Time (Minutes)
1,940	300	3	3.1
1,552	300	3	5
873	300	3	13.18
1,940	300	6	1.92
1,940	200	3	0.9
1,552	300	6	3.5
1,552	200	3	1.58
873	300	6	11.16
873	200	3	5.25

The third phase of the investigation is to determine available combat time for deck launched interceptors attacking a target at 30,000 feet. Here, the F4H-1 accelerates at sea level to climb speed, climbs to 30,000 feet and accelerates to maximum speed. Figures 71 thru 77 show the available combat times and their results are summarized on Table IX.

TABLE IX

EARLY WARNING DETECTION REQUIREMENTS
 (Co-Altitude Attacks at 30,000 Feet -
 Interceptor Deck Launched)

Target Velocity VT (Ft/Sec)	Early Warning Detection Range (Distance From Fleet Center) (n. mi.)	System Dead Time (Minutes)	Available Combat Time (Minutes)
1,897	300	3	0.42
1,518	300	3	1.83
854	300	3	9.33
1,897	300	6	0
1,897	200	3	0
1,518	300	6	0.25
1,518	200	3	0
854	300	6	7.17
854	200	3	1.08

Degradation Caused By Countermeasures

Basic work on this phase of the study has been reported in NRL Reports 4720, 4785 and 4949. The vulnerability of the AI radar to countermeasures is further detailed in a secret supplement to this report (see Volume VI).

Remaining Study

There are several areas where investigation is needed before the performance of the current system under tactical conditions can be clearly defined. These are as follows:

- (1) Extension of the co-altitude probability of success curves to include angles off the target's nose greater than 60° and to include smaller increments.
- (2) Conduct a flight simulator program to operationally verify the adequacy of model techniques in the present study. This would be a check, using the pilot in the loop, of the critical areas exposed by the current study.
- (3) Extension of the incremental altitude study to include azimuth angles other than head-on.
- (4) Determine by study and analysis the acceleration launching transients occurring during the Sparrow III missile launch and the effects of these transients upon dynamic performance of the missile internal functions and missile trajectory to the target.
- (5) Determine by study and analysis the effects of noise and missile orientation on system accuracy, both with and without "English Bias".
- (6) Determine by study and analysis the illumination requirements after Sparrow III launch in conjunction with break-away requirements and aircraft normal flight recovery requirements.
- (7) Investigation of limits imposed by hydraulics on pull-up capability.

PHASE IV-SYSTEM PERFORMANCE UNDER EXPECTED TACTICAL CONDITIONS WITH ADDITION OF CURRENTLY PROPOSED IMPROVEMENTS

The results presented previously in this report and those presented in Volume I indicate that improvement in subsystem performance is needed if successful missile launches at an acceptable probability level are to be achieved. When other degrading factors are considered, in addition to those included here, it is predictable that the probability of success curves shown previously will be degraded further. It is thus very important to investigate regions of possible improvement to the subsystem elements in order that overall system tactical use capability can be improved.

AN/APQ-72-AN/APQ-74 Improvements in Fair Weather

In Volume I of this report the improvements realized from search volume optimization, bandwidth switching, bright display, improved receiver crystals, and triangle vectoring were considered. It was estimated that these improvements would result in an 85% detection capability against a B-47 target at approximately 19 n.mi. head-on under high speed conditions. To date there is insufficient data in hand to verify the validity of these estimates. However, flight tests of some of these improvements have been made by the contractor². Figure 78 shows the results of some of these tests. The test altitude was 15,000 feet. Runs were made against an F2H-2, head-on aspect, with a closing rate of 800 knots. For these tests an improved receiver was used (improved NF from 10.7 to 8.94 db), the bandwidth of the IF was narrowed in the search mode (from 4mc to 1.1mc), the search employed was 64° azimuth by 6.4° elevation and the dish size was increased to 30 in. While it is not the intent to compare these results with test results obtained by NATC, Patuxent, on the AN/APQ-50 (test conditions were different) the trend is apparent. With the modified system the 85% probability of detection occurred at 31 n.mi. Referring to Volume I, it is seen that the 85% probability of detection for the AN/APQ-50 as obtained by Patuxent was 16.8 n.mi. It should be remembered that the results of Fig. 78 have not been degraded in any way. Thus they do not represent tactical capability.

Probability of Successful Arrival to Missile Launch - Improved Radar

In Volume I the results of using the improved radar, which had an 85% probability of detecting a B-47 size target head-on at 19 n.mi. and ± 57° azimuth and elevation gimbal coverage, were presented for attacks occurring at 50,000 feet altitude. These results are repeated here on Fig. 79.

Corresponding results for attacks occurring at 30,000 and 1,000 feet altitude are given on Figs. 80 and 81. These results are summarized on Table X.

TABLE X
COMPARISON OF PROBABILITY OF SUCCESSFUL ARRIVAL TO MISSILE LAUNCH
FOR SYSTEMS USING IMPROVED AND UNIMPROVED RADAR
(Co-Altitude Attacks - Nonmaneuvering Target)

Altitude (ftx10 ³)	Inter- ceptor Velocity V_F (Ft/Sec)	Speed Ratio V_T/V_F	Aspect Angle \uparrow (Deg)	Probability of Successful Arrival to Missile Launch (%)	
				Improved Radar	Unimproved Radar
50	1,940	1.0	0	75	46
50	1,940	1.0	30	89	52
50	1,940	1.0	60	8	0
50	1,940	0.8	0	84	48
50	1,940	0.8	30	91	73
50	1,940	0.8	60	89	44
50	1,940	0.45	0	97	69
50	1,940	0.45	30	98	86
50	1,940	0.45	60	100	85
30	1,897	1.0	0	75	45
30	1,897	1.0	30	88	53
30	1,897	1.0	60	8	0
30	1,897	0.8	0	84	52
30	1,897	0.8	30	92	75
30	1,897	0.8	60	89	44
30	1,897	0.45	0	97	79
30	1,897	0.45	30	98	90
30	1,897	0.45	60	100	89
1	1,189	0.8	0	82	52
1	1,189	0.8	30	84	60
1	1,189	0.8	60	76	47

Comparing the results given on Table X, it is seen that there is an insignificant difference due to altitude in the 30,000 and 50,000 feet cases. As stated previously, the 1,000 feet altitude case has not been investigated thoroughly because of the lack of test data. Based on the theoretical calculations and limited test data presented previously, one probability of successful arrival to missile launch curve has been presented.

To date the effects of adding the estimated improvement in AI radar performance resulting from the use of a second operator has not been investigated fully (12% range improvement). However, the effects on probability of successful arrival to missile launch can be inferred. Figure 79a shows the sensitivity of the probability of successful arrival to missile launch, using the improved system, to range increase. The conditions are the same as those of Fig. 79. When $V_T/V_F = 1.0$ and $V_F = M 2.0$ the improvement resulting from using a 12% range increase are:

- (1) From 75% to 84% for $\gamma = 0^\circ$
- (2) From 89% to 92% for $\gamma = 30^\circ$.

Probability of Successful Arrival to Missile Launch -
Improved Radar - Maneuvering Target

The effects of target maneuvers on the probability of successful arrival to missile launch on a system using the improved radar are shown on Fig. 82. The altitude of attack is 30,000 feet and $V_T/V_F = 1.0$ where $V_F = M 1.91$. The radar has an 85% probability of detection at 19 n.mi. The gimbal angle coverage is $\pm 57^\circ$ in azimuth and elevation. On this figure, the solid line shows the results of initial target maneuvers toward the interceptor (initial right turn) and the dashed line shows the results of initial target maneuvers away from the interceptor (initial left turn). These results are shown on Table XI and a comparison is made with the results obtained with a system using the unimproved radar.

TABLE XI

COMPARISON OF PROBABILITY OF SUCCESSFUL ARRIVAL TO MISSILE LAUNCH
FOR SYSTEMS USING IMPROVED AND UNIMPROVED RADAR
(Co-Altitude Attacks—Maneuvering Target)

Interceptor Velocity V_F (Ft/Sec)	Speed Ratio V_T/V_F	Aspect Angle \uparrow (Deg)	Probability of Successful Arrival to Missile Launch (%)			
			Improved Radar		Unimproved Radar	
			Initial Right Turn	Initial Left Turn	Initial Right Turn	Initial Left Turn
1,897	1.0	0	72	72	42.5	42.5
1,897	1.0	30	79	90	51	56
1,897	1.0	60	8	8	0	0
1,897	0.8	0	82	82	53	53
1,897	0.8	30	87	94	62	77
1,897	0.8	60	89	89	44	44
1,897	0.45	0	97	97	77	77
1,897	0.45	30	96	99	84	92
1,897	0.45	60	100	100	89	89

Referring to the results given on Table XI, it is seen that as in the case of the unimproved radar target maneuvers initially to the left and initially to the right yield the same results for $\uparrow = 0$. Comparison of results shows that there is a significant improvement in probability of successful arrival to missile launch with the improved radar particularly when a high speed target is involved. Comparing the results of Table XI for the improved radar against the maneuvering target with the corresponding results of Table X for the nonmaneuvering target, and using the case $V_T/V_F = 1.0$, we see that target maneuvers result in 3% degradation for $\uparrow = 0^\circ$. When $\uparrow = 30^\circ$ there is 10% degradation for an initial right maneuver by the target and a 1% improvement for an initial left turn by the target because of the additional time available. When $\uparrow = 60^\circ$ there is no difference between each of the assumed maneuvers and the nonmaneuvering target. The reason is the same as stated previously (gimbal angle limits predominate in the assumed model).

Figure 83 compares the probability of successful arrival to missile launch for nonmaneuvering and for maneuvering targets. The attack occurs at 30,000 feet. The improved radar is used. Here again, the curves plotted for the maneuvering target give the results for a combination of worst possible maneuvers. This assumes that the target has a large amount of information related to interceptor range and angle of approach. For $\gamma = 60^\circ$, the probabilities are the same for both the maneuvering and nonmaneuvering targets for the same reason as stated previously (gimbal angle limits predominate in the assumed model). When $\gamma = 30^\circ$ and $V_T/V_F = 1.0$, the probability of success for the maneuvering target is 78% as compared to 88% for the nonmaneuvering target. When $\gamma = 0^\circ$, the probability of success for the maneuvering target is 66% as compared to 75% for the nonmaneuvering target.

When the speed ratio is reduced to 0.8 and $\gamma = 30^\circ$, the probability of success for the maneuvering target is 88% as compared to 92% for the nonmaneuvering target. When $\gamma = 0^\circ$, the probability of success for the maneuvering target is 76% as compared to 84% for the nonmaneuvering target. Corresponding results are also presented for the case of $V_T/V_F = 0.45$.

Probability of Successful Arrival to Missile Launch - Improved Radar Pull-Up Attacks

The next phase of the study is that of pull-up attacks with a system which incorporates the improved radar. The results of this phase are detailed in Appendix V of Volume IV. Samples of the results are shown on Figs. 84 thru 87. The model assumes head-on attacks with an azimuth distribution of vectoring errors about this head-on attack of $1\sigma = \pm 3$ n.mi. The 85% probability of detection on the range distribution corresponds to that of the improved radar (19 n.mi.). The gimbal limits are those of the improved radar ($\pm 57^\circ$ in elevation and azimuth). No corrections in altitude or azimuth are made until lock-on (10 secs. after detection). Upon lock-on the interceptor starts an immediate 3 g pull-up until it is on a lead-pursuit course. The criteria for success is that the error can be reduced to 10° or less between the R_{\max} and R_{\min} boundary without a requirement of load factor exceeding 3 or CL_{\max} , the gimbal angles of the AI radar are not exceeded, and a minimum recovery of $L/W = 0.5$ is required. The interceptor parameters used are those of the F4H-1. As stated previously, the useful zone would be extended in altitude if the F8U-3 were considered due to its greater altitude capability. The results are summarized on Table XII.

TABLE XII

PROBABILITY OF SUCCESSFUL ARRIVAL TO MISSILE LAUNCH
(Pull-Up Attacks - Improved Radar)

Target Alt. (ftx10 ³)	Target Velocity (Mach)	Interceptor Alt. at Start of Pull-Up (ftx10 ³)	Interceptor Velocity at Start of Pull-Up	Probability of Success- ful Arrival to Launch (%)	Primary Reasons for Failures
65	2.0	25	V_{Fmax}	17	Error Could Not be Re- duced to 10°
65	2.0	45	M 2.0	50	Error Could Not be Re- duced to 10°
65	2.0	55	M 2.0	75	Error Could Not be Re- duced to 10°
65	0.9	15	V_{Fmax}	56	Recovery Problems $L/W < 0.5$
65	0.9	25	V_{Fmax}	95	Error Could Not be Re- duced to 10°
65	0.9	35	M 2.0	90	Error Could Not be Re- duced to 10°
65	0.9	55	M 2.0	97	Error Could Not be Re- duced to 10°
50	2.0	10	V_{Fmax}	16	Error Could Not be Re- duced to 10° Excessive Gimbal Angle

TABLE XII (CONT)

PROBABILITY OF SUCCESSFUL ARRIVAL TO MISSILE LAUNCH
(Pull-up Attacks - Improved Radar)

Target Altitude (ftx10 ³)	Target Velocity (Mach)	Interceptor Altitude at Start of Pull-up (ftx10 ³)	Interceptor Velocity at Start of Pull-up	Probability of Successful Arrival to Missile Launch (%)	Primary Reasons for Failures
50	2.0	20	V _{Fmax}	46	Error could not be reduced to 10°
50	2.0	40	M 2.0	75	Error could not be reduced to 10°
50	2.0	50	M 2.0	75	Error could not be reduced to 10°
50	0.9	10	V _{Fmax}	99	
50	0.9	30	V _{Fmax}	98	Excessive gimbal angle
50	0.9	40	M 2.0	98	Error could not be reduced to 10°
50	0.9	50	M 2.0	98	Error could not be reduced to 10°

Comparing the results for the system using the improved radar (summarized on Table XII) with those for the system using the unimproved radar (summarized on Table V), it is seen that there is a tremendous improvement in the probability of successful arrival to missile launch. For example, a system using the unimproved radar had no capability for attacking M 2.0 targets flying at 65,000 feet when pull-ups were initiated below 38,000 feet. For pull-ups starting at 45,000 feet, the probability of success was 6%. When the pull-ups were started from 55,000 feet there

was a 13% probability of success. Inspection of Table XII immediately shows the advantages of using the improved radar.

System Performance Resulting From the Use of Advanced Interceptor Performance

Earlier in this report, it was stated that since the speed of the F8U-3 is restricted to M 2.0 because of limits other than engine limits, the resulting co-altitude capability (neglecting altitude ceiling) would be the same as for the F4H-1. In addition, it was shown that the basic difference in pull-up capability was that due to the greater altitude ceiling of the F8U-3. It is now of interest to investigate the resulting system performance when a higher speed interceptor is used. For this portion of the study the V_{\max} capability of the F8U-3 is employed.

Figures 88 thru 90 show the polar plots resulting from the high speed interceptor attacking targets at 50,000 feet. For this cursory look at the problem, we have returned to the barrier analysis. All barriers are representative of 85 to 90% probability. The target speeds are the same as those used in the preceding investigations. The situation assumes no vectoring errors and the interceptor is on a perfect lead pursuit course at detection. Figure 85 shows the results of co-altitude attacks against a target flying at 1,940 ft/sec. The interceptor speed at the beginning of the run is 2,134 ft/sec. Comparing this with Fig. 22 of Volume I (interceptor velocity of 1,940 ft/sec) it is seen that the basic advantage is that now around-the-clock attacks can be made because of the speed advantage. However, the penetration will be high for attacks aft of the beam. For example, the run which originates at 120° off the target's nose required approximately 220 secs. before the interceptor closes to R_{\max} . Attacks originating in the zone up to 30° off the target's nose were marginal for the conditions of Fig. 22 (interceptor velocity 1,940 ft/sec). This region is made even more marginal when the higher speed interceptor of Fig. 88 is used. This is due to the fact that at the higher speeds R_{\min} is increased and the range covered by the interceptor in the lock-on interval is increased. Figures 89 and 90 give corresponding plots for the advanced interceptor attacking targets at 30,000 feet altitude and 1,000 feet altitude. The comparison given for the 50,000 feet case applies equally well here.

The results of the settling time study using the advanced interceptor are shown on Figs. 91 thru 99. These runs were made at 30,000 feet. The interceptor speed was 2,185 ft/sec. The criteria throughout is that the error must be reduced to some value, say 10° , and held there for 3 seconds. The solid curves are those resulting from the use of a cockpit

simulator and REAC. The dashed curves show the results of IBM runs. As stated previously the 50% settling time and 3 second criteria do not apply to the IBM runs because the IBM gives the perfect solution (man not in loop). The IBM results are shown in this fashion to allow direct comparison with the REAC runs. The results of this portion of the study are summarized on Table XIII.

TABLE XIII

SYSTEM SETTLING TIME REQUIRED AFTER AI RADAR LOCK-ON (Advanced Interceptor - 30,000 Feet Altitude) $V_F = 2,185$ ft/sec						
Target Velocity V_T (ft/sec)	AI Radar Lock-On Range (n.mi.)	Aspect Angle \uparrow (Deg)	Heading Error At Lock-On ϵ (Deg)	Status of Run		
				85% Settling Time	50% Settling Time	IBM Settling Time
1,897	10	20	20	Could Not Re- duce Error	Could Not Reduce Error Below 17°	Could Not Re- duce Error Below 15°
1,897	10	20	30	Could Not Re- duce Error		Could Not Reduce Error Below 27°
1,897	10	40	20	Error Could Only be Re- duced to 16°	Error Could Only be Reduced to 13°	Error Could Only be Re- duced to 16°
1,897	10	40	30	Could Not Reduce Error		Error Could Only be Re- duced to 29°
1,518	10	20	20	Error Could Only be Re- duced to 14°	Error Re- duced to 10° in 9 Seconds	Error Re- duced to 10° in 10 Secs.
1,518	10	20	30	Could Not Re- duce Error	Could Not Reduce Error	Error Could Only be Re- duced to 27°

TABLE XIII (Cont'd)

SYSTEM SETTLING TIME REQUIRED AFTER AI RADAR LOCK-ON
 (Advanced Interceptor - 30,000 Feet Altitude)
 $V_T = 2,185$ ft/sec

Target Velocity V_T (ft/sec)	AI Radar Lock-On Range (n.mi.)	Aspect Angle \uparrow (Deg)	Heading Error At Lock-On ϵ (Deg)	Status of Run		
				85% Settling Time	50% Settling Time	IRM Settling Time
1,518	7.5	40	20	Could Not Reduce Error	Could Not Reduce Error	Error Could Only be Reduced to 18°
1,518	10	40	20	Error Reduced to 10° in 10 Secs.	Error Reduced to 10° in 8 Secs.	Error Could Only be Reduced to 12°
1,518	10	40	30	Error Could Only be Reduced to 28°	Error Could Only be Reduced to 26°	Error Could Only be Reduced to 28°
1,518	10	60	20	Error Reduced to 10° in 9 Secs.	Error Reduced to 10° in 7 Secs.	Error Reduced to 10° in 10 Secs.
1,518	15	60	20	Error Reduced to 10° in 6.5 Secs.	Error Reduced to 10° in 5.5 Secs.	Error Reduced to 10° in 7 Secs.
1,518	10	60	30	Error Could Only be Reduced to 28°	Error Could Only be Reduced to 22°	Error Could Only be Reduced to 27°
1,518	10	60	40	Error Could Only be Reduced to 38°	Error Could Only be Reduced to 37°	Error Could Only be Reduced to 39°
1,518	15	60	30	Error Reduced to 10° in 14 Secs.	Error Reduced to 10° in 12 Secs.	Error Reduced to 10° in 16 Secs.
1,518	15	60	40	Error Could Only be Reduced to 22°	Error Reduced to 10° in 24 Secs.	Error Could Only be Reduced to 28°
854	10	40	20	Error Reduced to 10° in 10 Secs.	Error Reduced to 10° in 8 Secs.	Error Reduced to 10° in 7.8 Secs.
854	10	40	30	Error Could Only be Reduced to 26°	Error Could Only be Reduced to 25°	Error Could Only be Reduced to 24°

The following general comments can be made about the curves of Figs. 91 thru 99. In general, the error could be reduced to a much lower value with the slower speed interceptor than with this advanced interceptor (comparison of Figs. 91 and 28). This is expected since the turning radius is smaller at the lower speeds. Referring to Fig. 92, it is seen that the IBM run resulted in a lesser reduction of error than the EEAC run. This implies that the pilot, even though a positive indication in the form of a buzzer was used, may have pulled slightly more than 3 g's. This is borne out by the sample brush recordings in Appendix IV.

Remaining Study:

There are still several areas where additional analysis is needed to allow more complete definition of the performance of the improved system. Among these are:

1. Extension of the analysis of the F4H-1 and F8U-3 incremental altitude capabilities with the improved system at aspects other than head-on.
2. Extension of the analysis of co-altitude probability of success to include angles greater than 60° off the nose and to include smaller increments.
3. Verify by flight simulator tests the adequacy of the results obtained from the described model.
4. Inclusion of actual missile performance during ejection launch and after launch. This includes transient effects during launch..
5. Inclusion of the effects of noise and missile orientation both with and without "English Bias".
6. Verify by flight simulation study the effects of a situation display on system probability of success and develop optimum approach tactics.
7. Determine by study and analysis the sensitive elements of the F4H-1 and F8U-3 weapon systems mechanization and their accuracy tolerances.

8. Determine by study and analysis the feasibility and possible advantages of using alternate guidance systems (different from those covered in this volume) in the F4H-1 and F8U-3 Weapon Systems.

In addition to these areas there are several areas of improvement which are under investigation. These are as follows:

1. The effects of countermeasures on the AJ radar has been investigated and reported separately in NRL Report 4949. In addition, analysis of the improvements made to date is described in a secret supplement to this report. (See Volume VI.)
2. While the results of use of a larger antenna have not been detailed, they have been implied by the effects of range variation on the probability of success given in Volume I and this study. In addition the controlled flight tests resulting from the use of a larger antenna along with other improvements are described by Fig. 78. The calculation of the range improvement realized by the use of a larger antenna is straightforward and will be included in the analysis at a later date.
3. NRL has investigated the AJ features desired for the Sparrow III seeker. The results of this investigation have been reported to BuAer (NRL Report 4720).

PHASE V - STUDY TO DETERMINE AND ASSESS REALIZABLE IMPROVEMENTS

This phase is of necessity a continuing one. In those areas where it appeared that important gains could be made by incorporation of improvements which could be realized within a useful time scale, actions recommendations have been made to the Bureau. In Volume I of this report it was recommended, based on the analysis to date, that the following actions be prosecuted:

1. The incorporation of optimized search areas, bandwidth switching and bright display (enhanced operator environment) can be achieved during the time available for the development of this system. Collectively they represent a major improvement in system performance. The first two of these items have been tested (in part) by the contractor and the resulting improvement is detailed in this volume.

2. While the exact availability date for a situation display such as the Triangle System is not predictable at the present time, concerted effort should be directed towards its development. The incorporation of such a display will represent a major improvement in overall system performance capability. The Bureau of Aeronautics is pursuing a program which will result in incorporation of the airborne elements of a situation display.
3. While the analysis to date has indicated that additional range above that realized from Items (1) and (2) above is very desirable, the incorporation of such items as a larger dish should be delayed until sufficient analysis is completed either under this study program or by the fire control contractor to allow arrival at an optimum balance between dish size and gimbal angle coverage. For example, a currently proposed "improved" version of the antenna calls for a usefully large gimbal angle. However, the diameter and conditions of mounting cause the antenna to be obstructed by extraneous material. Thus the total gimbal angle is not in fact usable. Based on the work of this study and on contractor analyses, a reasonable compromise between unobstructed gimbal coverage and dish size can be reached.

PHASE VI - STUDY OF IR TIE-IN FOR AI FIRE CONTROL SYSTEMS

To date, a survey of government agencies and contractors working in the field of IR has revealed that data on performance of equipment operating in the band of the proposed IR search and track equipment and data on the IR radiation from high speed aircraft at altitudes of interest is practically non-existent. The limited data that is available has in general resulted from a multiplicity of scaling of test data taken under unrealistic conditions (target aircraft tied down on the deck). Thus the statements made in Volume I (data lacking) still apply. To date, the undefined state of the IR capability in the AI fire control system is such that analysis is not warranted. Thus the Navy study has concentrated on revealing the deficient areas of the primary fire control system. As soon as results from tests currently underway at NOTS, Aerojet, Eglin Air Force Base, etc. become available, an investigation will be made to see if IR can supplement the deficient areas of the primary system.

PHASE VII - REPEAT STUDY PHASES I - VI FOR SPARROW III WITH IR SEEKER

The statements made above in the section on IR search and track are even more applicable to the proposed long wavelength IR Sp. III. In addition, they apply equally well to the currently available IR seeker (DAN-5) when a supersonic target is involved (afterburners). About the only data available where there is general agreement on the results, is that related to the DAN-5 seeker performance when operating against a subsonic jet target.

Figures 100 and 101 show the resulting polar plots for attacks made by an interceptor flying at M 2.0 or V_{max} . Figure 100 shows the results of attacks made at 50,000 feet. The target velocity is 873 ft/sec. It is seen that the seeker restricts the attack zones to within $\pm 70^\circ$ off the target's tail. The resulting attack courses are restricted to approaches from 90° back to tail-on. Figure 101 shows the results for attacks made at 30,000 feet. The results are essentially the same.

As soon as reliable data becomes available on the performance of long wavelength and short wavelength detectors and on target radiation characteristics they will be included in the study. Since the attack courses are already generated (same courses apply to Sparrow III conventional), it is a relatively simple task to include the resulting attack zones.

PHASE VIII - REPEAT STUDY PHASE I-VI FOR SIDEWINDER

To date, data on the performance of the proposed Sidewinder IC has not been received from NOTS. This includes aerodynamic as well as seeker performance data. NOTS is currently preparing this data and expects to complete the work in the near future.

In lieu of and in anticipation of data on the Sidewinder IC, pure pursuit trajectories were generated for various speed and altitude conditions. Figures 102 thru 104 give examples of some of the resulting polar plots. More complete coverage is given in Appendix VIII of Volume IV. The Sidewinder IA launch zones (prepared by NOTS - aerodynamic restrictions) are shown on these polar plots. The approximate effective launch zones are enclosed by heavy lines. The polar plot of Fig. 102 shows the results of attacks made at 30,000 feet altitude when $V_T/V_F = 1.0$ and $V_F = M 2.0$. If the same 3 g criteria is applied as was used in the preceding portions of the study, it is seen that entry, under these conditions, into the usable launch zone (labeled D) cannot be made.

Figure 103 shows the results when the speed ratio (V_T/V_F) is reduced to 0.8. Here it is seen that attacks must originate aft of 65° (3 g limitation) if entry into the launch zone is to be made. Attacks aft of 90° will result in large penetration distances.

Figure 104 shows the results of reducing the speed ratio to 0.45 (today's target). For this condition the results are essentially the same as those for $V_T/V_F = 0.8$. Penetration distances, however, will not be large for any attack aspect.

Figure 105 gives a comparison of probable performance of Sidewinder IC as compared to Sidewinder IA at 50,000 feet when launched from an interceptor whose speed is 1,940 ft/sec and $V_T/V_F = 1.0$. The zone given for Sidewinder IC is based on very preliminary estimates made by NOTS and is restricted only by aerodynamic considerations. It is seen that when the 3 g criteria is applied, entry into the Sidewinder IA zone could not be made. However, over a narrow region beginning at 62° off the target's nose, entry could be made into the Sidewinder IC zone.

Based on the requirement of entry into a relatively narrow region about the tail of the target for Sidewinder launch and on the fact that pure pursuit trajectories are required for Sidewinder while lead pursuit courses are desired for Sparrow III, a cursory look at the mixed load compatibility with current vectoring practices (offset lead collision) has been started. Figure 106 gives an example of the type of analysis underway. This shows the probability of successful arrival to missile launch for the Sparrow III for various types of vectoring doctrine. The current radar is employed. The altitude of attack is 30,000 feet and $V_T/V_F = 1.0$ where $V_F = 1,897$ ft/sec. The solid curve shows the results for pure collision vectoring and is the same as presented before. The dashed curve shows the results of pure pursuit vectoring on probability of success. It is seen that for the head-on case, the probability of success for pure pursuit and pure collision is the same (46%). At $\gamma = 30^\circ$ the pure collision course results in the highest probability of success. This is as expected because the problem of converting to a lead pursuit course from a pure collision course (larger lead angle) is easier than converting from a pure pursuit to a lead pursuit in the small time available. At $\gamma = 60^\circ$ the pure pursuit vectoring is best because in this region gimbal angle is the primary restriction in the lead collision approach.

The remaining curve (that designated by — - — - — - —) gives the resulting probability for a deviated pursuit vectoring approach. For this case 15° lead angle was selected for examination. As could be expected, when $\gamma = 0^\circ$ this deviated pursuit approach yields the worst

results. This is because the lead angle is too large. However, for both $\tau = 30^\circ$ and 60° , the deviated pursuit approach yields the best results. This is because the gimbal angle restriction has been lessened in conjunction with a requirement for a lesser correction to get to the correct lead pursuit course.

It is obvious that this is a very preliminary analysis. The necessary steps are further analysis on optimum vectoring tactics for Sparrow III, comparable analysis of tactics for Sidewinder IC and reduction of results to a compromise compatible with fleet vectoring capability.

CONCLUSIONS AND RECOMMENDATIONS

Introduction

The conclusions and recommendations given in Volume I apply equally well here. They have been extended to cover the additional areas of investigation and are detailed below. Even though there are additional areas of needed study, as detailed in the text, much useful data is now available as a result of the Navy's study. As stated in Volume I, inferences can be drawn (and in fact have been drawn) which will be useful in,

- (1) formulation of the basic system configuration,
- (2) development of a situation display,
- (3) formulation of tactical doctrine guide lines,
- (4) revision of operational concept for usage of secondary missile seekers,
- (5) establishing applicability of secondary AI fire control systems, such as IR, to the deficient areas of the primary AI fire control system,
- (6) establishing lowest acceptable limits defining a useful Navy system, and
- (7) starting immediate action on Items 1 thru 6 above in order that useful attainment of operational requirement objectives can be achieved.

Detailed Conclusions and Recommendations

A. System Using Available Hardware

1. The results of the study using the barrier method of analysis (wherein each barrier represents 85%-90% probability) of the ideal situation for high altitude (co-altitude) attacks given in Volume I apply equally well here. Additional results for 1,000 feet altitude are presented in this volume. The following conclusions are indicated:

(a) When $V_T/V_F = 1.0$ where $V_F = V_{max}$, the interceptor must start his approach from forward of 70° off the target's nose if entry into the effective attack zone is to be made (see Fig. 5).

(b) When additional time is added representative of that encountered under tactical conditions (required to reduce initial vectoring errors down to allowable launch error of the missile) the effective attack zone, except for a small region aft of the beam is eliminated. This zone must be entered via a 10° corridor between 60° and 70° off the target's nose.

(c) When this total system settling time is considered, even the case of $V_T/V_F = 0.8$ will be extremely marginal. The forward effective attack zone is eliminated.

2. In Volume I the results of making attacks with the interceptor operating under V_{cruise} conditions were given. The study results given in this volume indicate that when attacks are against high-speed targets, there is only a minor change in capability when the interceptor starts at V_{cruise} and accelerates toward V_{max} . As would be expected, a slight increase in allowable approach aspect occurs.

3. If the F8U-3 is restricted to its design acceptance limit (M 2.0) the resulting co-altitude performance of the X1B system is essentially the same as that of the X1A (neglecting difference in altitude ceilings).

4. The pull-up capability of the X1B system is essentially the same as that of the X1A system when operating altitudes of the F4H-1 are considered. However, the resulting attack zones for the X1B will be extended in altitude over those of the X1A due to the greater altitude capability of the F8U-3. There is an approximate 4000 feet altitude capability difference between the two systems.

5. The allowable launch error for Sparrow III is a function of altitude, aspect angle at the time of entry into the launch zone, gimbal angle limits of the AI radar and the point in the launch zone where the interceptor is in a position to launch the weapon.

(a) Against a high-speed target, attacks entering the launch zone close to head-on result in very small allowable launch errors. As the attack moves around toward the beam, the allowable launch error increases.

- (b) For purposes of this study, the allowable launch error has been fixed at 10° . When a 26 value of noise is included the allowable launch errors will be much less than 10° for many of the situations investigated.

6. The probability of successful arrival to missile launch in co-altitude attacks against nonmaneuvering targets, when limited by some of the degrading factors such as gimbal angle limits and vectoring inaccuracies, are given in Volume I and this volume of the report. When the attack altitude is 50,000 feet and $V_T/V_F = M. 2.0$ the resulting probabilities of successful arrival to missile launch are:

(a) for $V_T/V_F = 1.0$ the probability starts out at 46% for the head-on case $\tau = 0$, increases to 52% at $\tau = 30^\circ$ and drops to zero when $\tau = 60^\circ$.

(b) for $V_T/V_F = 0.8$ the probability starts out at 48% for $\tau = 0^\circ$, increases to 73% at $\tau = 30^\circ$ (correction on Volume I results) and decreases to 44% at $\tau = 60^\circ$.

7. When the altitude of attack is 30,000 feet and $V_F = V_{max}$ the resulting probabilities of successful arrival to missile launch are:

(a) for $V_T/V_F = 1.0$ the probability starts out at 45% for $\tau = 0^\circ$, increases to 53% at $\tau = 30^\circ$ and decreases to 0% at $\tau = 60^\circ$.

(b) for $V_T/V_F = 0.8$ the probability starts out at 52% for $\tau = 0^\circ$, increases to 75% at $\tau = 30^\circ$ and decreases to 44% at $\tau = 60^\circ$.

8. When the altitude of attack is 1,000 feet and $V_T/V_F = 0.8$ ($V_F = M 1.07$) the probability of successful arrival to missile launch is 52% at $\tau = 0^\circ$, 60% at $\tau = 30^\circ$ and 47% at $\tau = 60^\circ$. (The AI radar ranges used in this study of the 1,000 ft altitude case are believed to be optimistic).

9. The effects of incorporating the currently estimated improvement in AI detection range resulting from the use of a separate operator as shown by the study for the 50,000 ft altitude case are:

(a) The improvement in probability of successful arrival to missile launch for the high speed target case ($V_T/V_F = 1.0$) is from 46% to 54% for $\tau = 0^\circ$ and from 52% to 60% for $\tau = 30^\circ$.

(b) When the speed ratio is reduced to $V_T/V_F = 0.8$, the resulting improvement in probability of success is from 47% to 66% for $\tau = 0^\circ$ and from 73% to 79% for $\tau = 30^\circ$.

10. In pull-up attacks against a M 2.0 nonmaneuvering target at 65,000 feet altitude by a M 2.0 or V_{max} interceptor the resulting probabilities of successful arrival to missile launch are as follows:

(a) When the pull-up is initiated from 30,000 feet the probability is zero.

(b) When the pull-up is initiated from 45,000 feet altitude the resulting probability is 6%. The primary limitation is inability to reduce the error down to that allowable for launch.

(c) When the pull-up is initiated from 55,000 feet the resulting probability is 13%. Here the primary restriction results from excessive gimbal angle.

11. When the target altitude is reduced to 50,000 feet the probability of successful arrival to missile launch varies from 6% for pull-ups initiated at 30,000 feet to 46% for the co-altitude case.

12. When co-altitude attacks are considered and the target initiates a relatively simple maneuver at AI radar lock-on (1 g crisscross maneuver) the effect depends upon the direction of the initial maneuver (except for the head-on case). This maneuver, although mild, is believed realistic since the primary job of the target is to deliver its own weapon.

(a) As would be expected, there is no difference in the probability resulting from an initial turn to the left (away from the interceptor) or to the right (toward the interceptor) on the part of the target for the head-on case. When the attack occurs at 30,000 feet and $V_T/V_F = 1.0$ the resulting probability is 42.5%. When the speed ratio is reduced to 0.8 the probability is 53%. Comparing these results with those given previously for the nonmaneuvering target it is seen that there is an insignificant difference in the probabilities.

(b) When the approach course is from 30° off the target's nose, a maneuver to the right results in a 51% probability of success and a maneuver to the left results in a 56% probability of success for $V_T/V_F = 1$. When the speed ratio is reduced to $V_T/V_F = 0.8$ the corresponding probabilities are 62% and 77%. Comparing these results to those obtained for the nonmaneuvering target it is seen that there is a negligible difference in the results. A maneuver to the right always decreases

the probability slightly while a maneuver to the left always increases the probability slightly (more time available).

13. As stated in Volume I, when additional degrading factors are considered, the probabilities listed above will be reduced still further.

14. Theoretical calculations of weather effects in the performance of the current AI radar indicate that rain will degrade the range capability to the point where it is completely unacceptable. The current radar has an 85% probability of detecting a B-47 size target (high speed case) at 12-13 n.mi. This would be reduced to 2.8 n.mi. in the presence of a light rain.

B. System Using Improved Radar

1. To date, the improvement resulting from the use of a bright display, bandwidth switching and optimized search have been included in the study. The resulting range improvement is from 12.7 n.mi. to 19 n.mi. for a M 2.0 interceptor attacking a M 2.0 target.

2. When the improvements of Item 1 are considered along with a system having gimbal angle limits of $\pm 57^\circ$ the resulting probabilities of successful arrival to missile launch for attacks occurring at 50,000 feet and $V_T = M 2.0$ are:

(a) 75% for $V_T/V_F = 1.0$ and $T = 0^\circ$. For the unimproved radar the corresponding probability was 46%.

(b) 89% for $V_T/V_F = 1.0$ and $T = 30^\circ$. For the unimproved radar the corresponding probability was 52%.

(c) 8% for $V_T/V_F = 1.0$ and $T = 60^\circ$. For the unimproved radar the corresponding probability was 0%.

(d) 84% for $V_T/V_F = 0.8$ and $T = 0^\circ$. For the unimproved radar the corresponding probability was 48%.

(e) 91% for $V_T/V_F = 0.8$ and $T = 30^\circ$. For the unimproved radar the corresponding probability was 73%.

(f) 89% for $V_T/V_F = 0.8$ and $T = 60^\circ$. For the unimproved radar the corresponding probability was 44%.

3. The probabilities of successful arrival to missile launch for attacks occurring at 30,000 feet are essentially the same as those resulting from attacks occurring at 50,000 feet (see Items 2 and 3).

4. When the attack occurs at 1,000 feet altitude and $V_T/V_F = 0.8$ where $V_F = V_{max}$ the resulting probabilities of successful arrival to missile launch are 82% for $\tau = 0^\circ$, 84% for $\tau = 30^\circ$ and 76% for $\tau = 60^\circ$. These results are based upon theoretical calculations of AI radar performance and upon limited test data from NATC and are believed to be optimistic.

5. When the estimated difference in performance of the AI radar in a two-place system versus single-place operation is considered (12%) a minor change in probability of successful arrival to missile launch occurs. For example when the attack occurs at 50,000 feet and $V_T/V_F = 1.0$ where $V_F = M 2.0$ and $\tau = 0^\circ$ there is an improvement from 75% to 84%. When $\tau = 30^\circ$ the improvement is from 89% to 92%.

6. For the target maneuver investigated in this study (1 g criss-cross) there is a negligible effect on probability of successful arrival to missile launch under co-altitude attack conditions.

7. When pull-up attacks are considered and a system employing the improved radar is investigated there is a major improvement in probability of successful arrival to missile launch. For example, attacks against a target flying at 65,000 feet and M 2.0 yield probabilities as follows:

(a) When the pull-up is started from 25,000 feet altitude the probability is 17%. With the unimproved system there was no probability for pull-ups initiated below 38,000 feet.

(b) When the pull-up is started from 45,000 feet the probability is 50%. For the unimproved system the corresponding probability was 6%.

(c) When the pull-up is started from 55,000 feet the probability is 75%. For the unimproved system the corresponding probability was 13%.

8. As stated previously, if the F8U-3 is restricted to M 2.0 operation the results obtained will be the same as for the F4H-1 (within the altitude envelope of the F4H-1). However, the F8U-3 has a greater altitude capability than the F4H-1 thus the resulting effective attack zones obtained in this study for pull-up attacks will be extended upward from 58,000 feet to 62,000 feet.

C. General System Considerations

1. The study results indicate that careful consideration must be given to placement of early warning equipment with respect to fleet center if a tactically useful system is to emerge.

2. When an advanced interceptor is employed (F8U-3 not restricted to M 2.0) rear hemisphere, co-altitude attacks can now be made against target speeds where the current systems fail. However, the marginal forward hemisphere area is made even more marginal by the use of the higher interceptor velocity.

3. To date, the undefined state of the IR capability in the AI fire control system is such that analysis is unwarranted. Thus the Navy study has concentrated on revealing the deficient areas of the primary fire control system.

4. To date, there is insufficient test data available to allow analysis of any of the proposed IR seekers except the DAN-5 when operating against a subsonic target. The resulting effective attack zone is restricted for high probability, to $\pm 70^\circ$ off the target's tail. The attack courses are restricted to approaches from 90° back to tail-on.

5. To date, available data on Sidewinder performance is restricted to Sidewinder IA. In general, when high speed targets are considered, Sidewinder IA is unsuitable for use in these two systems. NOTS is currently preparing launch envelopes for Sidewinder IC. The increased range of Sidewinder IC will result in overall system capability in some regions where the Sidewinder IA launch area cannot be entered by the interceptor when attacking a target whose speed is nearly equal to his own speed.

Recommendations for Further Study Effort

There are several areas where investigation is needed before the performance of the current system under tactical conditions can be clearly defined. These are as follows:

1. Further study effort is needed on the low altitude investigation when results of planned tests become available.

2. If tests prove that there is a significant difference between the F8U-3 and F4H-1 Weapon Systems due to a separate operator, the results of the study to date should be modified to include this difference.

3. Extension of the co-altitude probability of success curves to include angles off the target's nose greater than 60° and to include smaller angular increments is needed.

4. A flight simulator program should be conducted to operationally verify the adequacy of model techniques used in the present study. This would be a check, using the pilot in the loop, of the critical areas exposed by the current study.

5. Extension of the incremental altitude study to include azimuth angles other than head-on is needed.

6. Determine by study and analysis the acceleration launching transients occurring during the Sparrow III missile launch and the effects of these transients upon dynamic performance of the missile internal functions and missile trajectory to the target.

7. Determine by study and analysis the effects of noise and missile orientation on system accuracy, both with and without "English Bias".

8. Determine by study and analysis the illumination requirements after Sparrow III launch in conjunction with breakaway requirements and aircraft normal flight recovery requirements.

9. Investigation of limits imposed by hydraulics on pull-up probability is needed.

There are still several areas where additional analysis is needed to allow more complete definition of the performance of the improved system. Among these are:

1. Extension of the analysis of the F4H-1 and F8U-3 incremental altitude capabilities with the improved system at aspects other than head-on.

2. Extension of the analysis of co-altitude probability of success to include angles greater than 60° off the nose and to include smaller angular increments.

3. Verify by flight simulator tests the adequacy of the results obtained from the described model.

4. Inclusion of actual missile performance during ejection launch and after launch. This includes transient effects during launch.

5. Inclusion of the effects of noise and missile orientation both with and without "English Bias".

6. Verify by flight simulation study the effects of a situation display on system probability of success and develop optimum approach tactics.

7. Determine by study and analysis the sensitive elements of the F4H-1 and the F8U-3 Weapon Systems mechanization and their accuracy tolerances.

8. Determine by study and analysis the feasibility and possible advantages of using alternate guidance systems (different from those covered in this volume) in the F4H-1 and the F8U-3 Weapon Systems.

In addition to the preceding basic system areas of investigation, there are several areas where data is lacking. These are:

1. Performance data on the Sidewinder IC.
2. Performance data on the Sparrow III-IR.
3. Performance data on the IR Search and Track.

As soon as data on these areas becomes available, it should be included in the study effort.

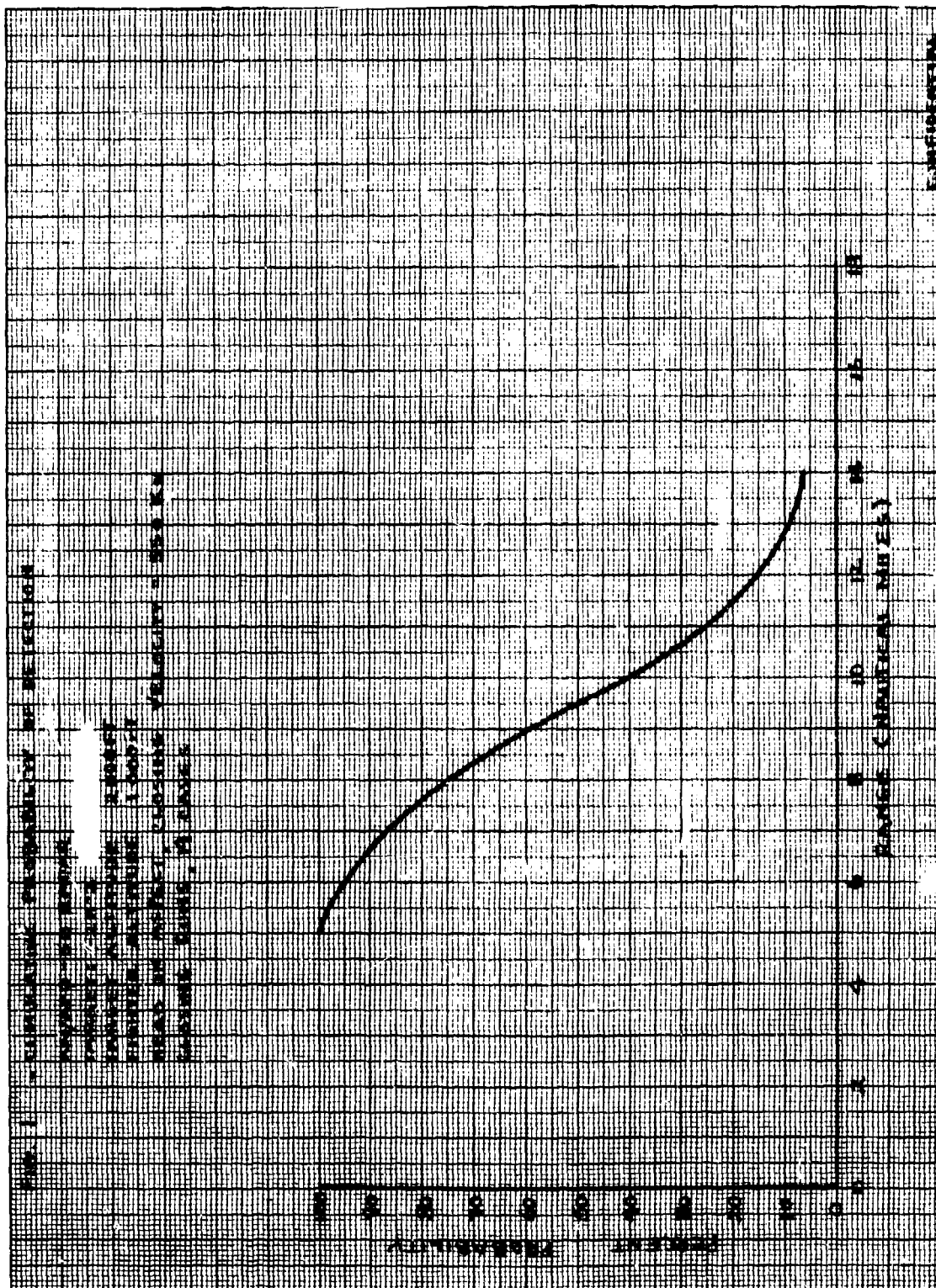
ACKNOWLEDGEMENTS

The data presented in this report represents the results, to date, of the Navy's Air-to-Air Missile Study Program. The analytical results including those from which figures were derived are in part the results of the computational work underway at Westinghouse Air Arm Division. In addition, results of analysis underway at NAMTC, Pt. Mugu are included. The authors would like to thank the analytical section of the Westinghouse Air Arm Division and the Laboratory Evaluation Department of NAMTC, Pt. Mugu, for their contribution to this report. The authors would also like to thank those agencies such as NOTS, Inyokern, NATC, Patuxent which supplied test data used in this report.

Personnel of the NRL who contributed importantly to the preparation of this report are Peter Waterman and Laurence Gilchrist of the Equipment Research Branch of the Radar Division; Charles Dodge, Radar Division Consultant; and John Barry and S. F. George, Mathematics Branch of the Radar Division.

REFERENCES

1. "Flight Test of AN/APQ-50 Radar Set, Report #1, Final Report," NATC, 1 Nov 1957, Confidential
2. "Prediction of the Maximum Range Boundary for the Supersonic Sparrow III Caused by the Exhaustion of Hydraulic Oil," NAMTC Memorandum Report No. LE -57, Confidential
3. "A Study of Allowable Launch Heading Error for the Sparrow III Aero X1A-X1B Systems," NAMTC Memorandum Report No. LE, Confidential
4. "Study of Effects of Rain on AI Radar Performance," NAMTC, Advance Copy - Laboratory Evaluation Department, Confidential
5. "Results of the Second and Third Phases of Flight Test of Aero 13F," Westinghouse Air Arm Report 1853, 22 Jan 1958, Confidential



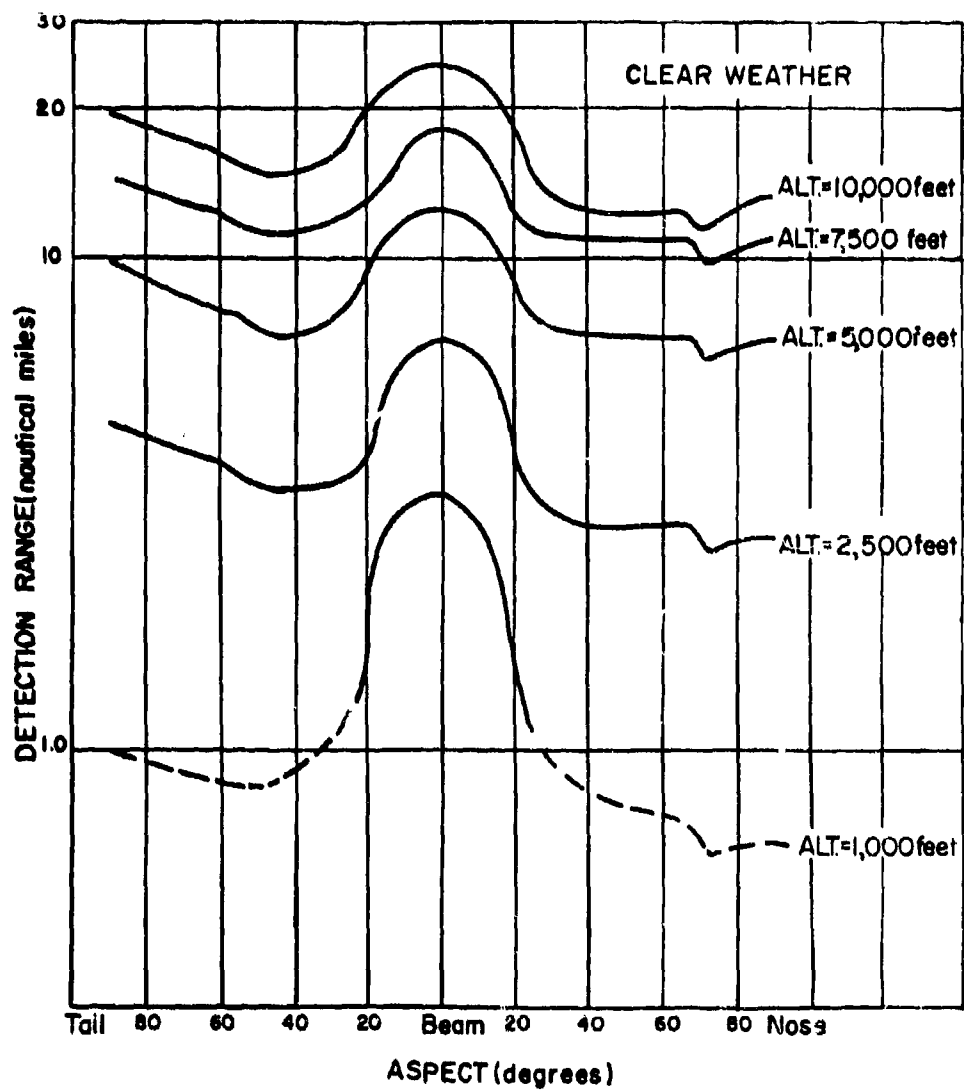
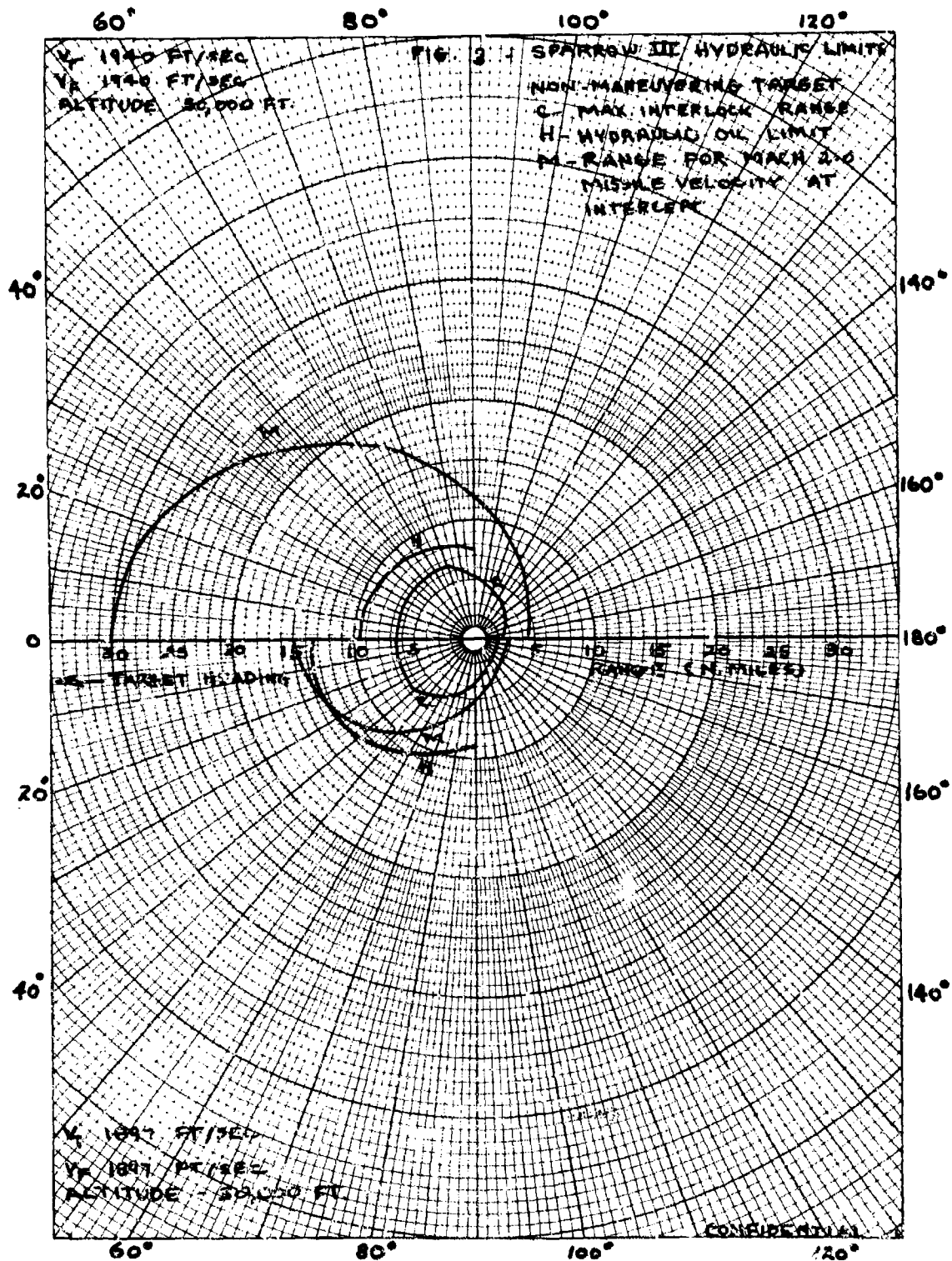
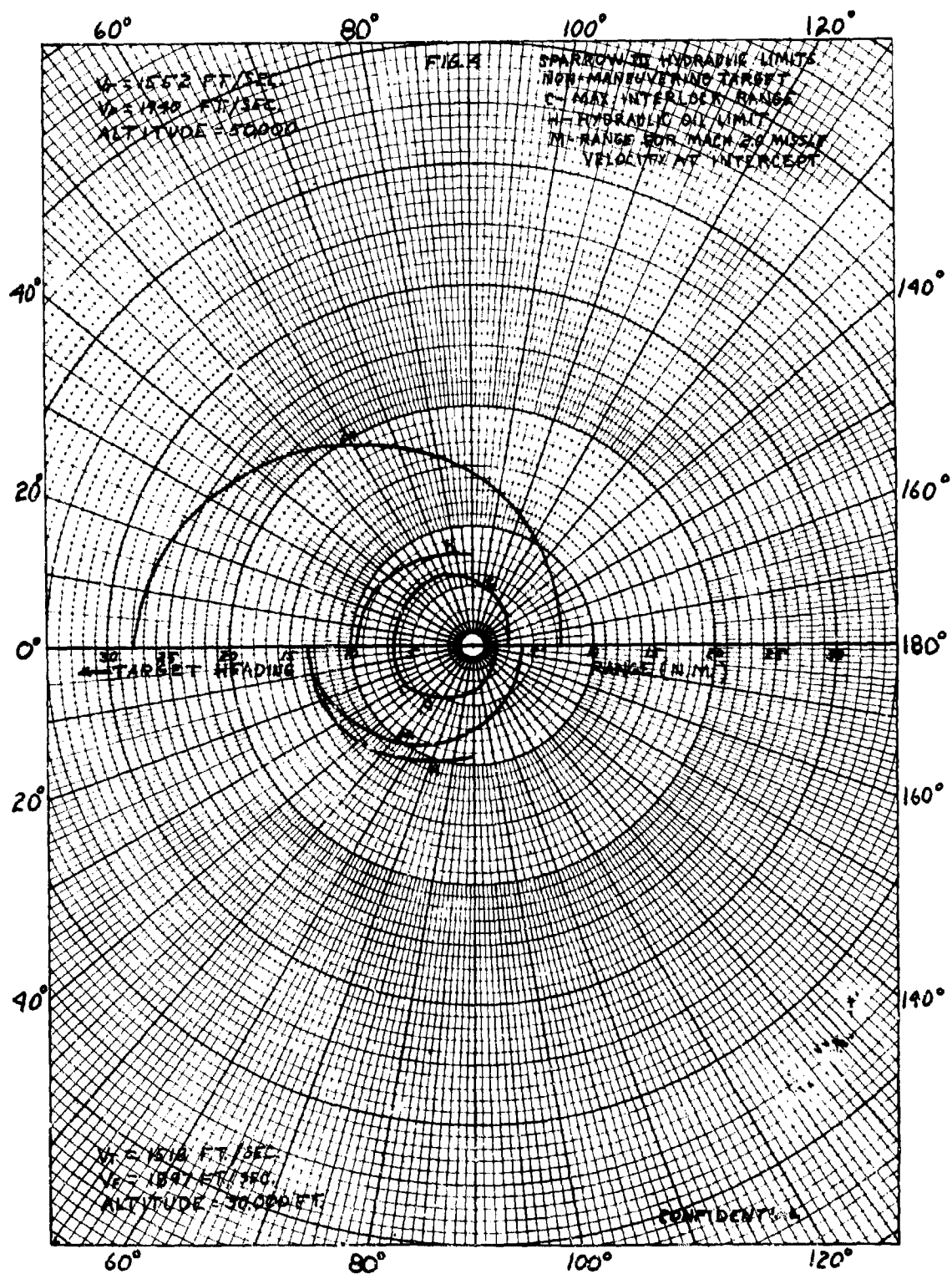
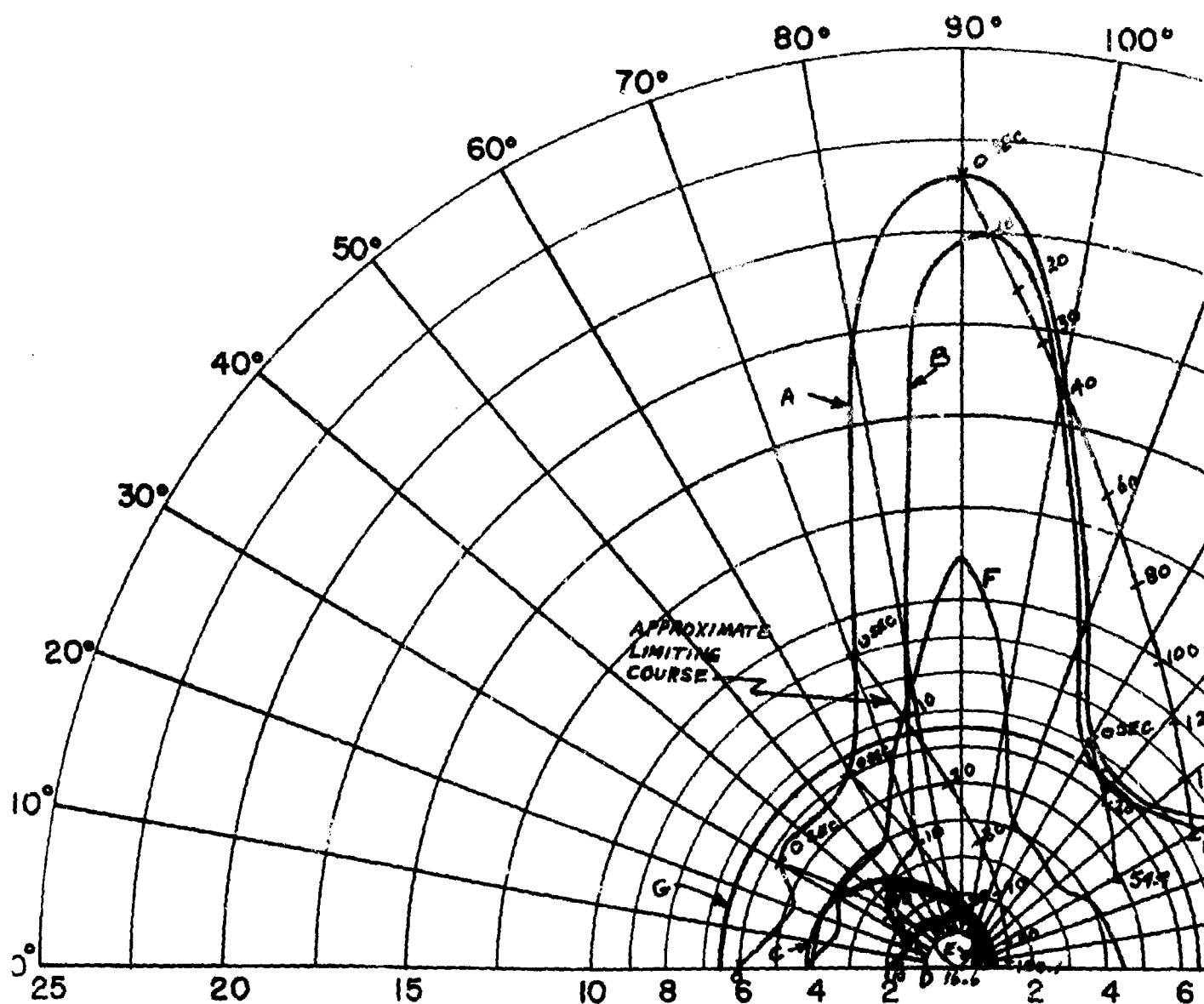


Figure 2. Low Altitude Detection Range - Vertical Polarization (Theoretical - B-47 TARGET)

CONFIDENTIAL







$V_F = 1189$ FT/SEC (F4H-1)(F8U-3)

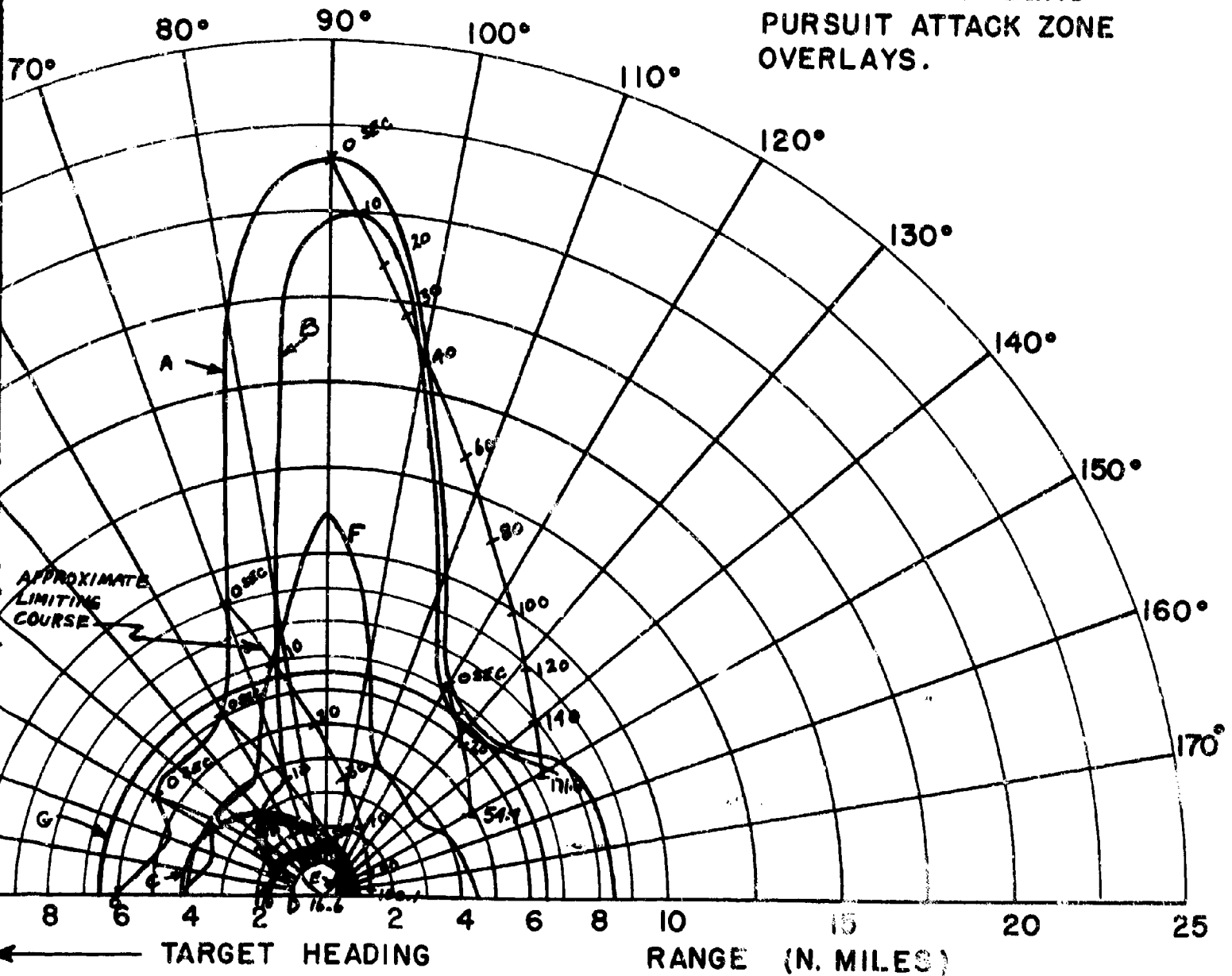
$V_T = 1189$ FT/SEC

ALTITUDE = 1000 FT.

← TARGET HEADING

- A - 85% DETECTION RANGE
- B - LOCK-ON RANGE (10 SEC. LOCK-ON)
- C - SPARROW III MAX. AERODYNAMIC
- D - SPARROW III MIN. AERODYNAMIC
- E - CONSTANT LOAD FACTOR LOCUS
- F - 90% SPARROW III SEEKER LOCK
- G - 6.5 N.M. INTERLOCK

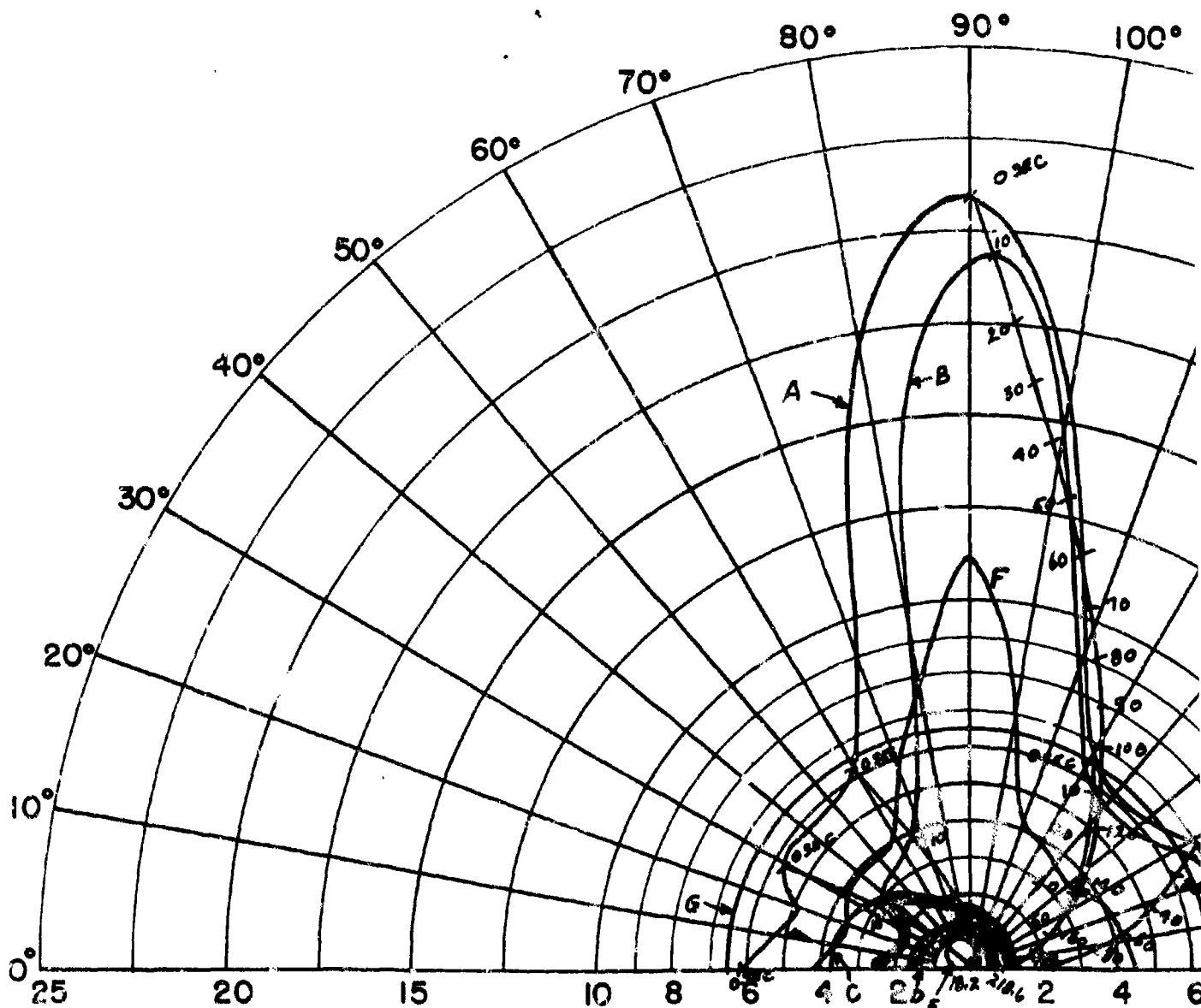
FIG. 5 - CO-ALTITUDE LEAD PURSUIT ATTACK ZONE OVERLAYS.



- 85% DETECTION RANGE
- LOCK-ON RANGE (10 SEC. LOCK-ON TIME)
- SPARROW III MAX. AERODYNAMIC RANGE
- SPARROW III MIN. AERODYNAMIC RANGE
- CONSTANT LOAD FACTOR LOCUS ($N_z = 3$)
- 90% SPARROW III SEEKER LOCK-ON RANGE
- 6.5 N.M. INTERLOCK

2

CONFIDENTIAL



$V_F = 1189$ FT/SEC (F4H-1)(F8U-3)

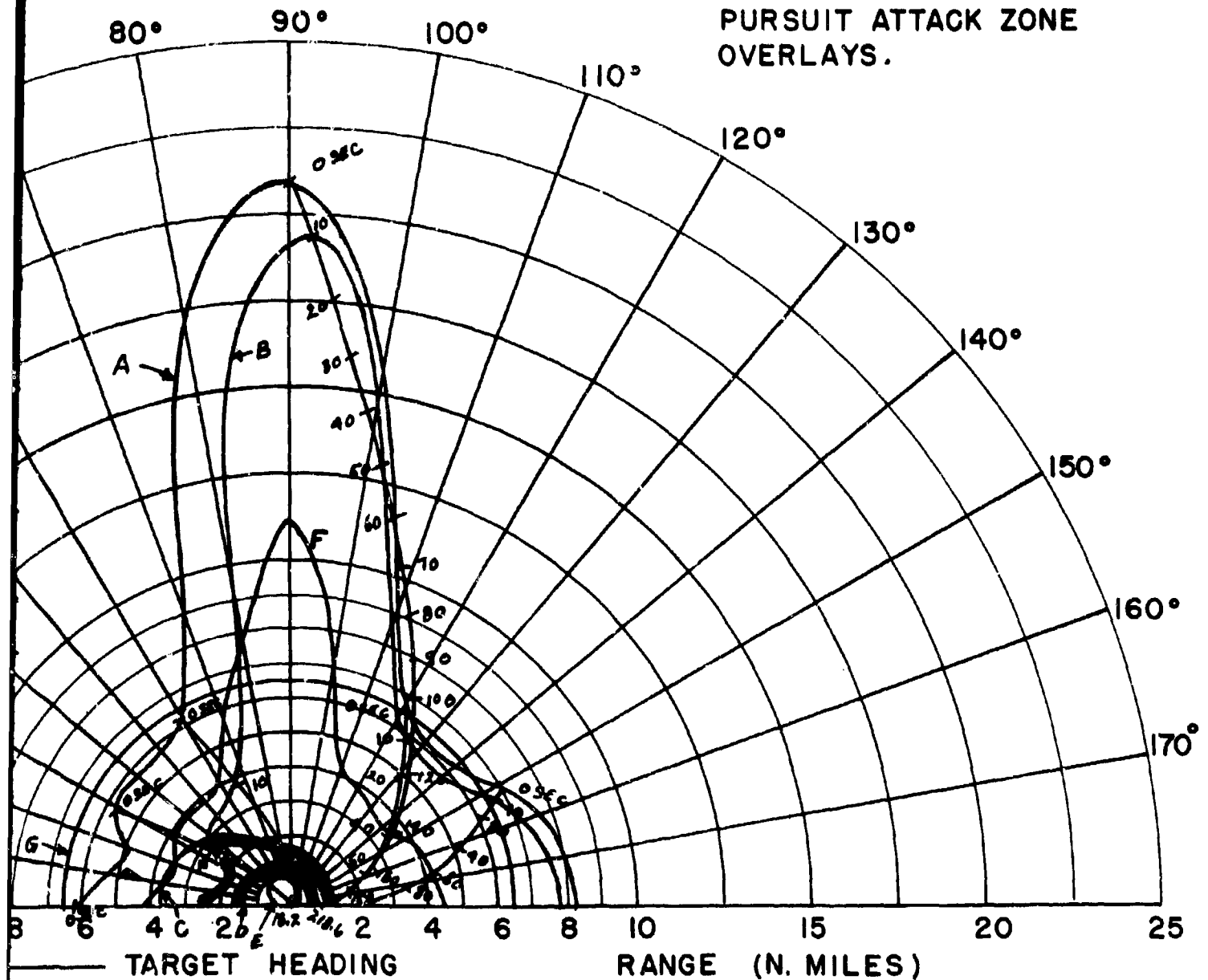
$V_T = 951$ FT/SEC

ALTITUDE = 1000 FT.

← TARGET HEADING

- A - 85% DETECTION RANGE
- B - LOCK-ON RANGE (10 SEC. LOCK-ON)
- C - SPARROW III MAX. AERODYNAMIC
- D - SPARROW III MIN. AERODYNAMIC
- E - CONSTANT LOAD FACTOR LOCUS
- F - 90% SPARROW III SEEKER LOCUS
- G - 6.5 N.M. INTERLOCK

FIG. 6 - CO-ALTITUDE LEAD
PURSUIT ATTACK ZONE
OVERLAYS.

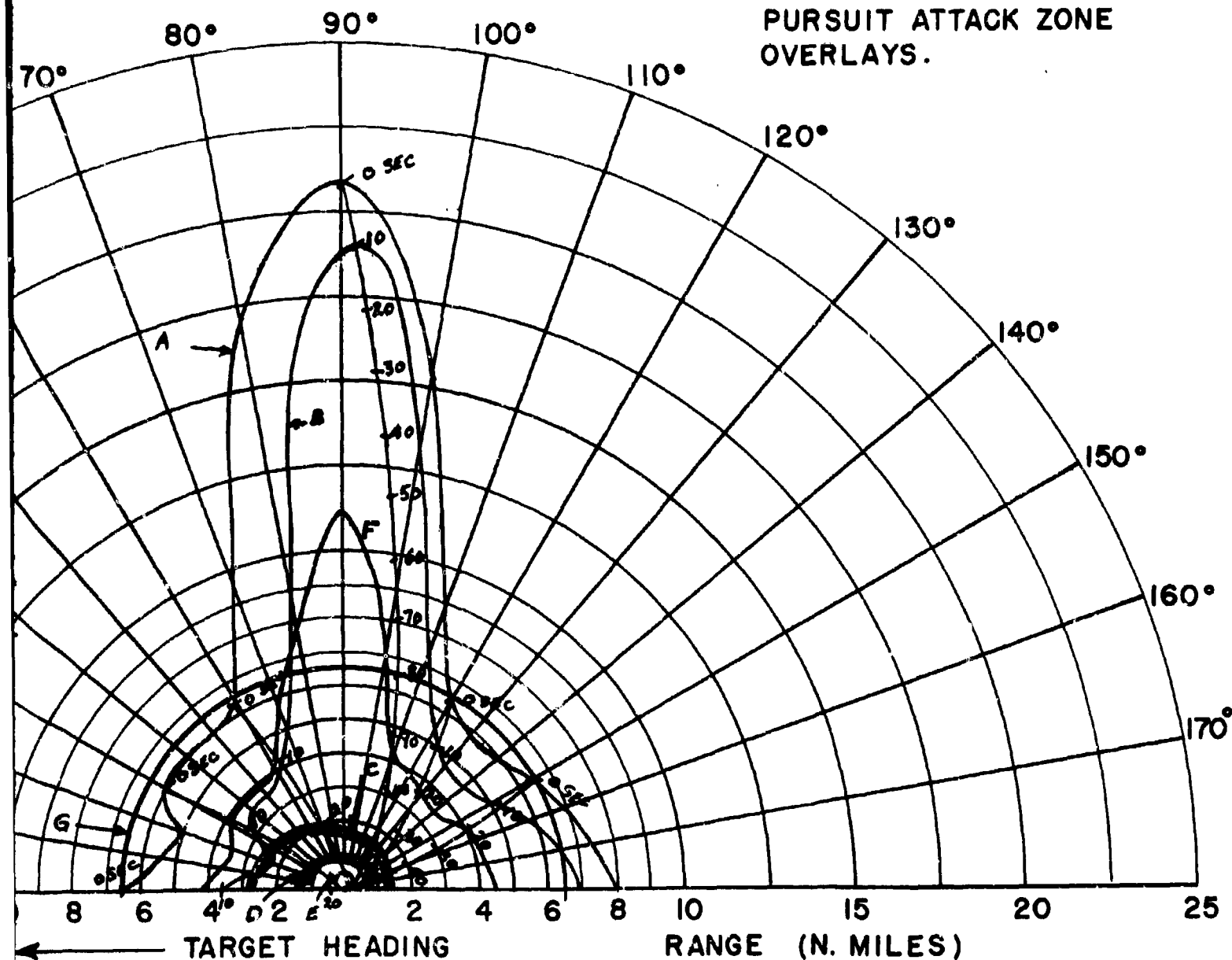


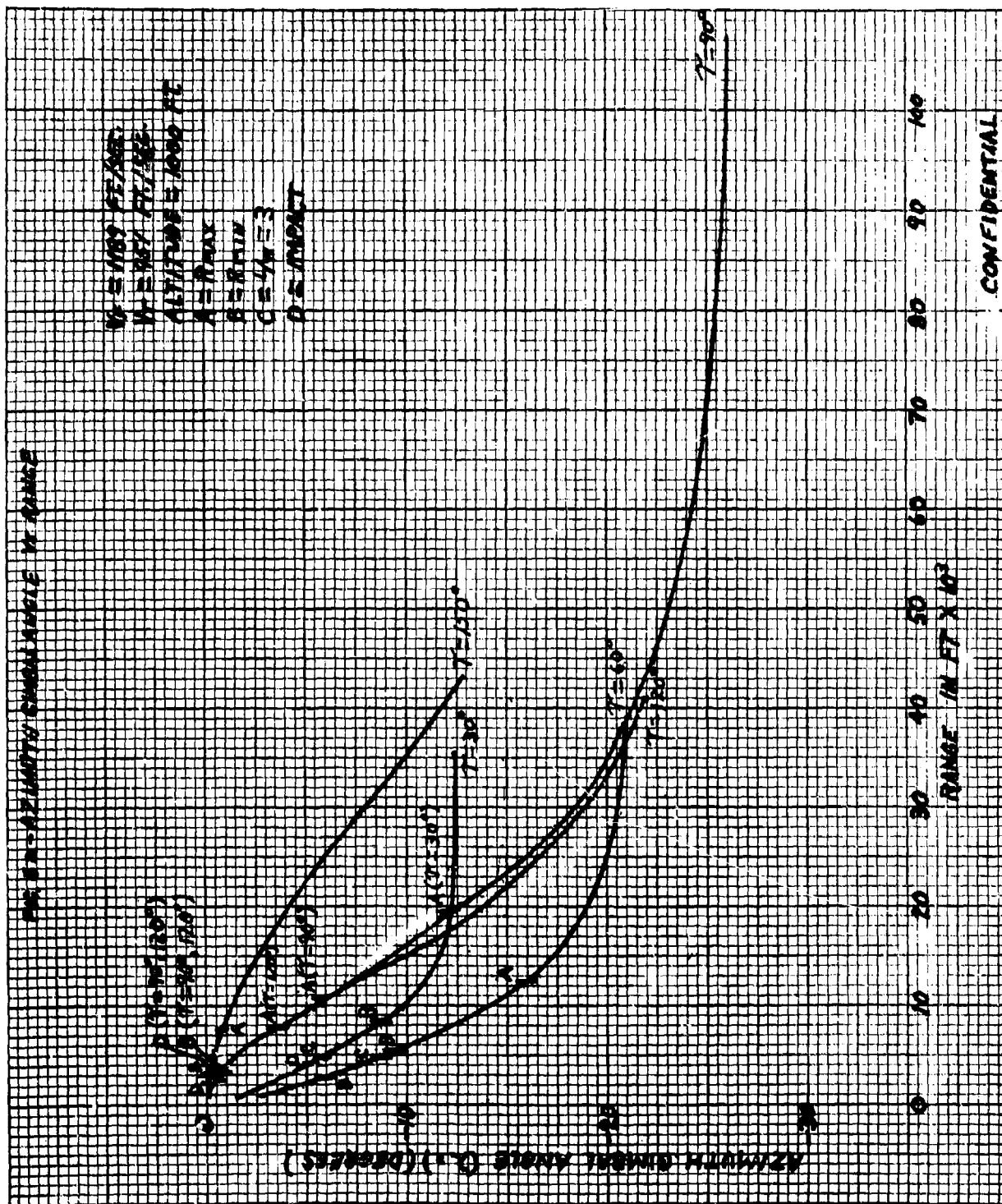
5% DETECTION RANGE
LOCK-ON RANGE (10 SEC. LOCK-ON TIME)
PARROW III MAX. AERODYNAMIC RANGE
PARROW III MIN. AERODYNAMIC RANGE
CONSTANT LOAD FACTOR LOCUS ($N_z = 3$)
0% SPARROW III SEEKER LOCK-ON RANGE
5 N.M. INTERLOCK

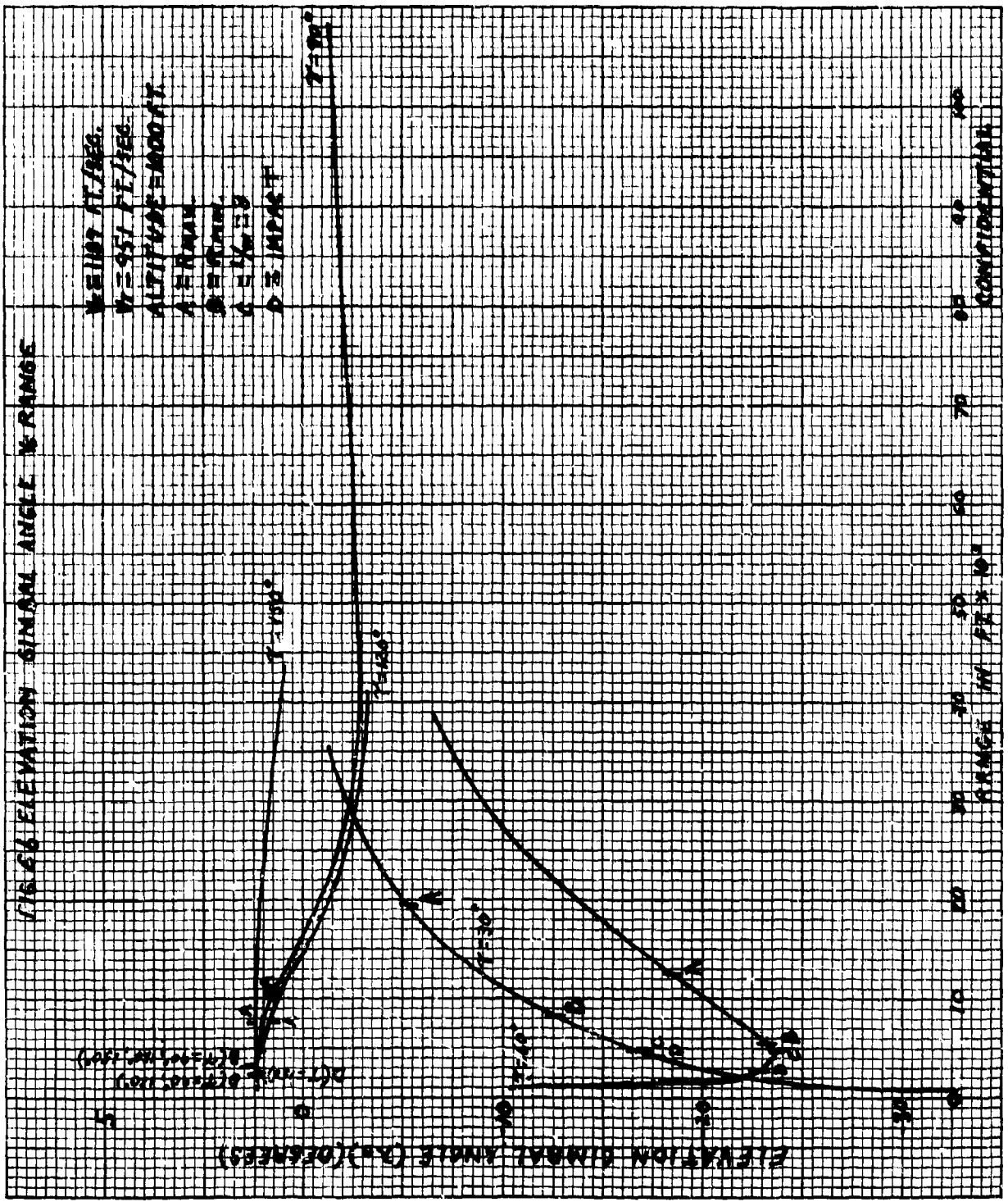
2

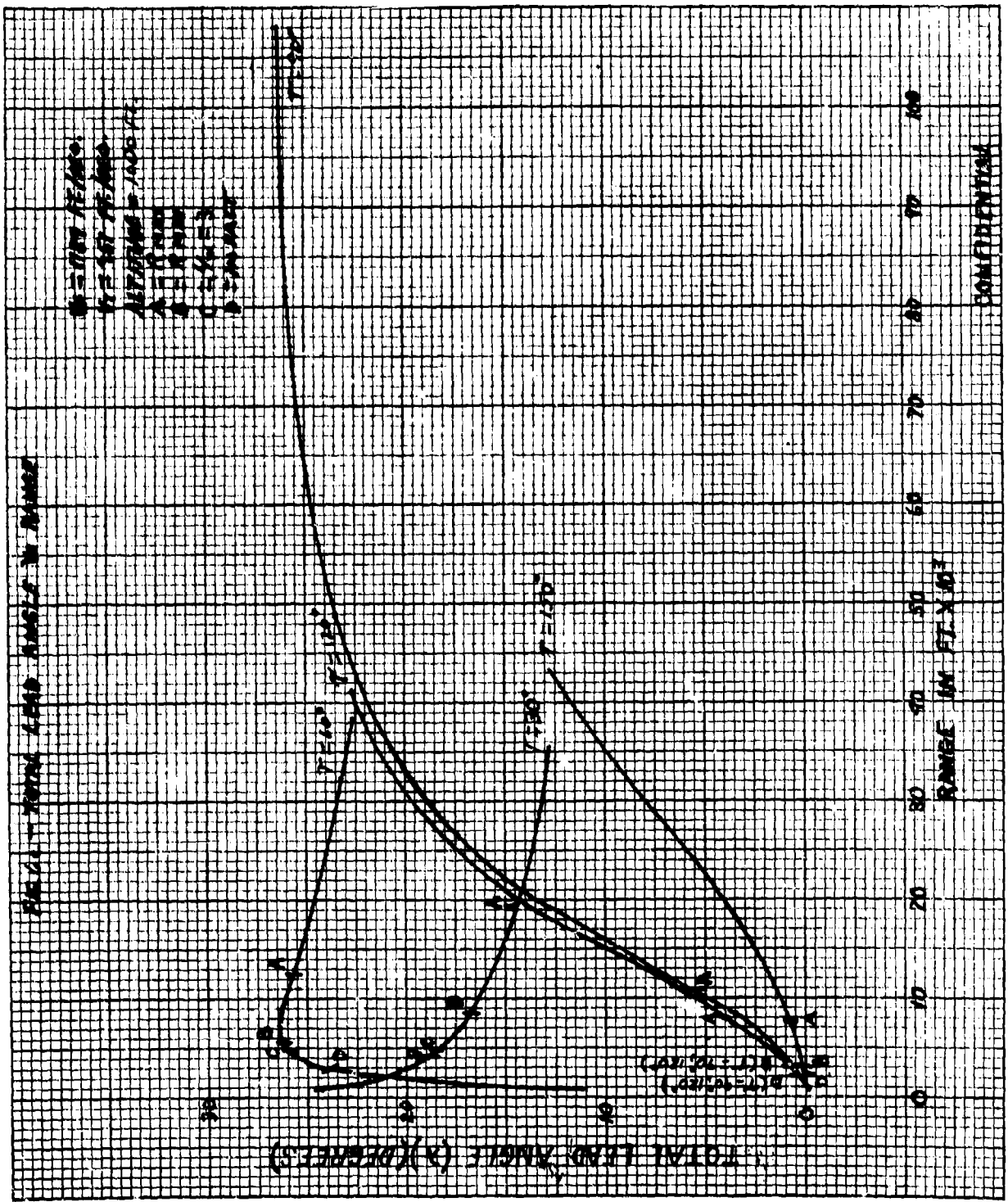
CONFIDENTIAL

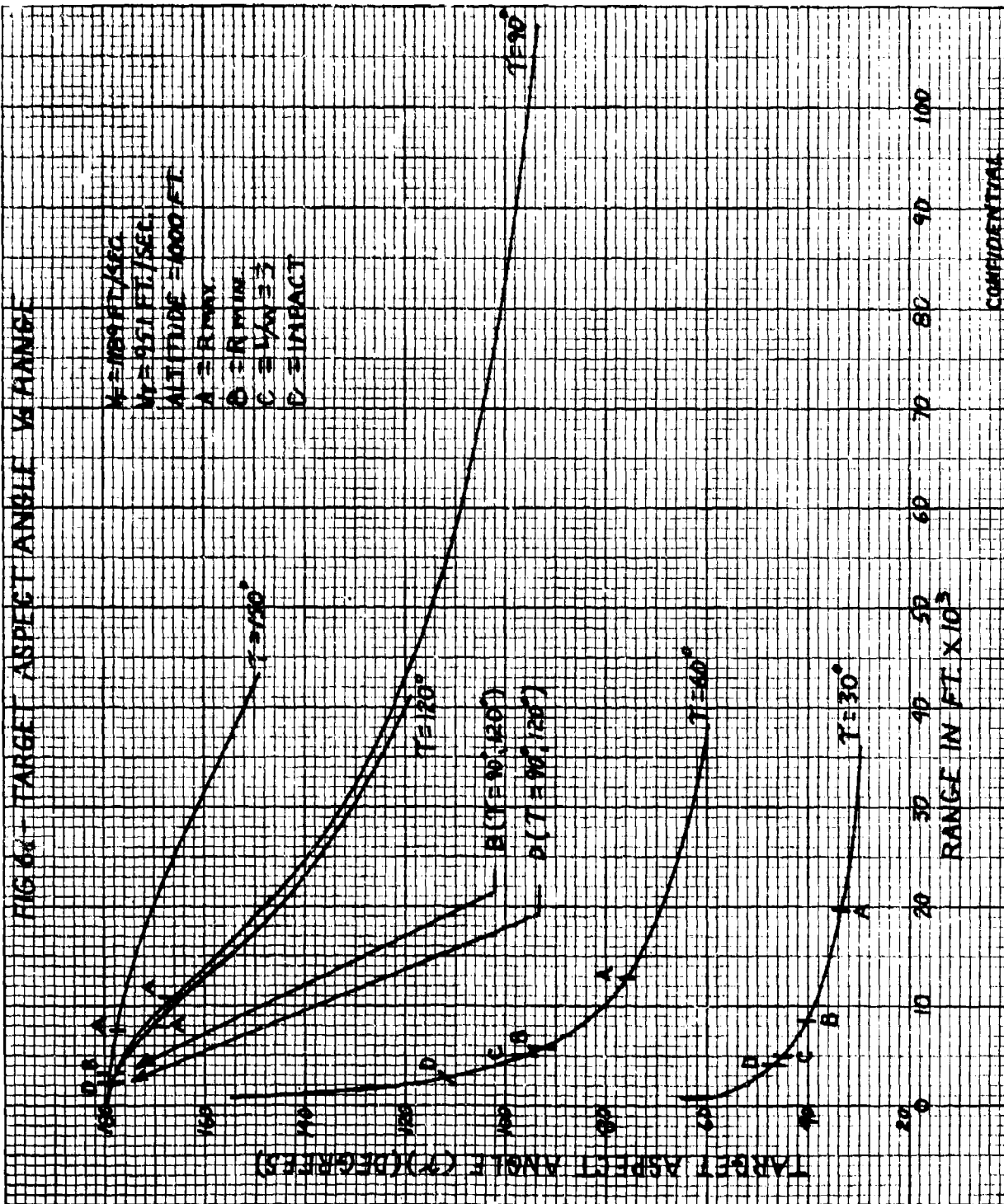
FIG. 7 - CO-ALTITUDE LEAD
PURSUIT ATTACK ZONE
OVERLAYS.

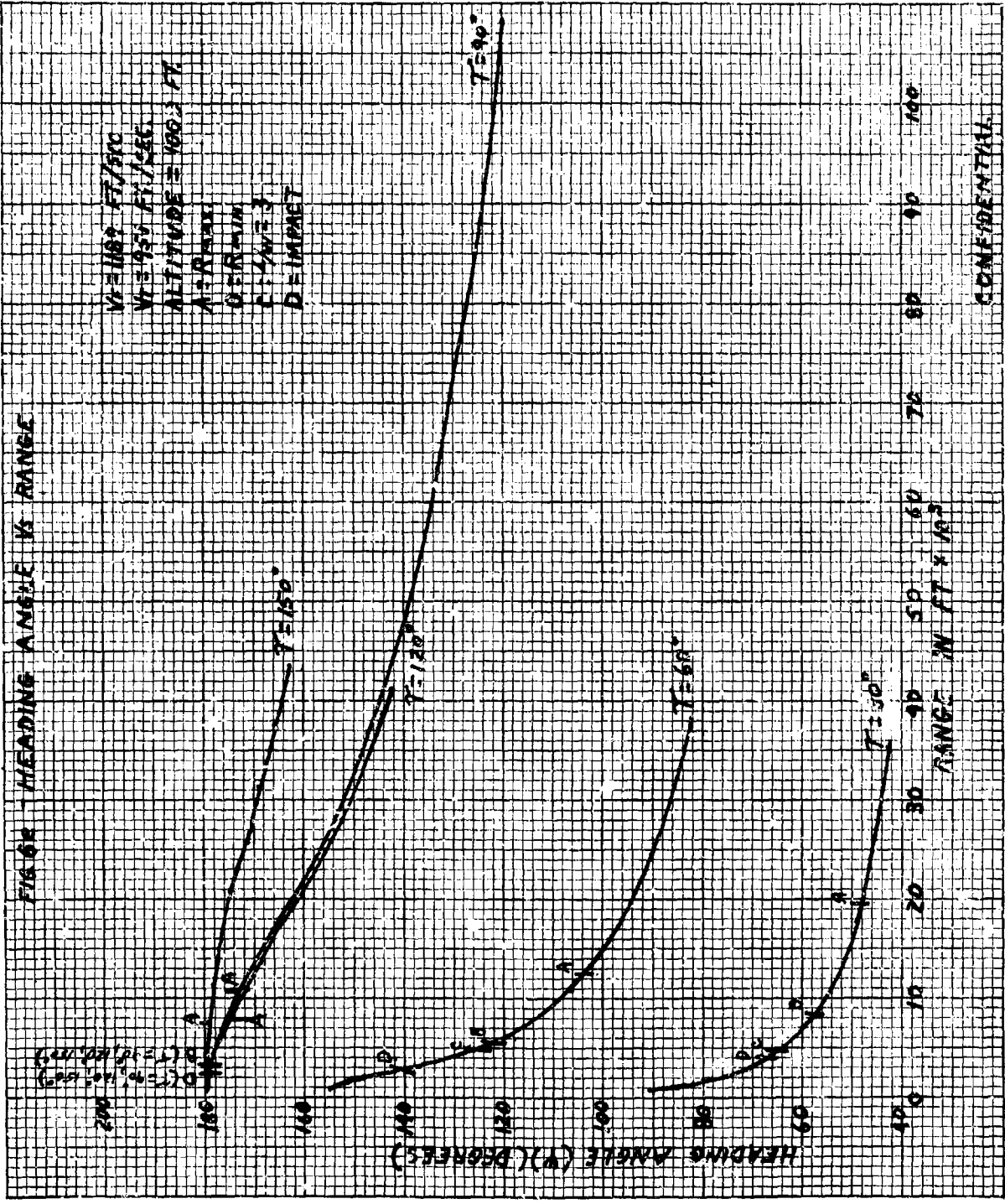




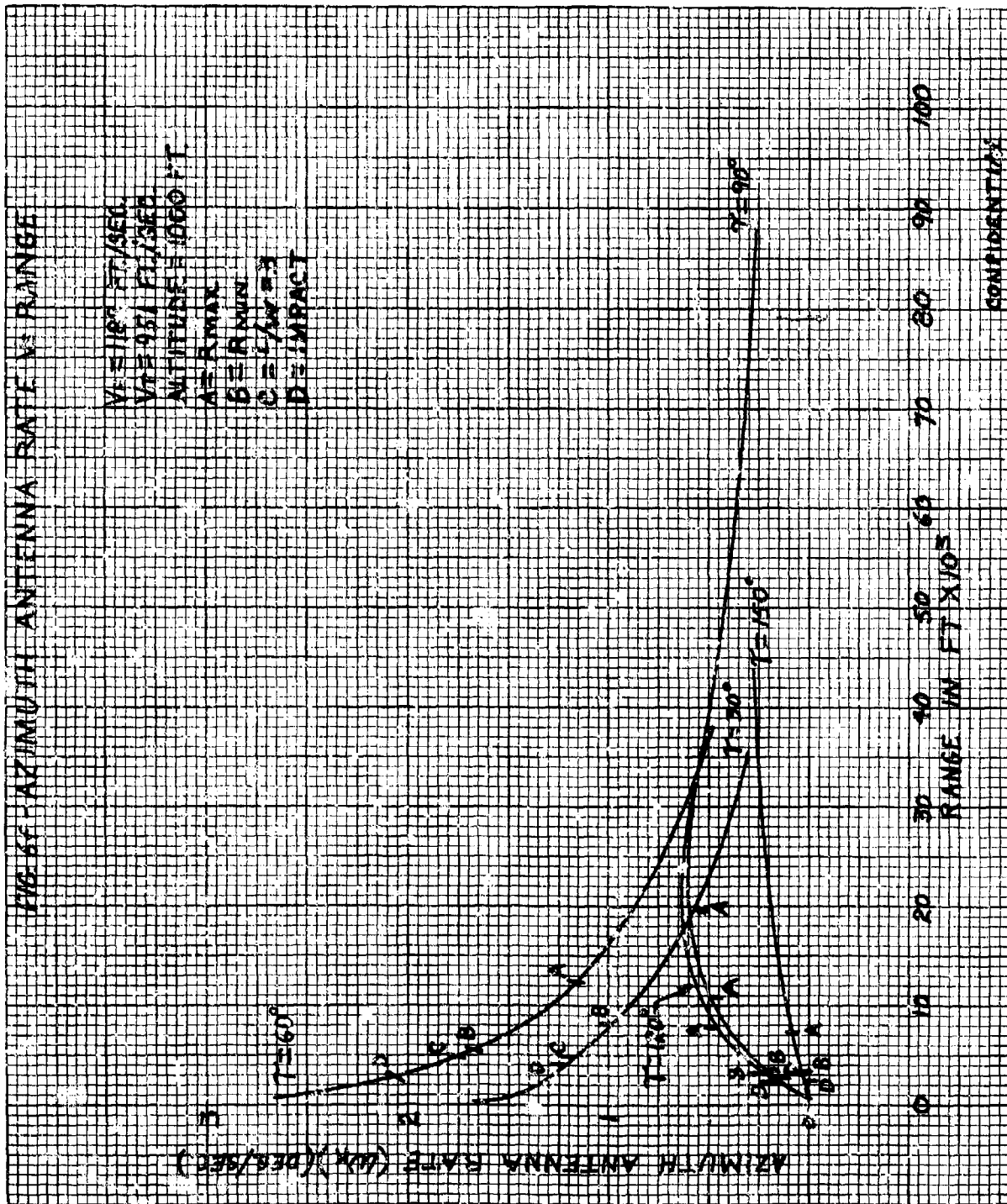




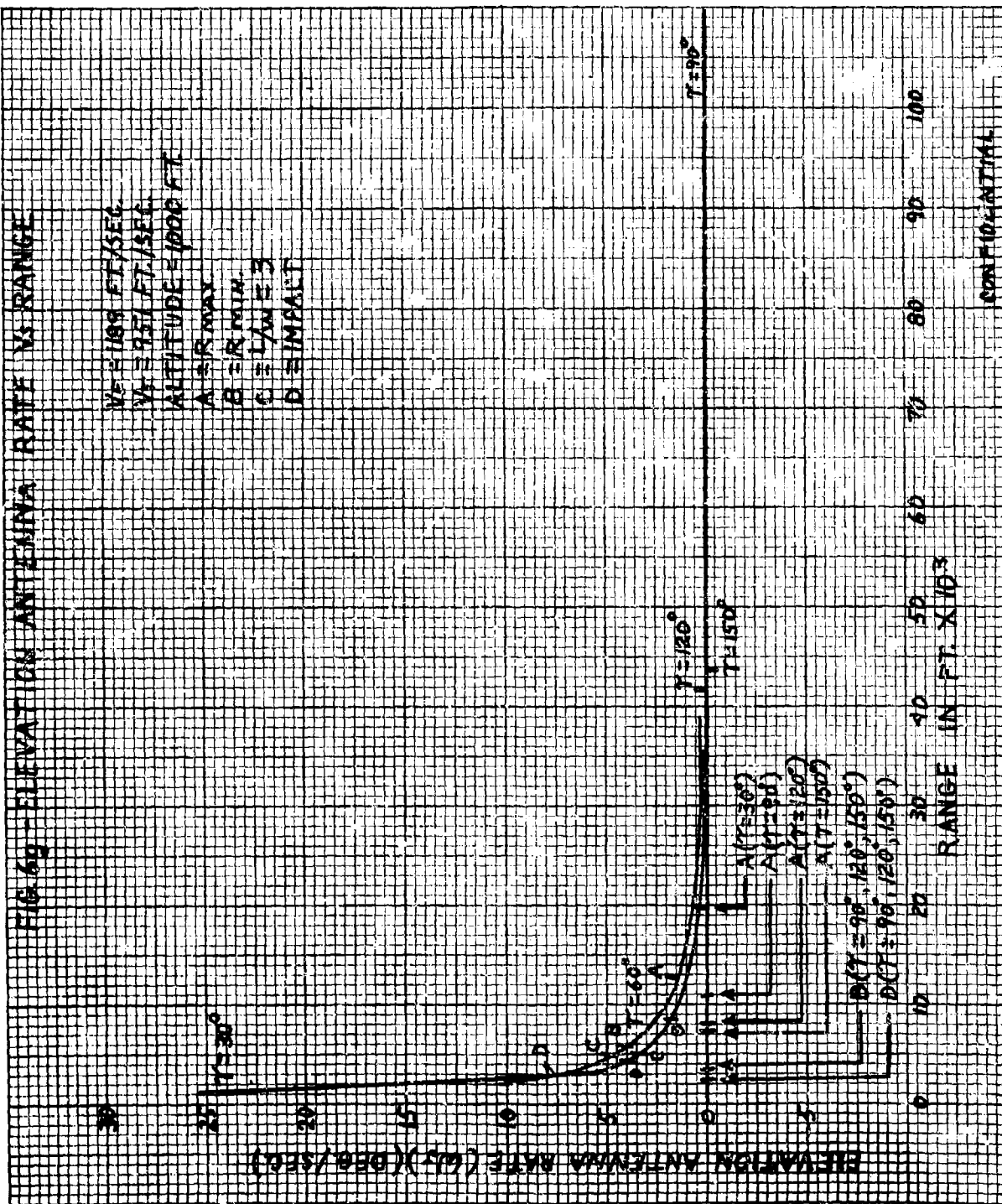




CONFIDENTIAL



CONFIDENTIAL



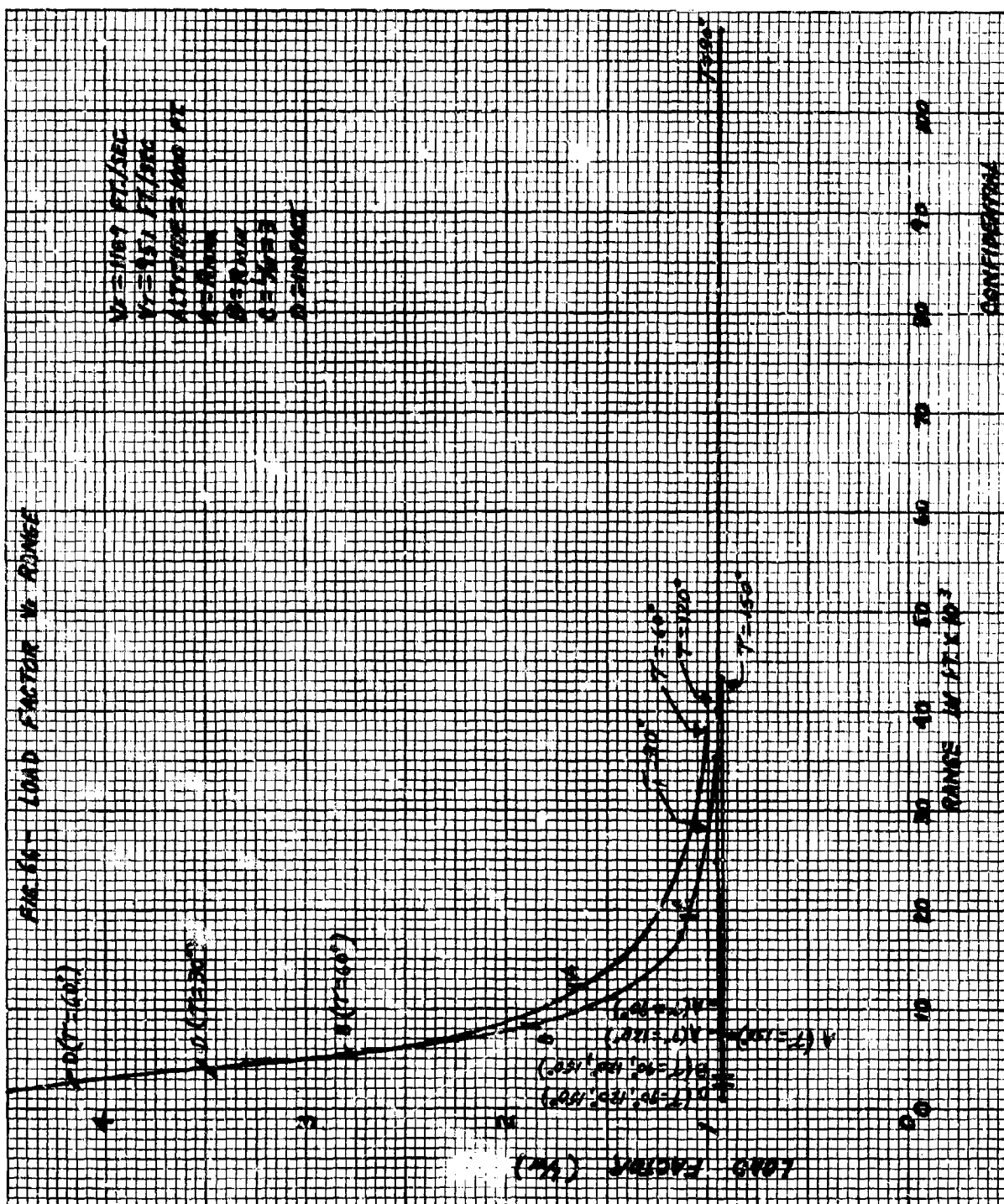
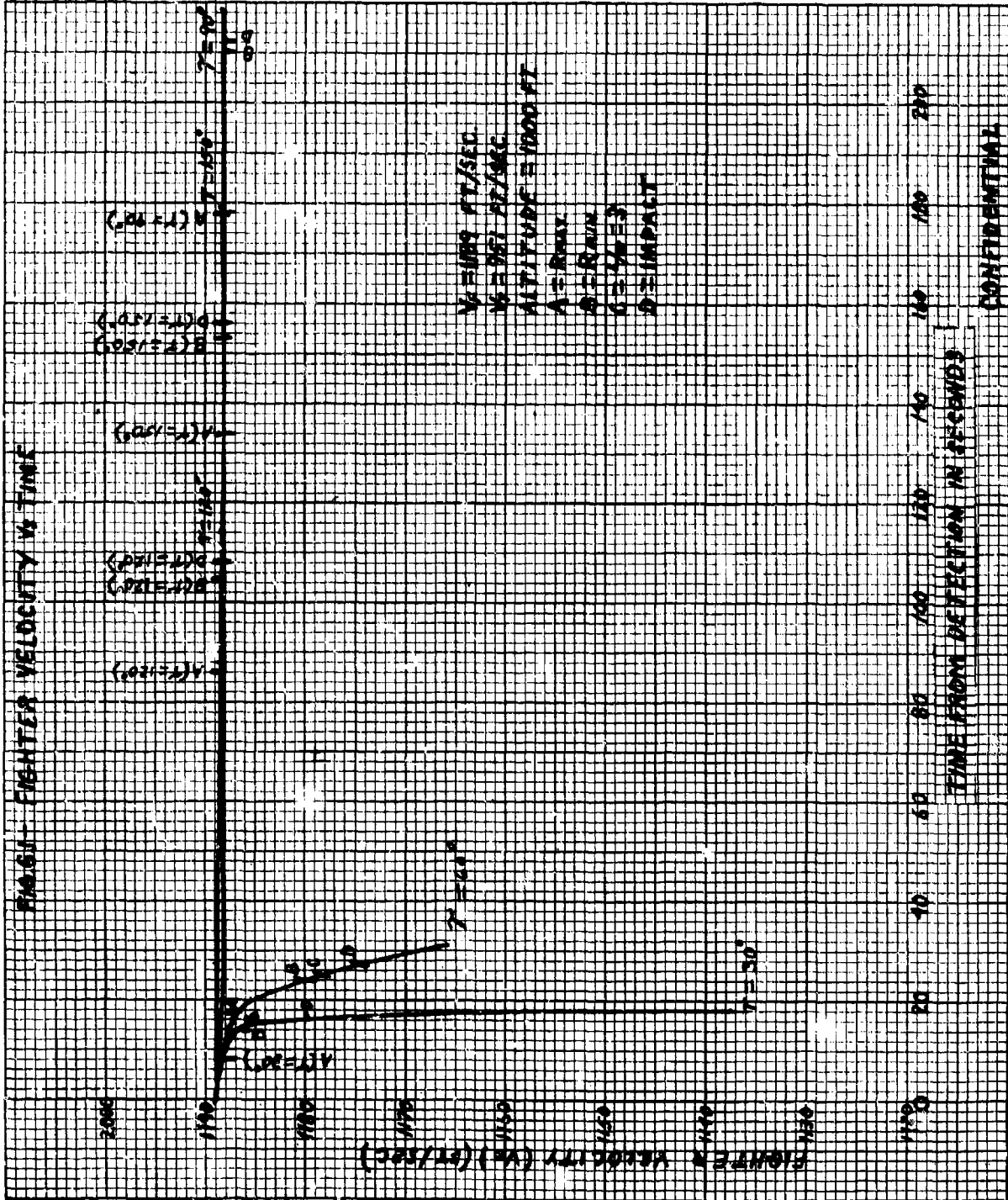
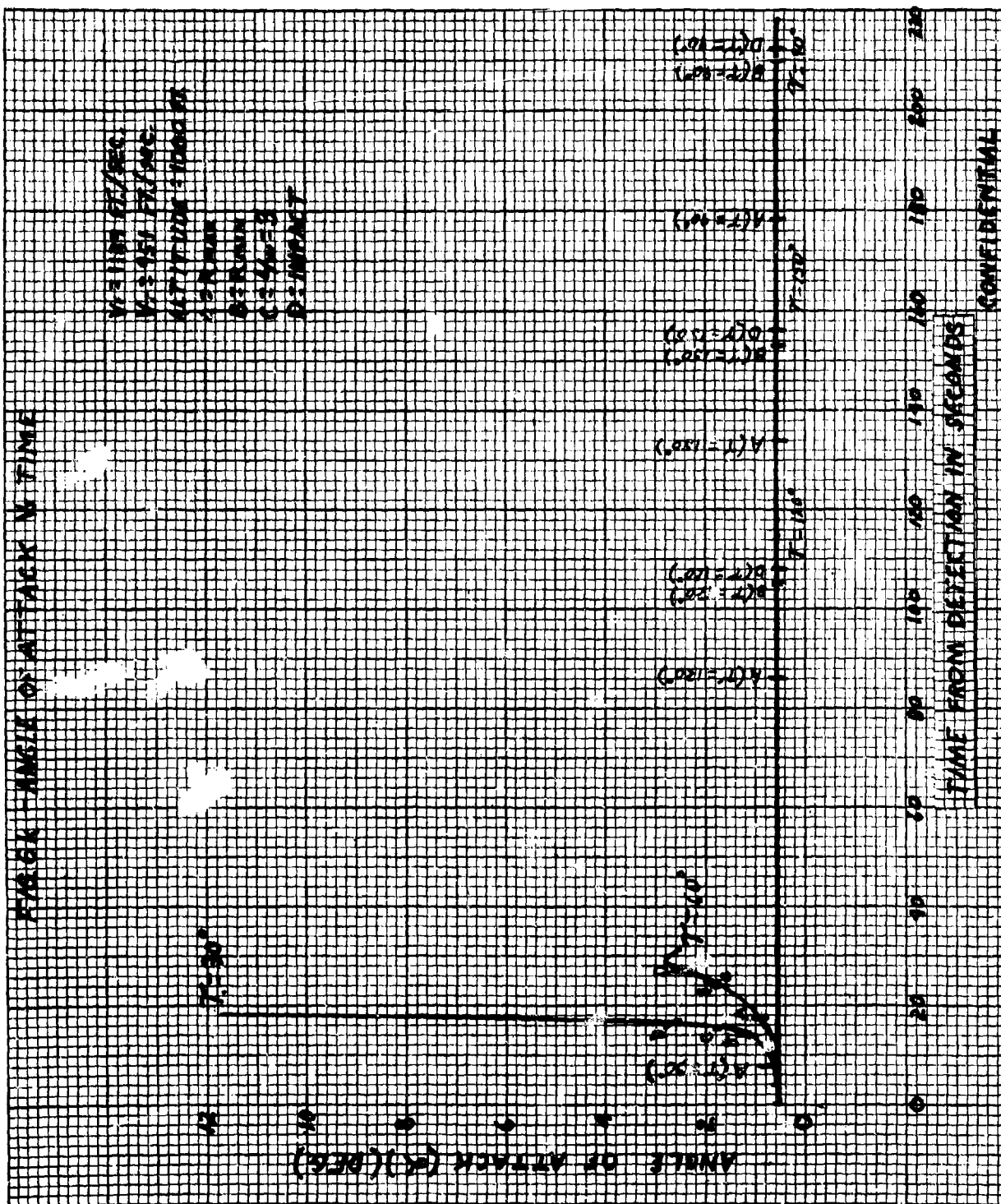


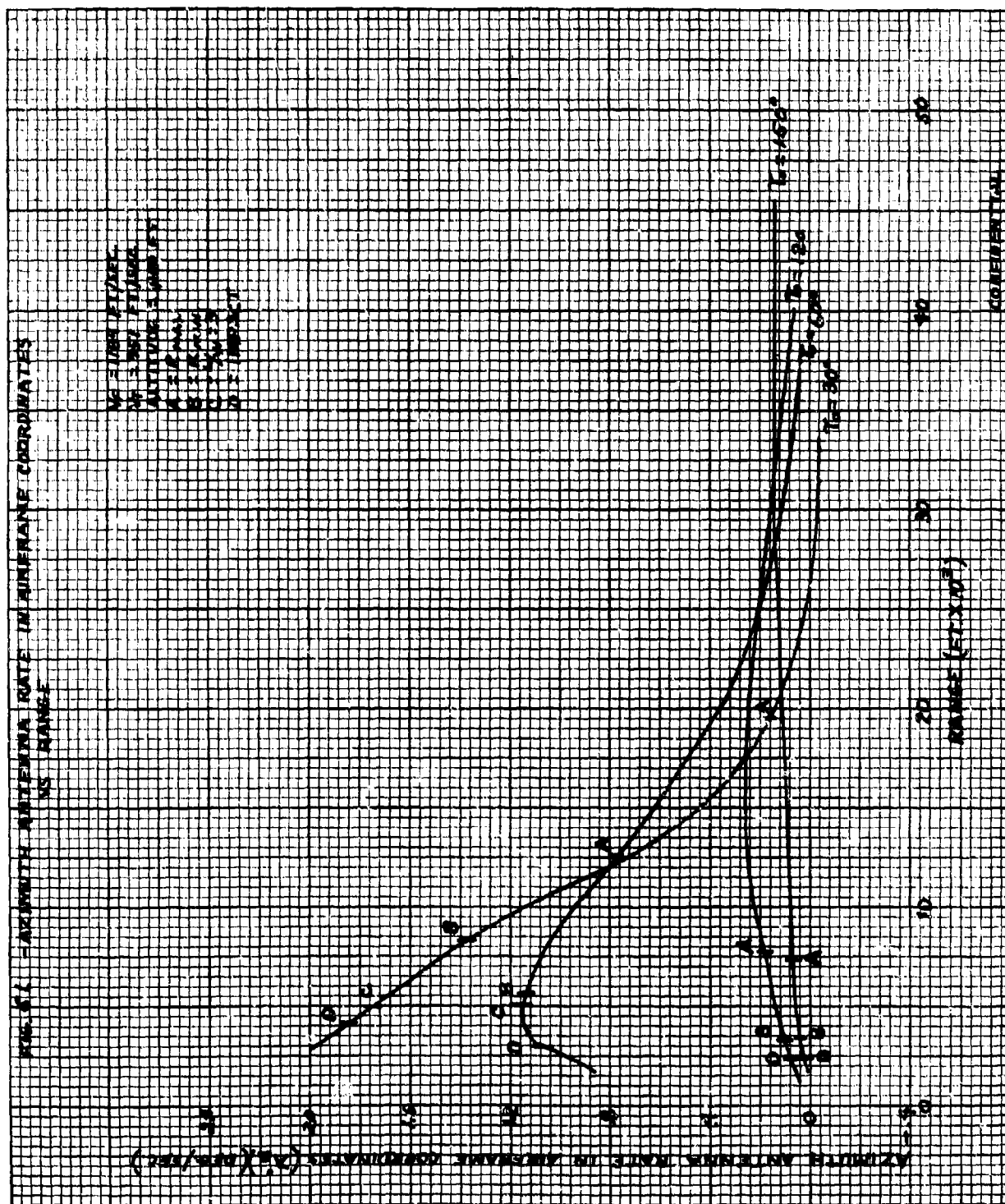


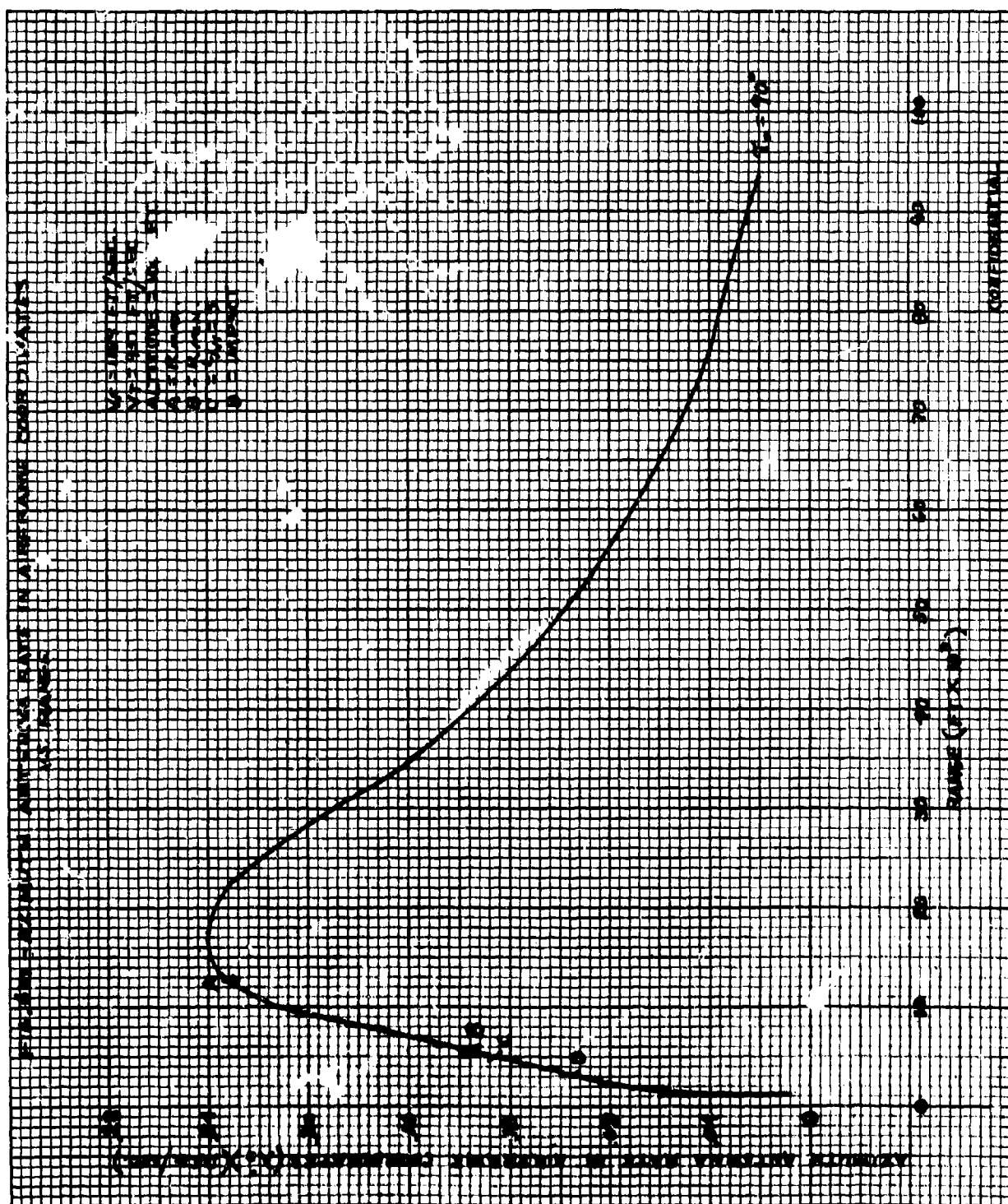
FIGURE 1- FIGHTER VELOCITY vs TIME

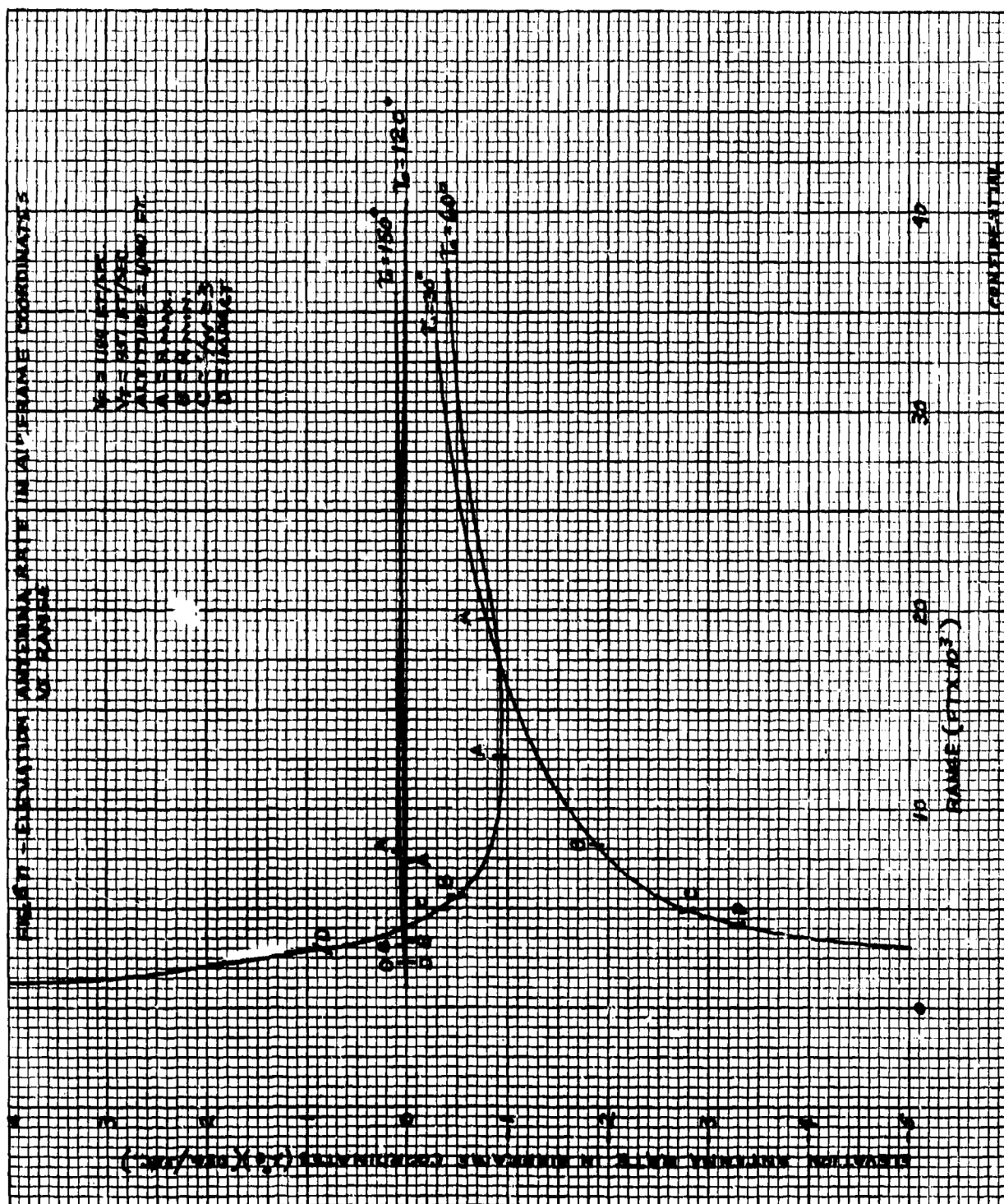


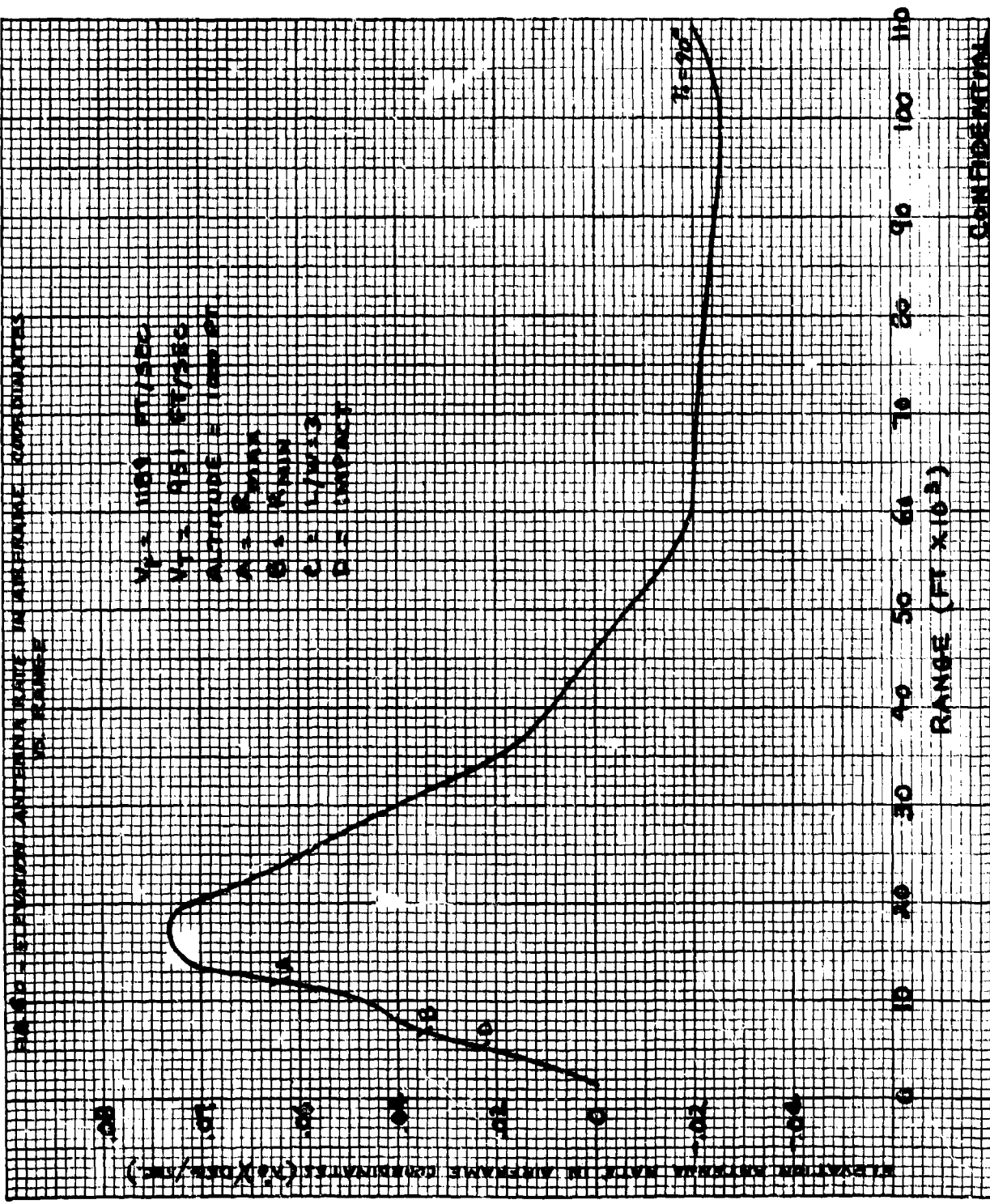
CONFIDENTIAL



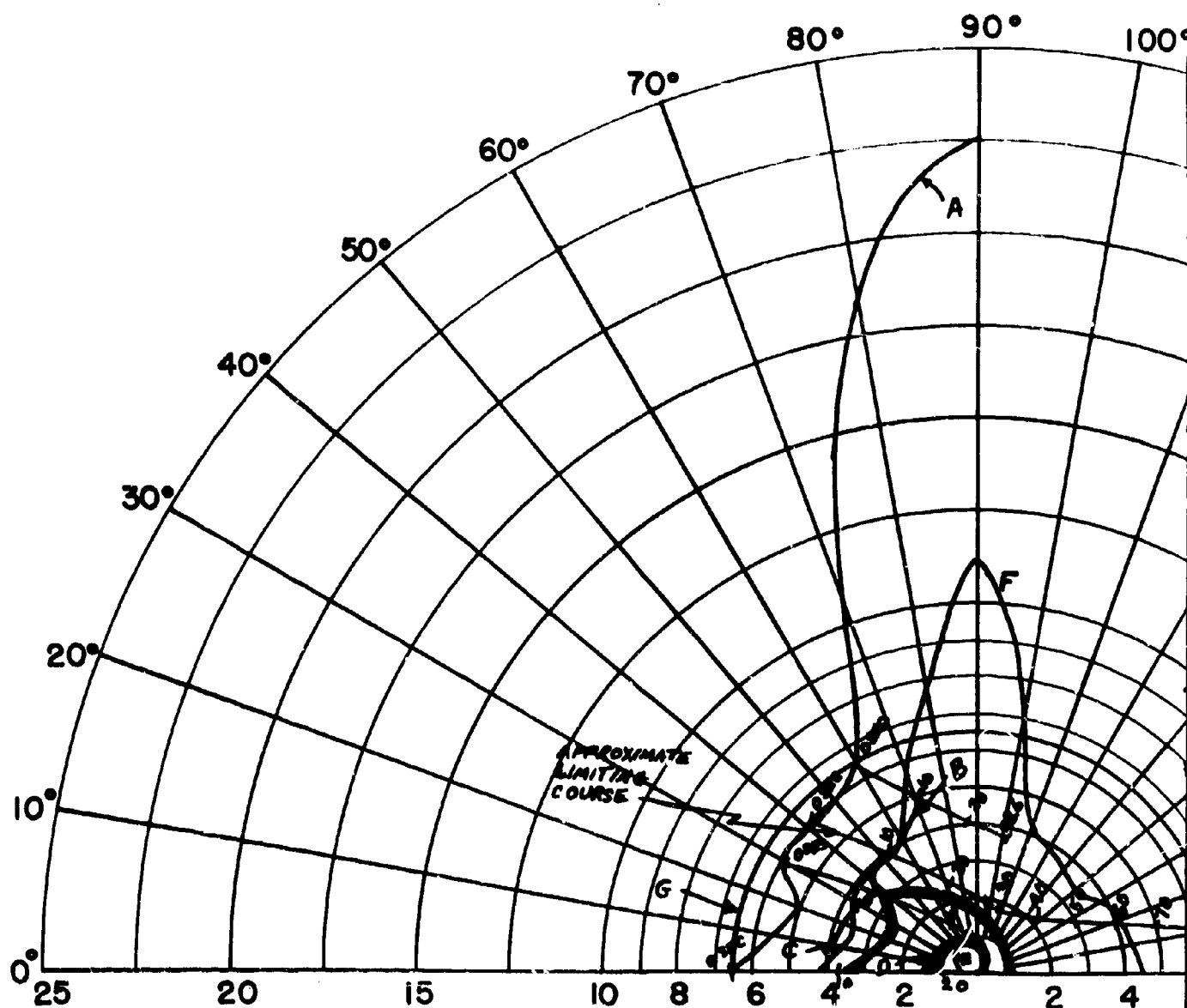








CONFIDENTIAL



$V_F = 556$ FT/SEC (F4H-1)(FBU-3)

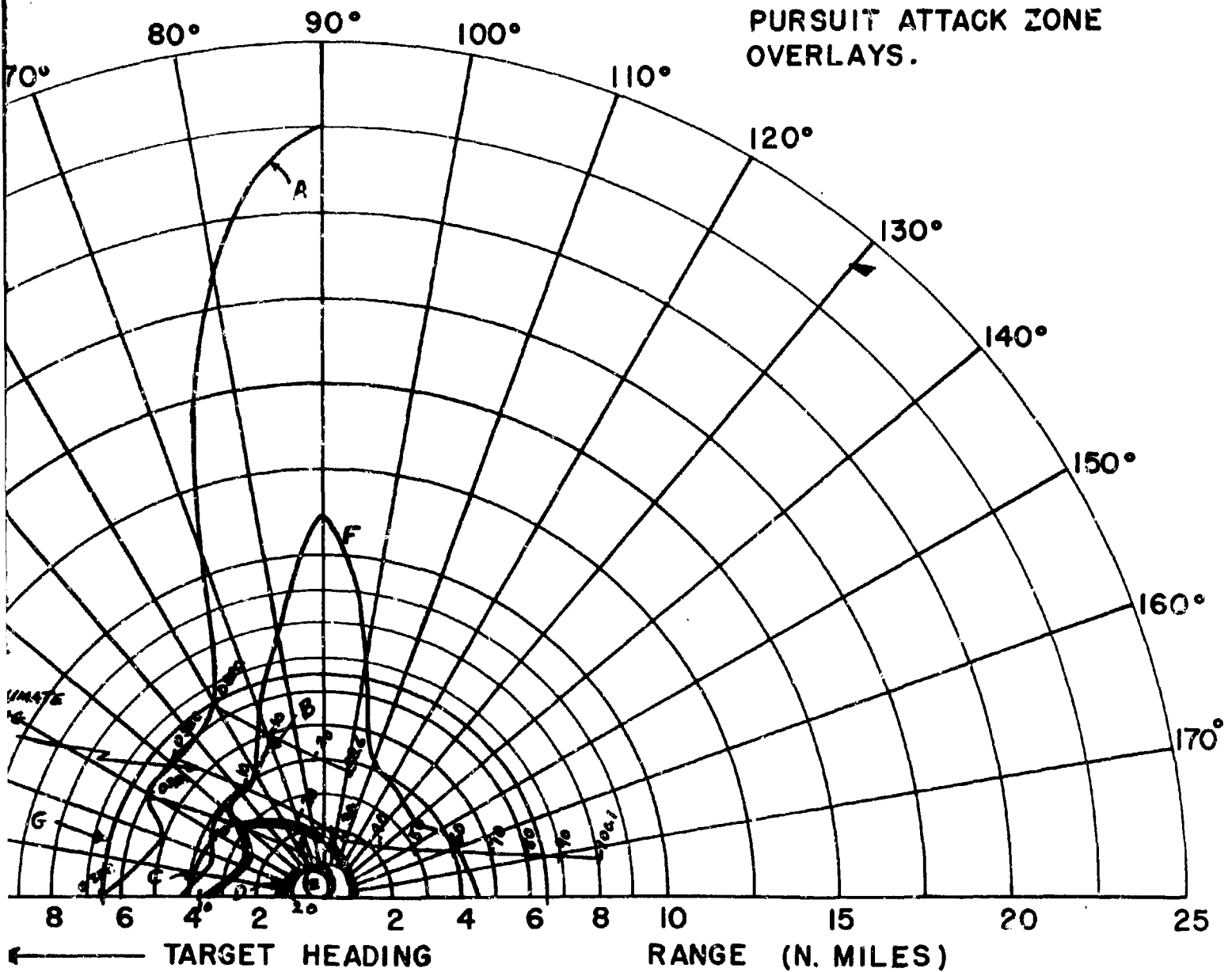
$V_T = 1189$ FT/SEC

ALTITUDE = 1000 FT.

← TARGET HEADING

- A - 85% DETECTION RANGE
- B - LOCK-ON RANGE (10 SEC. LOCK-ON)
- C - SPARROW III MAX. AERODYNAMIC
- D - SPARROW III MIN. AERODYNAMIC
- E - CONSTANT LOAD FACTOR LOG
- F - 90% SPARROW III SEEKER LOG
- G - 6.5 N.M. INTERLOCK

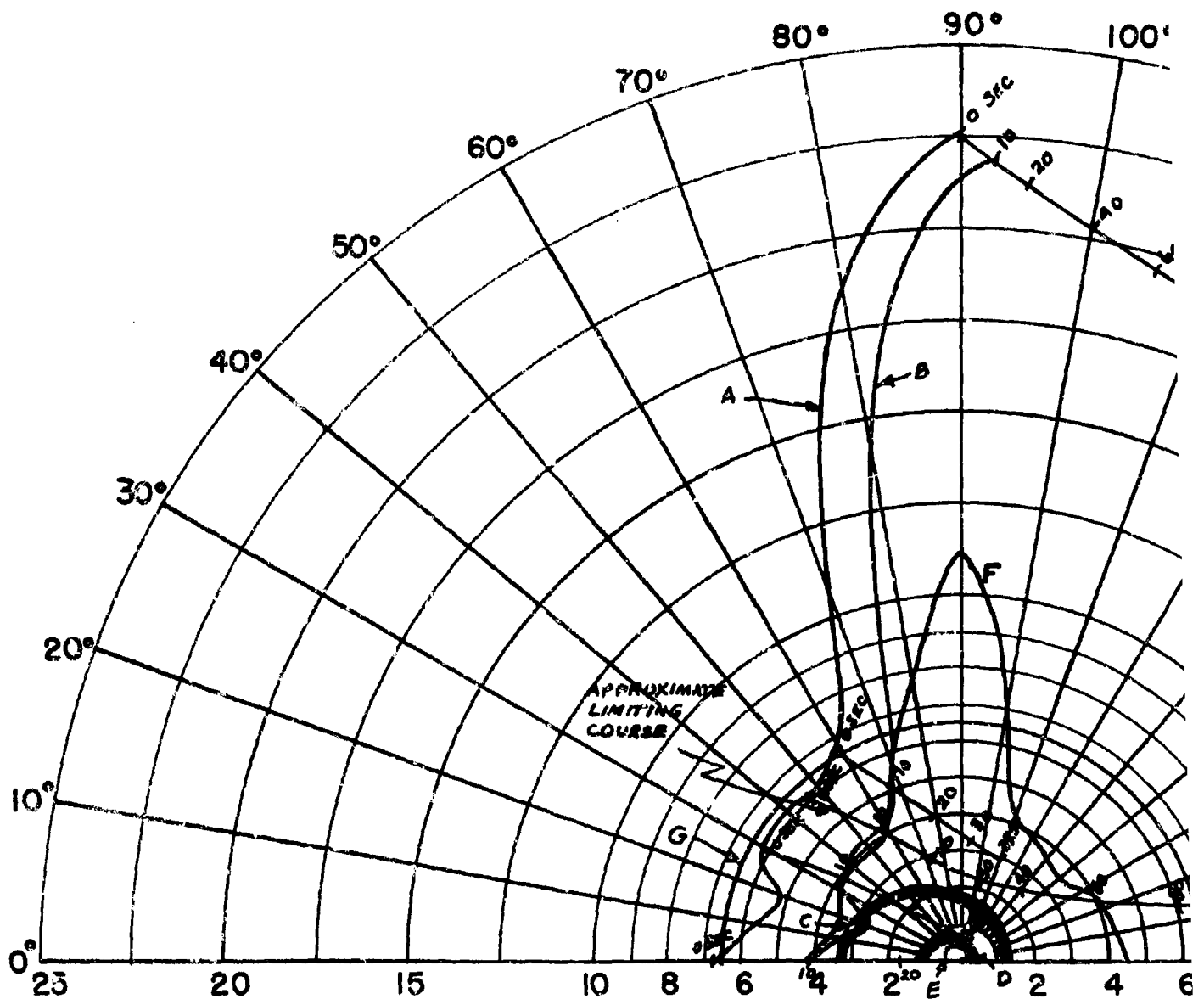
FIG. 8 - CO-ALTITUDE LEAD
PURSUIT ATTACK ZONE
OVERLAYS.



- 85% DETECTION RANGE
- LOCK-ON RANGE (10 SEC. LOCK-ON TIME)
- SPARROW III MAX. AERODYNAMIC RANGE
- SPARROW III MIN. AERODYNAMIC RANGE
- CONSTANT LOAD FACTOR LOCUS ($N_z = 3$)
- 90% SPARROW III SEEKER LOCK-ON RANGE
- 6.5 N.M. INTERLOCK

2

CONFIDENTIAL

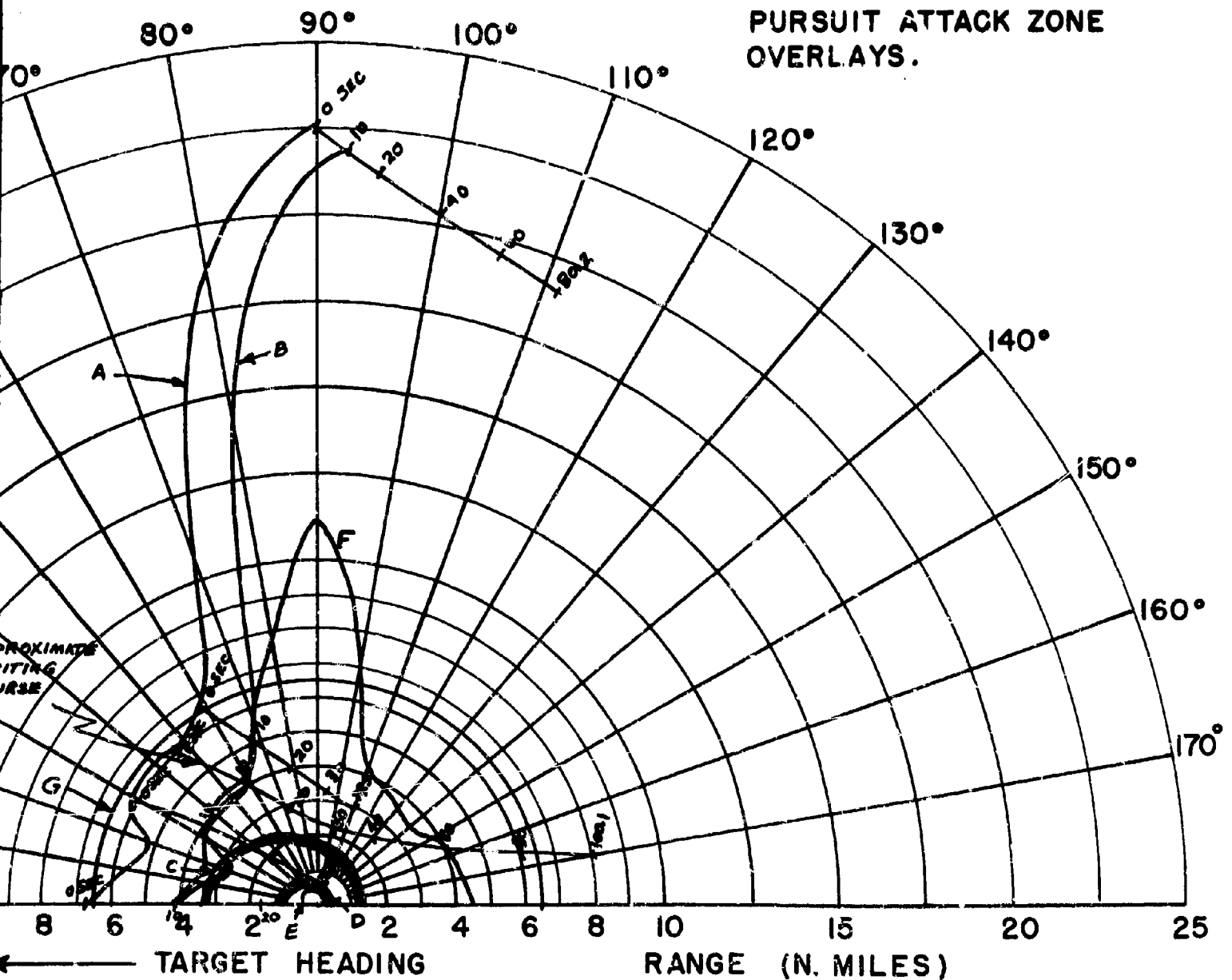


$V_F = 556$ FT/SEC (F4H-1)(F8U-3)
 $V_T = 951$ FT/SEC
 ALTITUDE = 1,000 FT.

← TARGET HEADING

- A - 85% DETECTION RANGE
- B - LOCK-ON RANGE (10 SEC. LOCK-ON)
- C - SPARROW III MAX. AERODYNAMIC
- D - SPARROW III MIN. AERODYNAMIC
- E - CONSTANT LOAD FACTOR LOCUS
- F - 90% SPARROW III SEEKER LOCUS
- G - 6.5 N.M. INTERLOCK

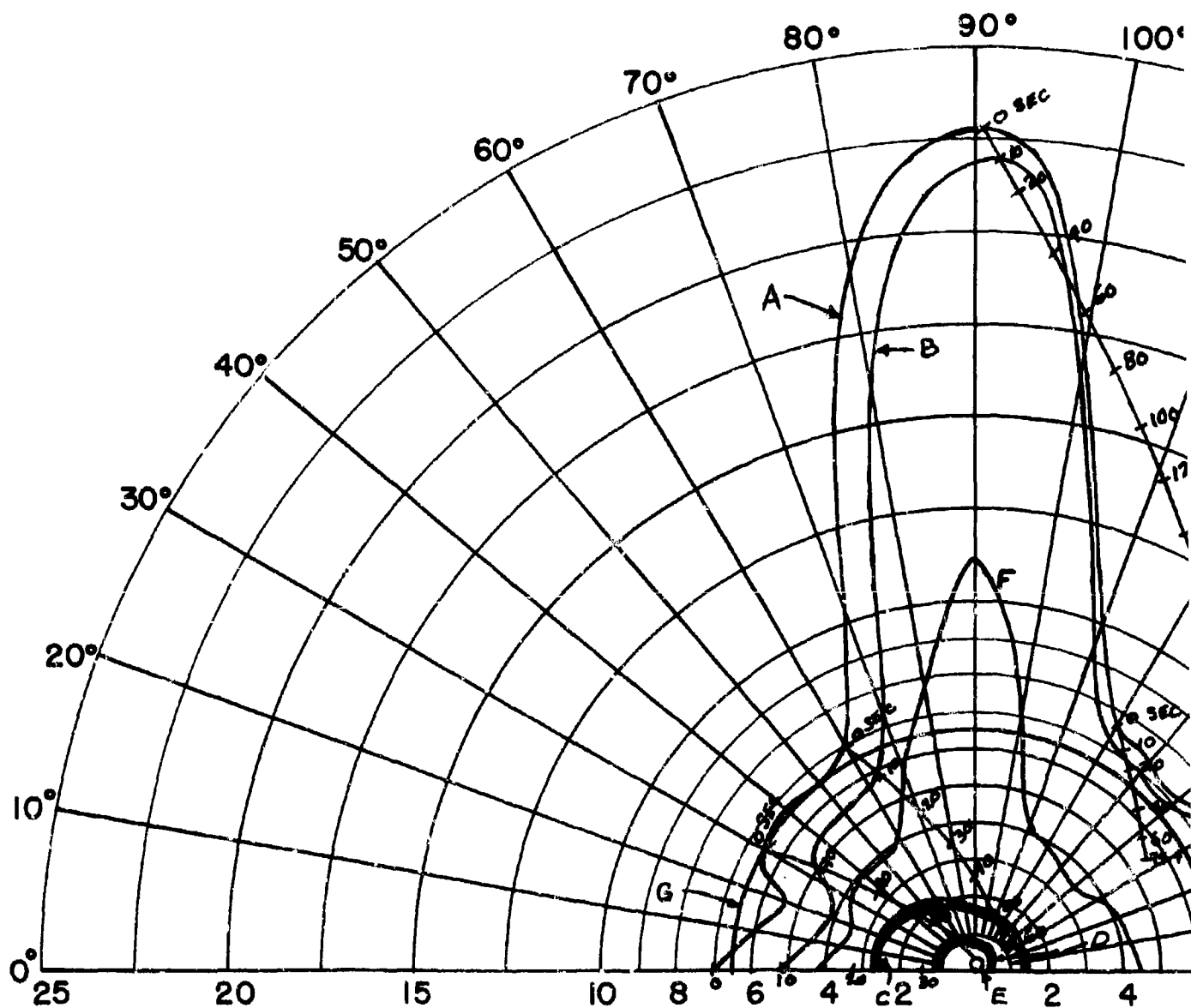
FIG. 9 - CO-ALTITUDE LEAD
PURSUIT ATTACK ZONE
OVERLAYS.



- 85% DETECTION RANGE
- LOCK-ON RANGE (10 SEC. LOCK-ON TIME)
- SPARROW III MAX. AERODYNAMIC RANGE
- SPARROW III MIN. AERODYNAMIC RANGE
- CONSTANT LOAD FACTOR LOCUS ($N_z = 3$)
- 90% SPARROW III SEEKER LOCK-ON RANGE
- 6.5 N.M. INTERLOCK

2

CONFIDENTIAL



$V_F = 556$ FT/SEC (F4H-1)(F8U-3)

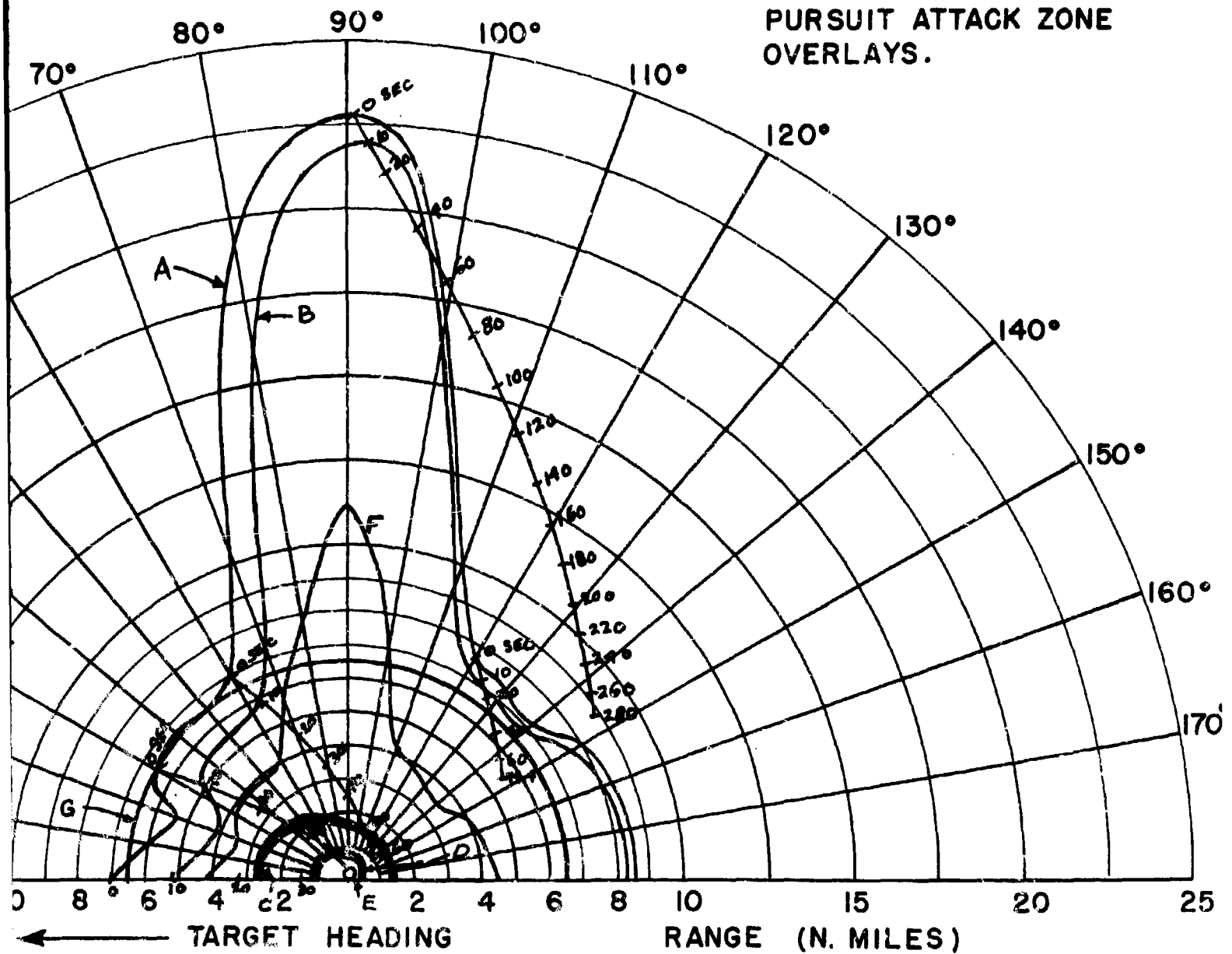
$V_T = 533$ FT/SEC

ALTITUDE = 1000 FT.

← TARGET HEADING

- A - 85% DETECTION RANGE
- B - LOCK-ON RANGE (10 SEC. LOCK-ON)
- C - SPARROW III MAX. AERODYNAMIC
- D - SPARROW III MIN. AERODYNAMIC
- E - CONSTANT LOAD FACTOR LOCUS
- F - 90% SPARROW III SEEKER LOCK
- G - 6.5 N.M. INTERLOCK

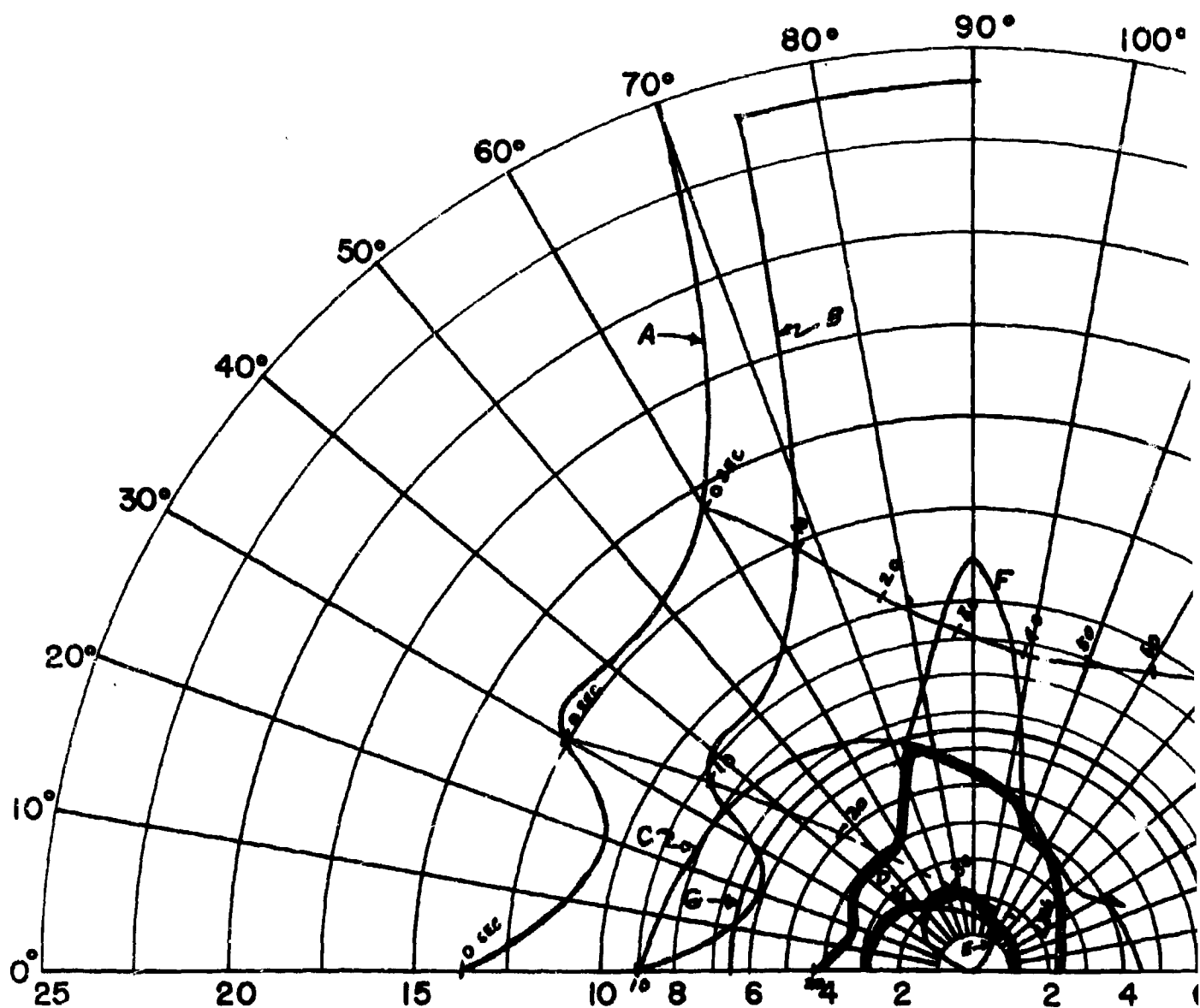
FIG. 10 - CO-ALTITUDE LEAD PURSUIT ATTACK ZONE OVERLAYS.



- A - 85% DETECTION RANGE
- B - LOCK-ON RANGE (10 SEC. LOCK-ON TIME)
- C - SPARROW III MAX. AERODYNAMIC RANGE
- D - SPARROW III MIN. AERODYNAMIC RANGE
- E - CONSTANT LOAD FACTOR LOCUS ($N_2 = 3$)
- F - 90% SPARROW III SEEKER LOCK-ON RANGE
- G - 6.5 N.M. INTERLOCK

2

CONFIDENTIAL



$V_F = 873$ FT/SEC (F4H-1)(F8U-3)

$V_T = 1940$ FT/SEC

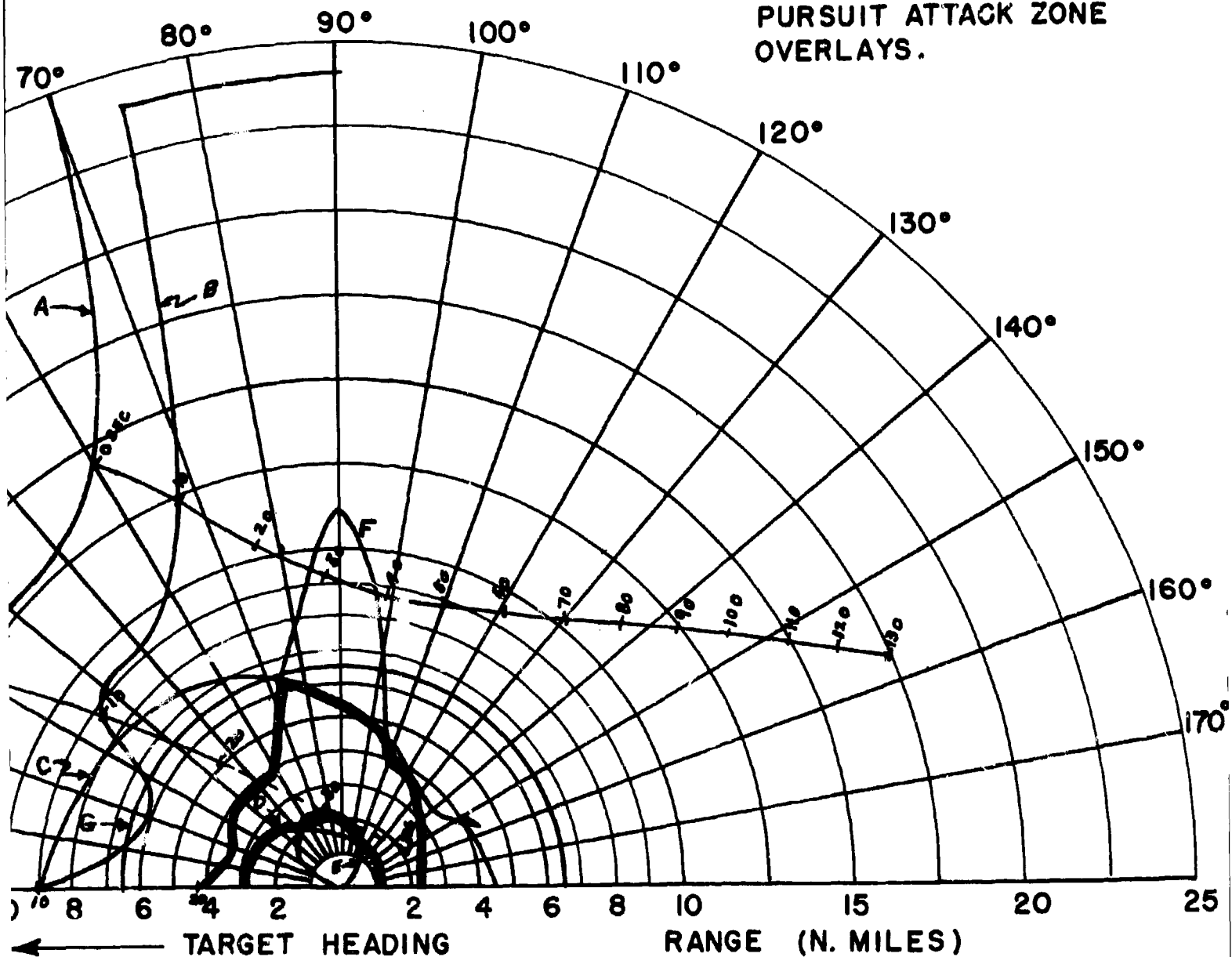
ALTITUDE = 50,000 FT.

INCREASED THRUST AT DETECTION

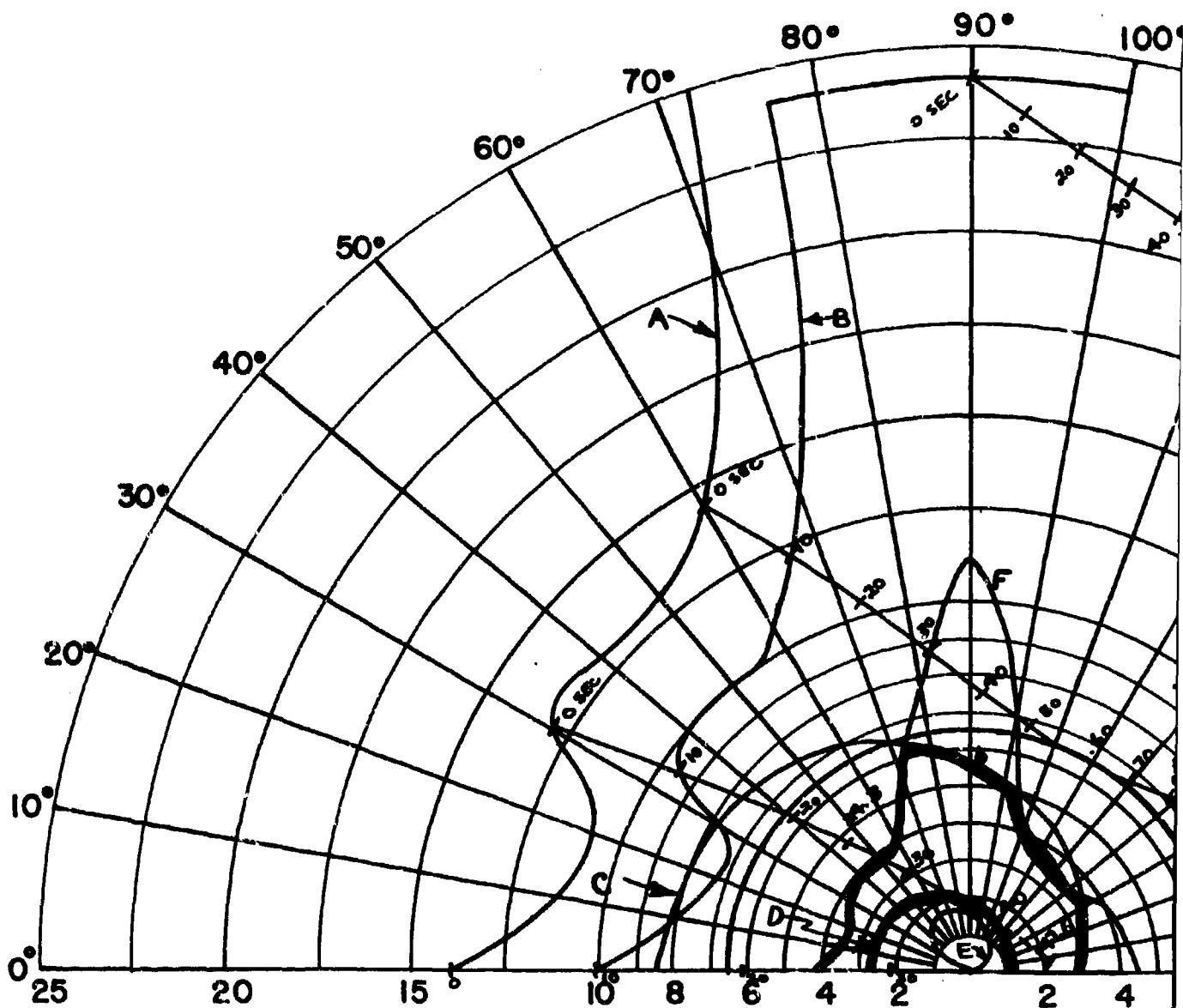
← TARGET HEADING

- A - 85% DETECTION RANGE
- B - LOCK-ON RANGE (10 SEC. LOCK-ON)
- C - SPARROW III MAX. AERODYNAMIC
- D - SPARROW III MIN. AERODYNAMIC
- E - CONSTANT LOAD FACTOR LOCUS
- F - 90% SPARROW III SEEKER LOCK
- G - 6.5 N.M. INTERLOCK

FIG. 11 - CO-ALTITUDE LEAD
PURSUIT ATTACK ZONE
OVERLAYS.



CONFIDENTIAL



$V_F = 873$ FT/SEC (F4H-1)(F8U-3)

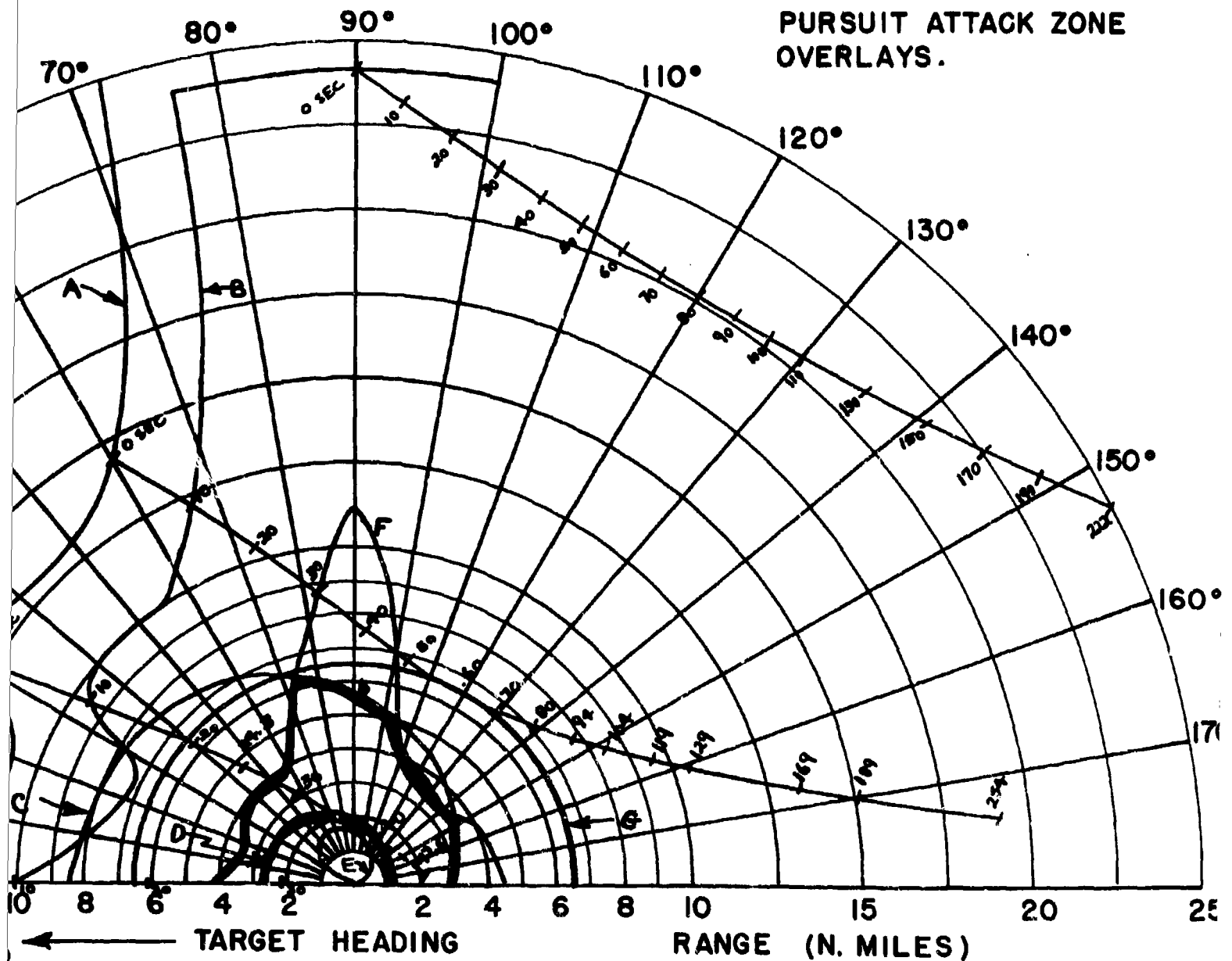
$V_T = 1552$ FT/SEC

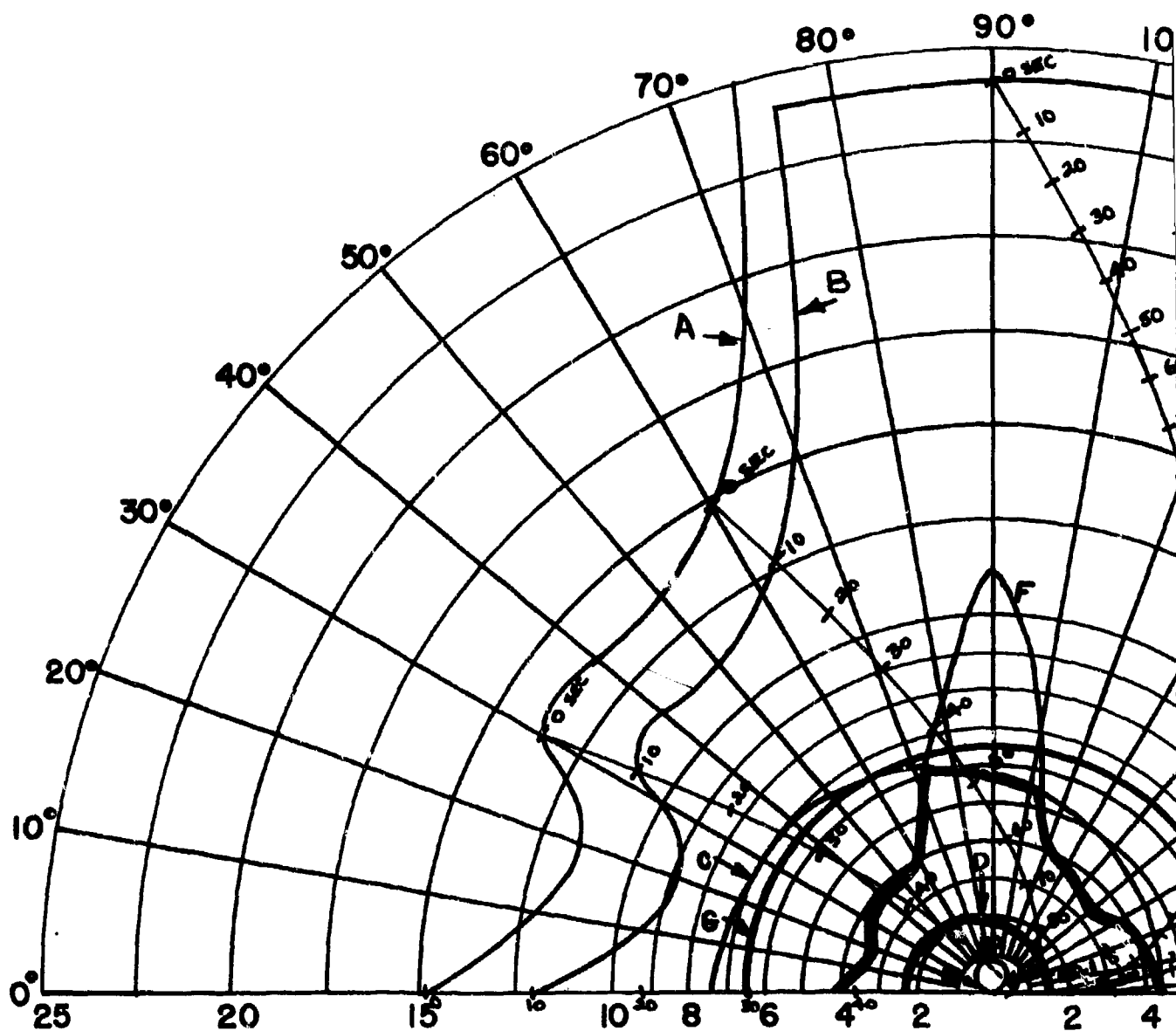
ALTITUDE = 50,000 FT.
INCREASED THRUST AT DETECTION

← TARGET HEADING

- A - 85% DETECTION RANGE
- B - LOCK-ON RANGE (10 SEC. LOCK)
- C - SPARROW III MAX. AERODYNAM
- D - SPARROW III MIN. AERODYNAM
- E - CONSTANT LOAD FACTOR LOC
- F - 90% SPARROW III SEEKER L
- G - 6.5 N.M. INTERLOCK

FIG. 12 - CO-ALTITUDE LEAD PURSUIT ATTACK ZONE OVERLAYS.





$V_F = 873$ FT/SEC (F4H-1)(F8U-3)

$V_T = 873$ FT/SEC

ALTITUDE = 50,000 FT.
INCREASED THRUST AT DETECTION

← TARGET HEADING

- A - 85% DETECTION RANGE
- B - LOCK-ON RANGE (10 SEC. LOCK)
- C - SPARROW III MAX. AERODYNAMIC
- D - SPARROW III MIN. AERODYNAMIC
- E - CONSTANT LOAD FACTOR
- F - 90% SPARROW III SEEKER
- G - 6.5 N.M. INTERLOCK

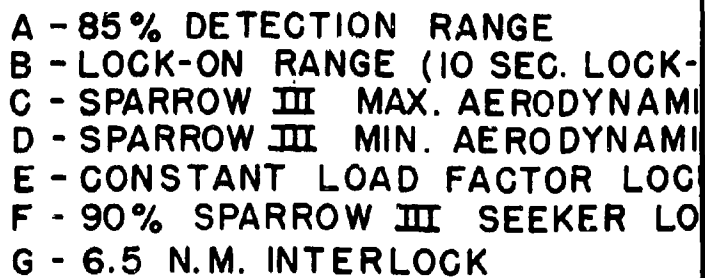
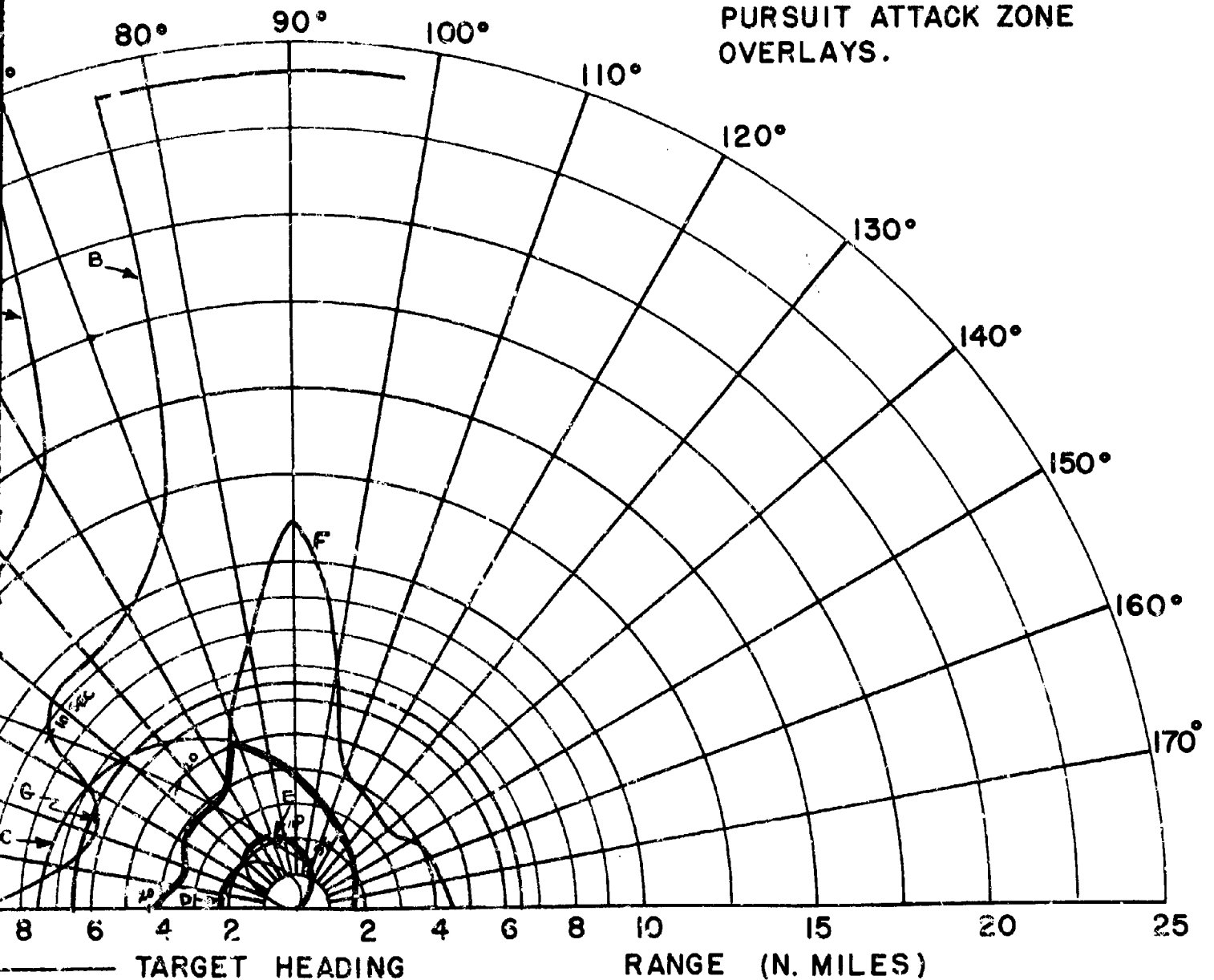


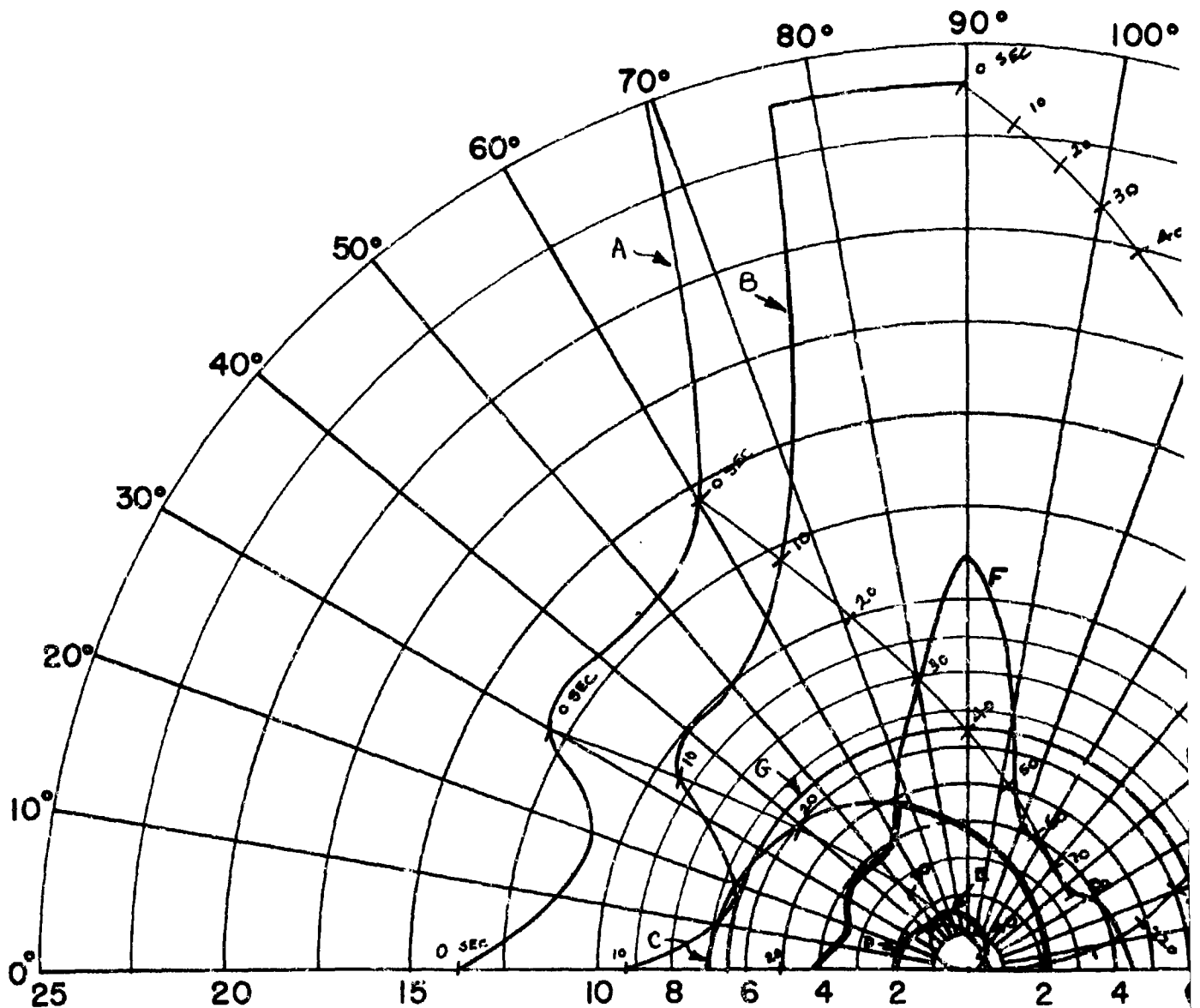
FIG. 14 - CO-ALTITUDE LEAD
PURSUIT ATTACK ZONE
OVERLAYS.



85% DETECTION RANGE
LOCK-ON RANGE (10 SEC. LOCK-ON TIME)
SPARROW III MAX. AERODYNAMIC RANGE
SPARROW III MIN. AERODYNAMIC RANGE
CONSTANT LOAD FACTOR LOCUS ($N_z = 3$)
90% SPARROW III SEEKER LOCK-ON RANGE
0.5 N.M. INTERLOCK

2

CONFIDENTIAL



$V_F = 894$ FT/SEC (F4H-1)(F8U-3)

$V_T = 1518$ FT/SEC

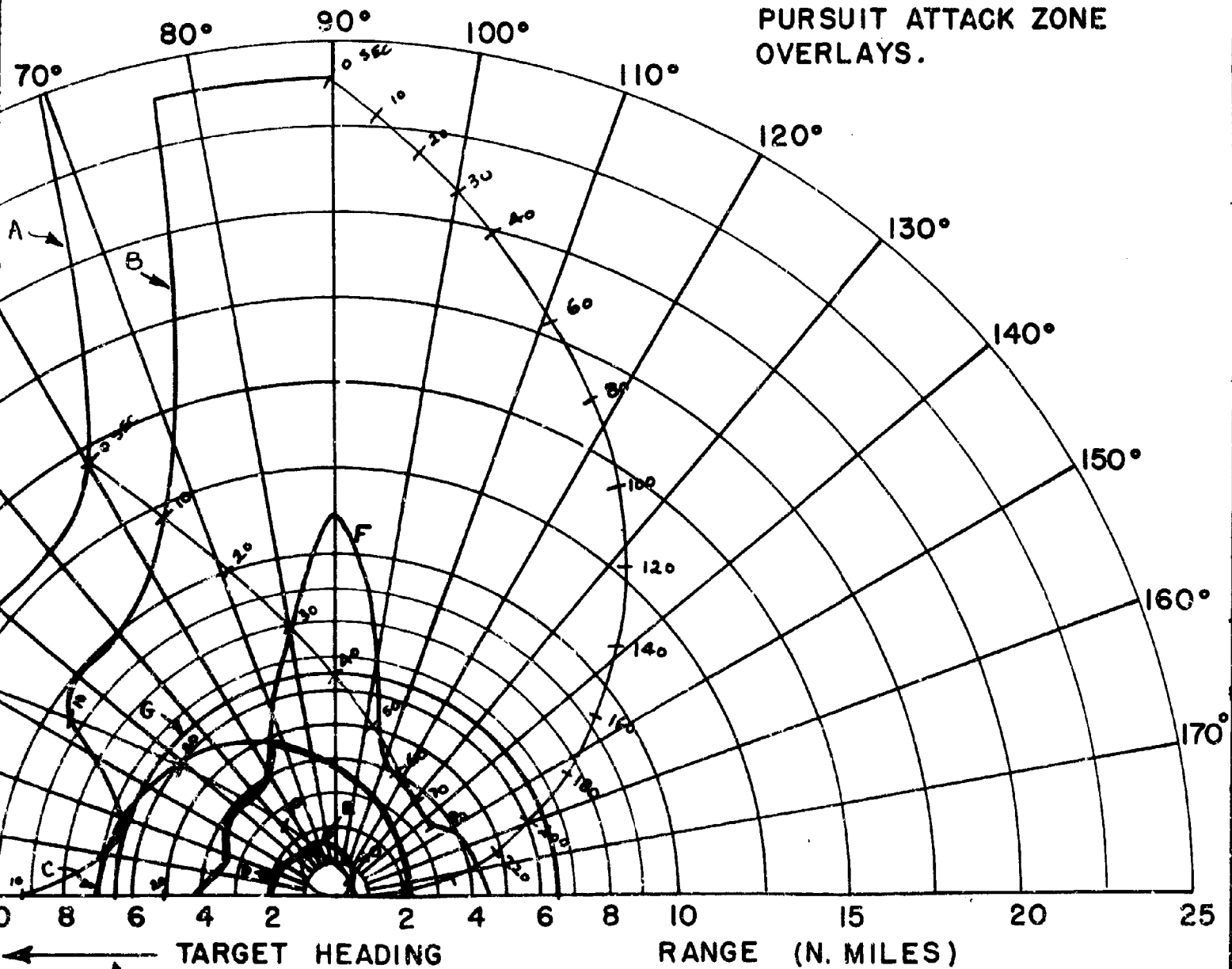
ALTITUDE = 30,000 FT.

INCREASED THRUST AT DETECTION

TARGET HEADING

- A - 85% DETECTION RANGE
- B - LOCK-ON RANGE (10 SEC. LOCK-ON)
- C - SPARROW III MAX. AERODYNAMIC
- D - SPARROW III MIN. AERODYNAMIC
- E - CONSTANT LOAD FACTOR LOCUS
- F - 90% SPARROW III SEEKER LOCK
- G - 6.5 N.M. INTERLOCK

FIG. 15 - CO-ALTITUDE LEAD
PURSUIT ATTACK ZONE
OVERLAYS.

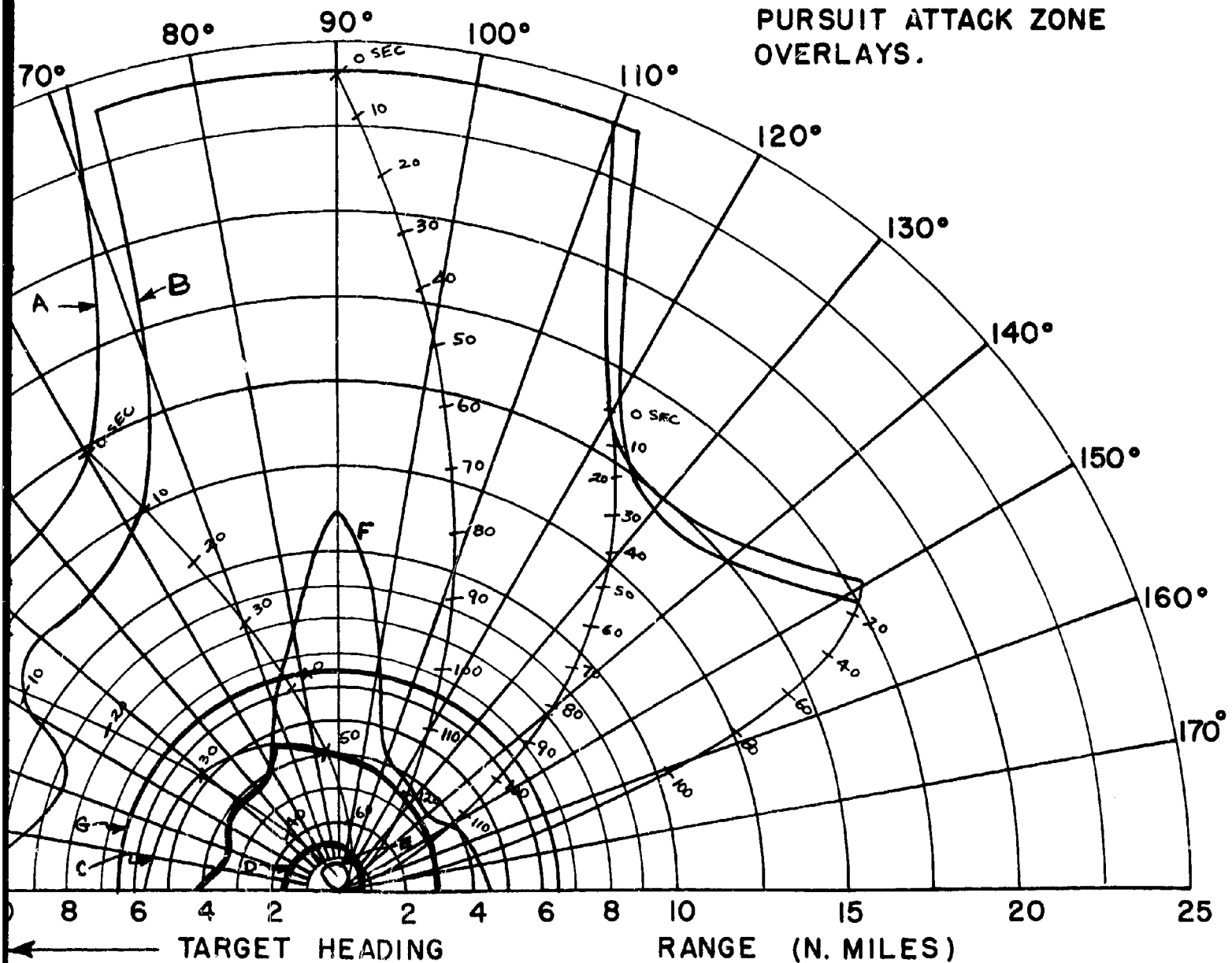


- A - 85% DETECTION RANGE
- B - LOCK-ON RANGE (10 SEC. LOCK-ON TIME)
- C - SPARROW III MAX. AERODYNAMIC RANGE
- D - SPARROW III MIN. AERODYNAMIC RANGE
- E - CONSTANT LOAD FACTOR LOCUS ($N_z = 3$)
- F - 90% SPARROW III SEEKER LOCK-ON RANGE
- G - 6.5 N.M. INTERLOCK

2

CONFIDENTIAL

FIG. 16 - CO-ALTITUDE LEAD
PURSUIT ATTACK ZONE
OVERLAYS.

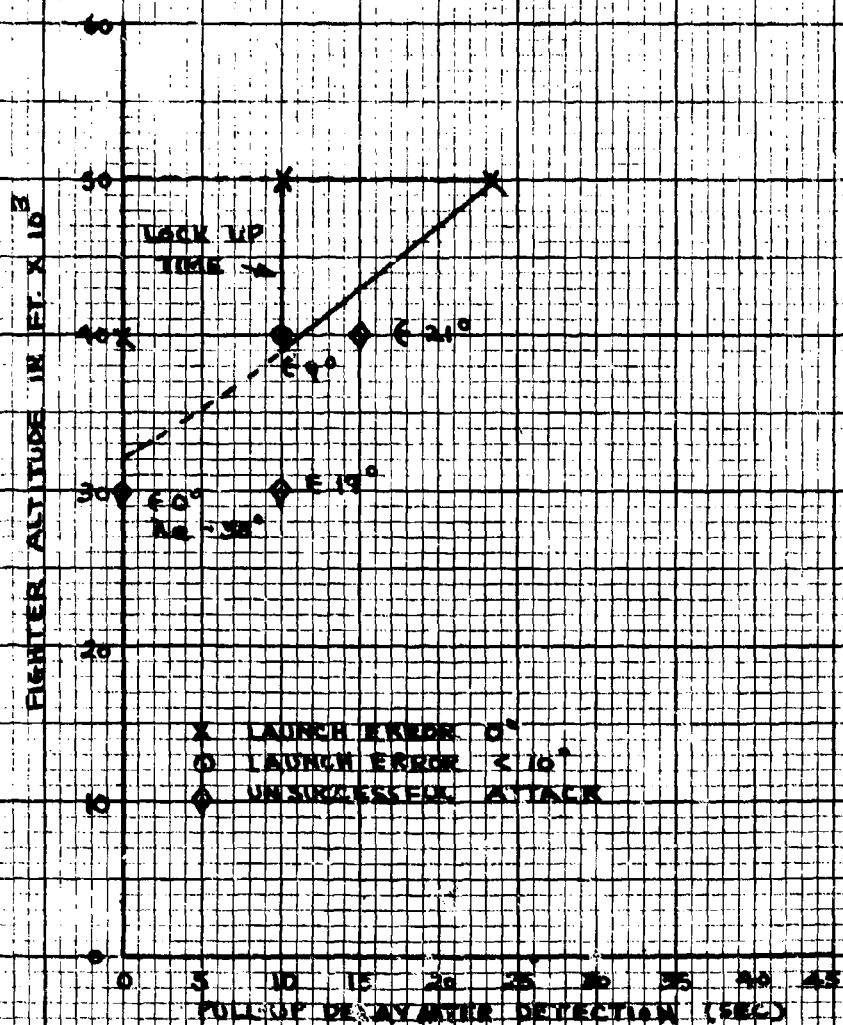


- 85% DETECTION RANGE
- LOCK-ON RANGE (10 SEC. LOCK-ON TIME)
- SPARROW III MAX. AERODYNAMIC RANGE
- SPARROW III MIN. AERODYNAMIC RANGE
- CONSTANT LOAD FACTOR LOCUS ($N_z = 3$)
- 90% SPARROW III SEEKER LOCK-ON RANGE
- 6.5 N.M. INTERLOCK

2

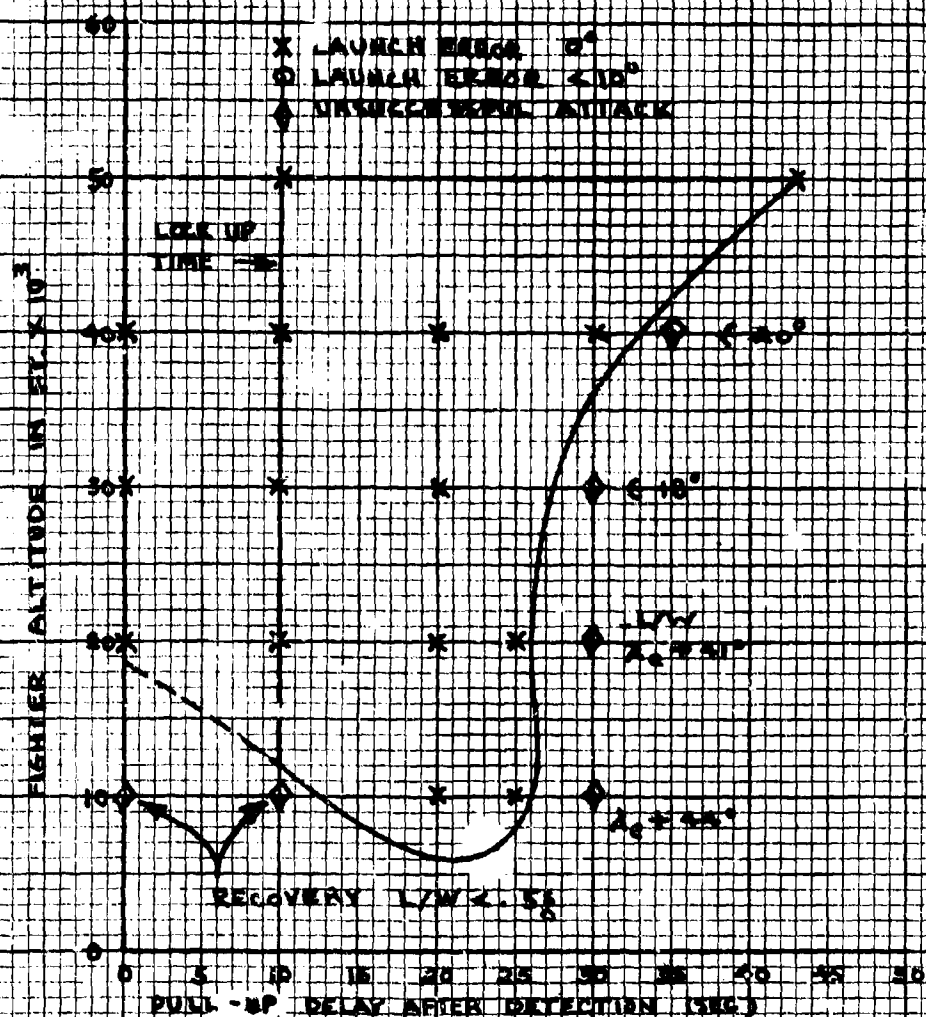
CONFIDENTIAL

FIG. 17 - PULL UP ATTACKS - HEAD ON
 MACH 2.0 TARGET 50,000 FT.
 85% DETECTION PROBABILITY - 641
 PULL UP 30 OR CL MAX
 V_f - MACH 0.9



CONFIDENTIAL

FIG. 18 - PULL-UP ATTACKS - HEAD ON
 RANGE TO TARGET 50,000 FT.
 95% DETECTION PROBABILITY - E-21
 PULL-UP 10 SEC. MAX
 V_p - TRACK 0.1

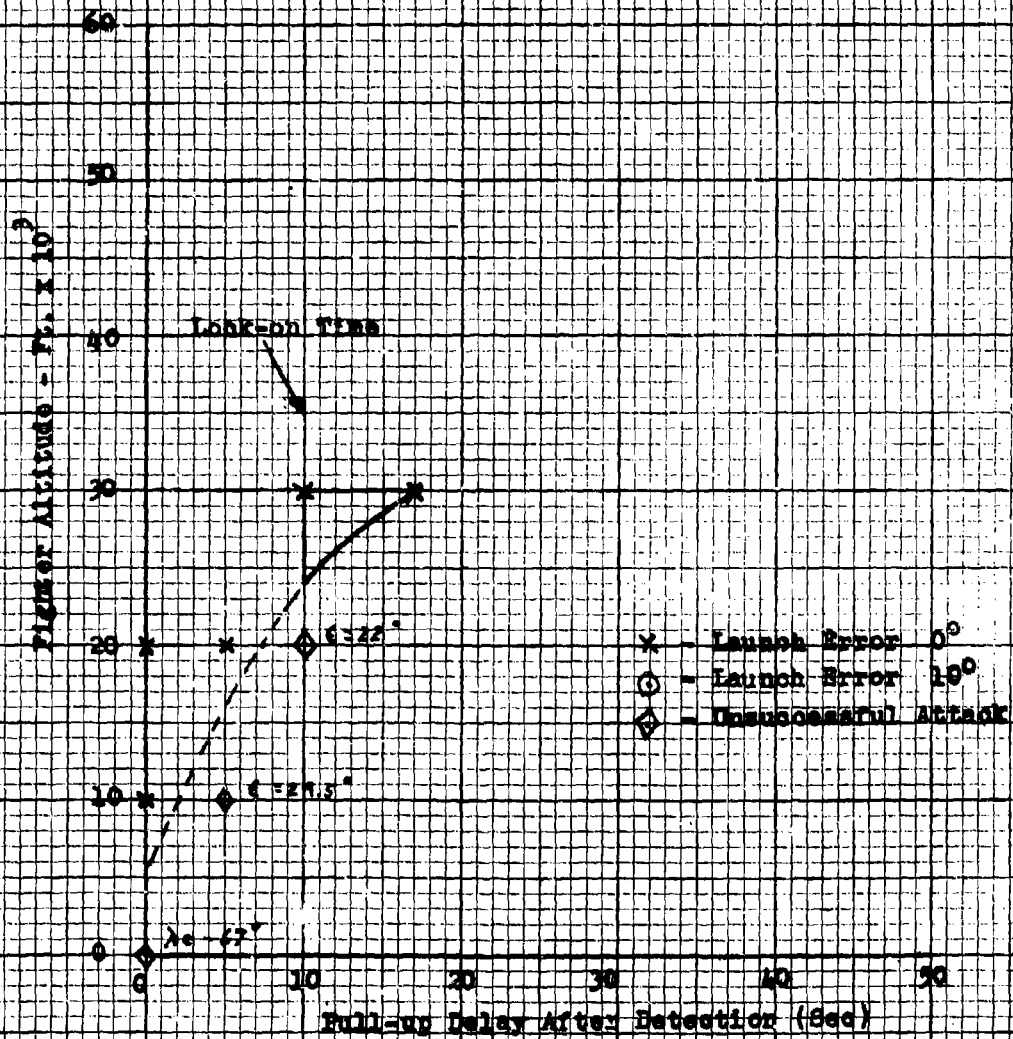


CONFIDENTIAL

Fig. 19 - Pull-up Attack - Head-on

Max 2.0 Target, 30,000 Ft.
 85% Detection Probability - R-17
 Pull-up 1g or 0

V_p Max 2.0 or V_p Max



CONFIDENTIAL

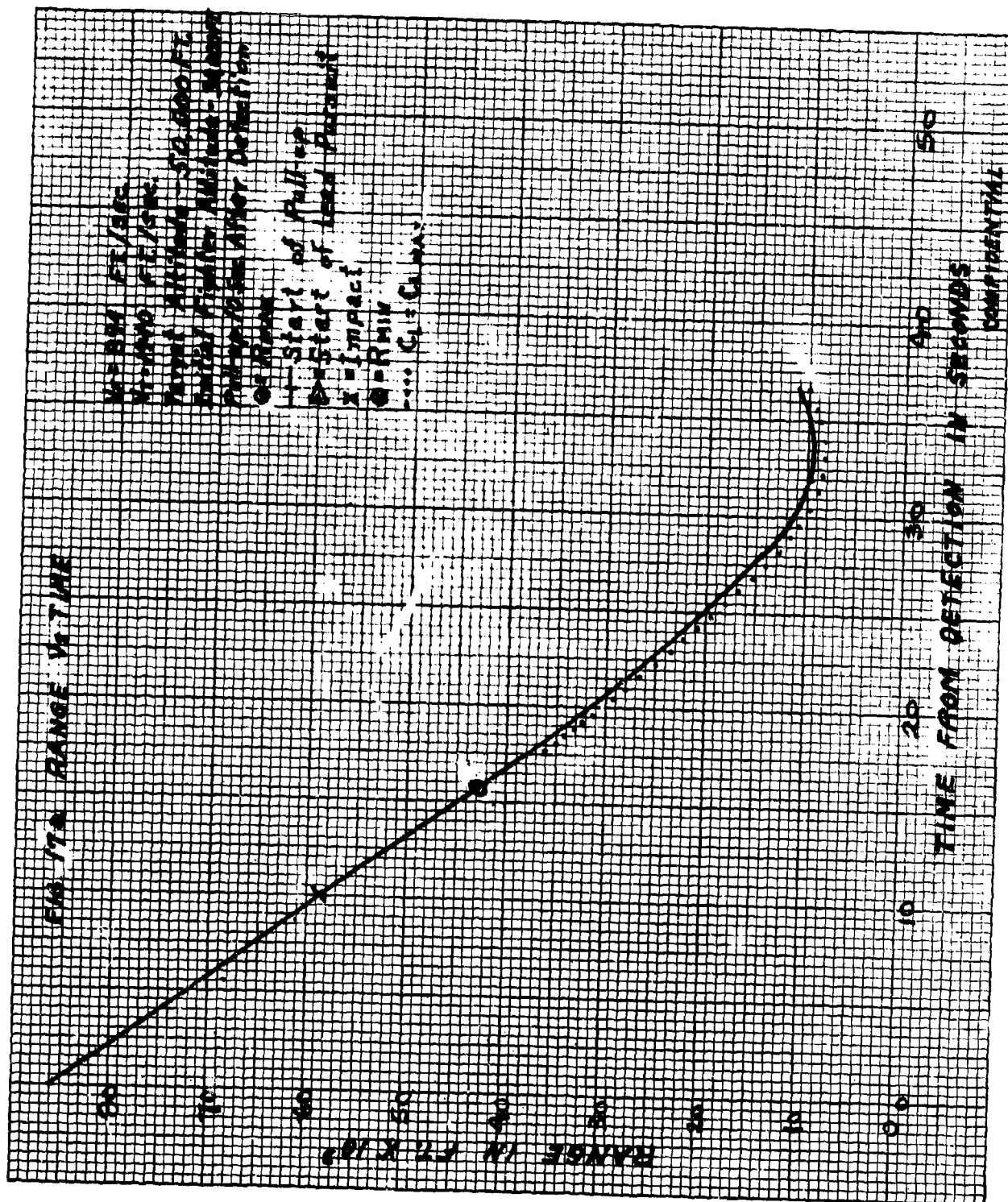
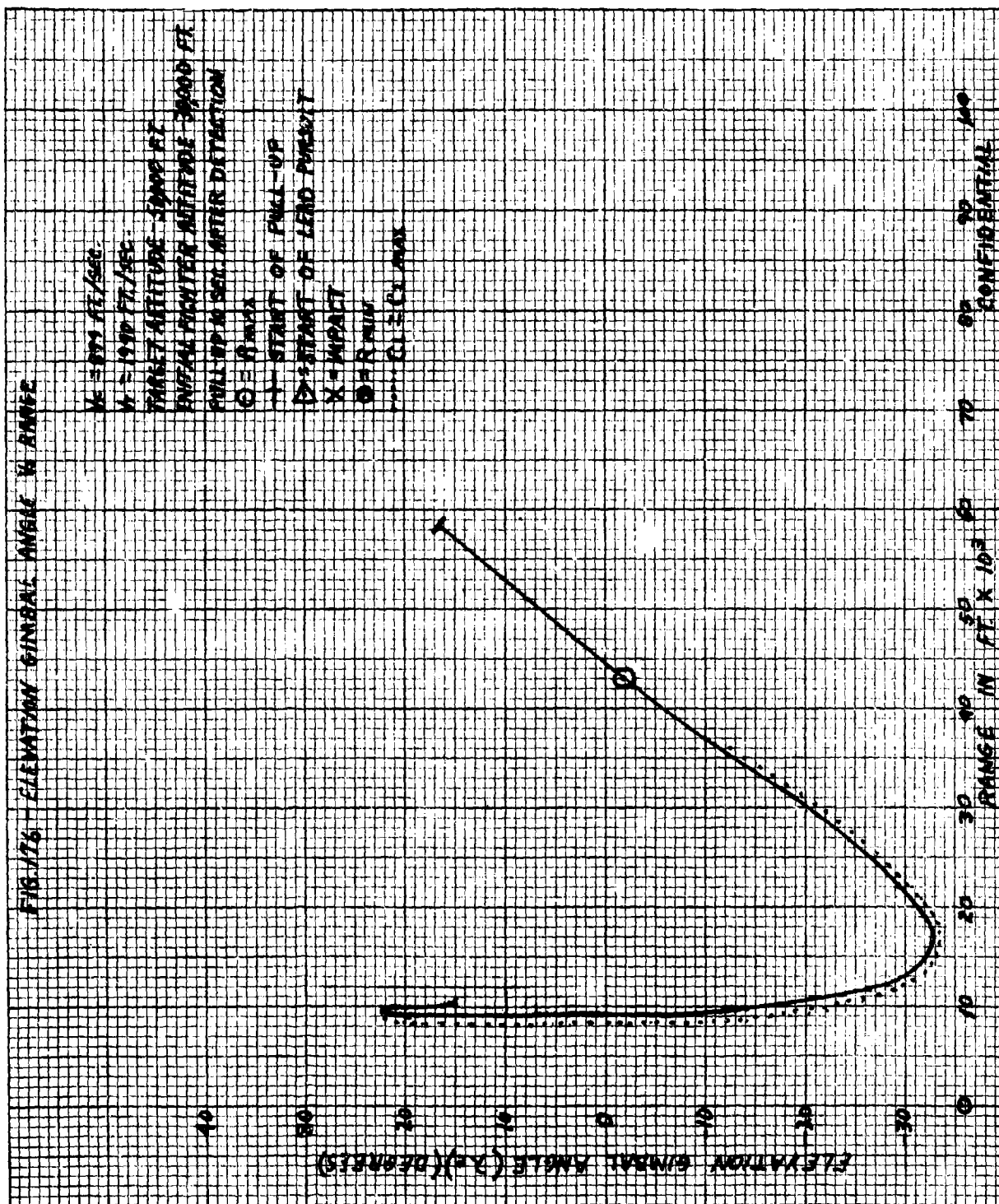


FIG. 176 ELEVATION GIMBAL ANGLE IN RANGE



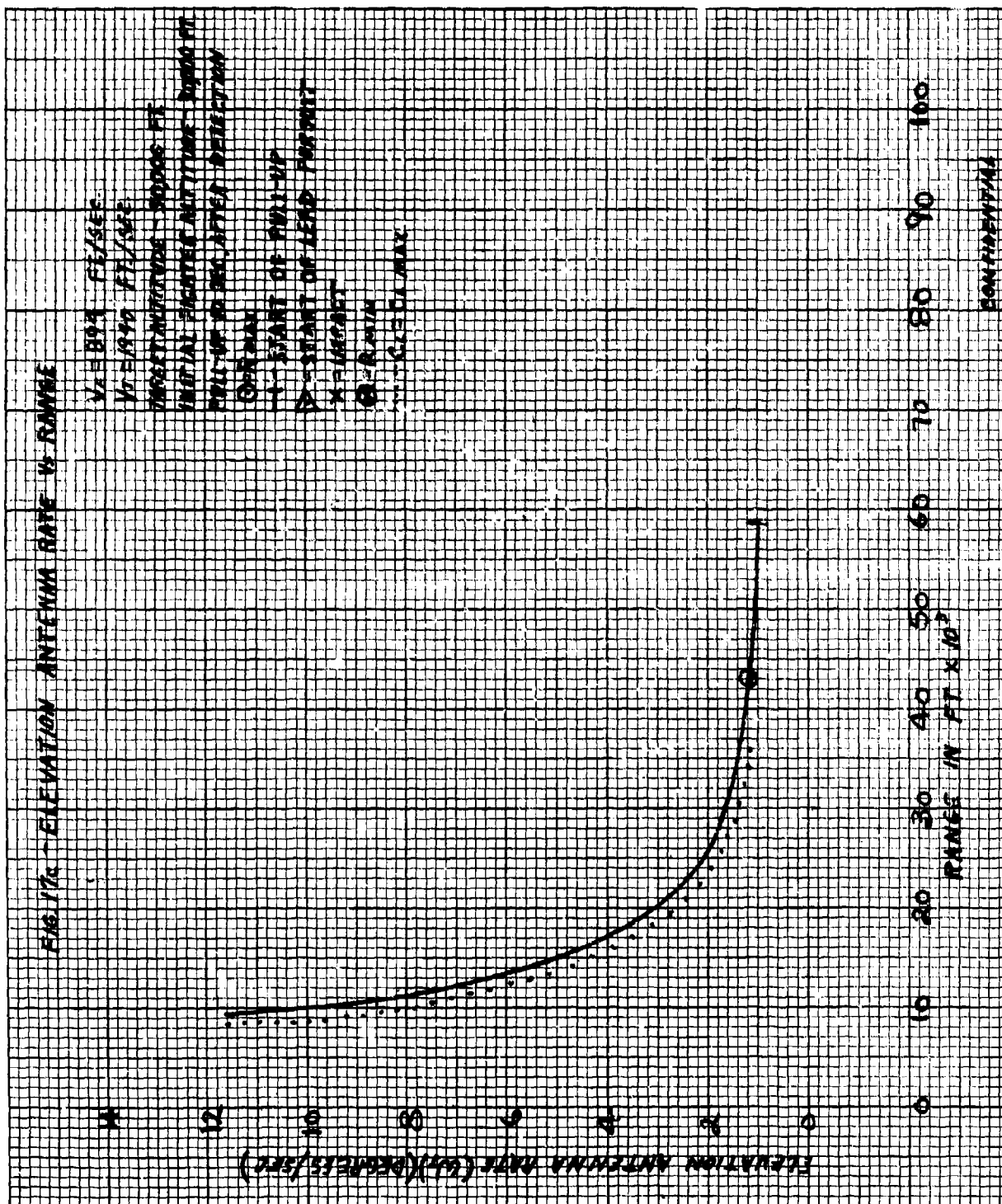
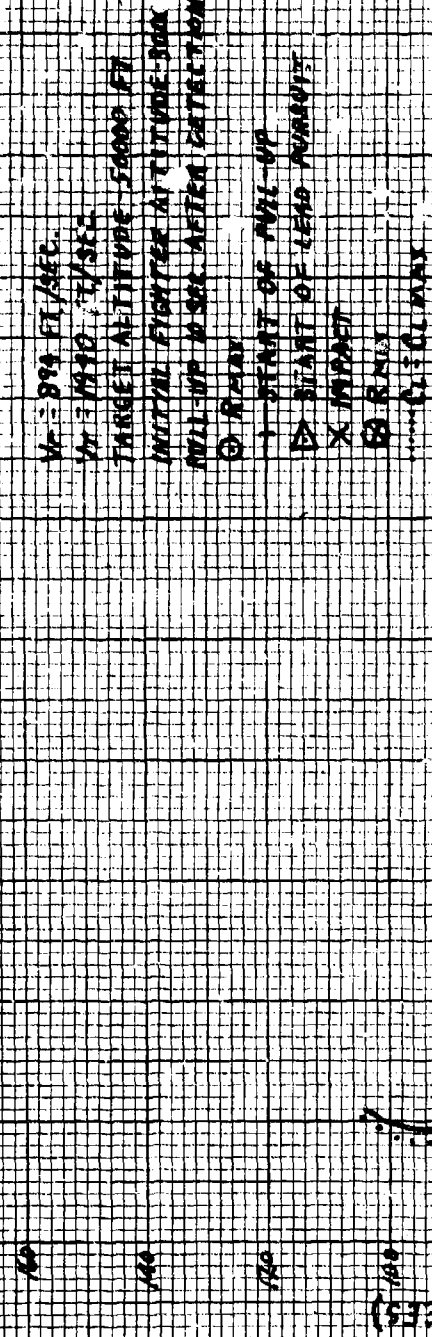
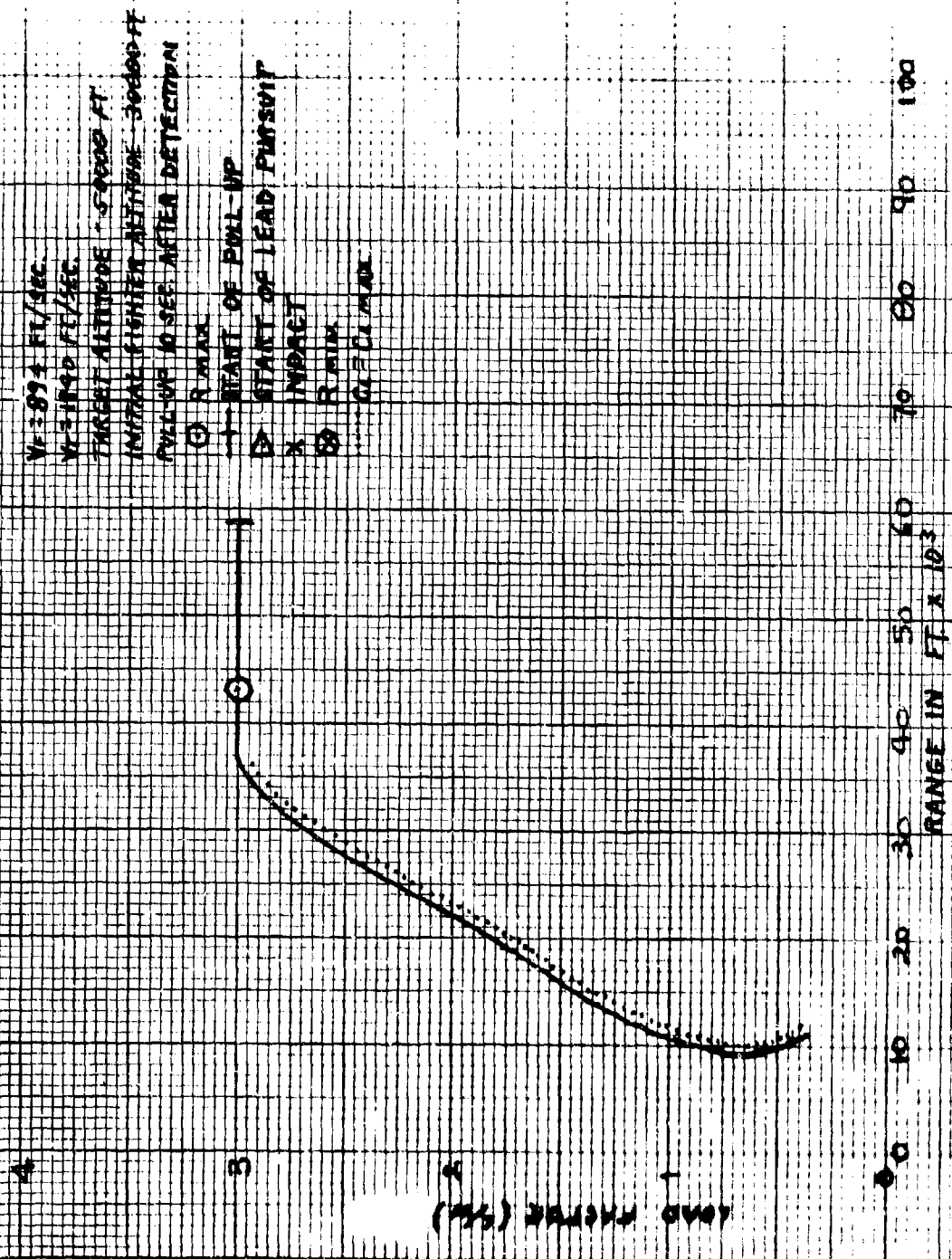


FIG 174 - HEADING ANGLE VS RANGE

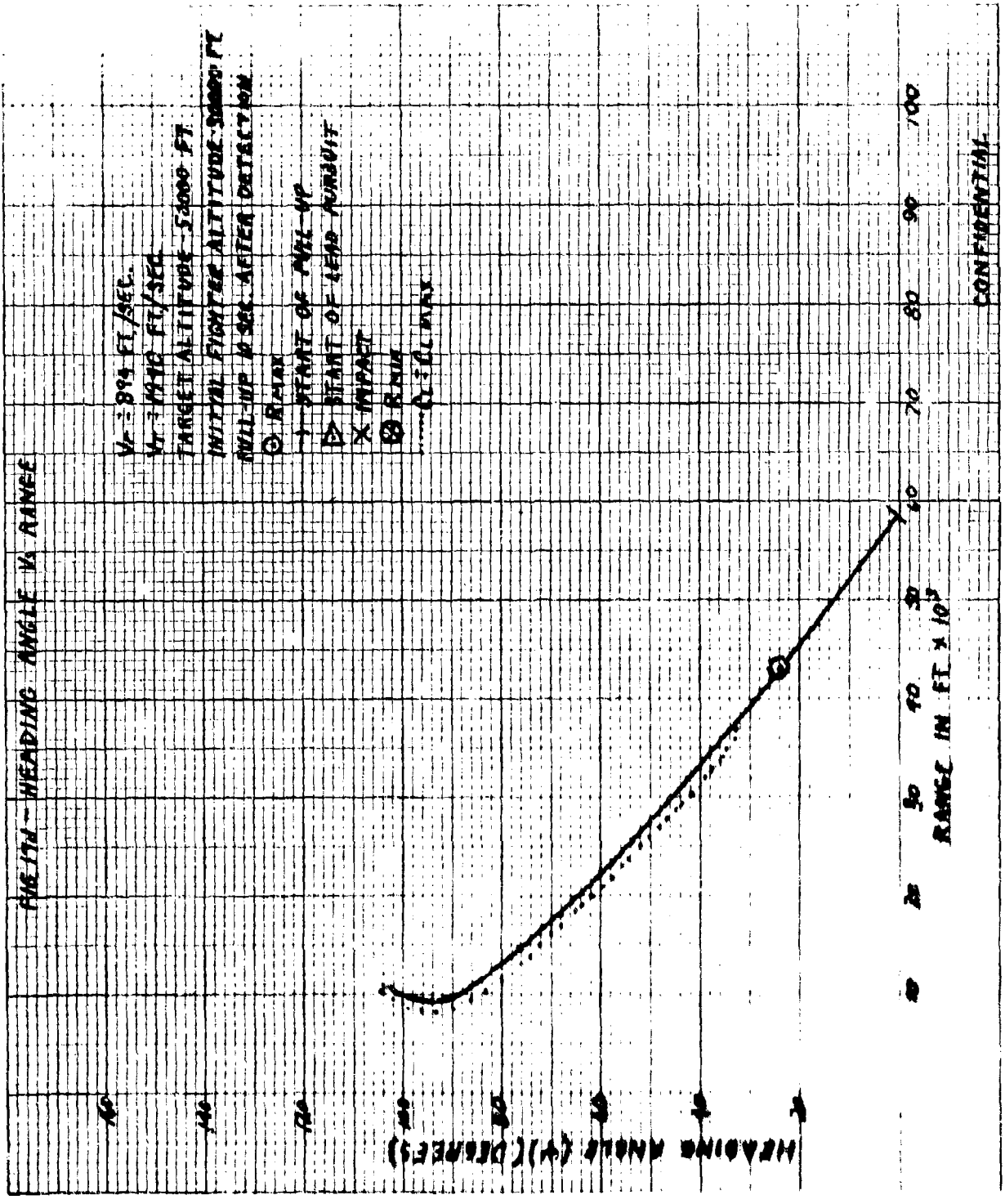


CONFIDENTIAL

FIG 17a LOAD FACTOR VS RANGE



CONFIDENTIAL



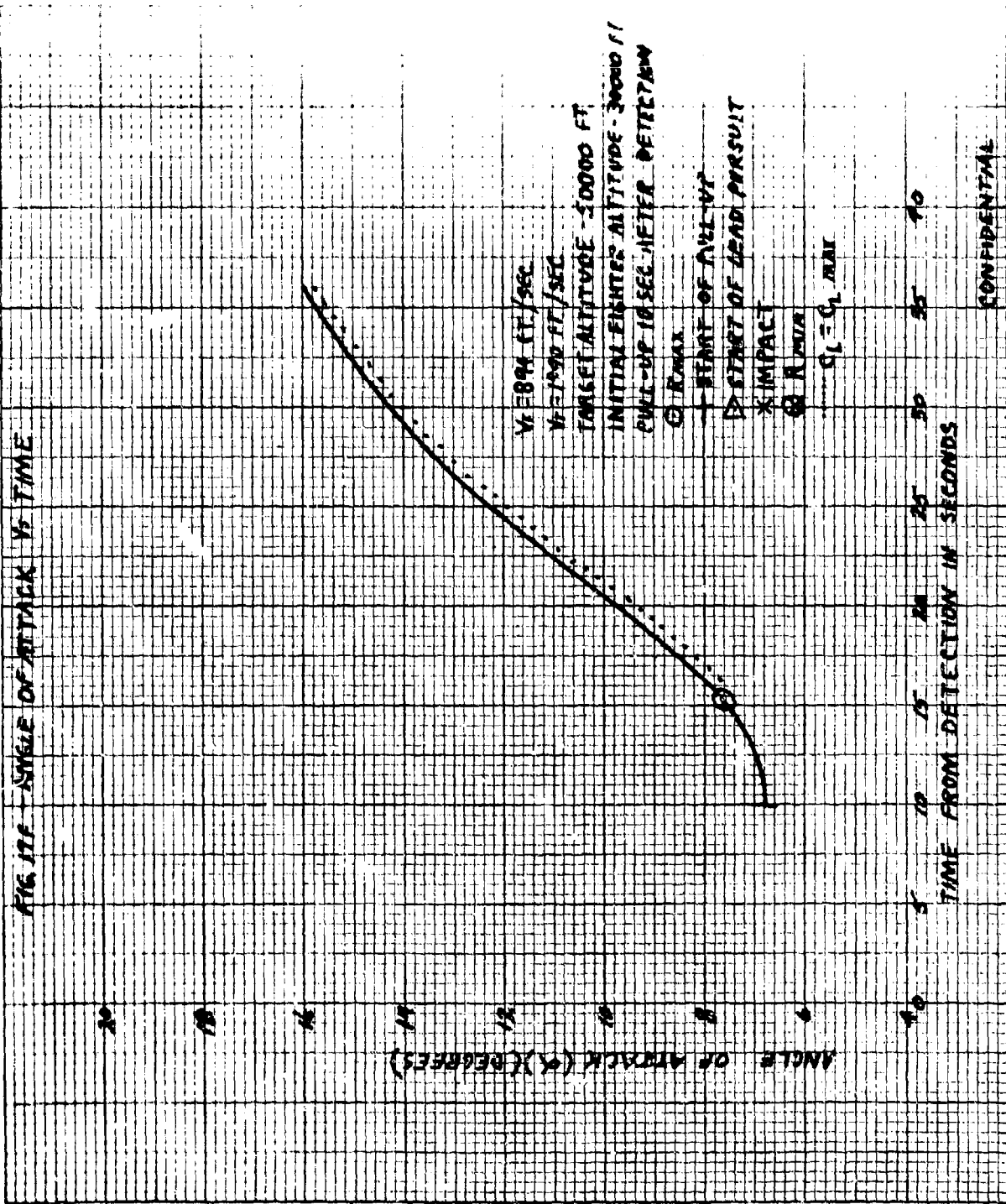
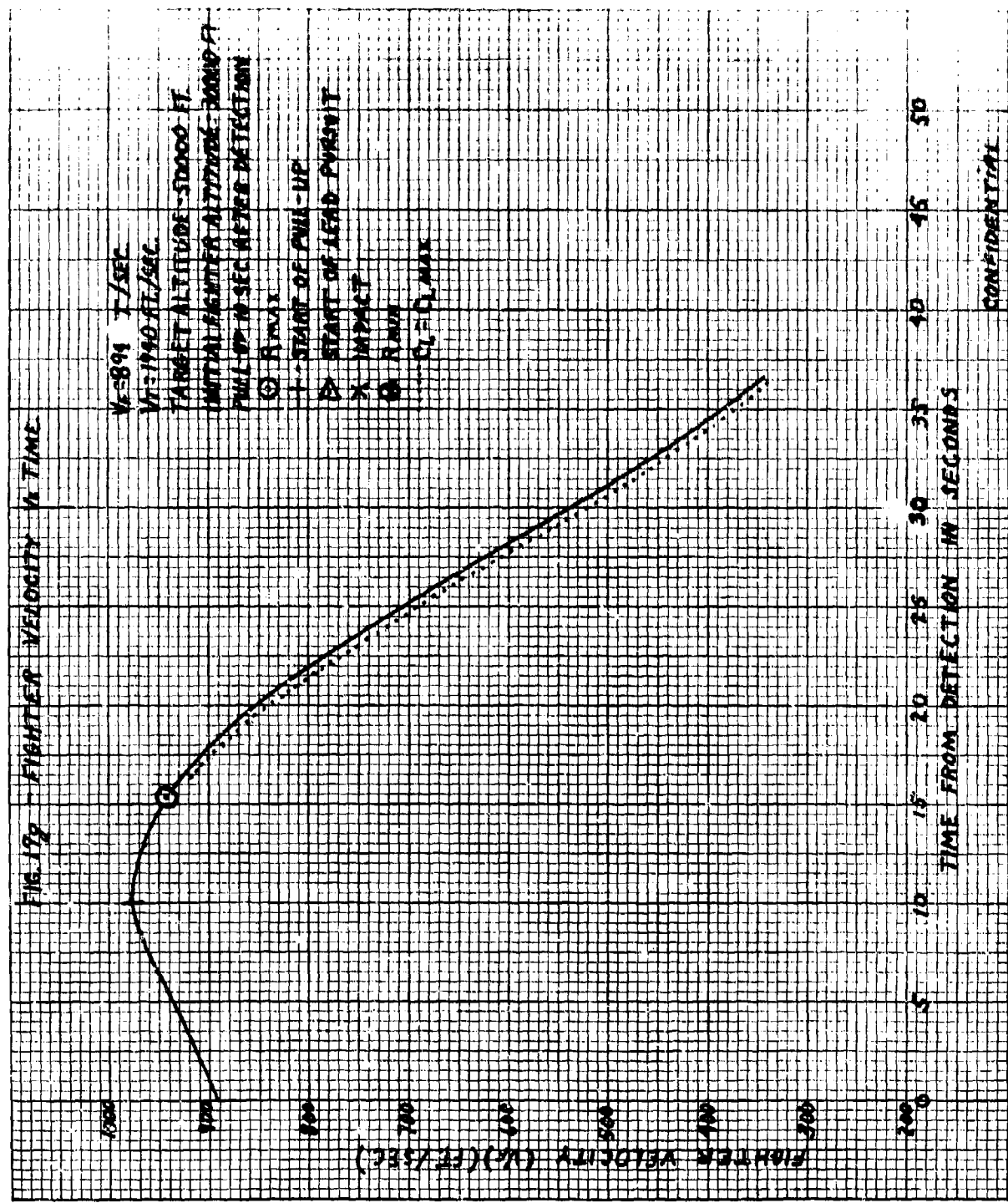
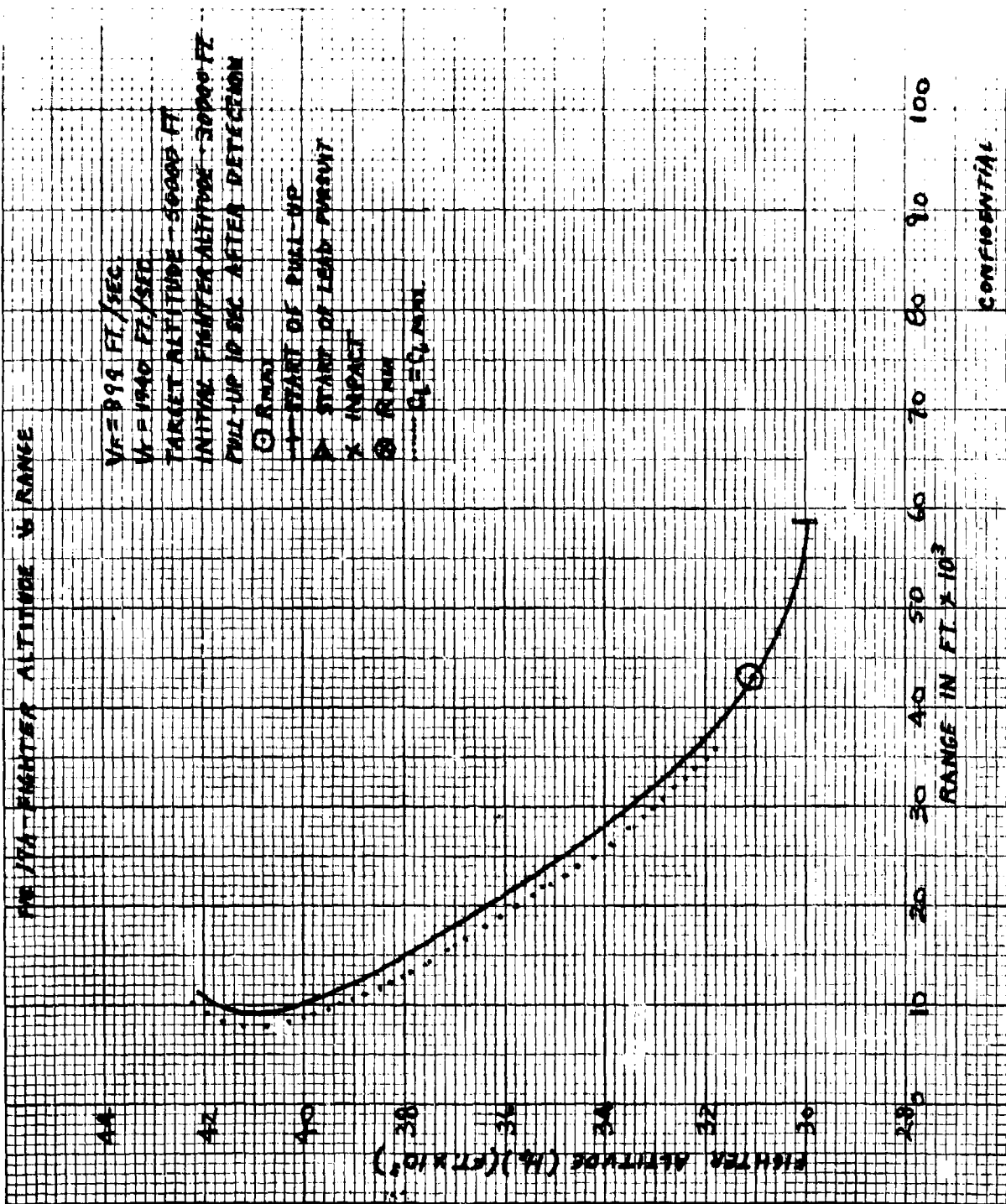


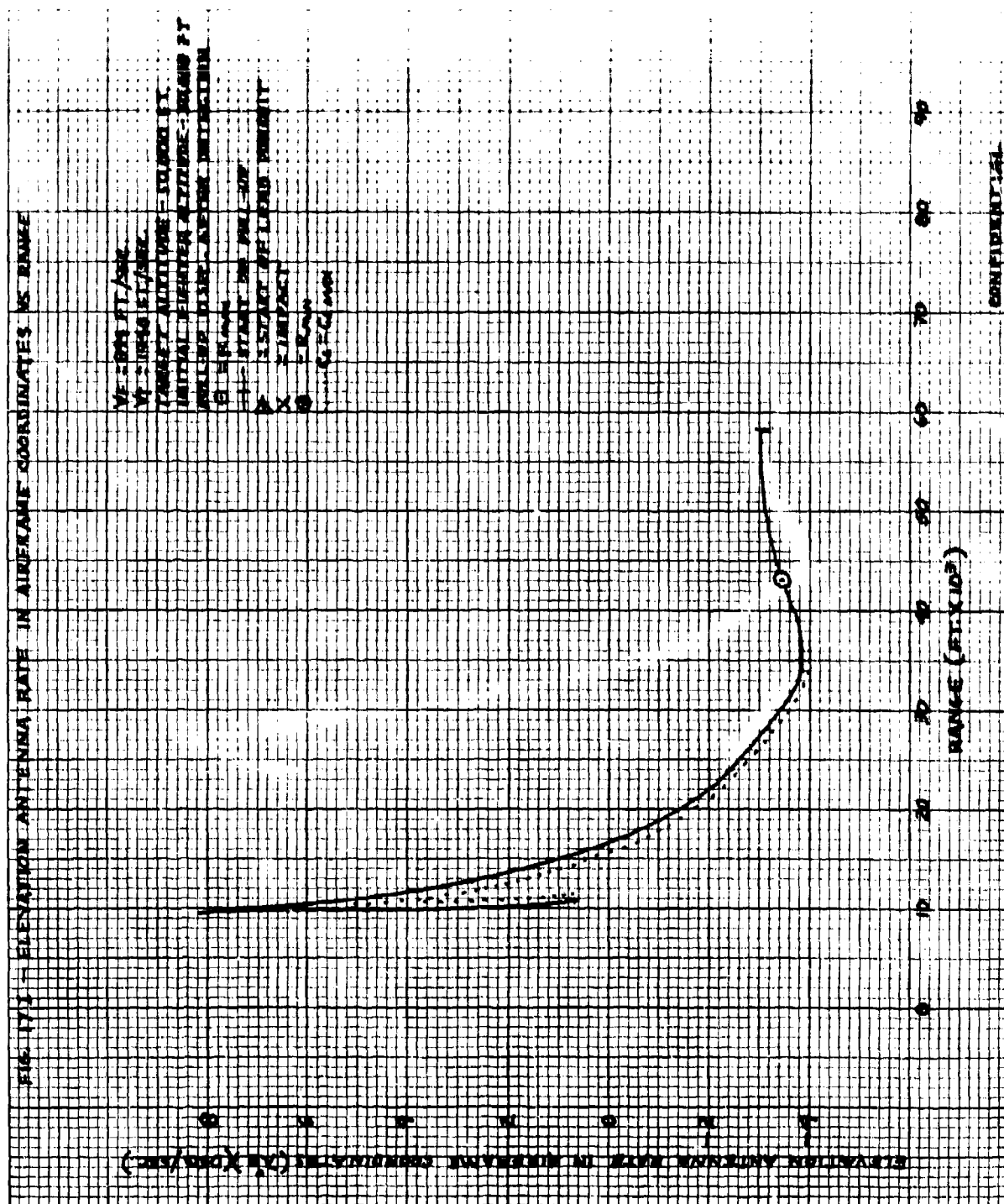
FIG. 199 - FIGHTER VELOCITY vs TIME



CONFIDENTIAL



CONFIDENTIAL



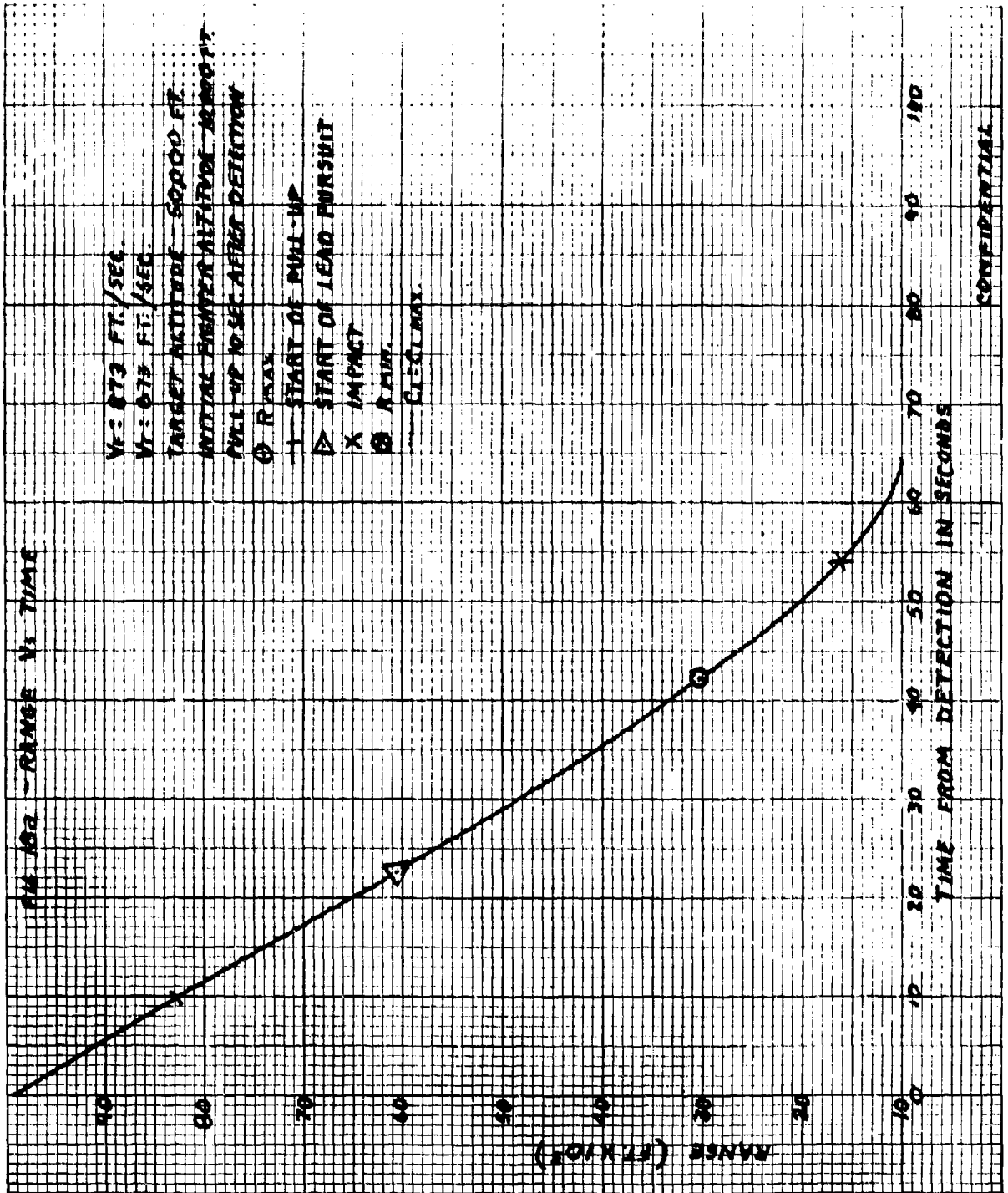
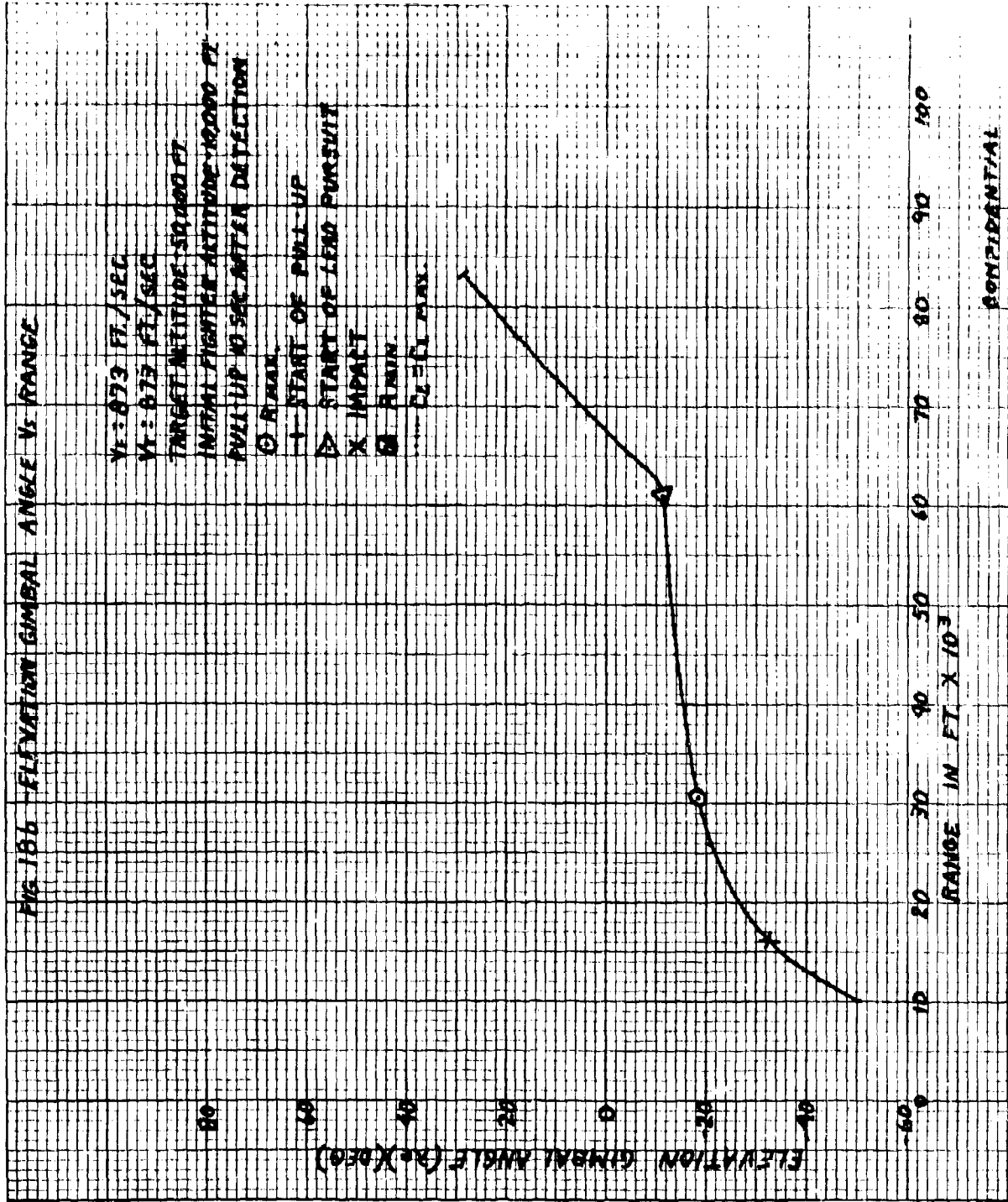
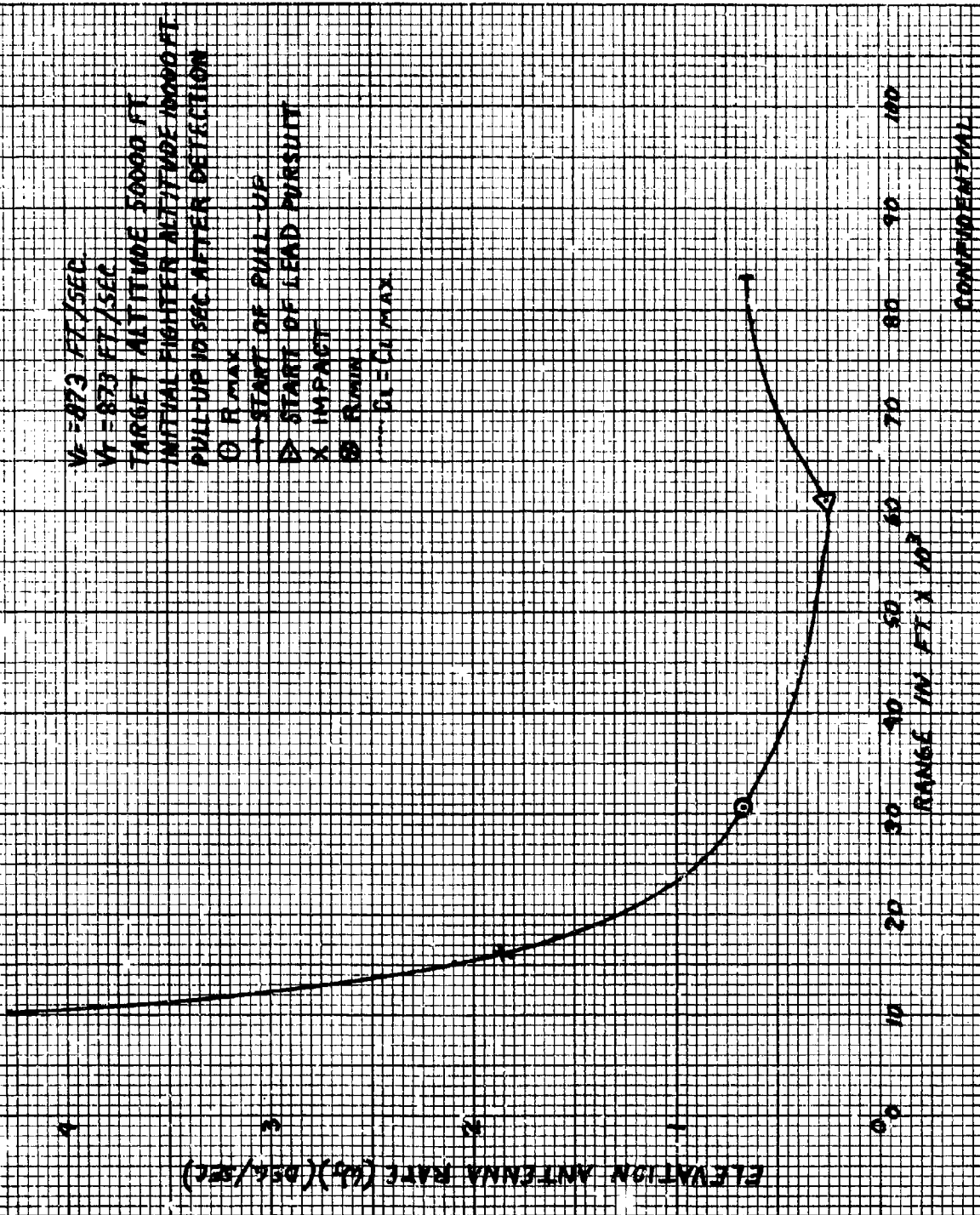


FIG 186 ELEVATION GMBAL ANGLE VS RANGE



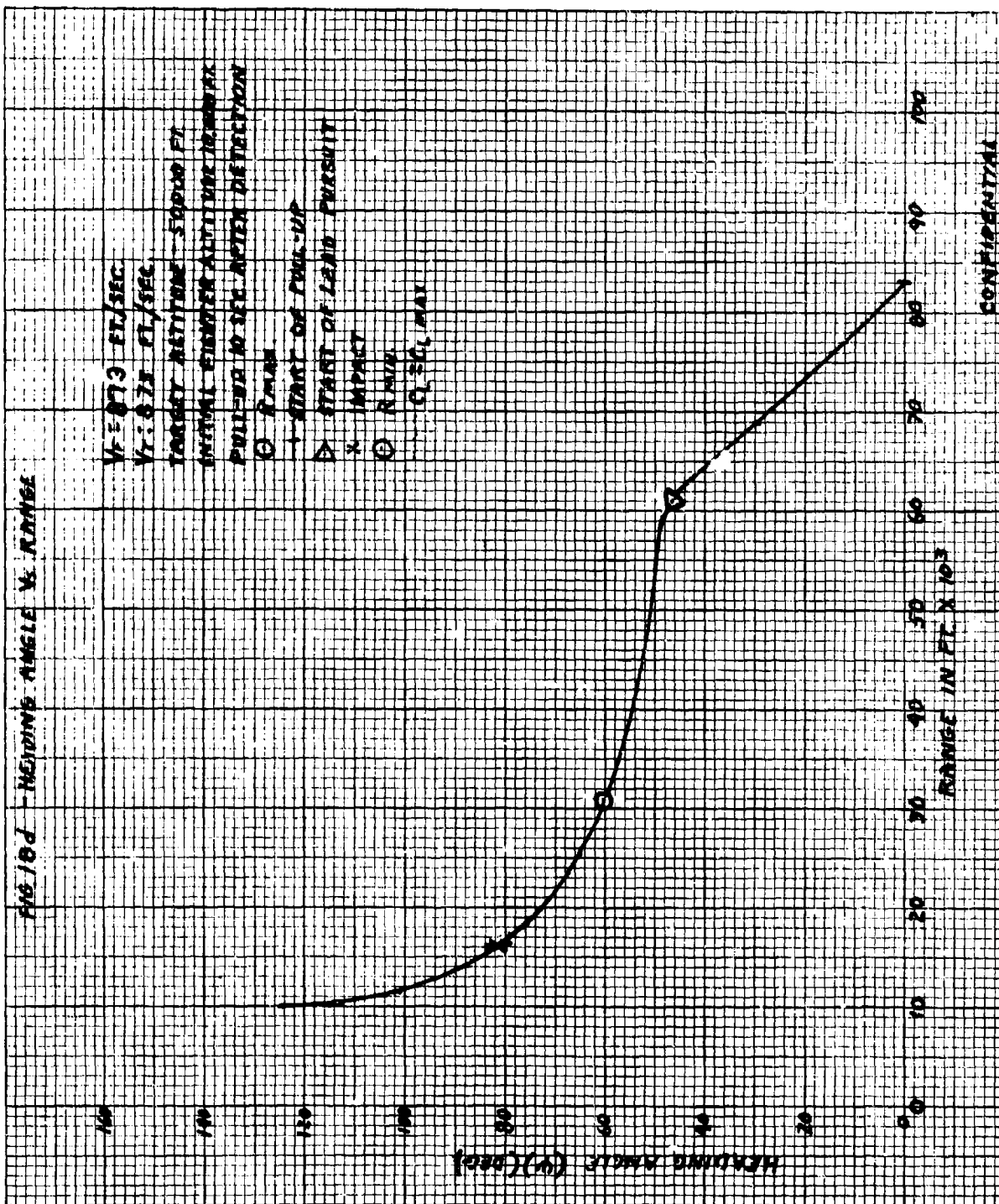
CONFIDENTIAL

FIG. 10C - ELEVATION ANTENNA RATE V. RANGE



CONFIDENTIAL

FIG 10d - HEADING ANGLE V. RANGE



CONFIDENTIAL

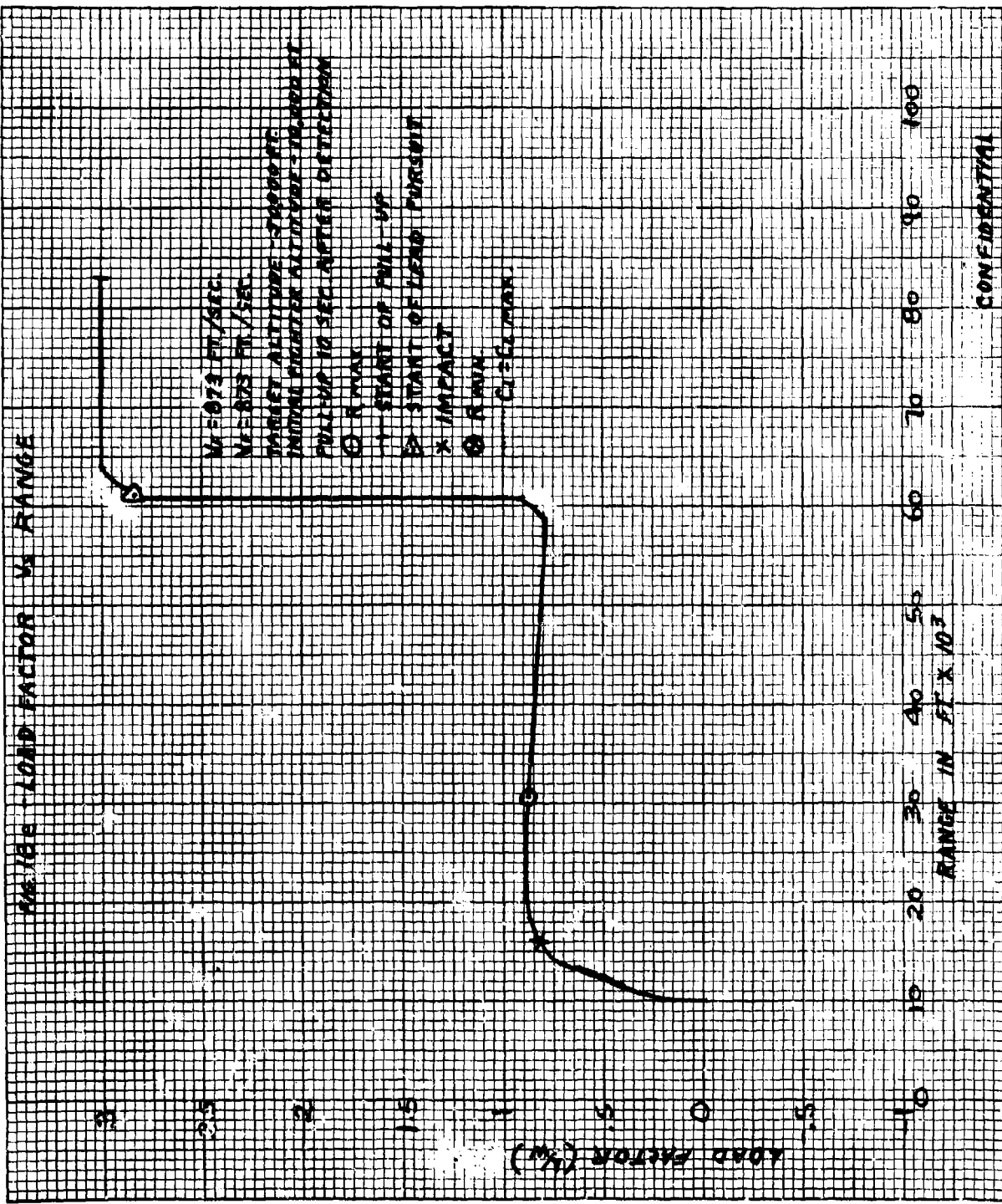
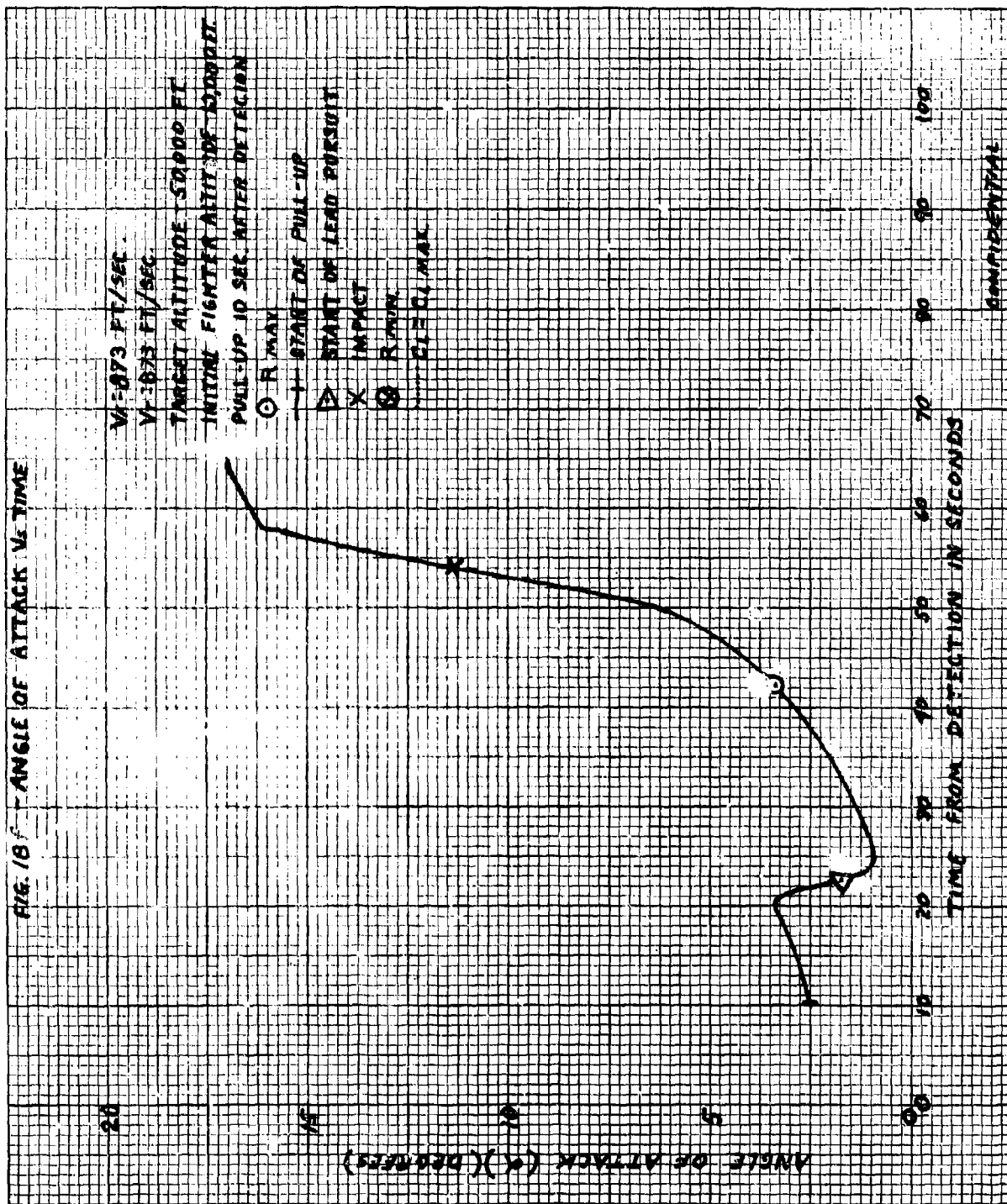


FIG. 18 - ANGLE OF ATTACK V_c TIME



CONFIDENTIAL

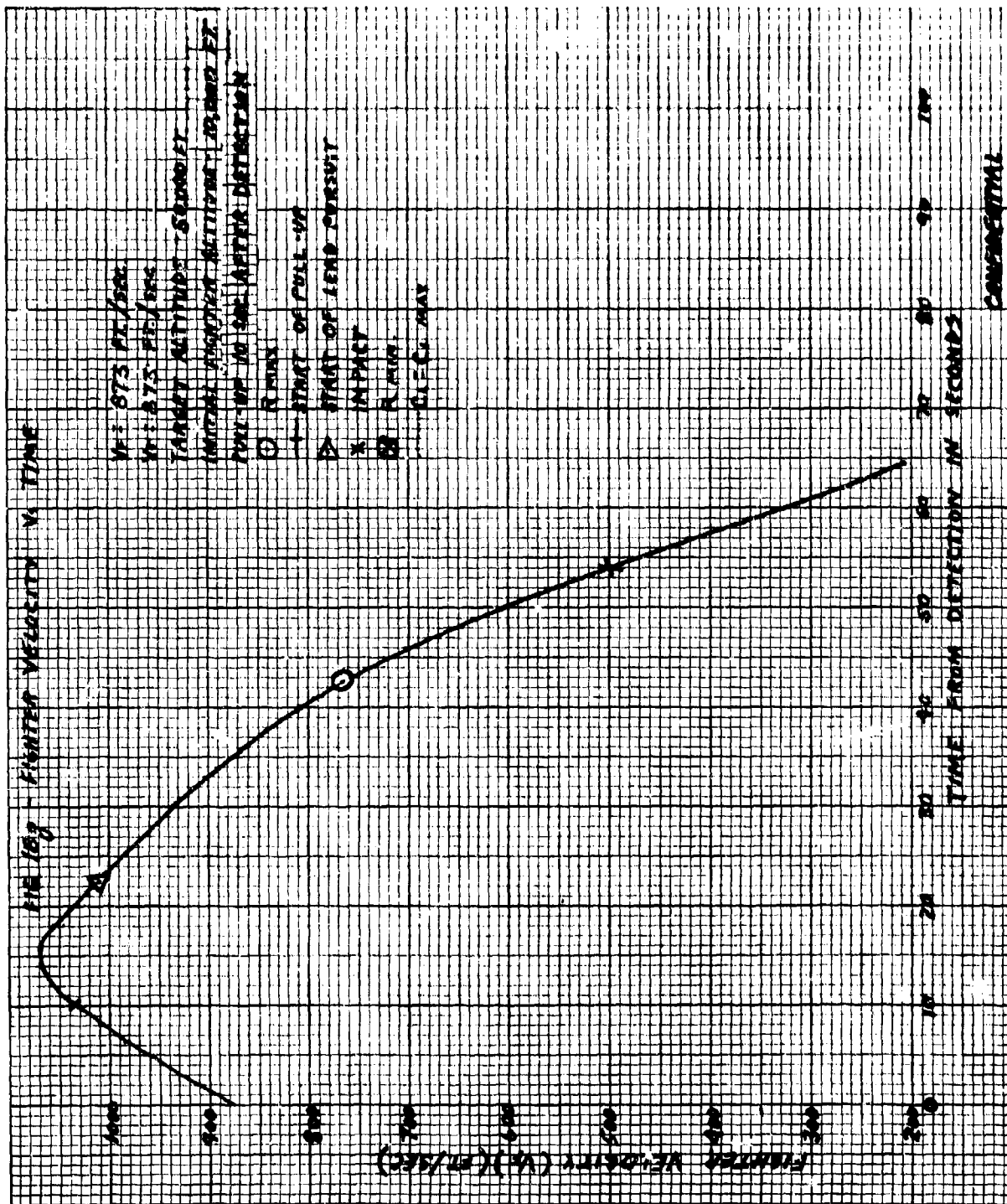
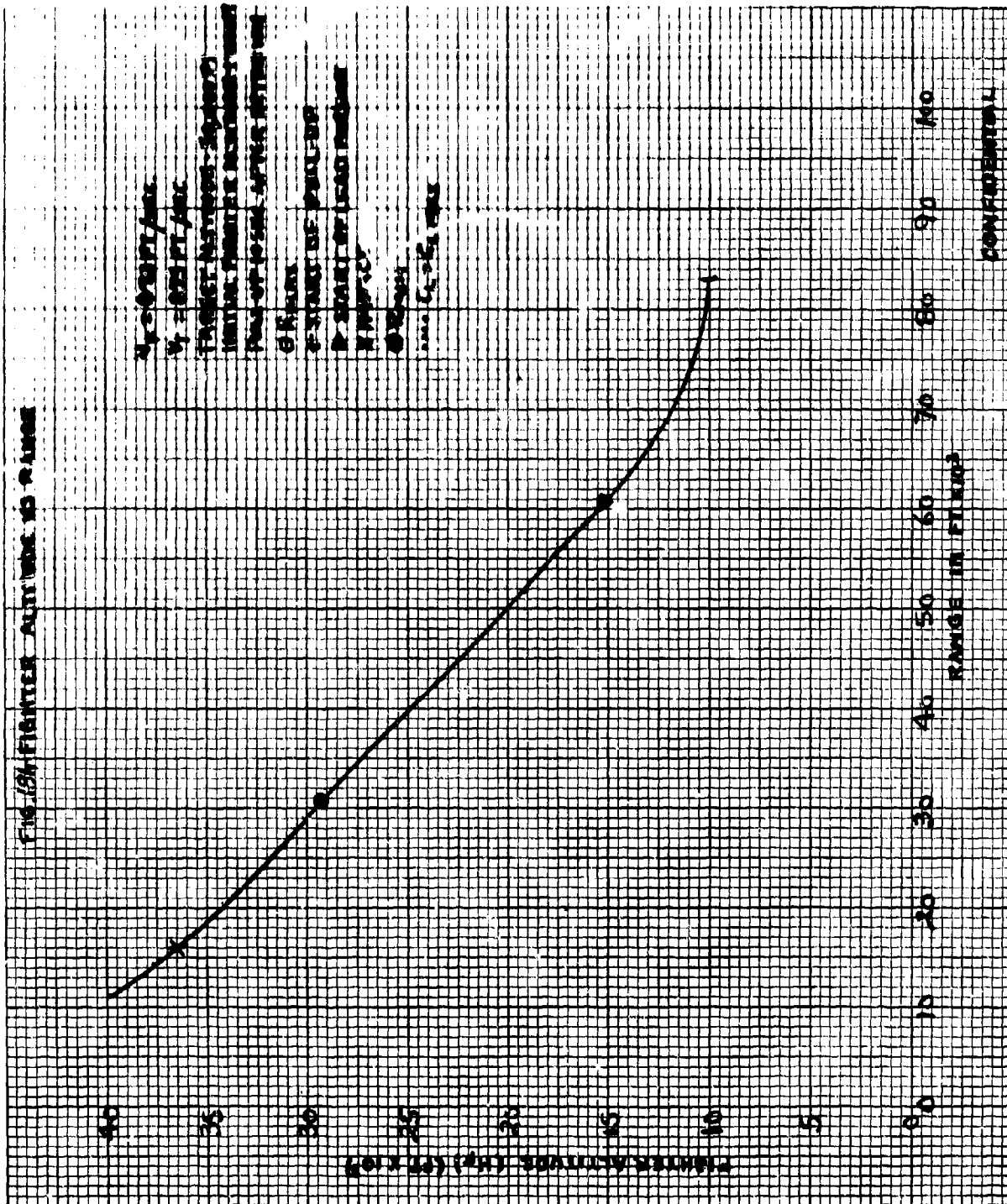
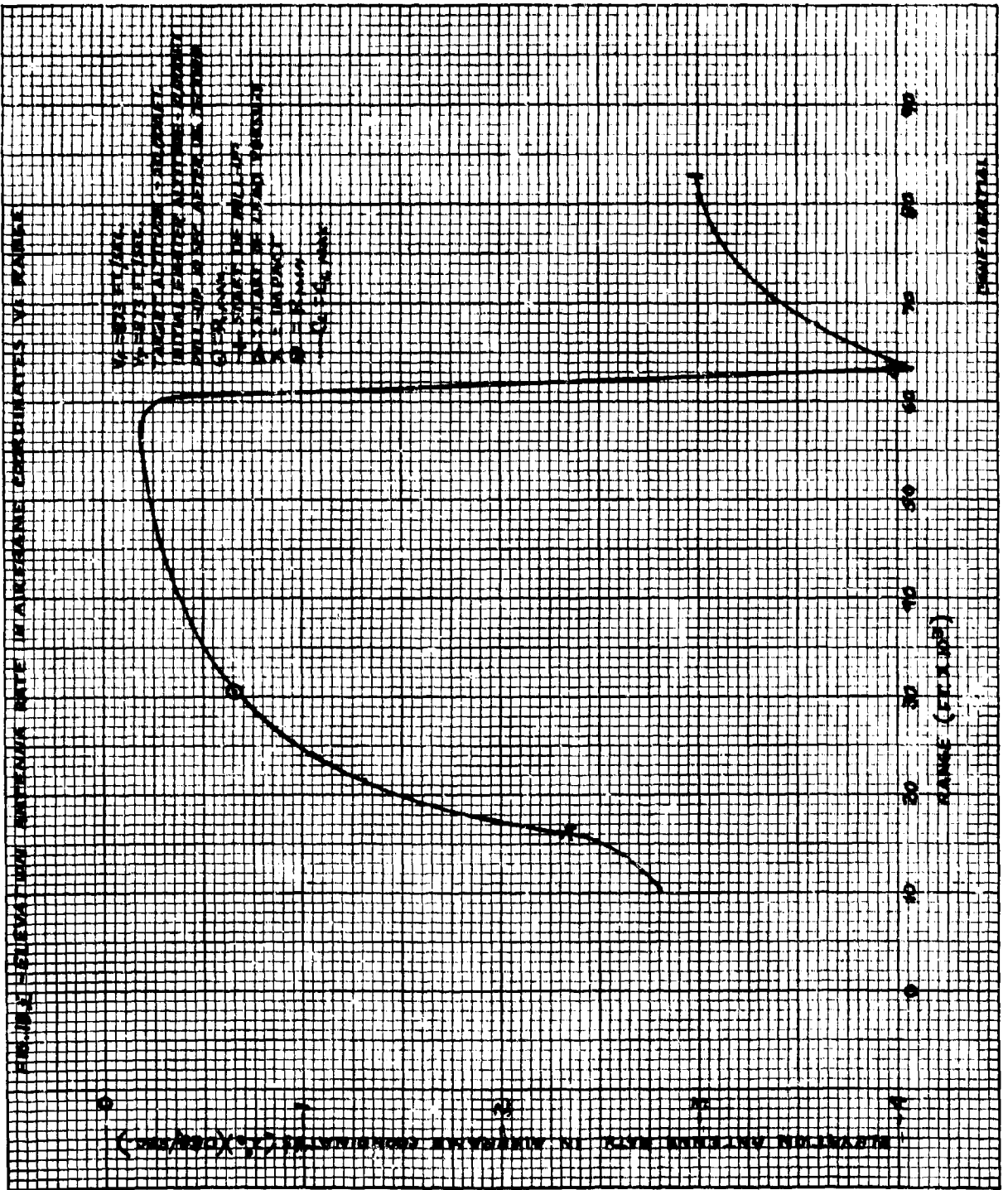


FIG. 18. FIGHTER AIRCRAFT TO RANGE





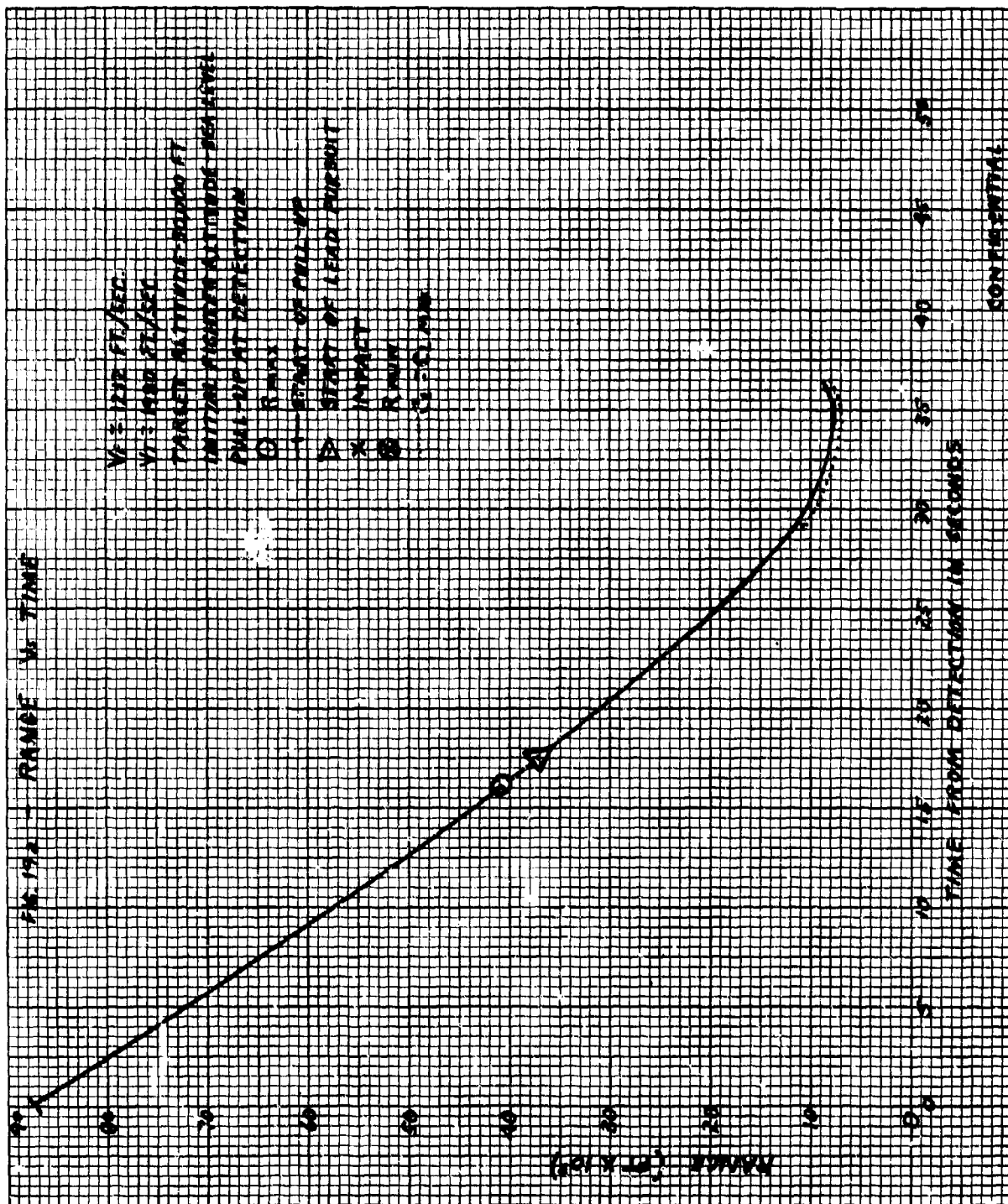
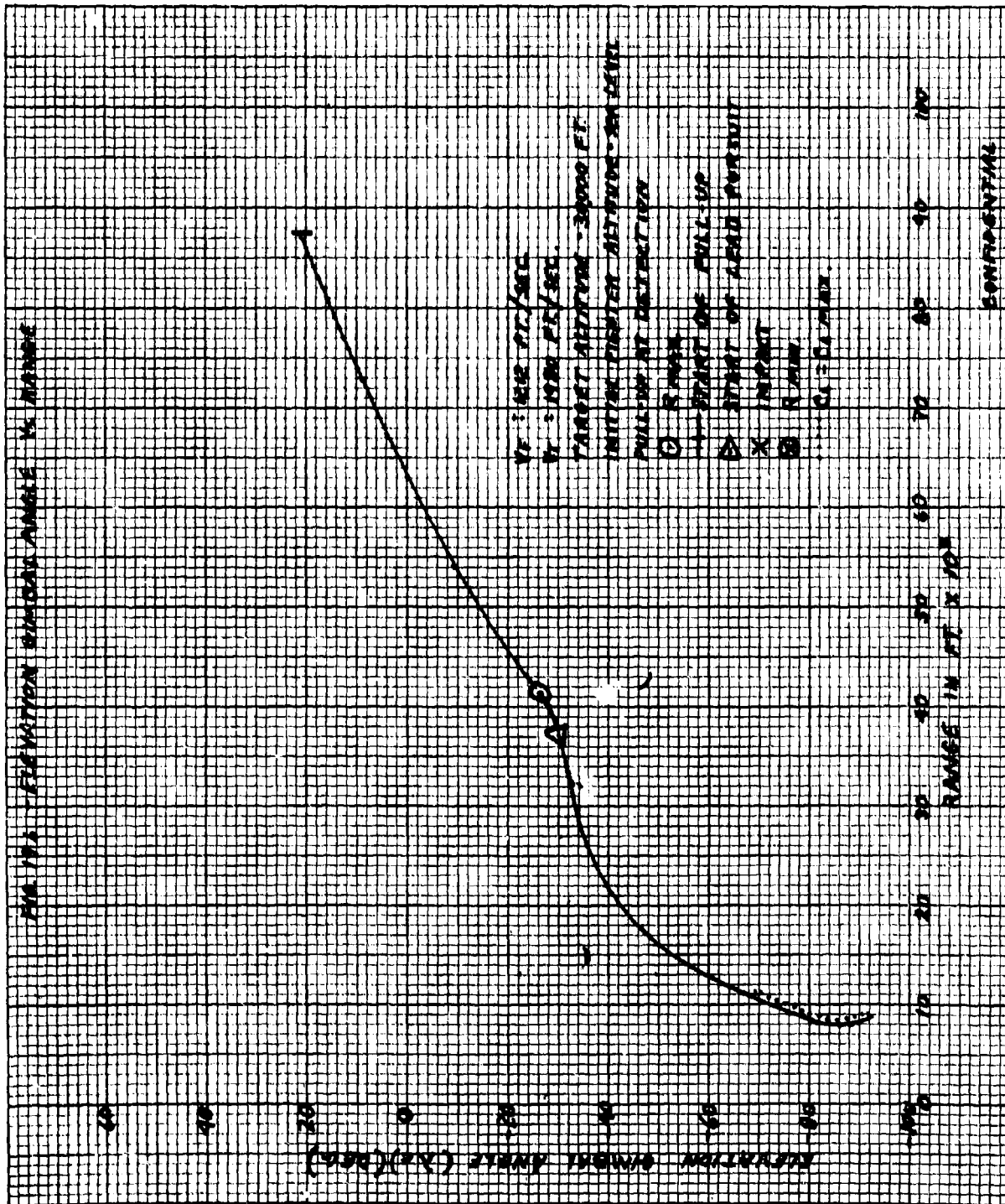
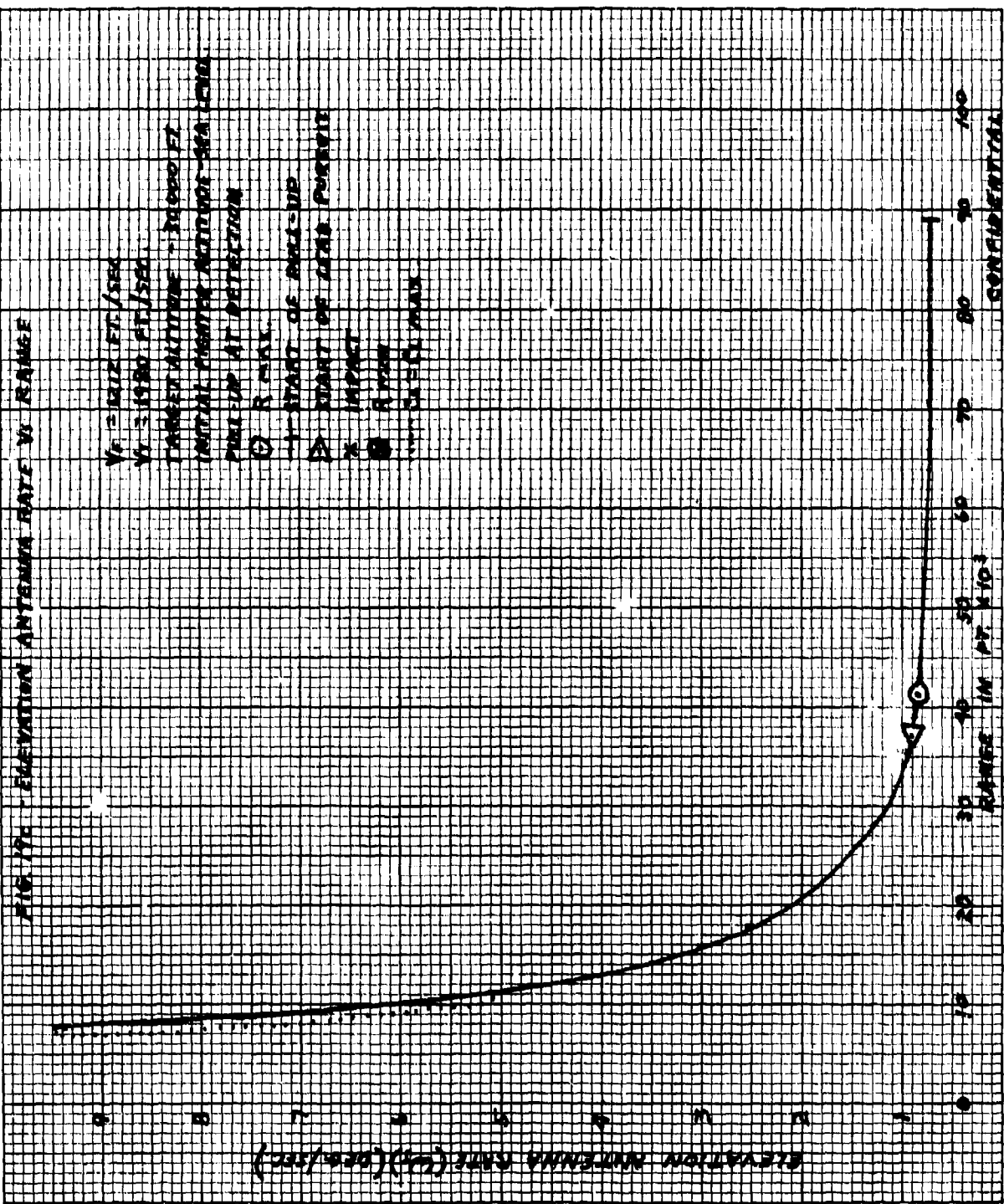
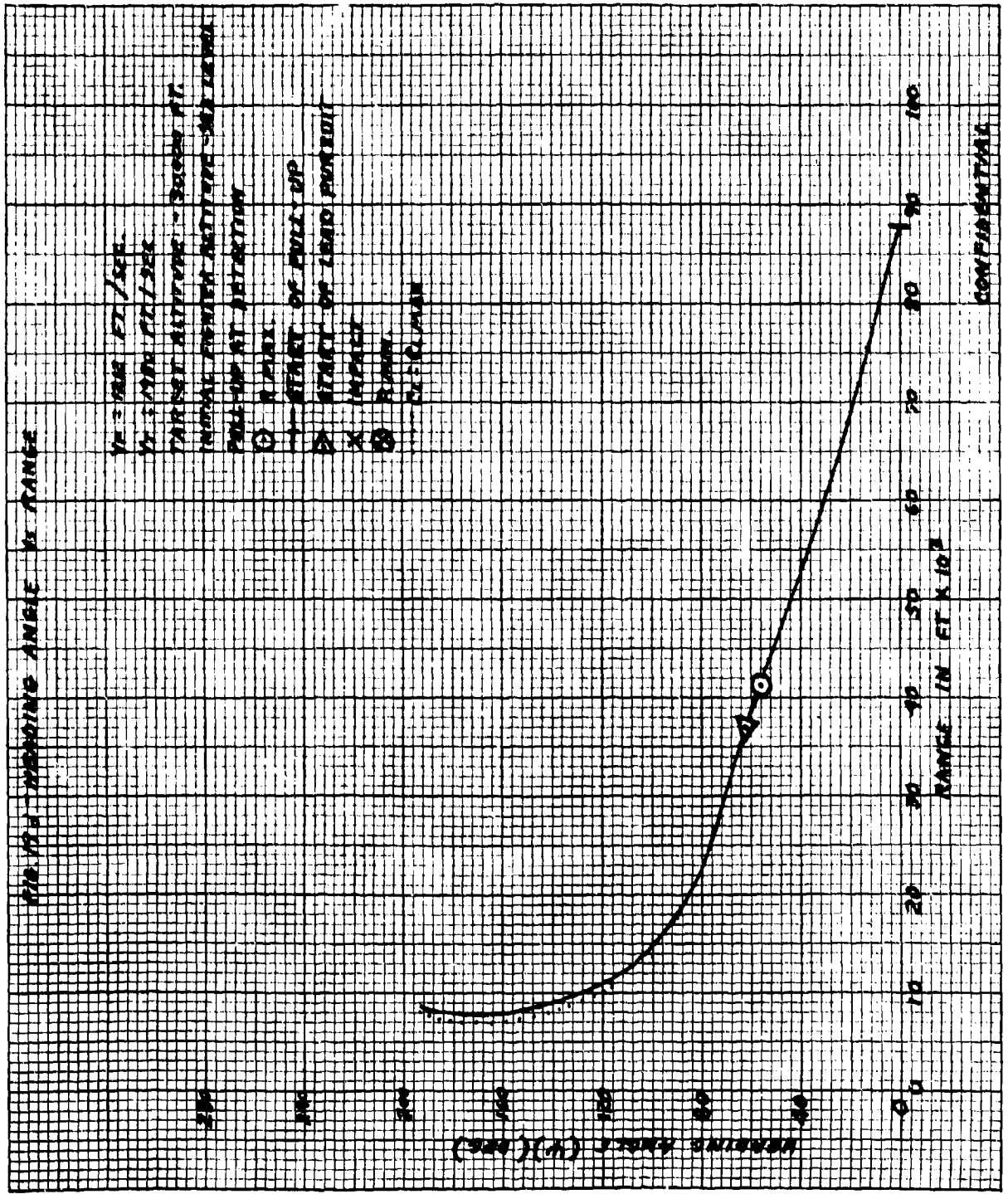
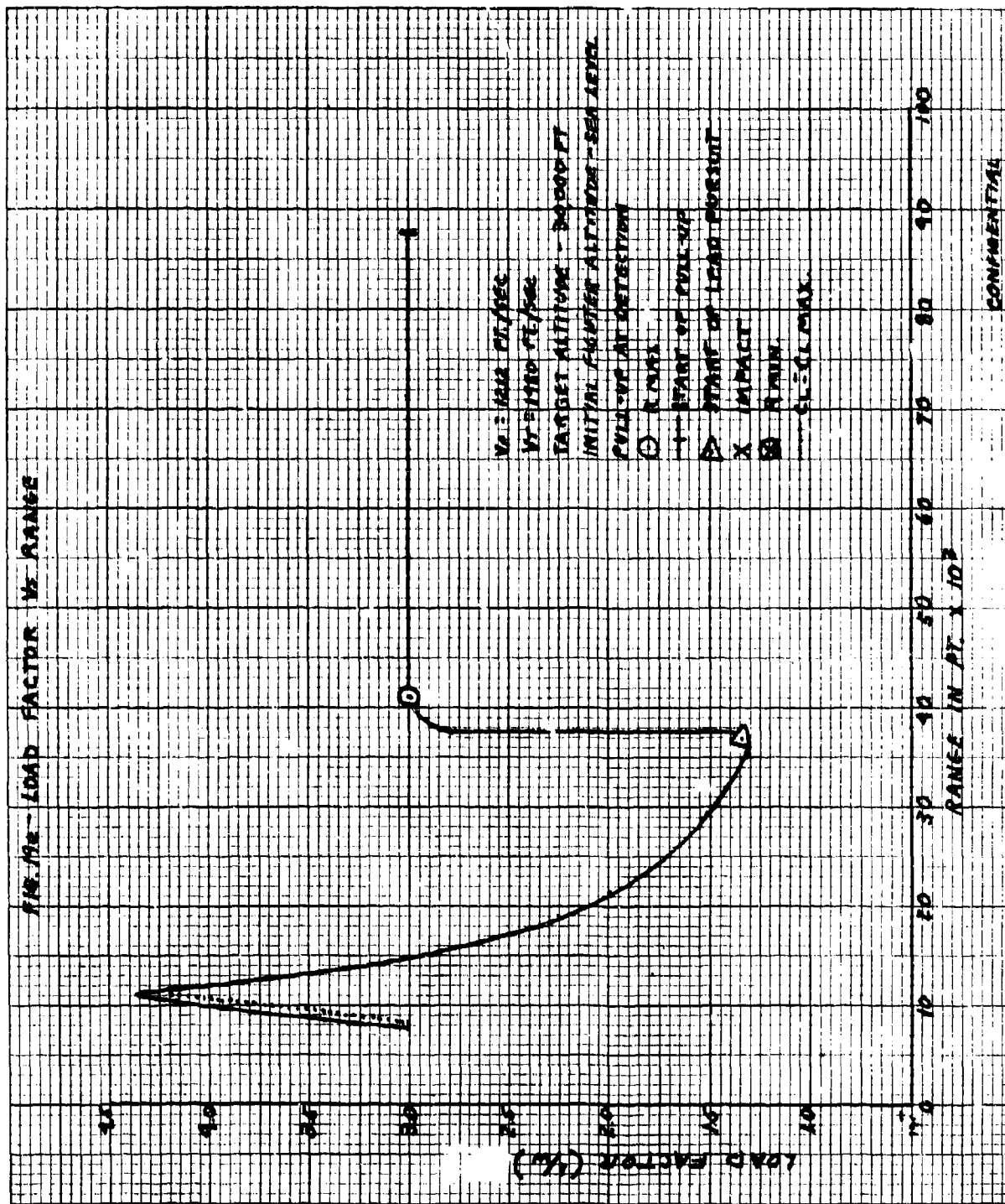


FIG. 19-1 ELEVATION SIGHTING ANGLES VS. RANGE

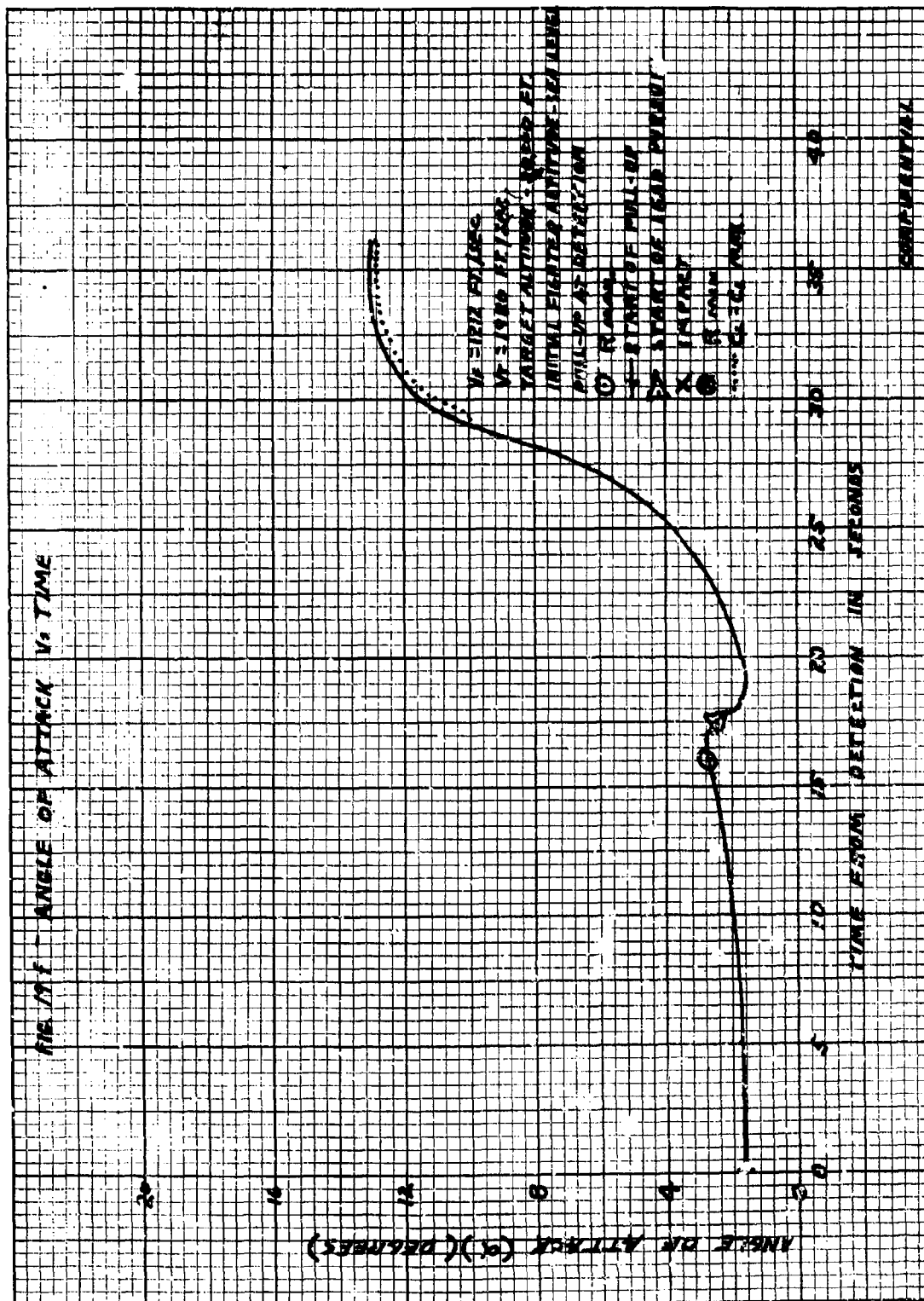


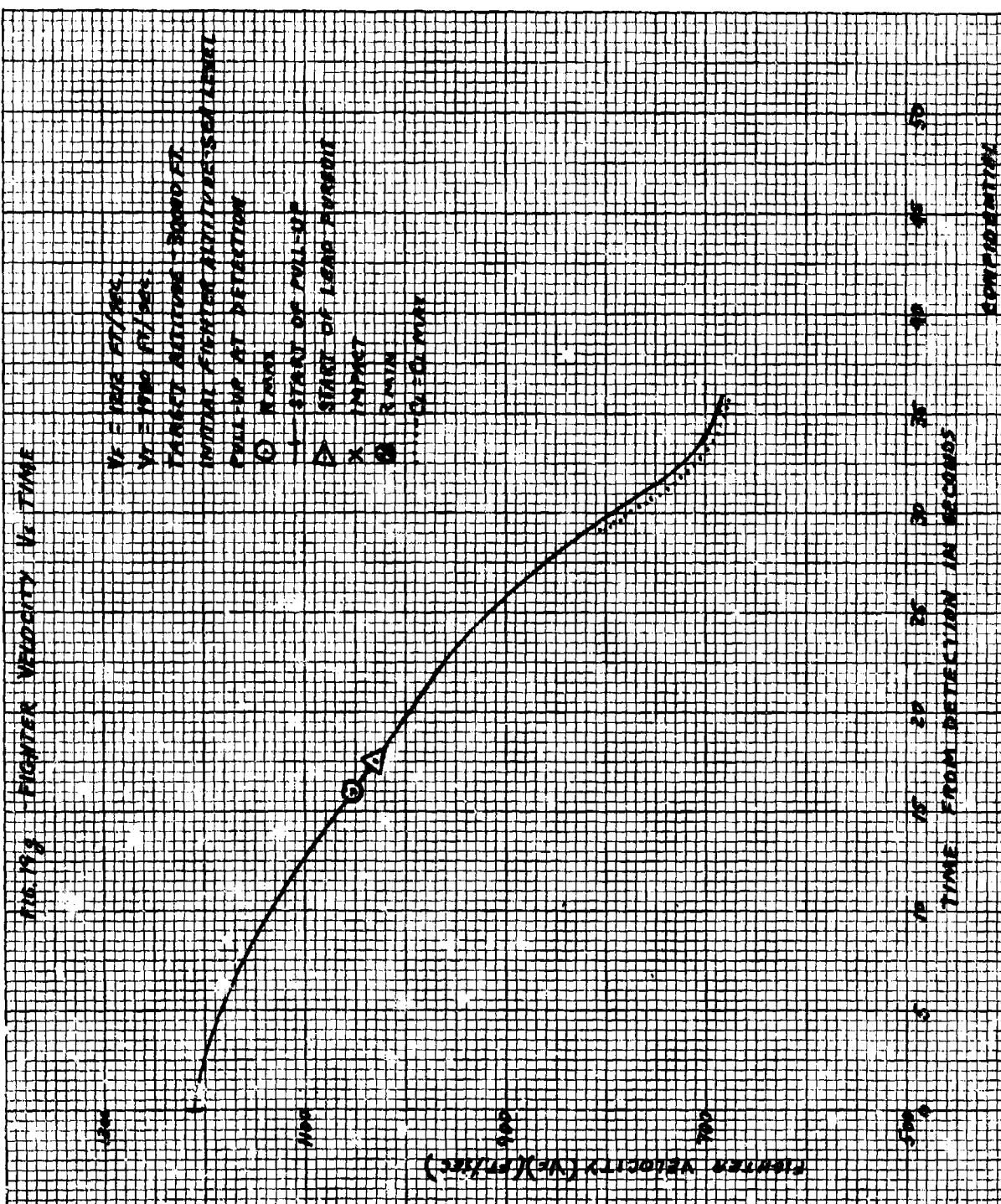


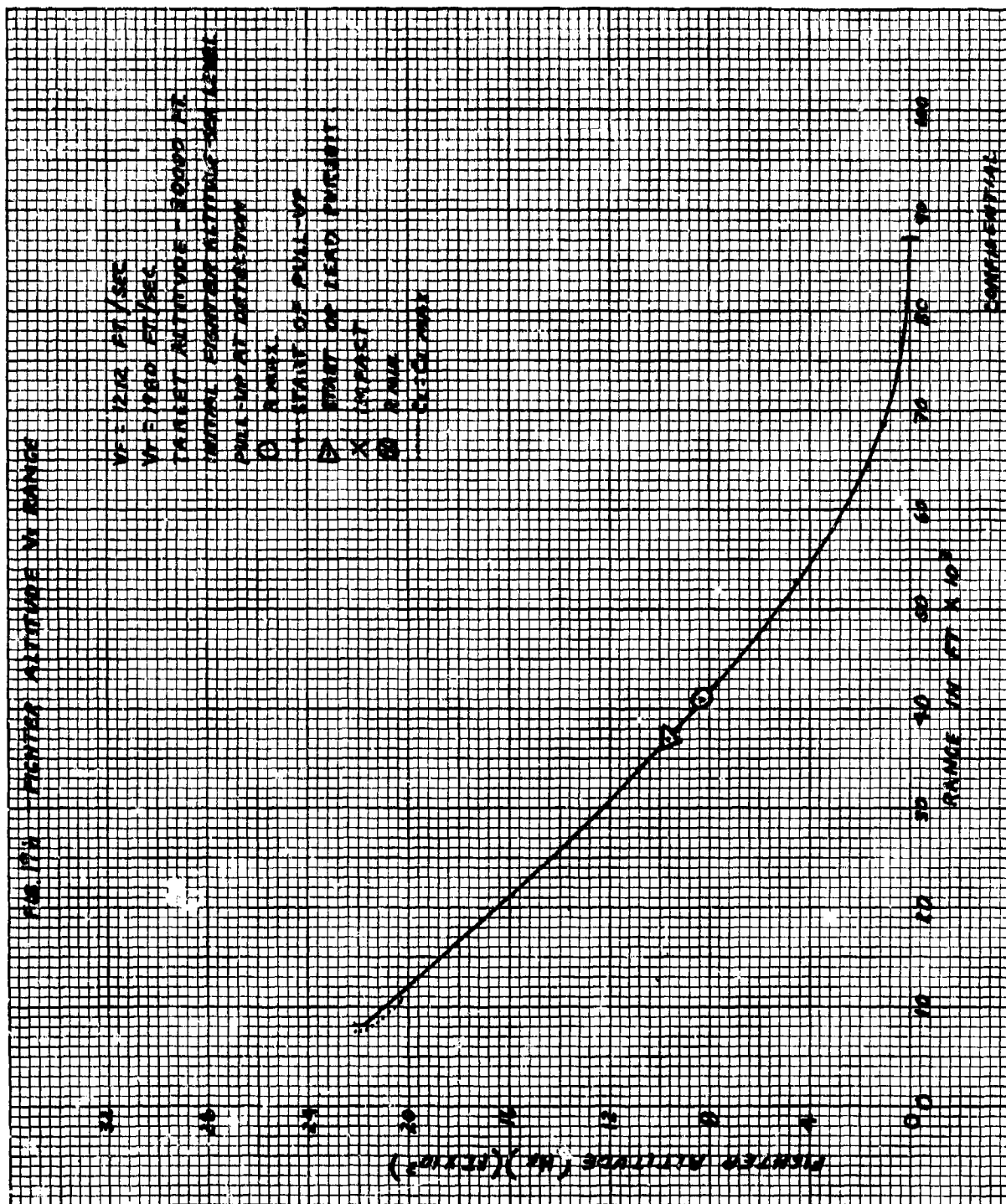




CONFIDENTIAL



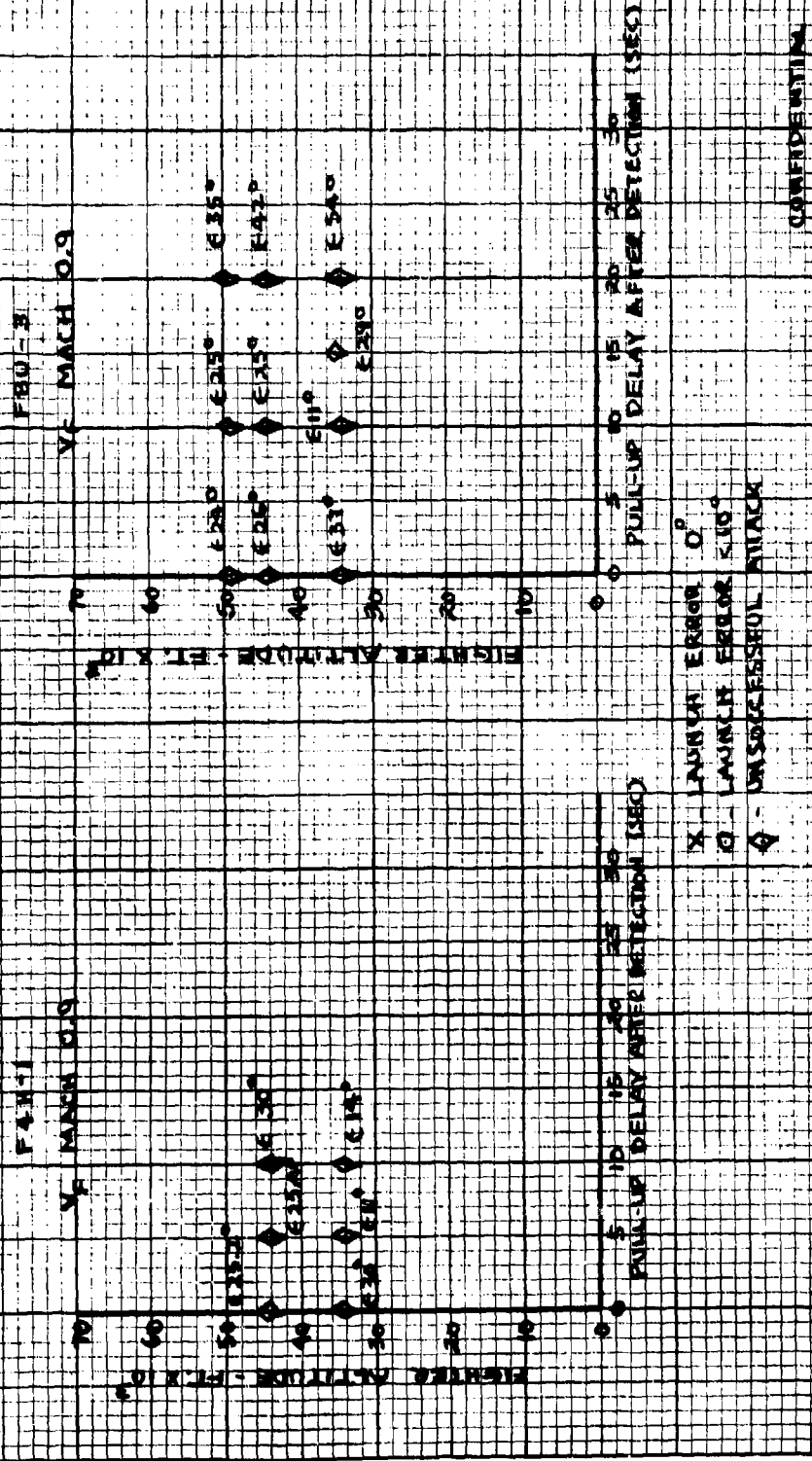




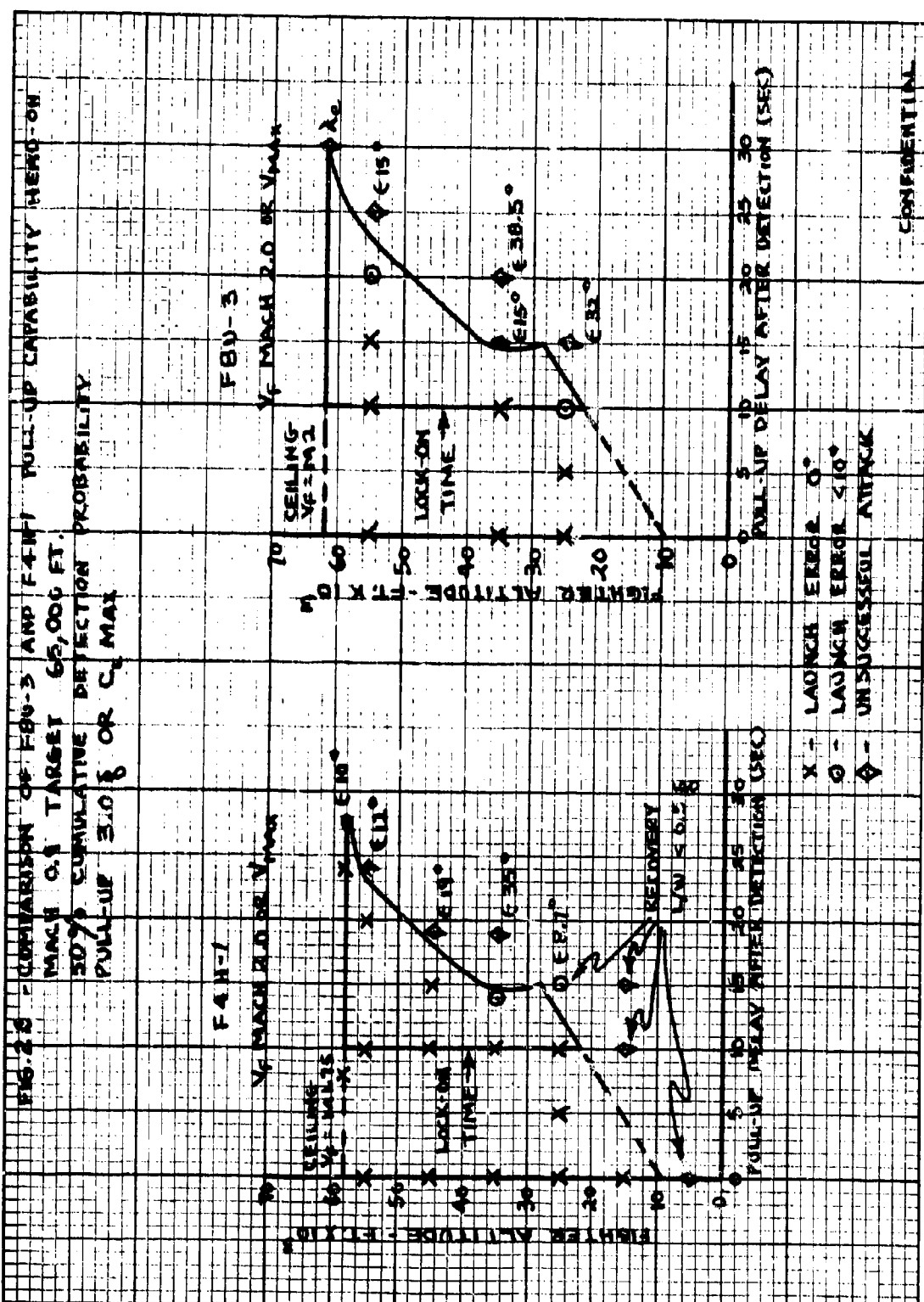
ALL INFORMATION CONTAINED HEREIN IS UNCLASSIFIED



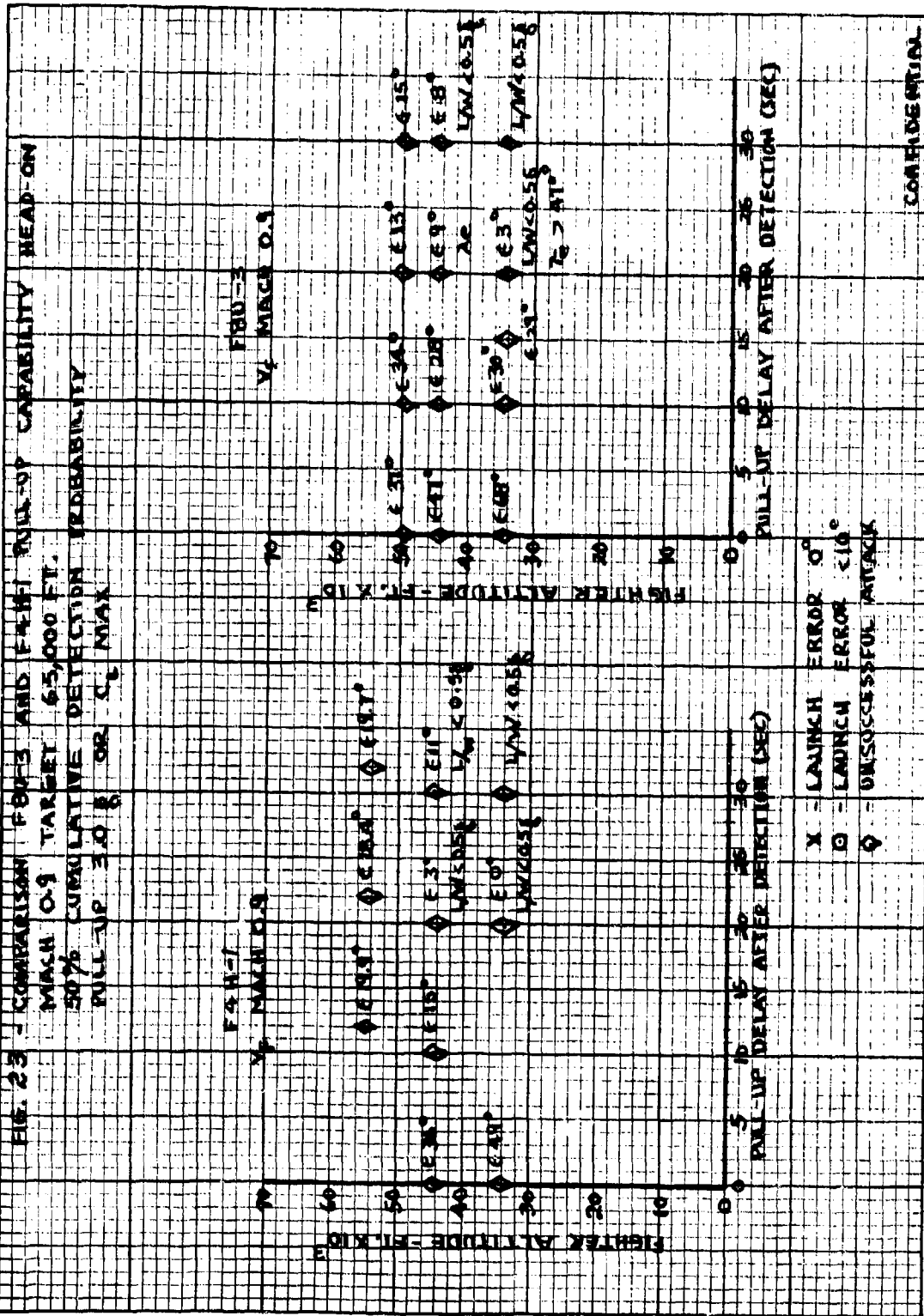
FIG. 21 - COMPARISON FBW-3 AND F4H-7 PULL-UP CAPABILITY HEAD-ON
 MACH 2.0 TARGET, 65,000 FT.
 50% COMBATIVE DETECTION PROBABILITY
 PULL-UP BLD 8 OR CL MAX



CONFIDENTIAL

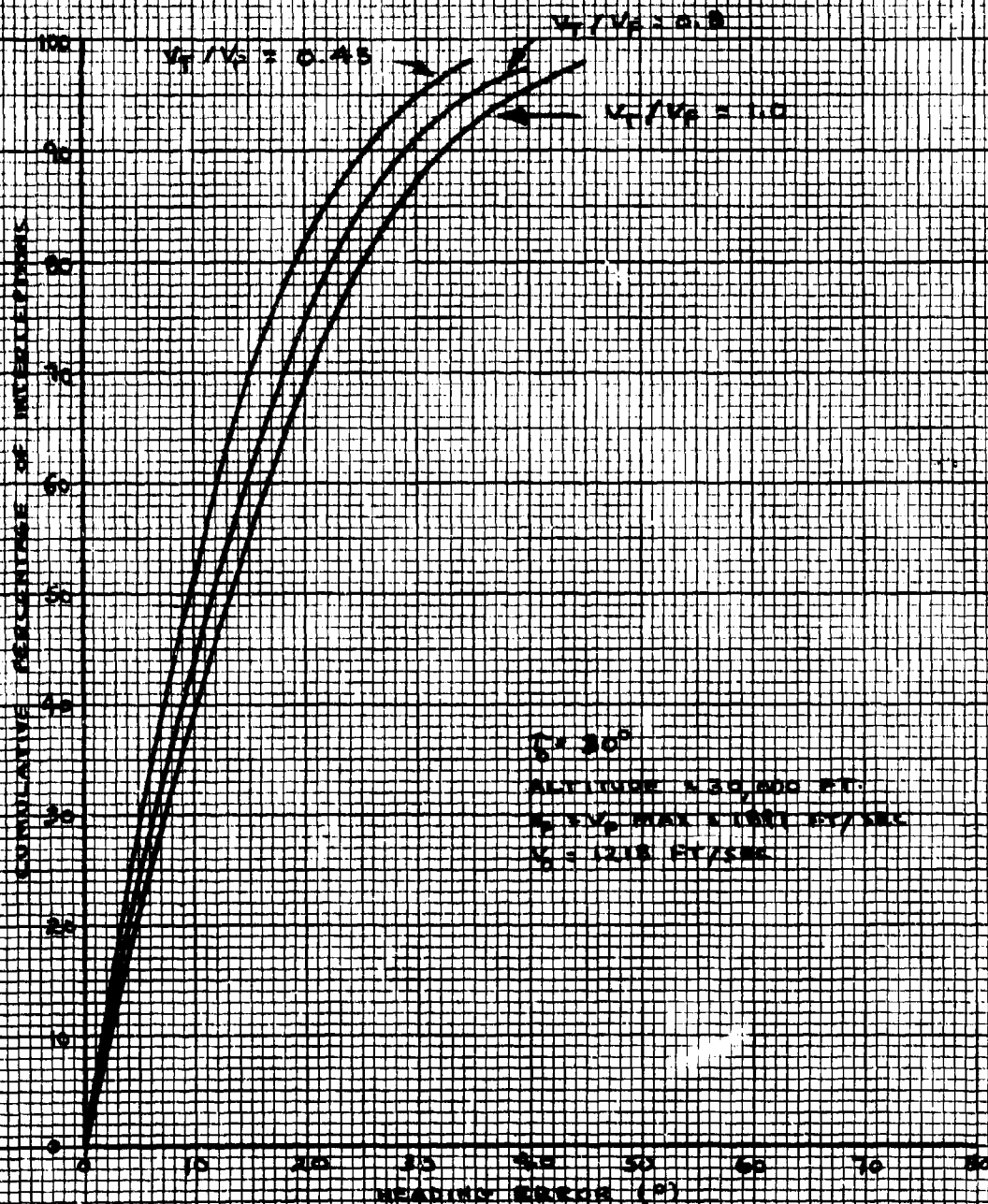


CONFIDENTIAL



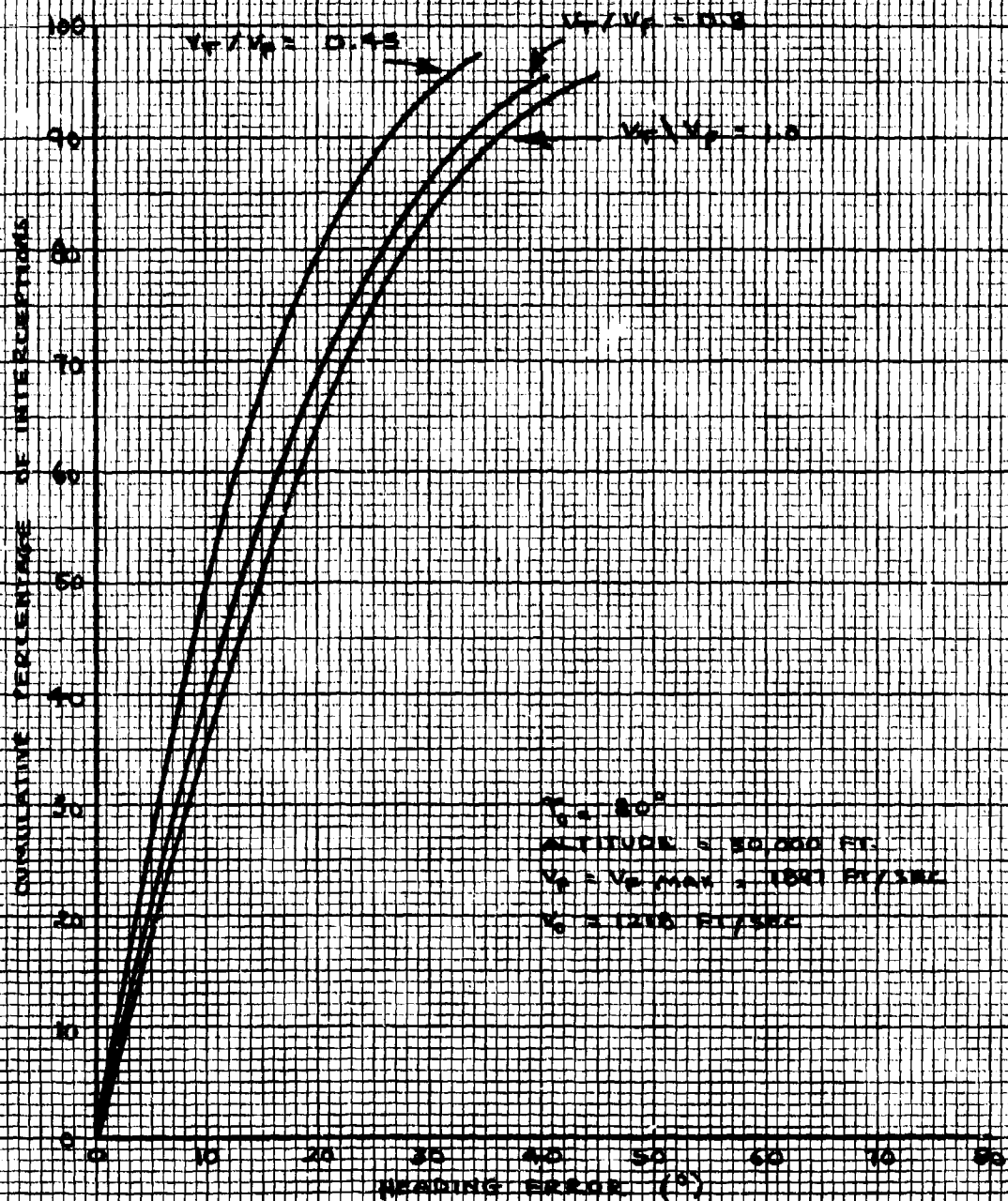
CONFIDENTIAL

FIG. 2-1 - CONVERSION OF VECTORING ERROR AT DETECTION
TO HEADING ERROR AT LOCK ON



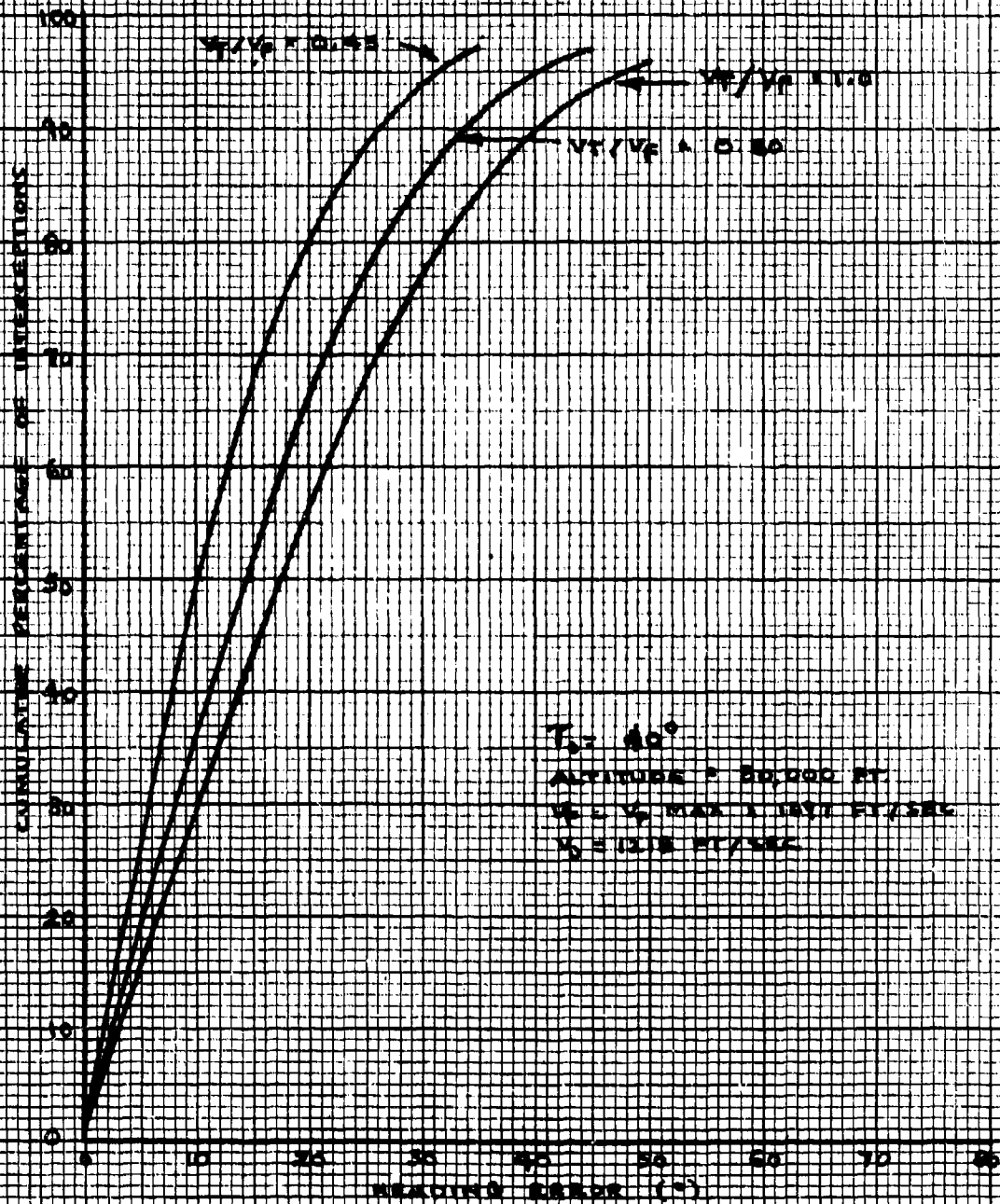
CONFIDENTIAL

FIG. 25 CONVERSION OF VELOCITY ERROR AT DETECTION
TO HEADING ERROR AT LOCK ON



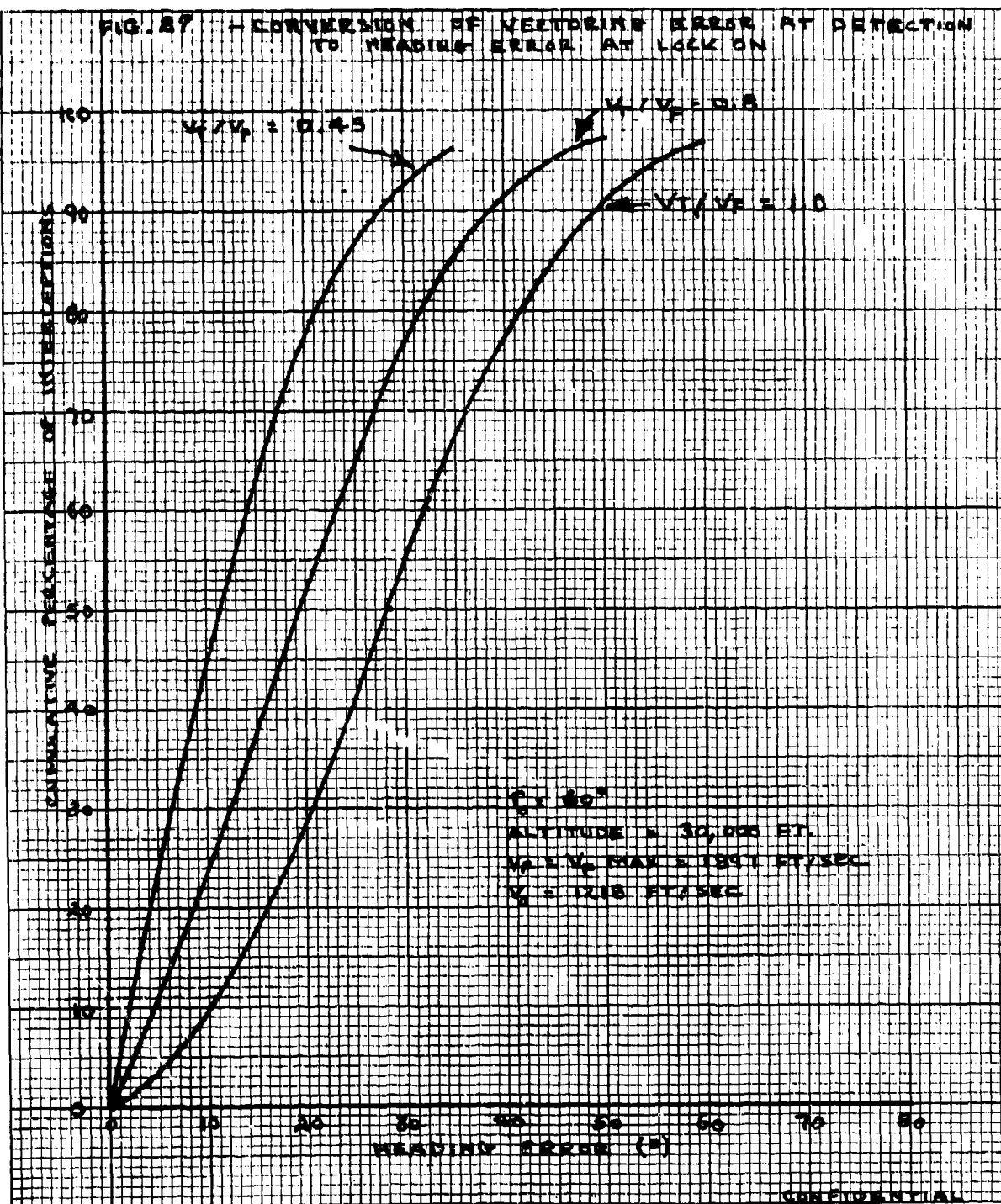
CONFIDENTIAL

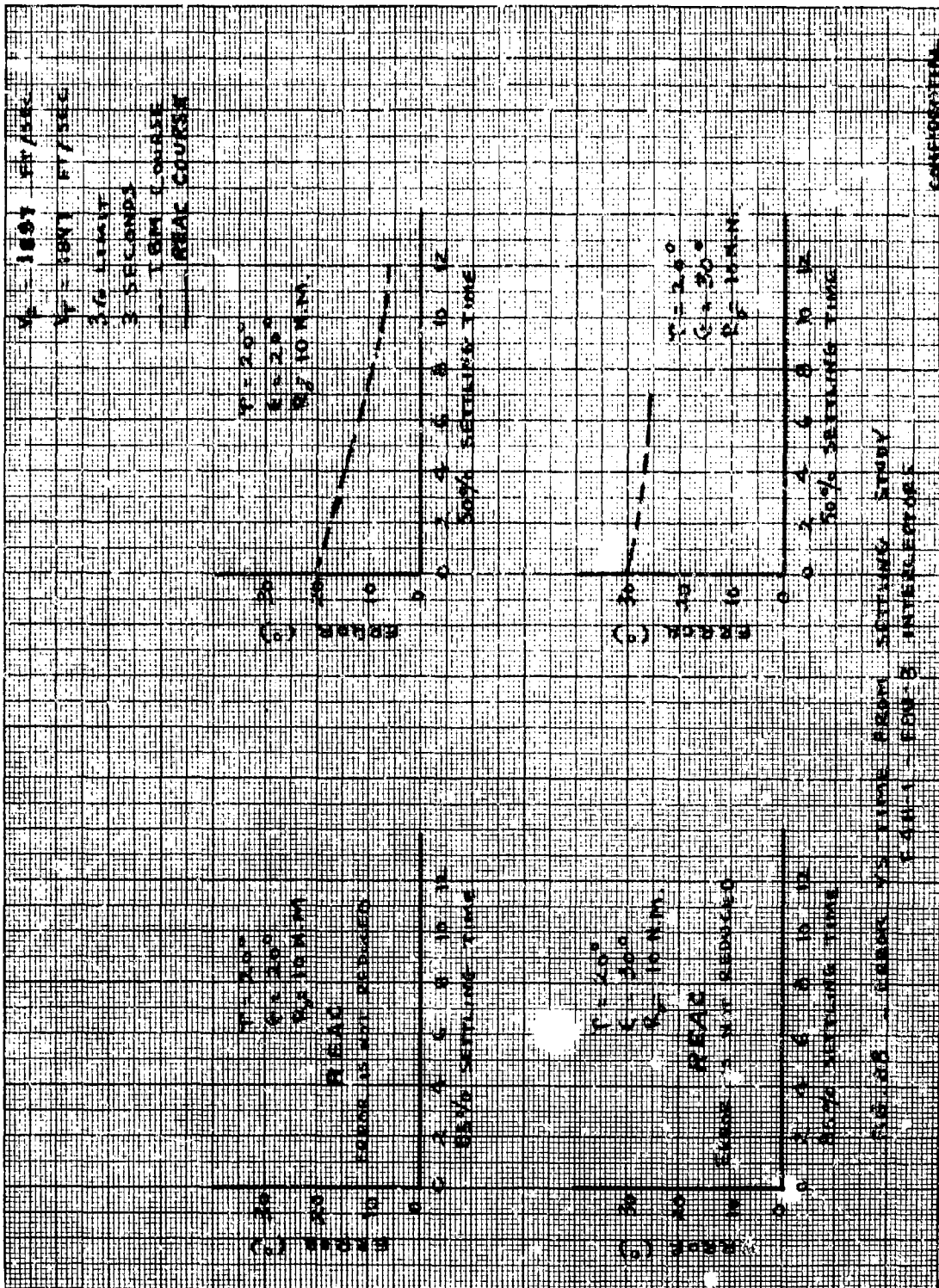
FIG. 28. CONVERSION OF VECTORING ERRORS AT DETECTION
TO HEADING ERRORS AT LOCK ON



CONFIDENTIAL

FIG. 87 - CONVERSION OF NEEDLE-DRIVE ERROR AT DETECTION TO READING ERROR AT LOCK ON





$V_0 = 1000$ FT/SEC
 $V_1 = 1000$ FT/SEC
 $V_2 = 1000$ FT/SEC
 $V_3 = 1000$ FT/SEC
 $V_4 = 1000$ FT/SEC
 $V_5 = 1000$ FT/SEC
 $V_6 = 1000$ FT/SEC
 $V_7 = 1000$ FT/SEC
 $V_8 = 1000$ FT/SEC
 $V_9 = 1000$ FT/SEC
 $V_{10} = 1000$ FT/SEC
 $V_{11} = 1000$ FT/SEC
 $V_{12} = 1000$ FT/SEC
 $V_{13} = 1000$ FT/SEC
 $V_{14} = 1000$ FT/SEC
 $V_{15} = 1000$ FT/SEC
 $V_{16} = 1000$ FT/SEC
 $V_{17} = 1000$ FT/SEC
 $V_{18} = 1000$ FT/SEC
 $V_{19} = 1000$ FT/SEC
 $V_{20} = 1000$ FT/SEC
 $V_{21} = 1000$ FT/SEC
 $V_{22} = 1000$ FT/SEC
 $V_{23} = 1000$ FT/SEC
 $V_{24} = 1000$ FT/SEC
 $V_{25} = 1000$ FT/SEC
 $V_{26} = 1000$ FT/SEC
 $V_{27} = 1000$ FT/SEC
 $V_{28} = 1000$ FT/SEC
 $V_{29} = 1000$ FT/SEC
 $V_{30} = 1000$ FT/SEC
 $V_{31} = 1000$ FT/SEC
 $V_{32} = 1000$ FT/SEC
 $V_{33} = 1000$ FT/SEC
 $V_{34} = 1000$ FT/SEC
 $V_{35} = 1000$ FT/SEC
 $V_{36} = 1000$ FT/SEC
 $V_{37} = 1000$ FT/SEC
 $V_{38} = 1000$ FT/SEC
 $V_{39} = 1000$ FT/SEC
 $V_{40} = 1000$ FT/SEC
 $V_{41} = 1000$ FT/SEC
 $V_{42} = 1000$ FT/SEC
 $V_{43} = 1000$ FT/SEC
 $V_{44} = 1000$ FT/SEC
 $V_{45} = 1000$ FT/SEC
 $V_{46} = 1000$ FT/SEC
 $V_{47} = 1000$ FT/SEC
 $V_{48} = 1000$ FT/SEC
 $V_{49} = 1000$ FT/SEC
 $V_{50} = 1000$ FT/SEC
 $V_{51} = 1000$ FT/SEC
 $V_{52} = 1000$ FT/SEC
 $V_{53} = 1000$ FT/SEC
 $V_{54} = 1000$ FT/SEC
 $V_{55} = 1000$ FT/SEC
 $V_{56} = 1000$ FT/SEC
 $V_{57} = 1000$ FT/SEC
 $V_{58} = 1000$ FT/SEC
 $V_{59} = 1000$ FT/SEC
 $V_{60} = 1000$ FT/SEC
 $V_{61} = 1000$ FT/SEC
 $V_{62} = 1000$ FT/SEC
 $V_{63} = 1000$ FT/SEC
 $V_{64} = 1000$ FT/SEC
 $V_{65} = 1000$ FT/SEC
 $V_{66} = 1000$ FT/SEC
 $V_{67} = 1000$ FT/SEC
 $V_{68} = 1000$ FT/SEC
 $V_{69} = 1000$ FT/SEC
 $V_{70} = 1000$ FT/SEC
 $V_{71} = 1000$ FT/SEC
 $V_{72} = 1000$ FT/SEC
 $V_{73} = 1000$ FT/SEC
 $V_{74} = 1000$ FT/SEC
 $V_{75} = 1000$ FT/SEC
 $V_{76} = 1000$ FT/SEC
 $V_{77} = 1000$ FT/SEC
 $V_{78} = 1000$ FT/SEC
 $V_{79} = 1000$ FT/SEC
 $V_{80} = 1000$ FT/SEC
 $V_{81} = 1000$ FT/SEC
 $V_{82} = 1000$ FT/SEC
 $V_{83} = 1000$ FT/SEC
 $V_{84} = 1000$ FT/SEC
 $V_{85} = 1000$ FT/SEC
 $V_{86} = 1000$ FT/SEC
 $V_{87} = 1000$ FT/SEC
 $V_{88} = 1000$ FT/SEC
 $V_{89} = 1000$ FT/SEC
 $V_{90} = 1000$ FT/SEC
 $V_{91} = 1000$ FT/SEC
 $V_{92} = 1000$ FT/SEC
 $V_{93} = 1000$ FT/SEC
 $V_{94} = 1000$ FT/SEC
 $V_{95} = 1000$ FT/SEC
 $V_{96} = 1000$ FT/SEC
 $V_{97} = 1000$ FT/SEC
 $V_{98} = 1000$ FT/SEC
 $V_{99} = 1000$ FT/SEC
 $V_{100} = 1000$ FT/SEC

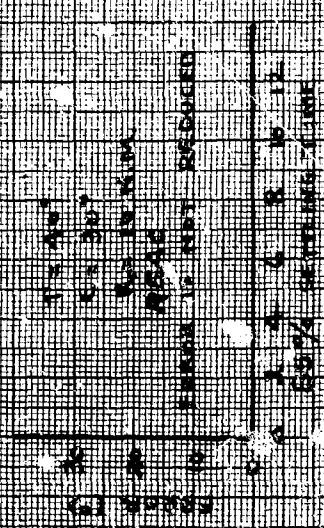
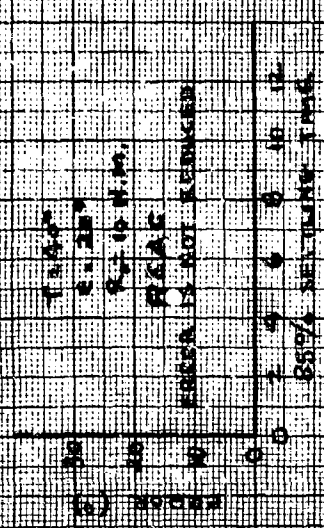
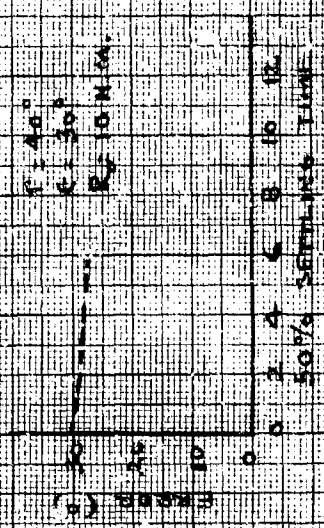
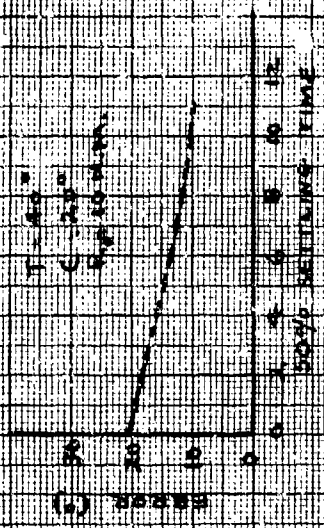
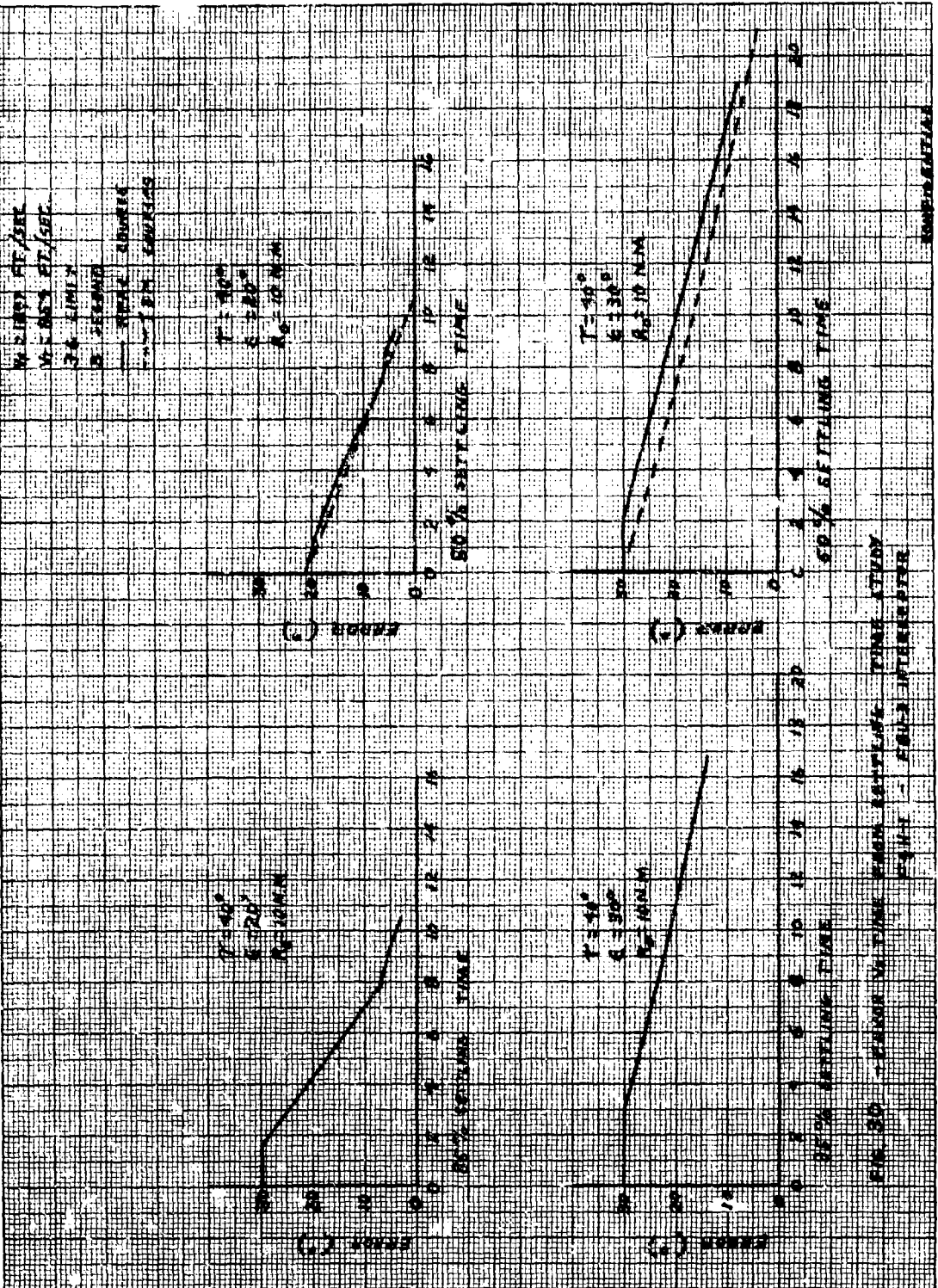
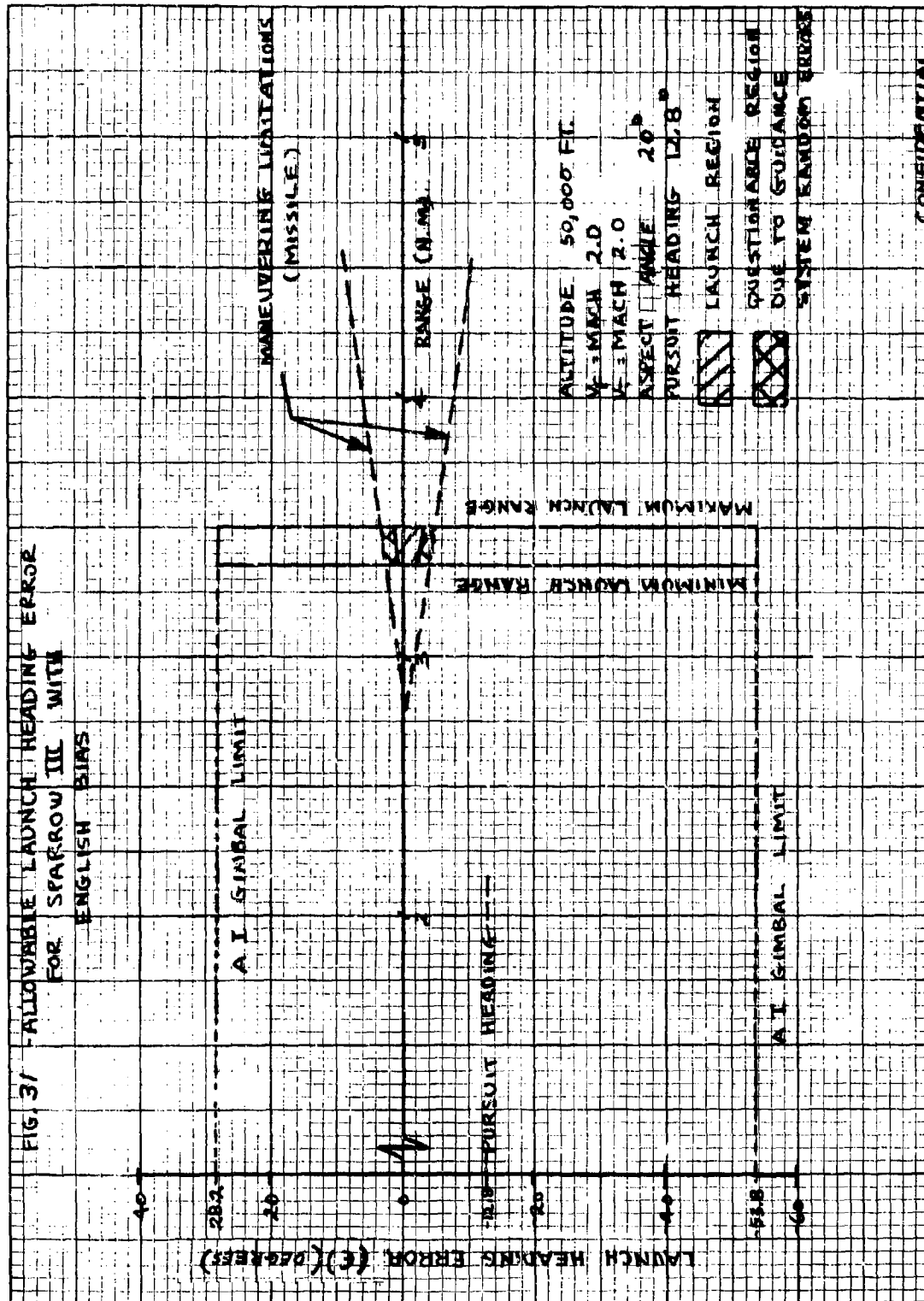


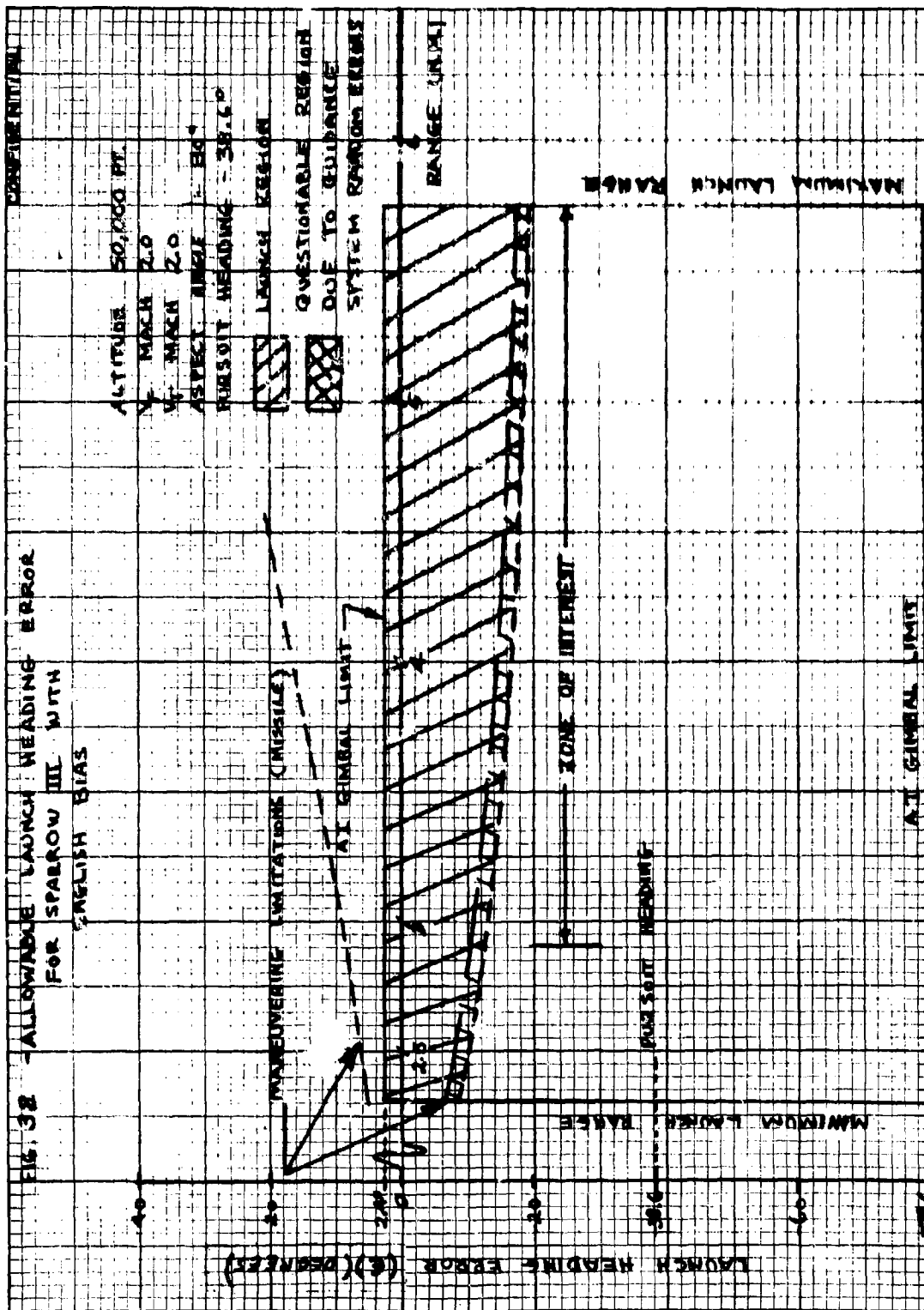
FIG. 20 - CURVE VS. TIME FROM SETTLING TIME STUDY
 FOR 1 - 1000 3 INTERFERE

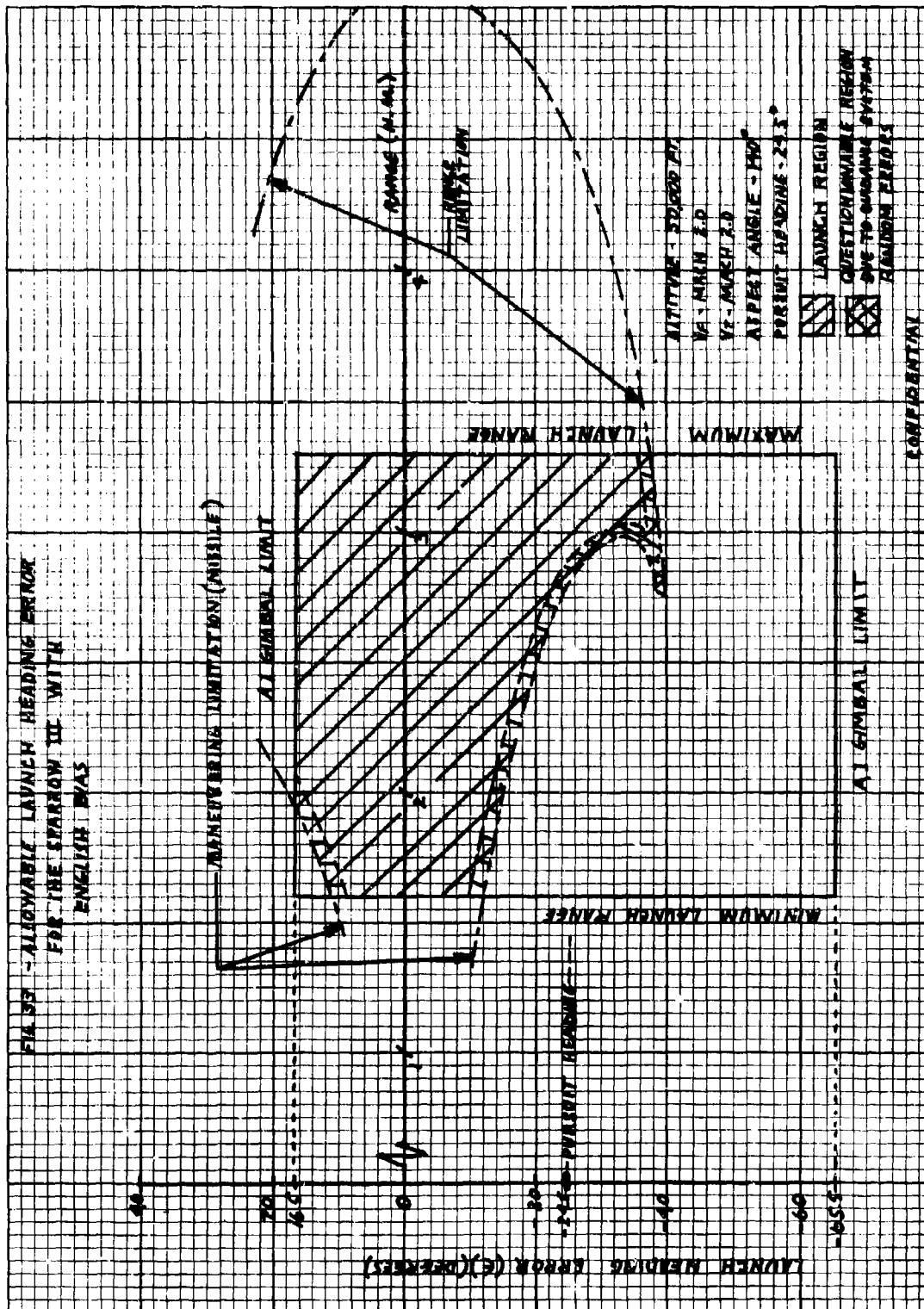
CONFIDENTIAL

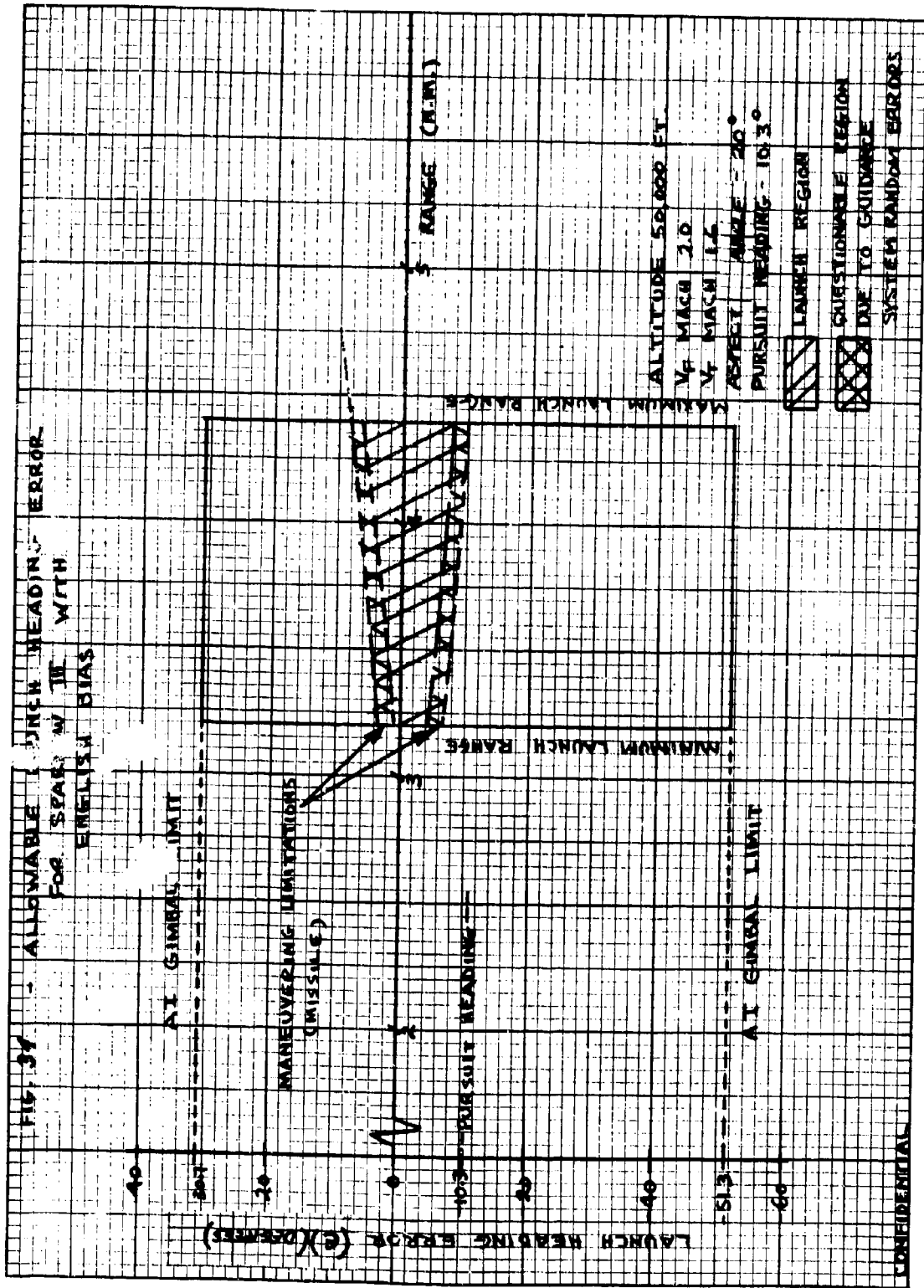


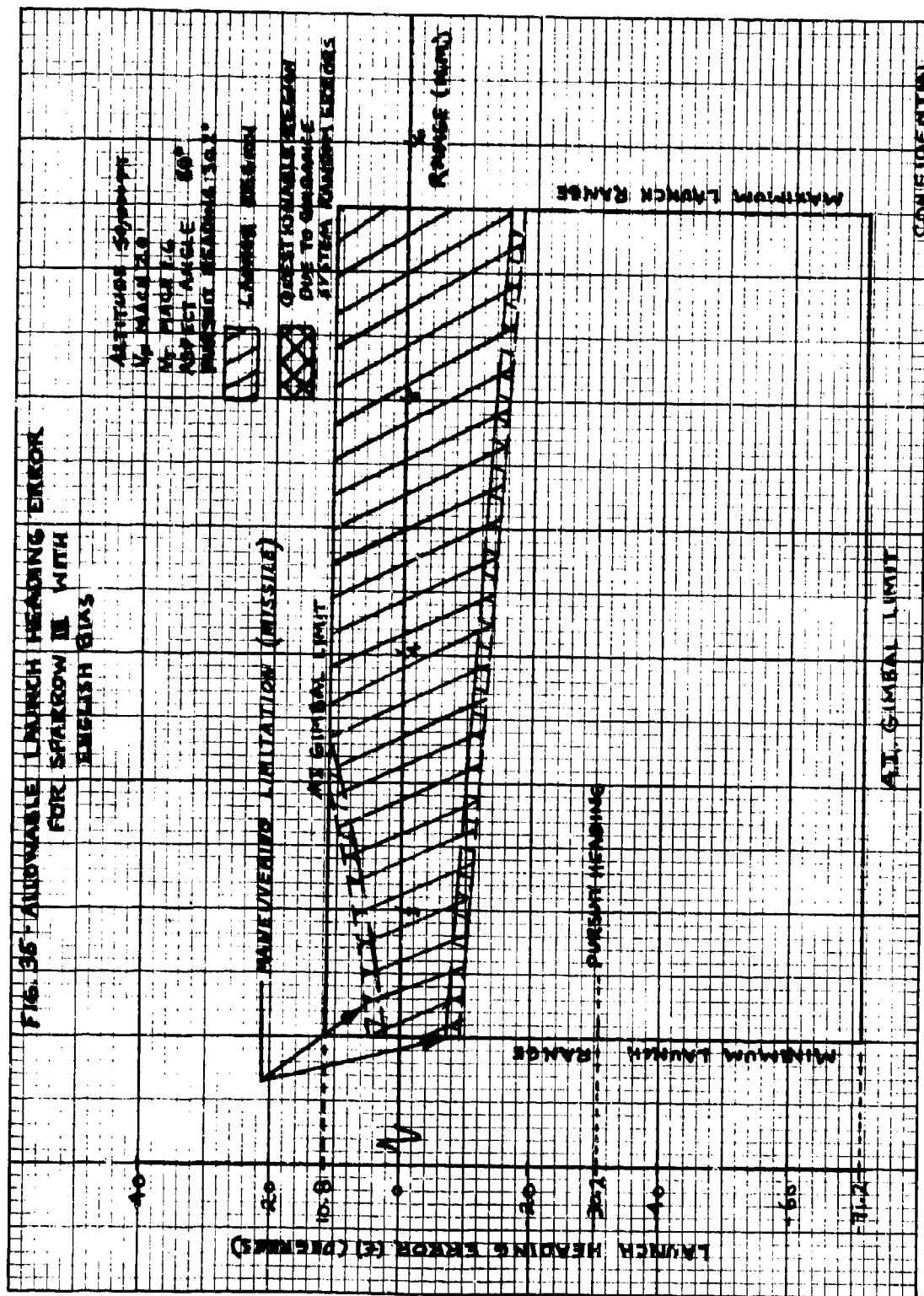


CONFIDENTIAL



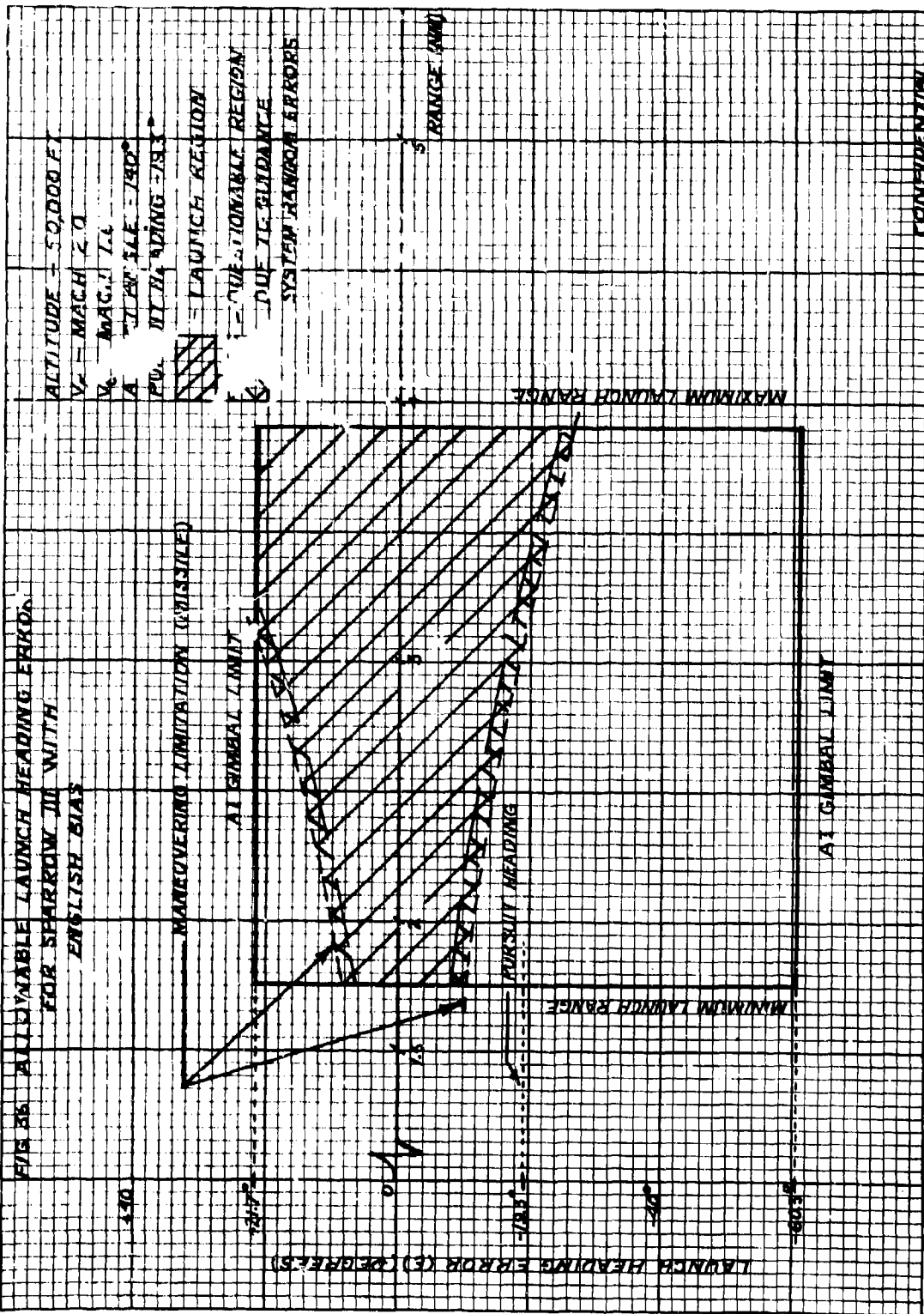


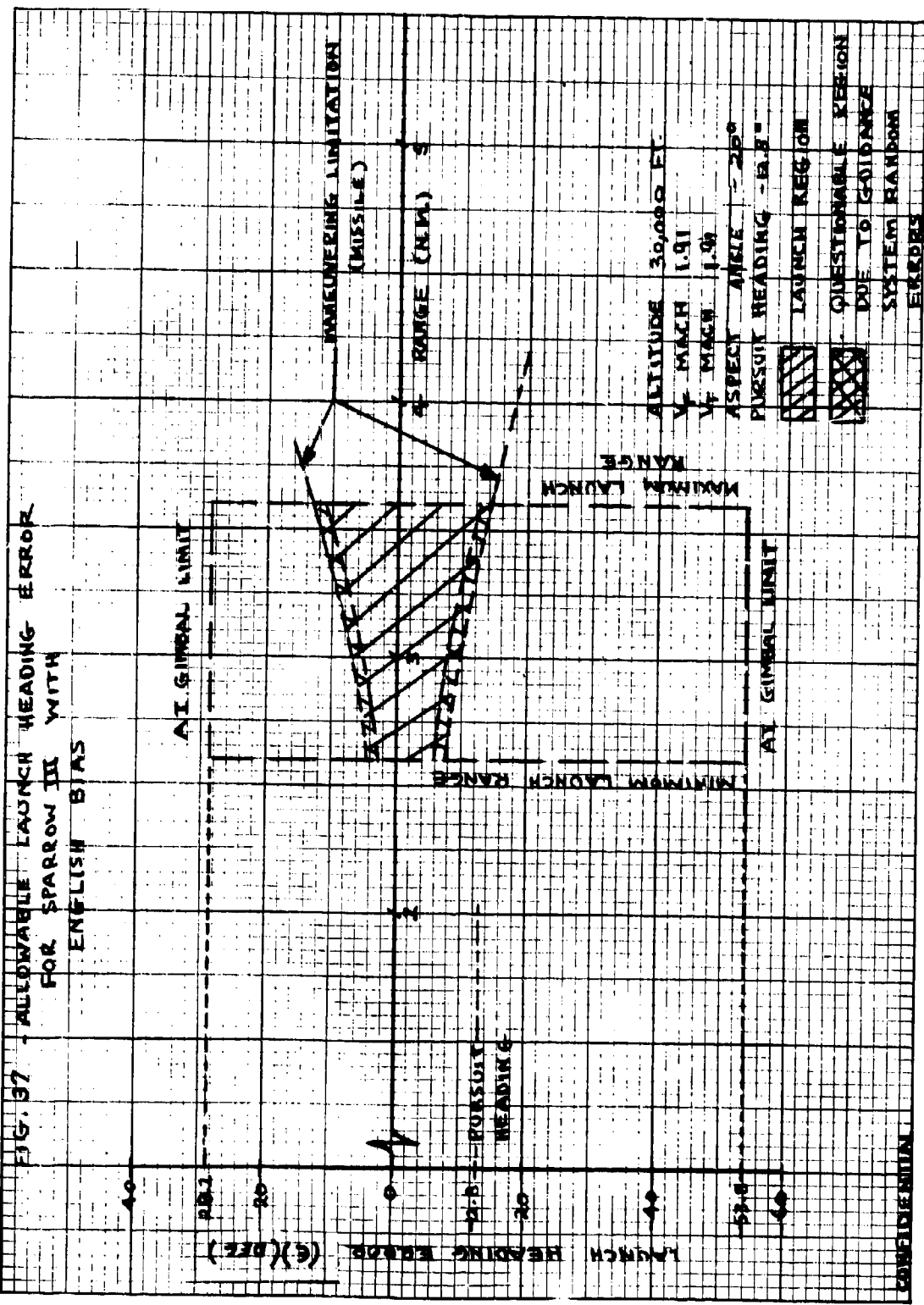




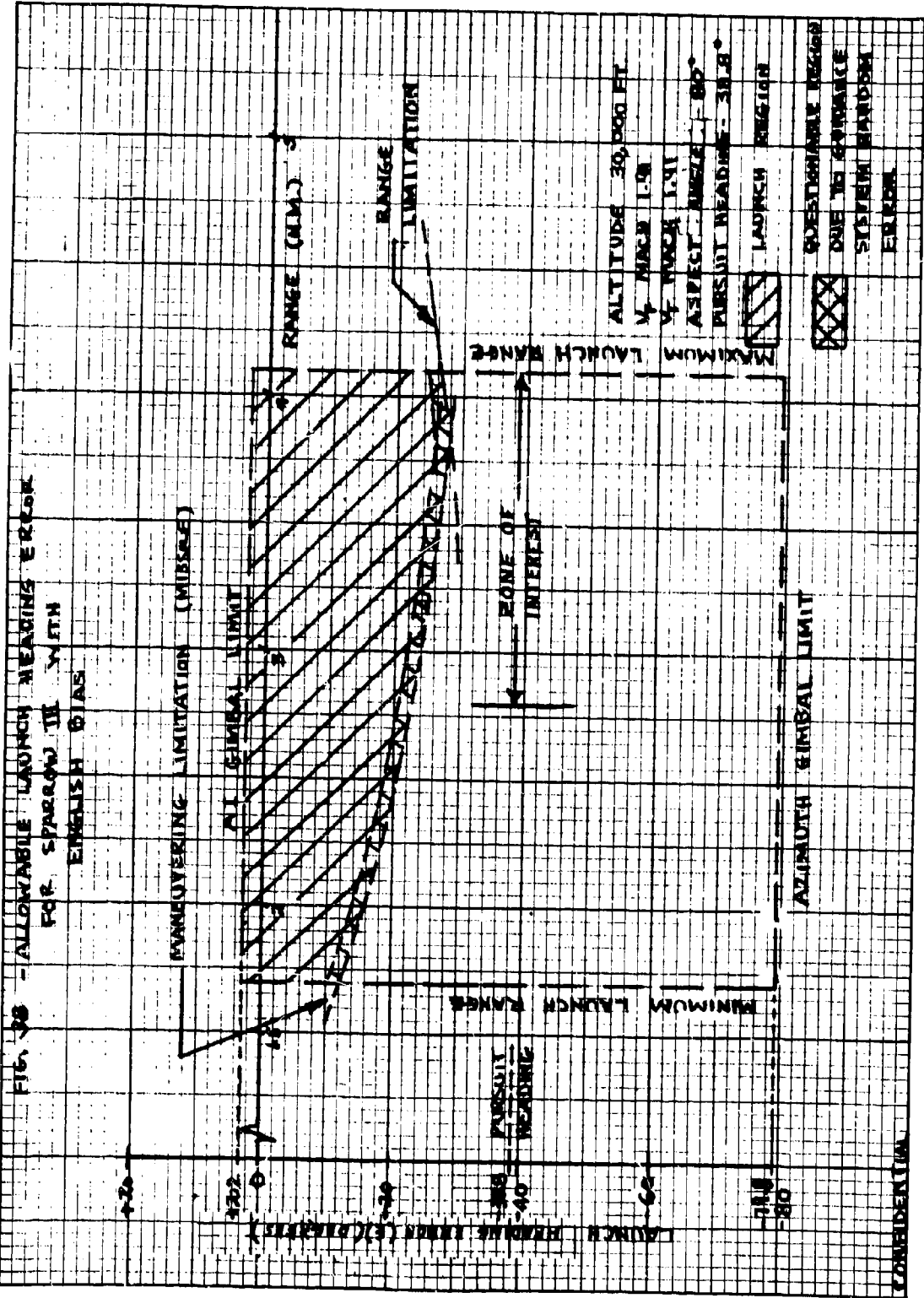
CONFIDENTIAL

FIG. 36. ADJUSTABLE LAUNCH HEADING ERROR FOR SPARROW 30 WITH ENGLISH BIAS





CONFIDENTIAL



CONFIDENTIAL

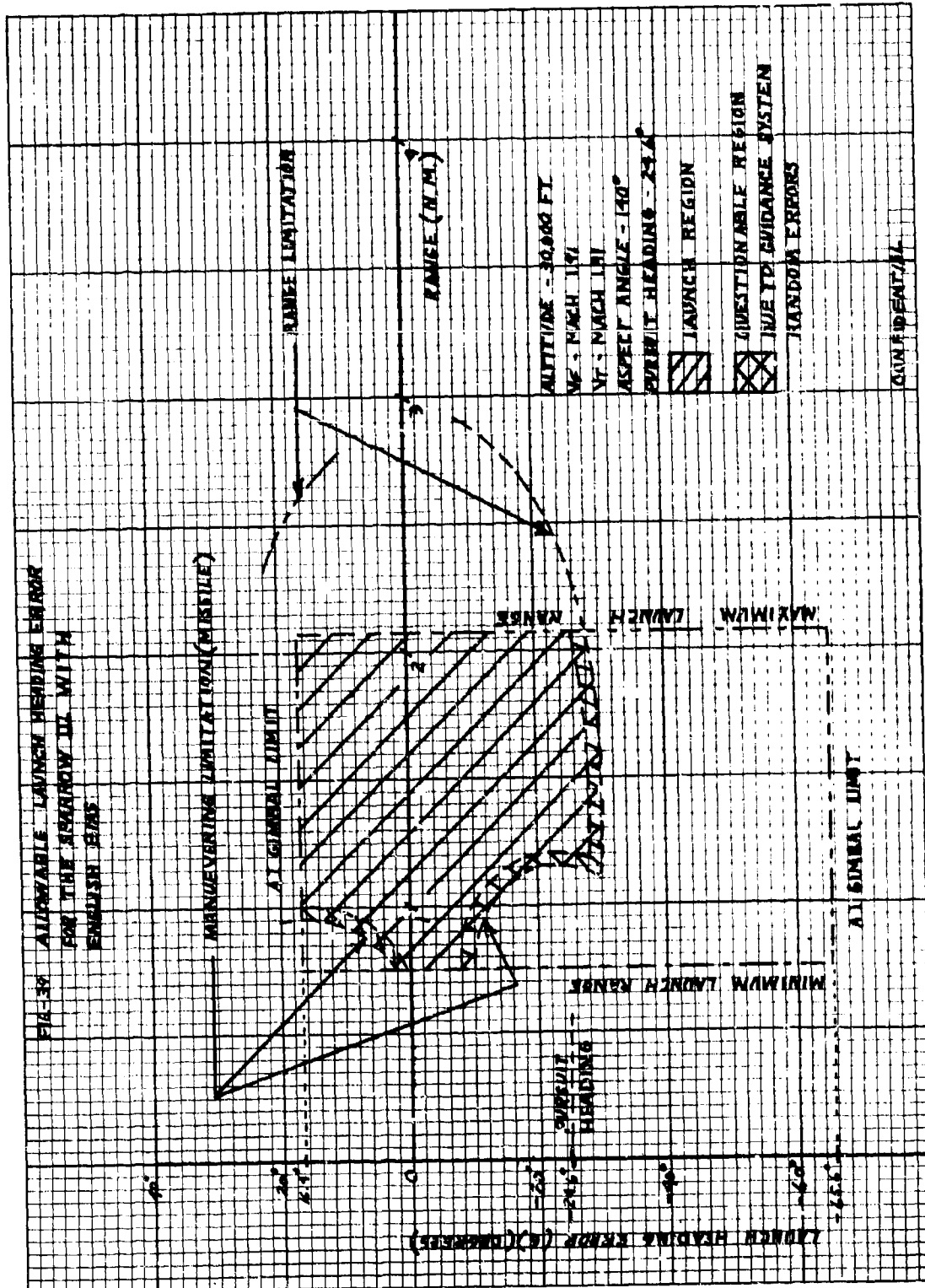
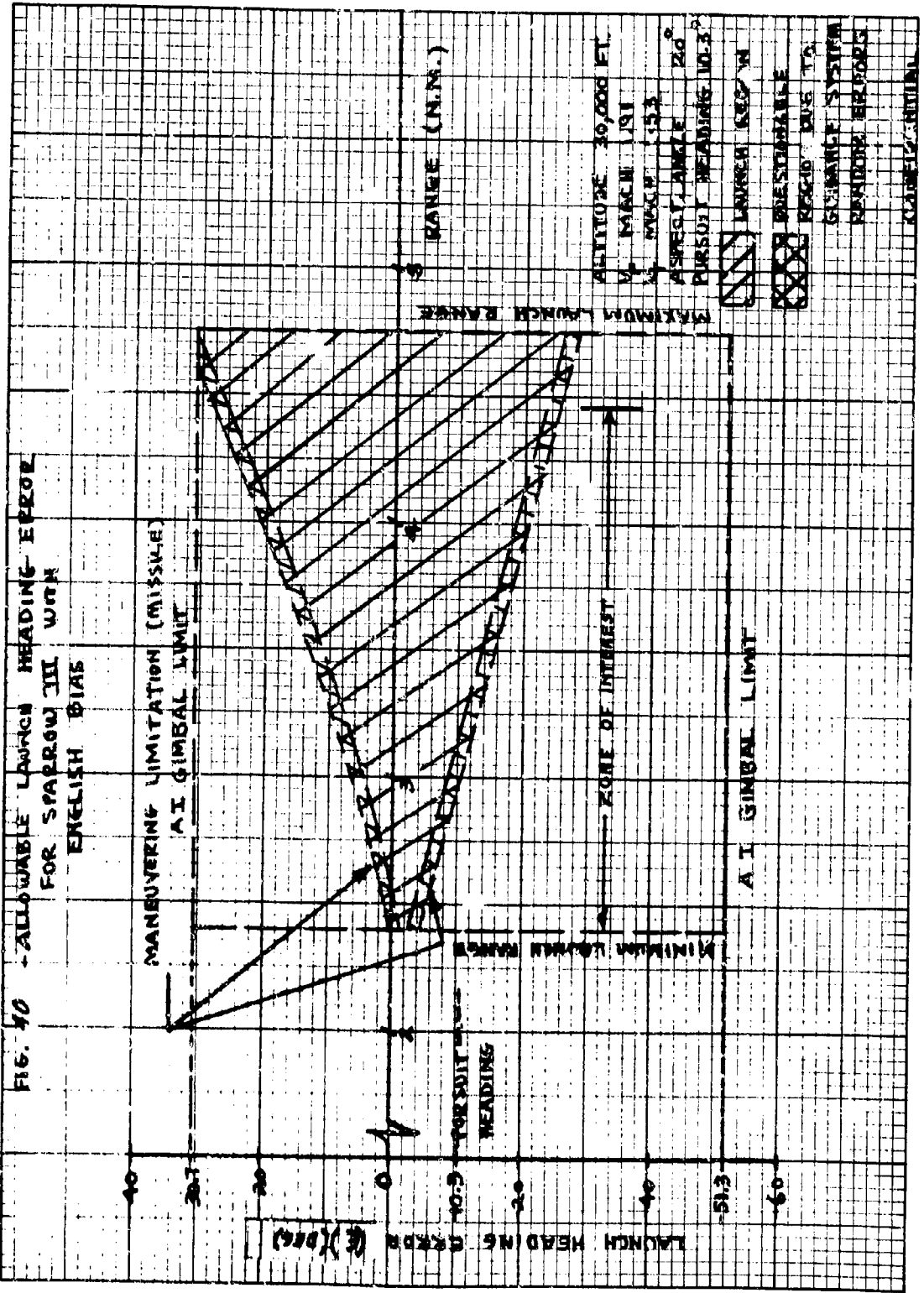
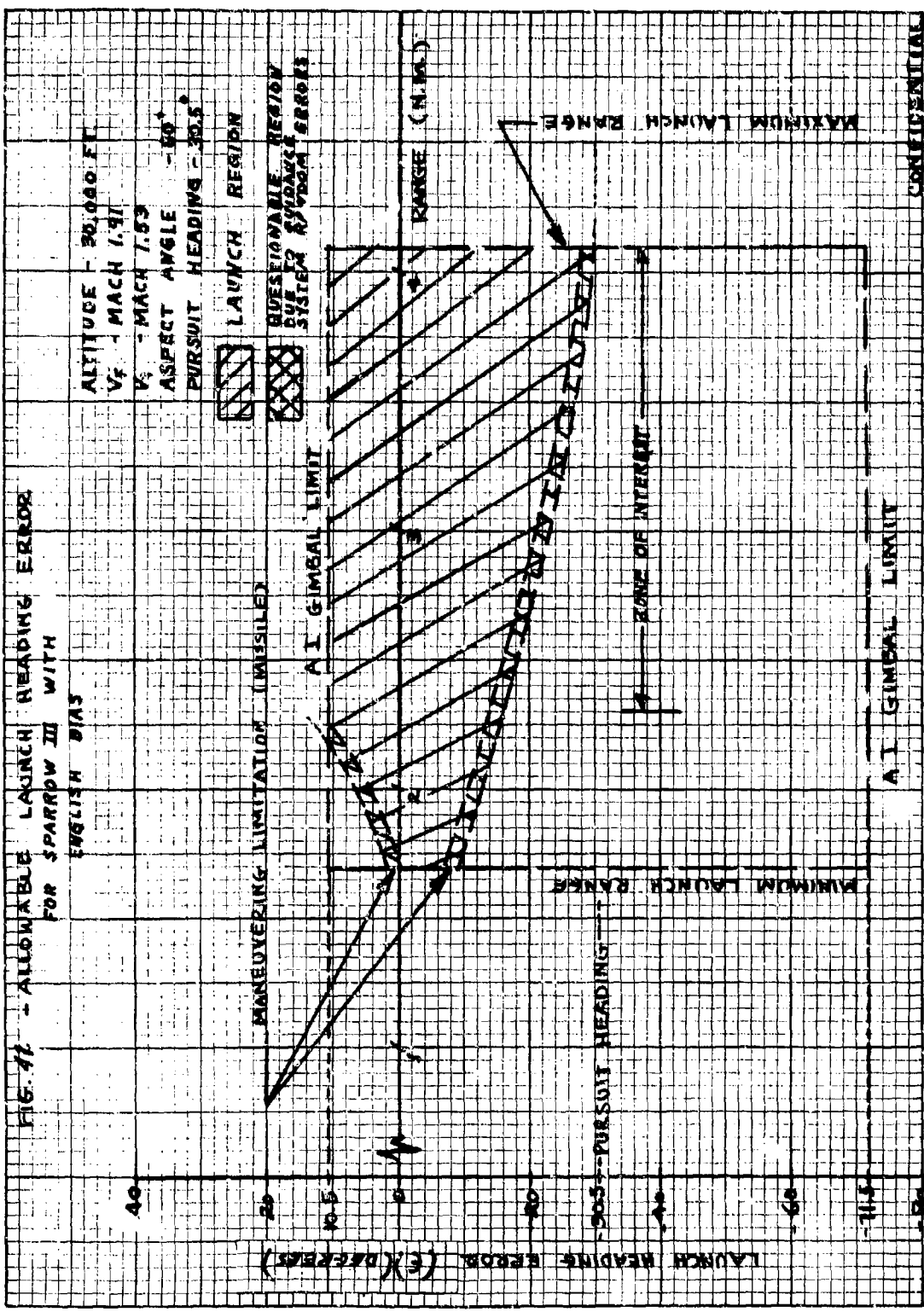


FIG. 40 - ALLOWABLE LAUNCH HEADING ERROR
FOR SPARROW III WITH
ENGLISH BIAS





CONFIDENTIAL

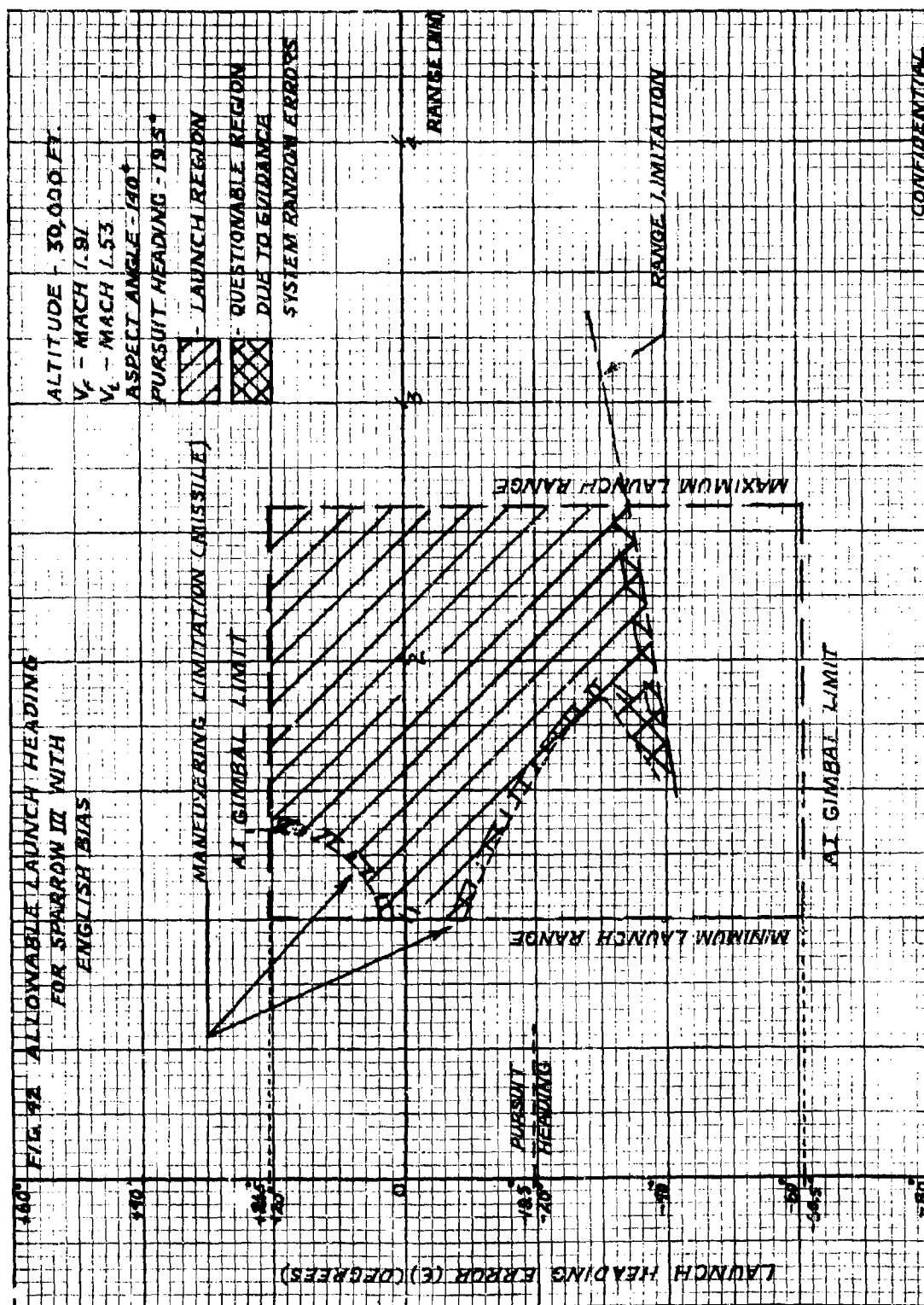
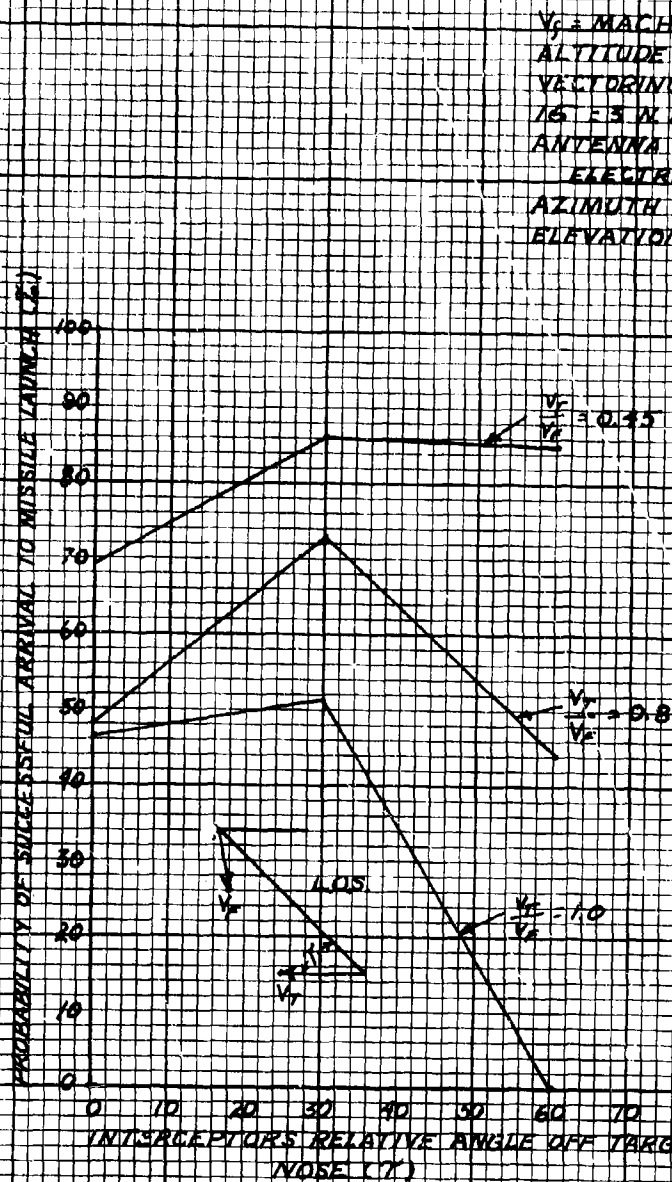


FIG. 43 - PROBABILITY OF SUCCESSFUL ARRIVAL TO MISSILE
LAUNCH VS VECTORIZING ANGLE



CONFIDENTIAL

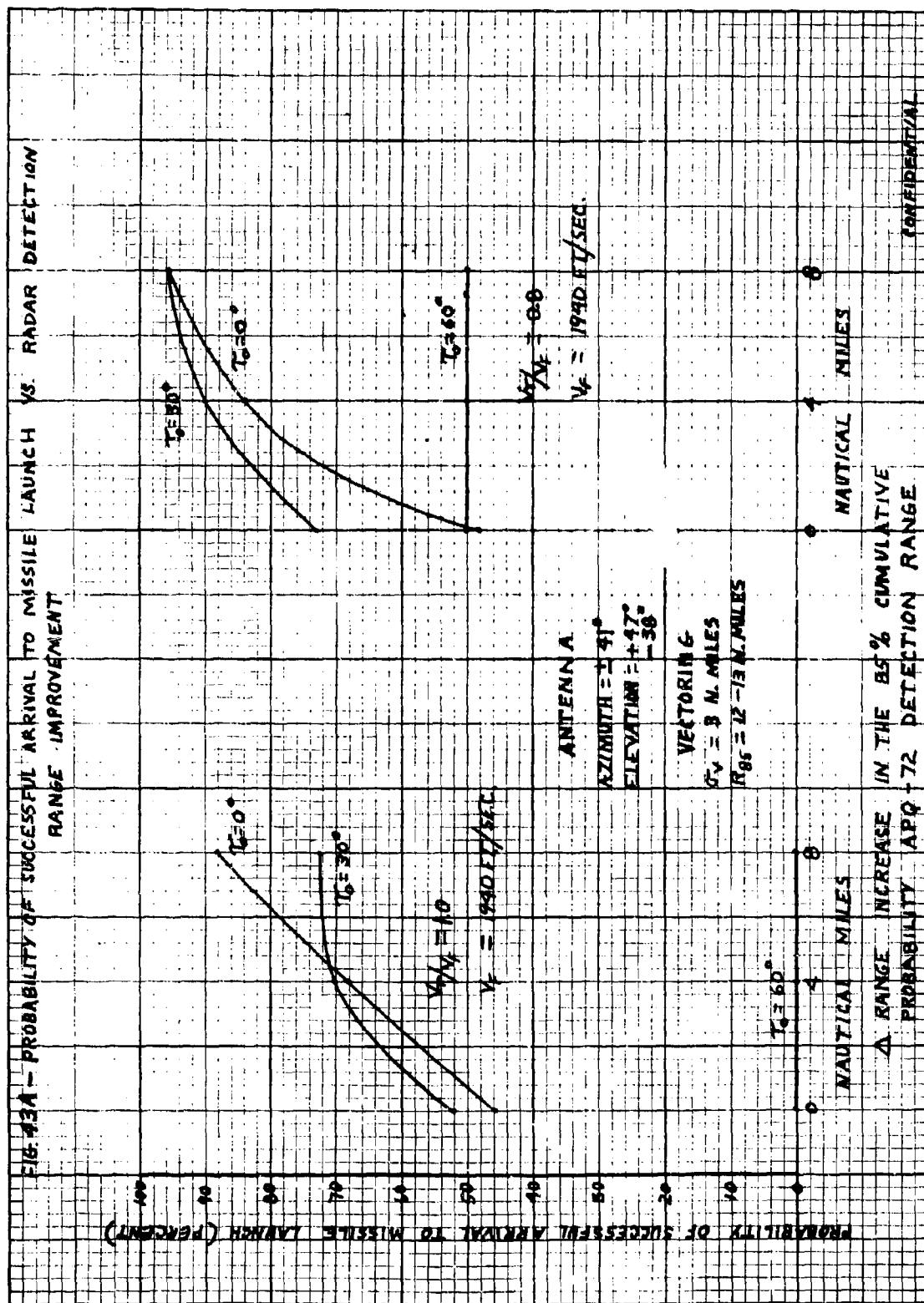
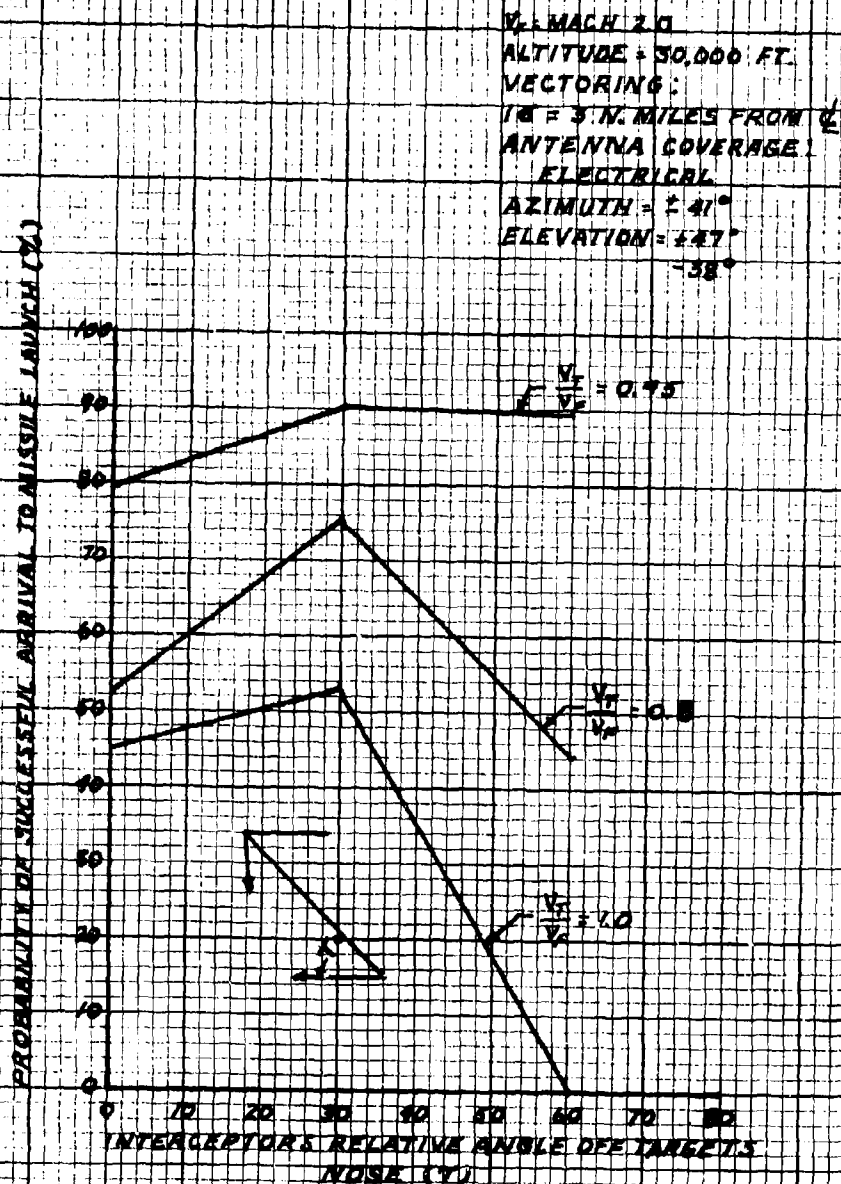


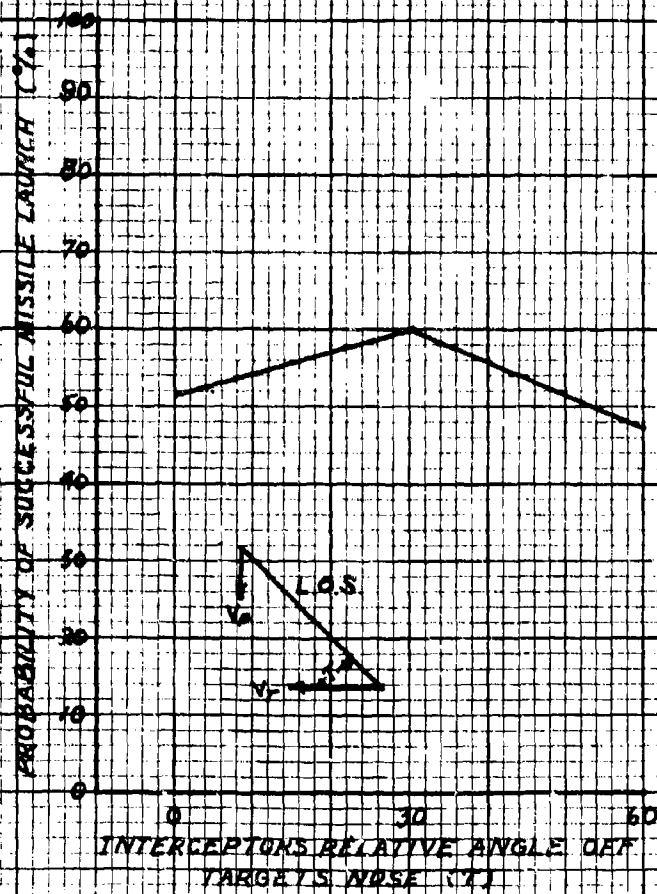
FIG. 24 - PROBABILITY OF SUCCESSFUL ARRIVAL TO MISSILE LAUNCH VS VECTORING ANGLE



CONFIDENTIAL

FIG. 13 PROBABILITY OF SUCCESSFUL ARRIVAL TO MISSILE
LAUNCH VS VECTORIZING ANGLE

ALTITUDE = 1000 FT
 $V_p = 183 \text{ FT/SEC} = \text{MIDT}$
 $V_p/V_t = 0.8$
 VECTORIZING
 $15^\circ \pm 3 \text{ N. MILES FROM } \frac{1}{2}$
 ANTENNA COVERAGE
 AZIMUTH $\pm 41^\circ$
 ELEVATION $\pm 27^\circ$
 -38°



CONFIDENTIAL

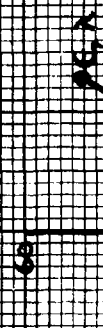
FIG 46 - PULL-UP ATTACKS, HEAD ON - UNIMPROVED MANEUVER

MIN 2.0 TARGET 25,000 FT.

PULL-UP 3.00 OR CL MAX

VELOCITY 2.0 OR V_{MAX}

VELOCITY ACCURACY 10% ± 5 NM IN ESTIMATING



E - RESTRICTION DUE TO EYES 710°

X - RESTRICTION DUE TO ISOMERAL ANGLE

PROBABILITY OF SUCCESSFUL MANEUVER TO MISSILE LAUNCH (%)

CONFIDENTIAL

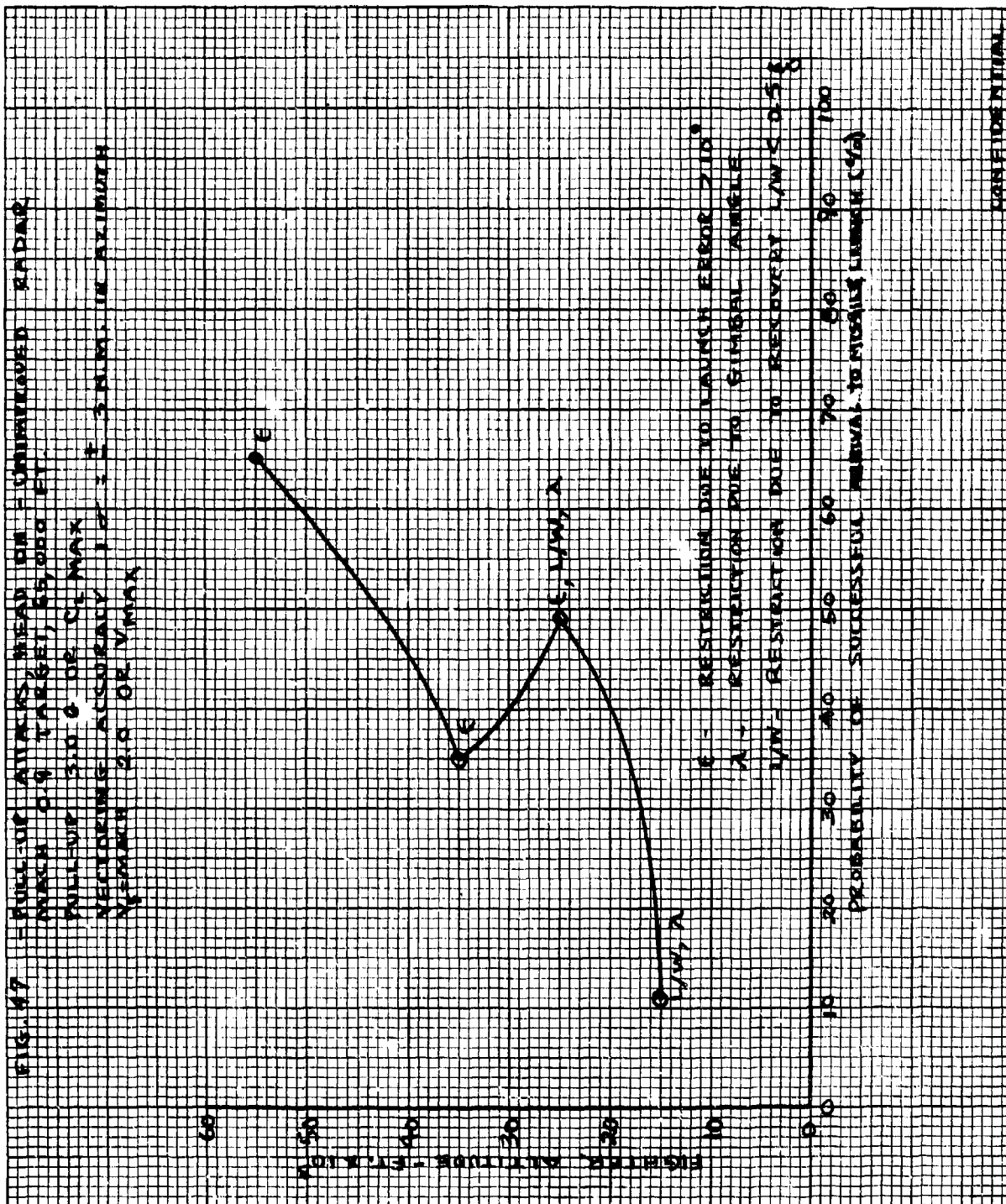
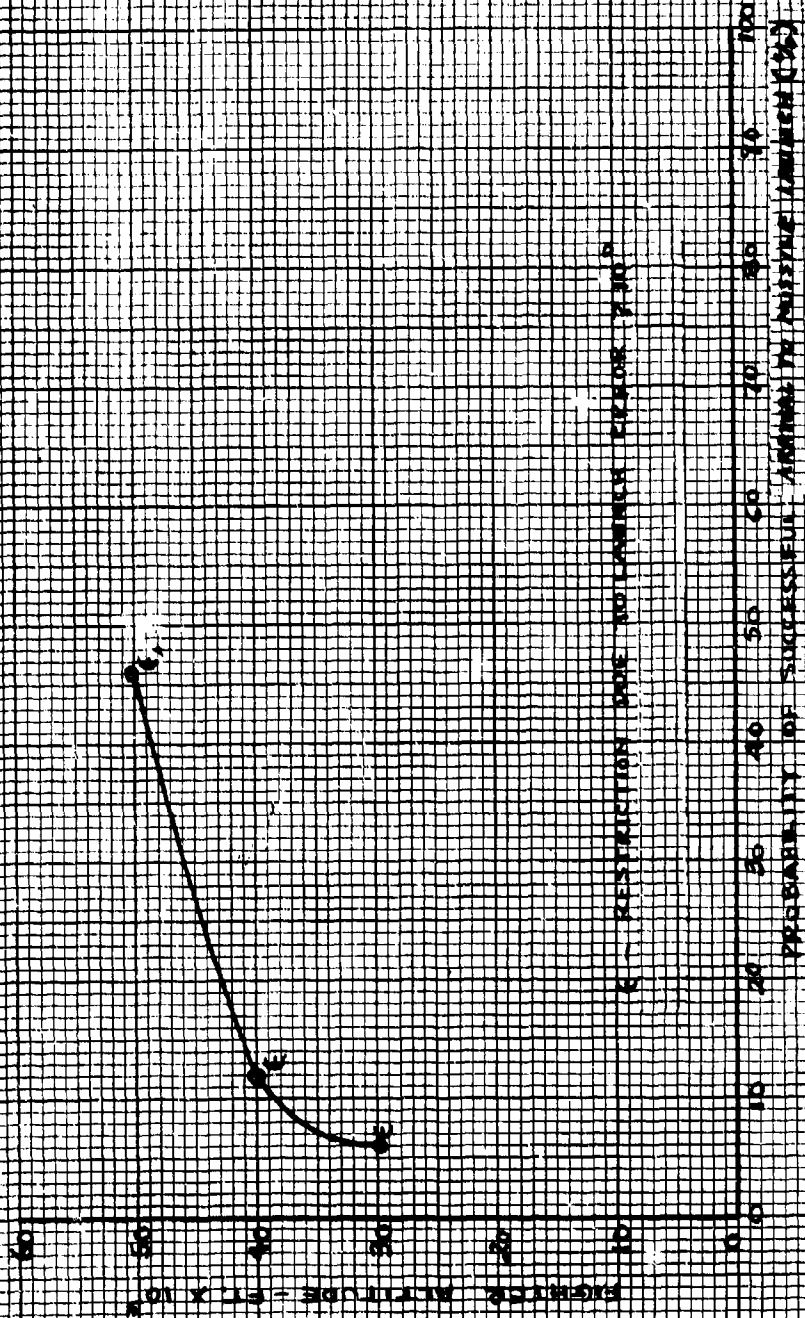
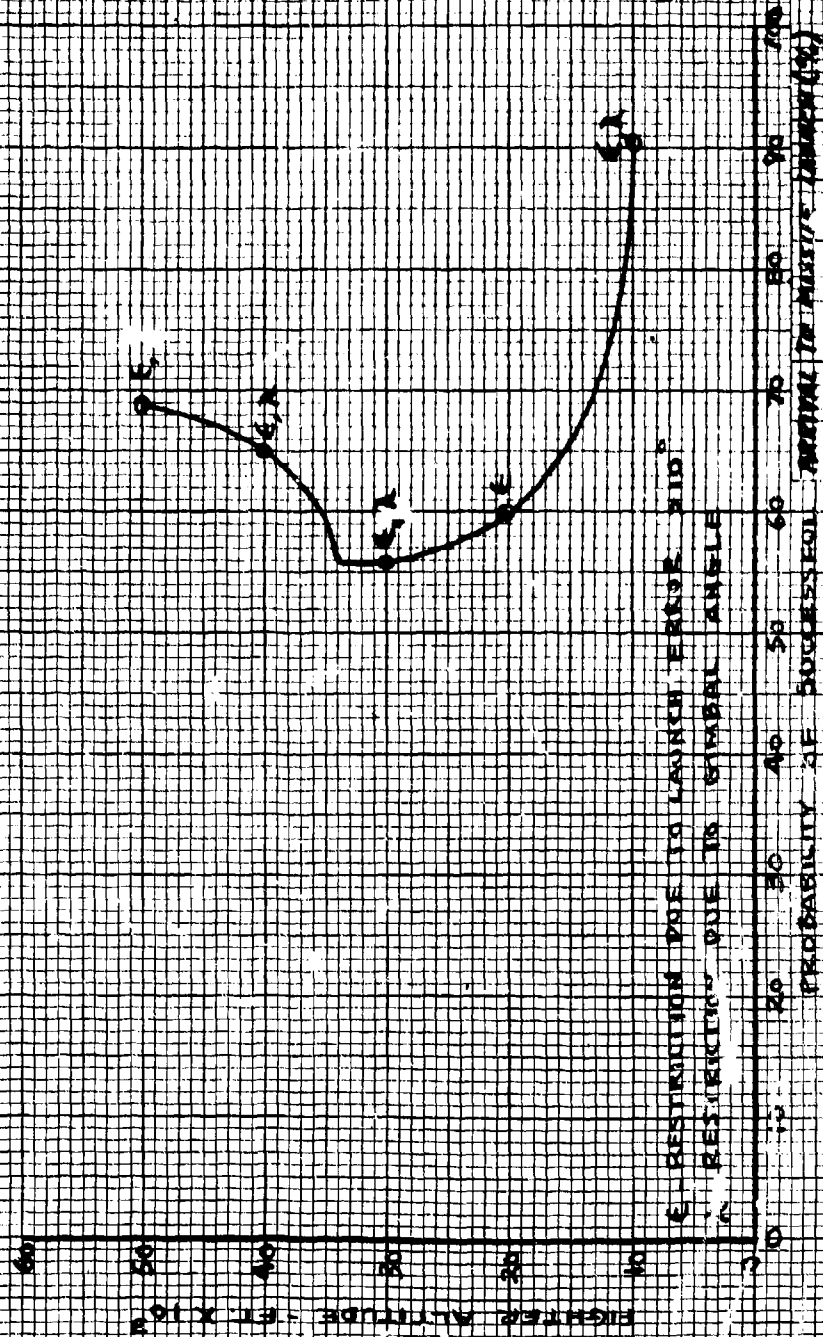


FIG. 28 - PULL-UP ATTACKS - HEAD ON - UNIMPROVED, CLADAR
 PULL-UP 2.0 TARGET, 50,000 FT.
 PULL-UP 3.0 TARGET, 50,000 FT.
 PULL-UP 4.0 TARGET, 50,000 FT.
 PULL-UP 5.0 TARGET, 50,000 FT.
 PULL-UP 6.0 TARGET, 50,000 FT.
 PULL-UP 7.0 TARGET, 50,000 FT.
 PULL-UP 8.0 TARGET, 50,000 FT.
 PULL-UP 9.0 TARGET, 50,000 FT.
 PULL-UP 10.0 TARGET, 50,000 FT.
 PULL-UP 11.0 TARGET, 50,000 FT.
 PULL-UP 12.0 TARGET, 50,000 FT.
 PULL-UP 13.0 TARGET, 50,000 FT.
 PULL-UP 14.0 TARGET, 50,000 FT.
 PULL-UP 15.0 TARGET, 50,000 FT.
 PULL-UP 16.0 TARGET, 50,000 FT.
 PULL-UP 17.0 TARGET, 50,000 FT.
 PULL-UP 18.0 TARGET, 50,000 FT.
 PULL-UP 19.0 TARGET, 50,000 FT.
 PULL-UP 20.0 TARGET, 50,000 FT.
 PULL-UP 21.0 TARGET, 50,000 FT.
 PULL-UP 22.0 TARGET, 50,000 FT.
 PULL-UP 23.0 TARGET, 50,000 FT.
 PULL-UP 24.0 TARGET, 50,000 FT.
 PULL-UP 25.0 TARGET, 50,000 FT.
 PULL-UP 26.0 TARGET, 50,000 FT.
 PULL-UP 27.0 TARGET, 50,000 FT.
 PULL-UP 28.0 TARGET, 50,000 FT.
 PULL-UP 29.0 TARGET, 50,000 FT.
 PULL-UP 30.0 TARGET, 50,000 FT.
 PULL-UP 31.0 TARGET, 50,000 FT.
 PULL-UP 32.0 TARGET, 50,000 FT.
 PULL-UP 33.0 TARGET, 50,000 FT.
 PULL-UP 34.0 TARGET, 50,000 FT.
 PULL-UP 35.0 TARGET, 50,000 FT.
 PULL-UP 36.0 TARGET, 50,000 FT.
 PULL-UP 37.0 TARGET, 50,000 FT.
 PULL-UP 38.0 TARGET, 50,000 FT.
 PULL-UP 39.0 TARGET, 50,000 FT.
 PULL-UP 40.0 TARGET, 50,000 FT.
 PULL-UP 41.0 TARGET, 50,000 FT.
 PULL-UP 42.0 TARGET, 50,000 FT.
 PULL-UP 43.0 TARGET, 50,000 FT.
 PULL-UP 44.0 TARGET, 50,000 FT.
 PULL-UP 45.0 TARGET, 50,000 FT.
 PULL-UP 46.0 TARGET, 50,000 FT.
 PULL-UP 47.0 TARGET, 50,000 FT.
 PULL-UP 48.0 TARGET, 50,000 FT.
 PULL-UP 49.0 TARGET, 50,000 FT.
 PULL-UP 50.0 TARGET, 50,000 FT.
 PULL-UP 51.0 TARGET, 50,000 FT.
 PULL-UP 52.0 TARGET, 50,000 FT.
 PULL-UP 53.0 TARGET, 50,000 FT.
 PULL-UP 54.0 TARGET, 50,000 FT.
 PULL-UP 55.0 TARGET, 50,000 FT.
 PULL-UP 56.0 TARGET, 50,000 FT.
 PULL-UP 57.0 TARGET, 50,000 FT.
 PULL-UP 58.0 TARGET, 50,000 FT.
 PULL-UP 59.0 TARGET, 50,000 FT.
 PULL-UP 60.0 TARGET, 50,000 FT.
 PULL-UP 61.0 TARGET, 50,000 FT.
 PULL-UP 62.0 TARGET, 50,000 FT.
 PULL-UP 63.0 TARGET, 50,000 FT.
 PULL-UP 64.0 TARGET, 50,000 FT.
 PULL-UP 65.0 TARGET, 50,000 FT.
 PULL-UP 66.0 TARGET, 50,000 FT.
 PULL-UP 67.0 TARGET, 50,000 FT.
 PULL-UP 68.0 TARGET, 50,000 FT.
 PULL-UP 69.0 TARGET, 50,000 FT.
 PULL-UP 70.0 TARGET, 50,000 FT.
 PULL-UP 71.0 TARGET, 50,000 FT.
 PULL-UP 72.0 TARGET, 50,000 FT.
 PULL-UP 73.0 TARGET, 50,000 FT.
 PULL-UP 74.0 TARGET, 50,000 FT.
 PULL-UP 75.0 TARGET, 50,000 FT.
 PULL-UP 76.0 TARGET, 50,000 FT.
 PULL-UP 77.0 TARGET, 50,000 FT.
 PULL-UP 78.0 TARGET, 50,000 FT.
 PULL-UP 79.0 TARGET, 50,000 FT.
 PULL-UP 80.0 TARGET, 50,000 FT.
 PULL-UP 81.0 TARGET, 50,000 FT.
 PULL-UP 82.0 TARGET, 50,000 FT.
 PULL-UP 83.0 TARGET, 50,000 FT.
 PULL-UP 84.0 TARGET, 50,000 FT.
 PULL-UP 85.0 TARGET, 50,000 FT.
 PULL-UP 86.0 TARGET, 50,000 FT.
 PULL-UP 87.0 TARGET, 50,000 FT.
 PULL-UP 88.0 TARGET, 50,000 FT.
 PULL-UP 89.0 TARGET, 50,000 FT.
 PULL-UP 90.0 TARGET, 50,000 FT.
 PULL-UP 91.0 TARGET, 50,000 FT.
 PULL-UP 92.0 TARGET, 50,000 FT.
 PULL-UP 93.0 TARGET, 50,000 FT.
 PULL-UP 94.0 TARGET, 50,000 FT.
 PULL-UP 95.0 TARGET, 50,000 FT.
 PULL-UP 96.0 TARGET, 50,000 FT.
 PULL-UP 97.0 TARGET, 50,000 FT.
 PULL-UP 98.0 TARGET, 50,000 FT.
 PULL-UP 99.0 TARGET, 50,000 FT.
 PULL-UP 100.0 TARGET, 50,000 FT.

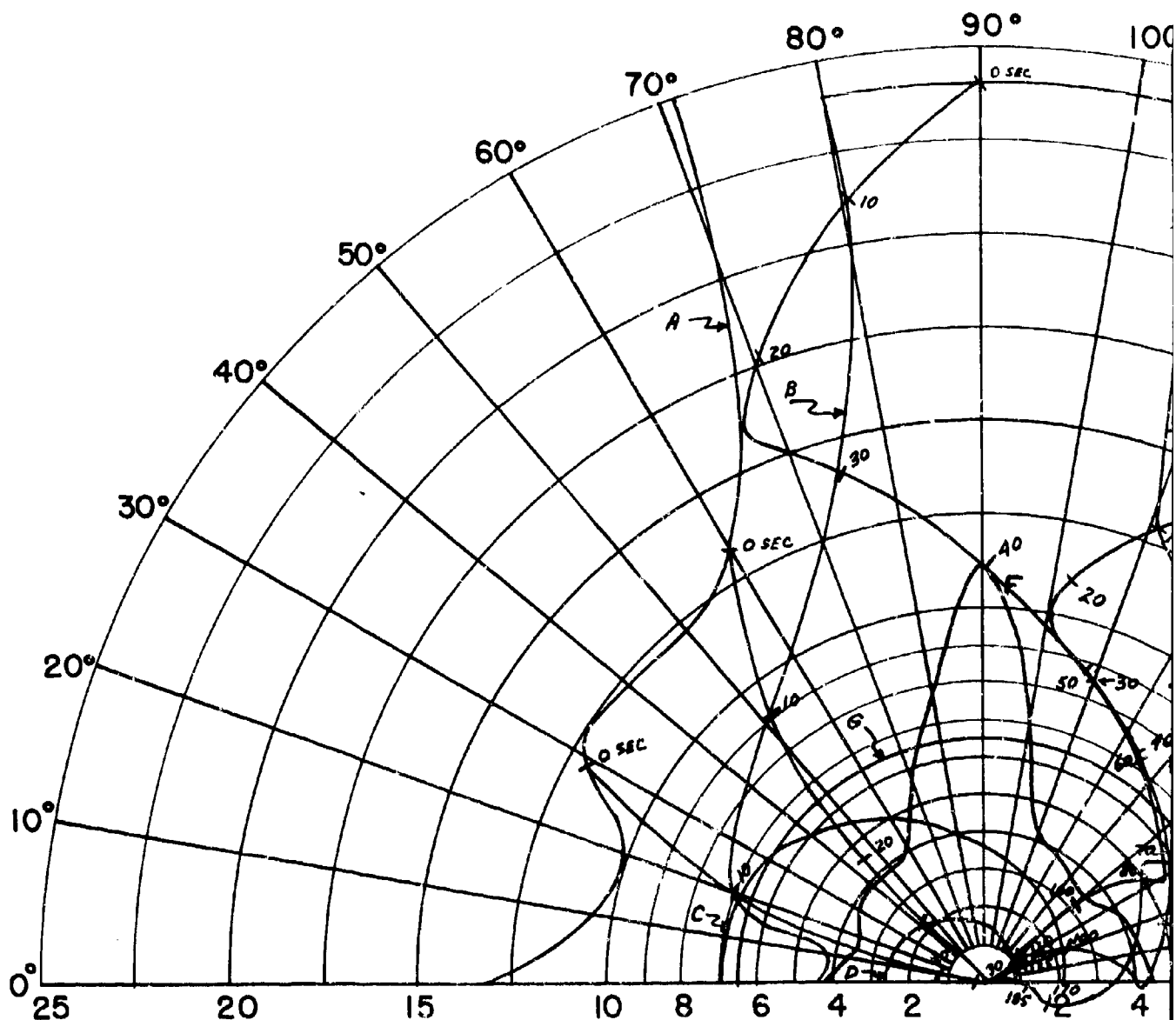


CONFIDENTIAL

FIG. 49 - PULL-UP ATTACKS, HEAD ON - UNIMPROVED RADAR:
 MAKE 0.9 TARGET, 50,000 FT.
 PULL-UP 3.0 G OR CL MAX
 V_F MAX 2.0 OR V_{MAX}
 VECTORING ACCURACY $1^\circ \pm 2^\circ$ 3 N. W. IN AZIMUTH



E - RESTRICTION DUE TO LAUNCH RANGE 210°
 A - RESTRICTION DUE TO GIMBAL ANGLE



$V_F = 1897$ FT/SEC (F4H-1)(F8U-3)

$V_T = 1518$ FT/SEC

ALTITUDE = 30,000 FT.

MANEUVERING TARGET—IN TARGET

COORDINATES

INITIAL RIGHT TURN

TARGET HEADING

A - 85% DETECTION RANGE

B - LOCK-ON RANGE (10 SEC. LOCK)

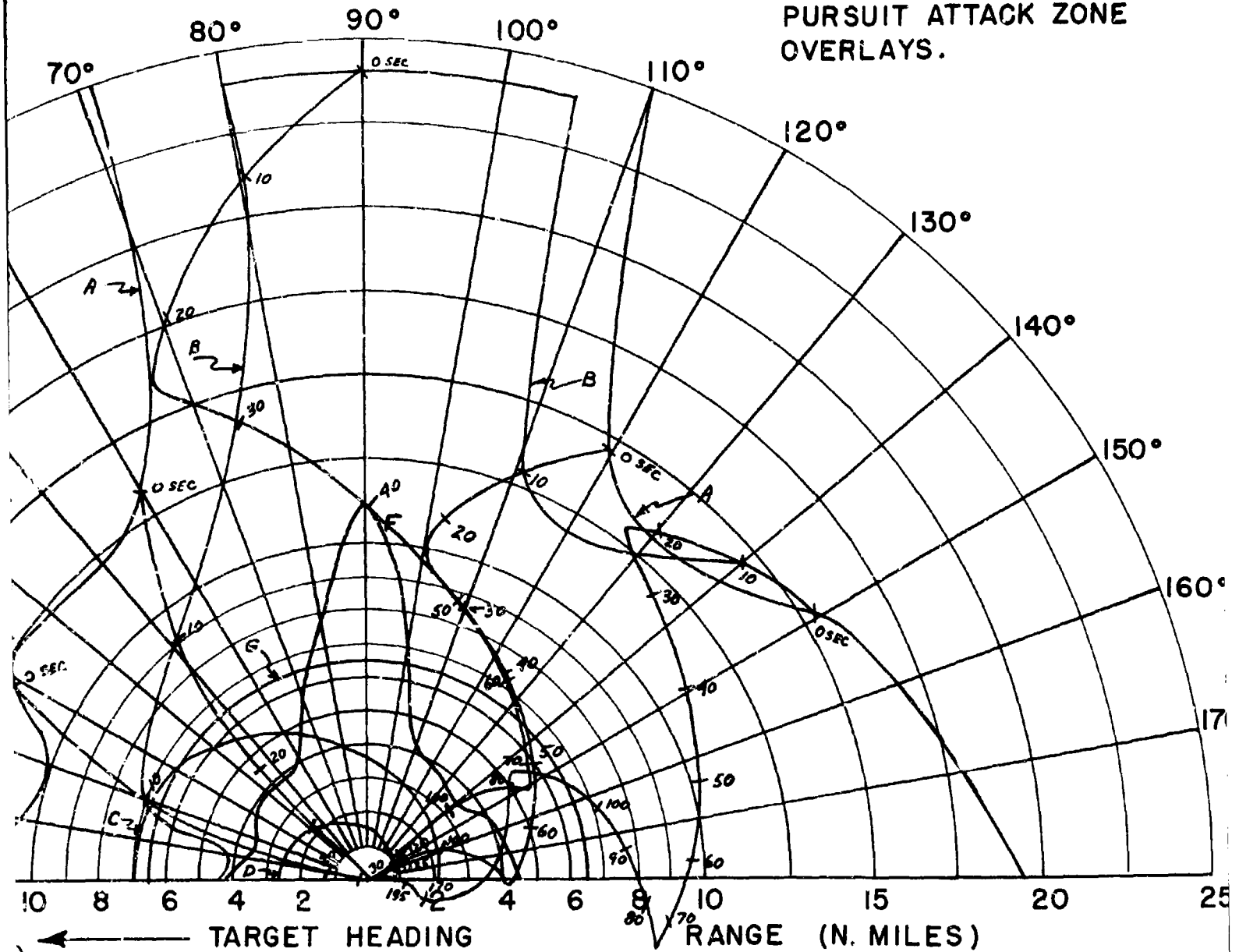
C - SPARROW III MAX. AERODYNAMIC

D - SPARROW III MIN. AERODYNAMIC

F - 90% SPARROW III SEEKER

G - 6.5 N.M. INTERLOCK

FIG. 50 - CO-ALTITUDE LEAD
PURSUIT ATTACK ZONE
OVERLAYS.

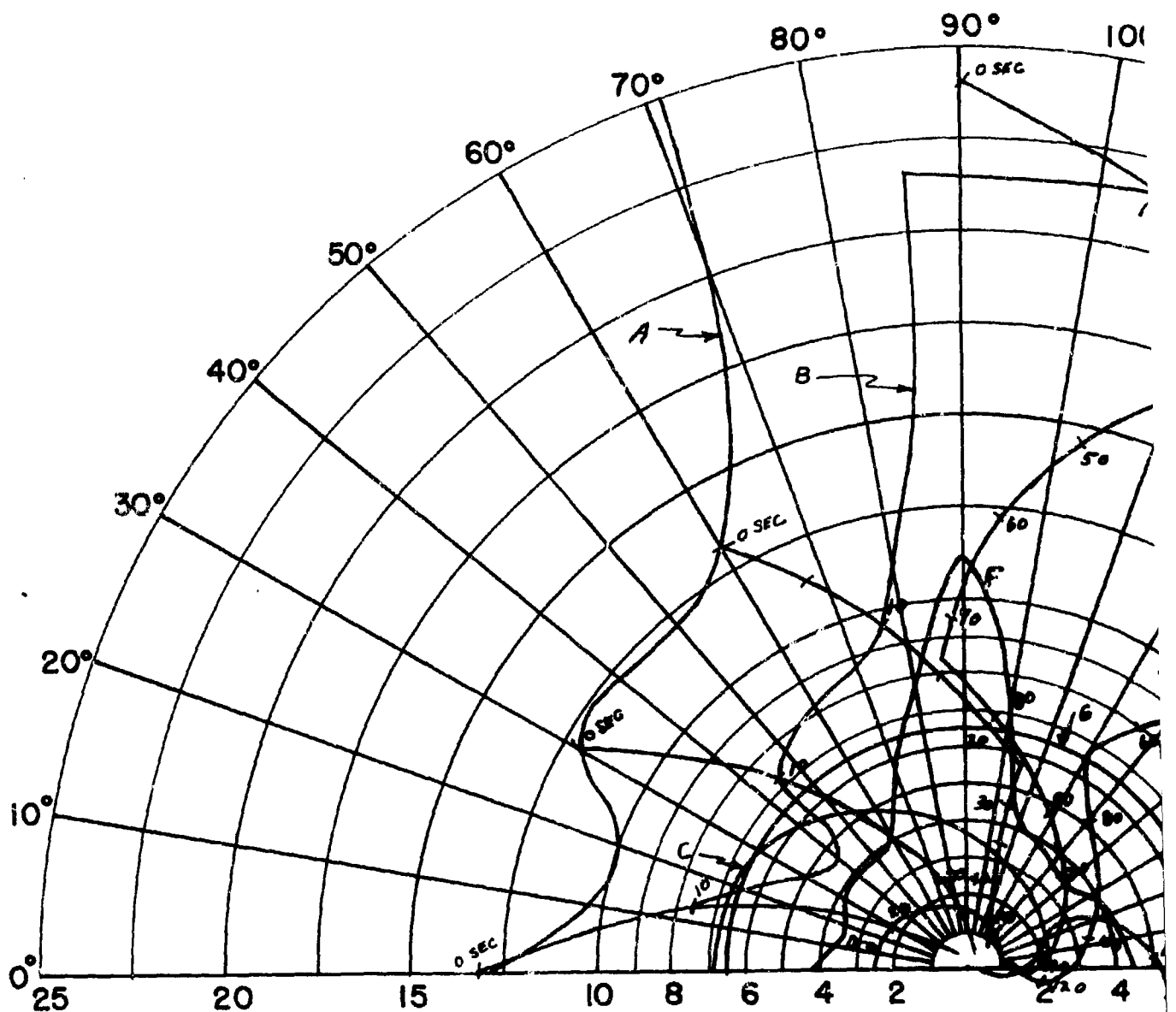


A - 85% DETECTION RANGE
B - LOCK-ON RANGE (10 SEC. LOCK-ON TIME)
C - SPARROW III MAX. AERODYNAMIC RANGE
D - SPARROW III MIN. AERODYNAMIC RANGE

F - 90% SPARROW III SEEKER LOCK-ON RANGE
G - 6.5 N.M. INTERLOCK

2

CONFIDENTIAL



$V_F = 1897$ FT/SEC (F4H-1)(F8U-3)

$V_T = 1518$ FT/SEC

ALTITUDE = 30,000 FT.

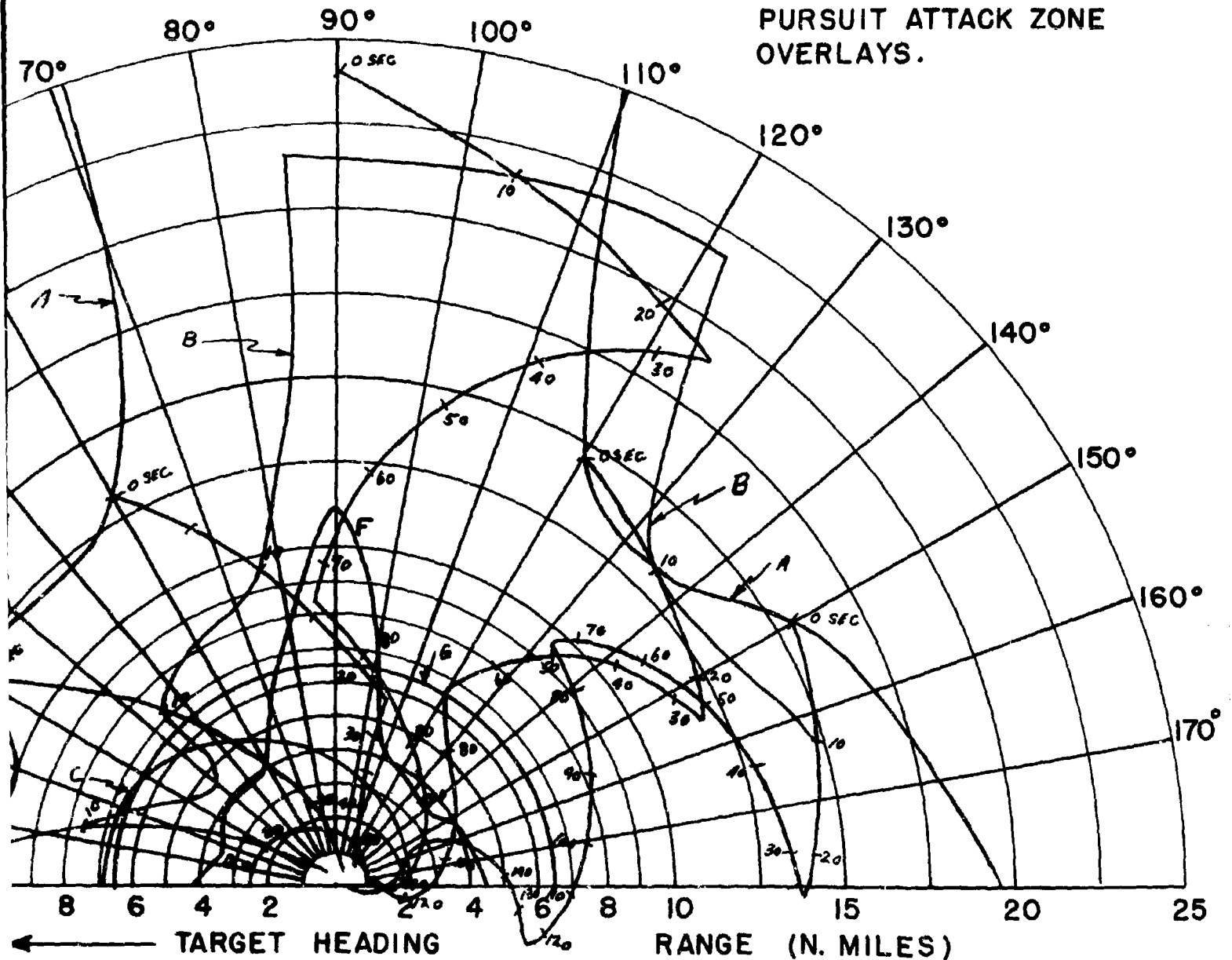
MANEUVERING TARGET - IN TARGET COORDINATES

INITIAL LEFT TURN

← TARGET HEADING

- A - 85% DETECTION RANGE
- B - LOCK-ON RANGE (10 SEC. LOCK)
- C - SPARROW III MAX. AERODYNAM
- D - SPARROW III MIN. AERODYNAM
- F - 90% SPARROW III SEEKER LO
- G - 6.5 N.M. INTERLOCK

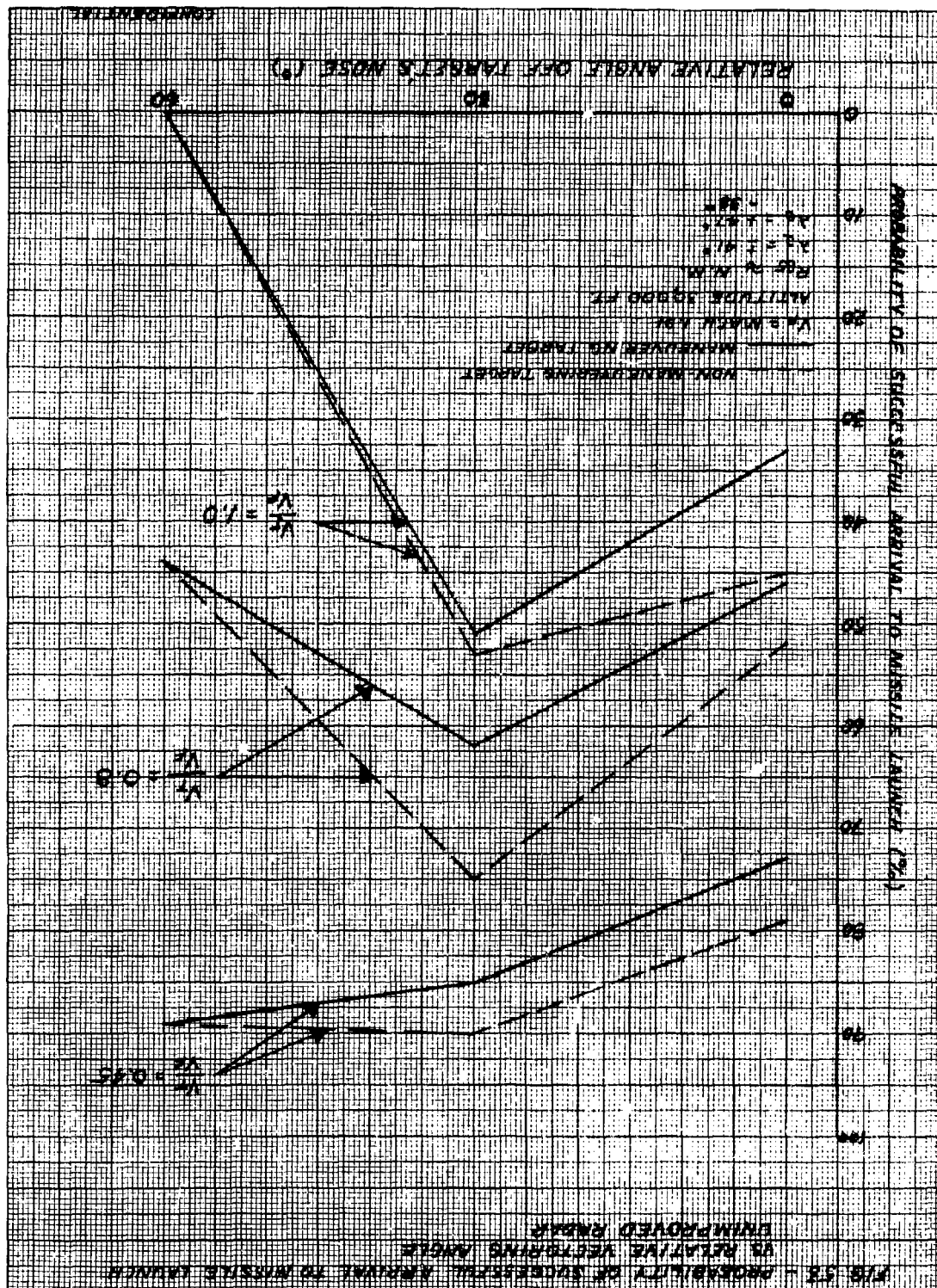
FIG. 51 - CO-ALTITUDE LEAD
PURSUIT ATTACK ZONE
OVERLAYS.

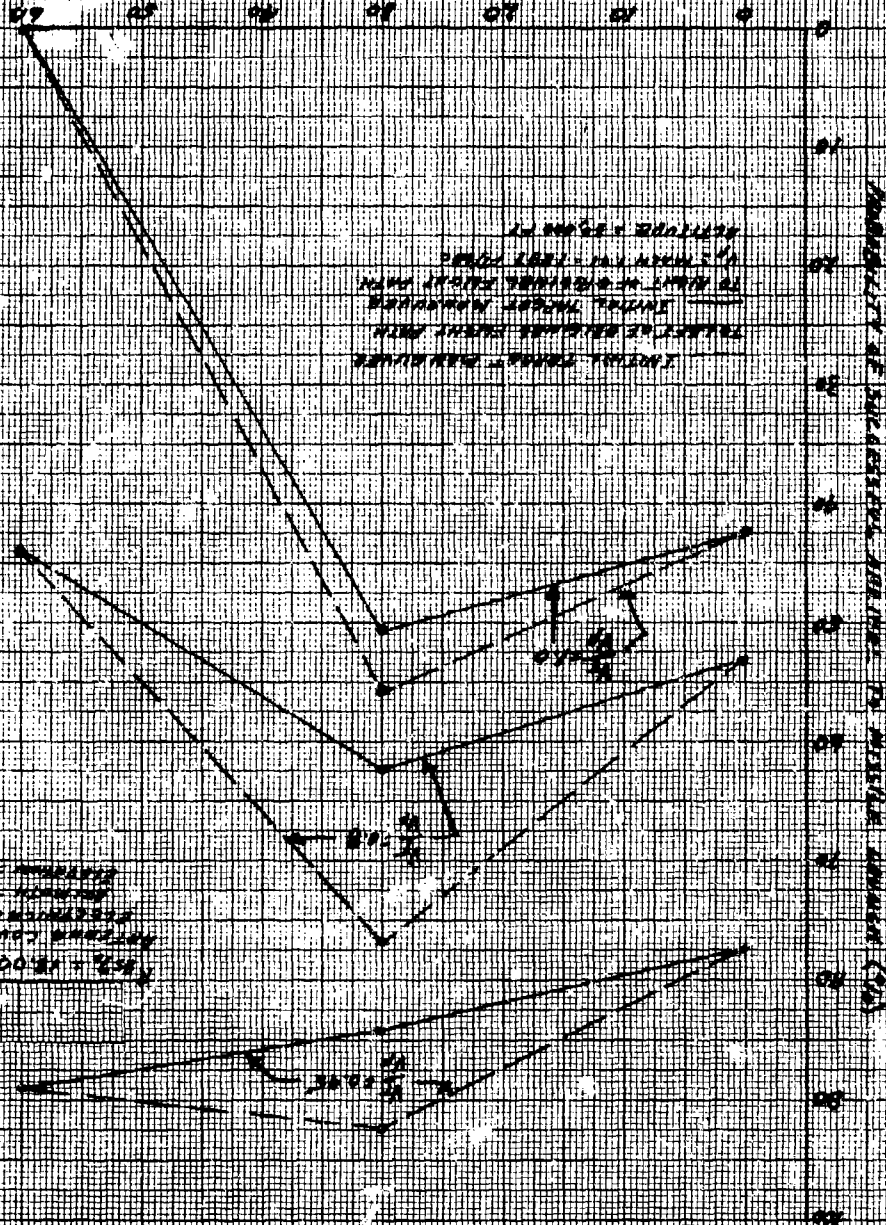


- 85% DETECTION RANGE
- LOCK-ON RANGE (10 SEC. LOCK-ON TIME)
- SPARROW III MAX. AERODYNAMIC RANGE
- SPARROW III MIN. AERODYNAMIC RANGE

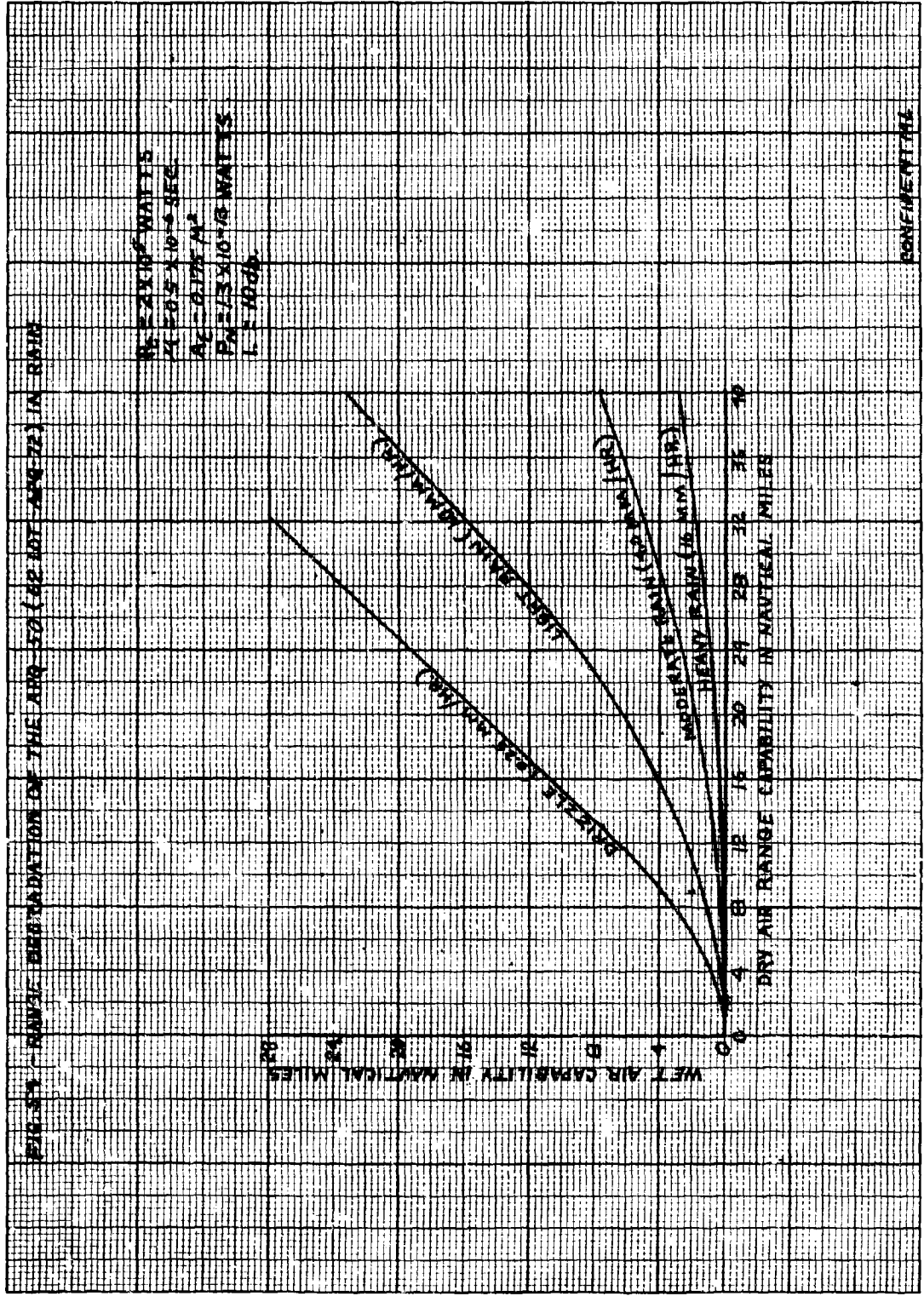
- 90% SPARROW III SEEKER LOCK-ON RANGE
- 6.5 N.M. INTERLOCK

2 CONFIDENTIAL





1. RESEARCH DESIGN



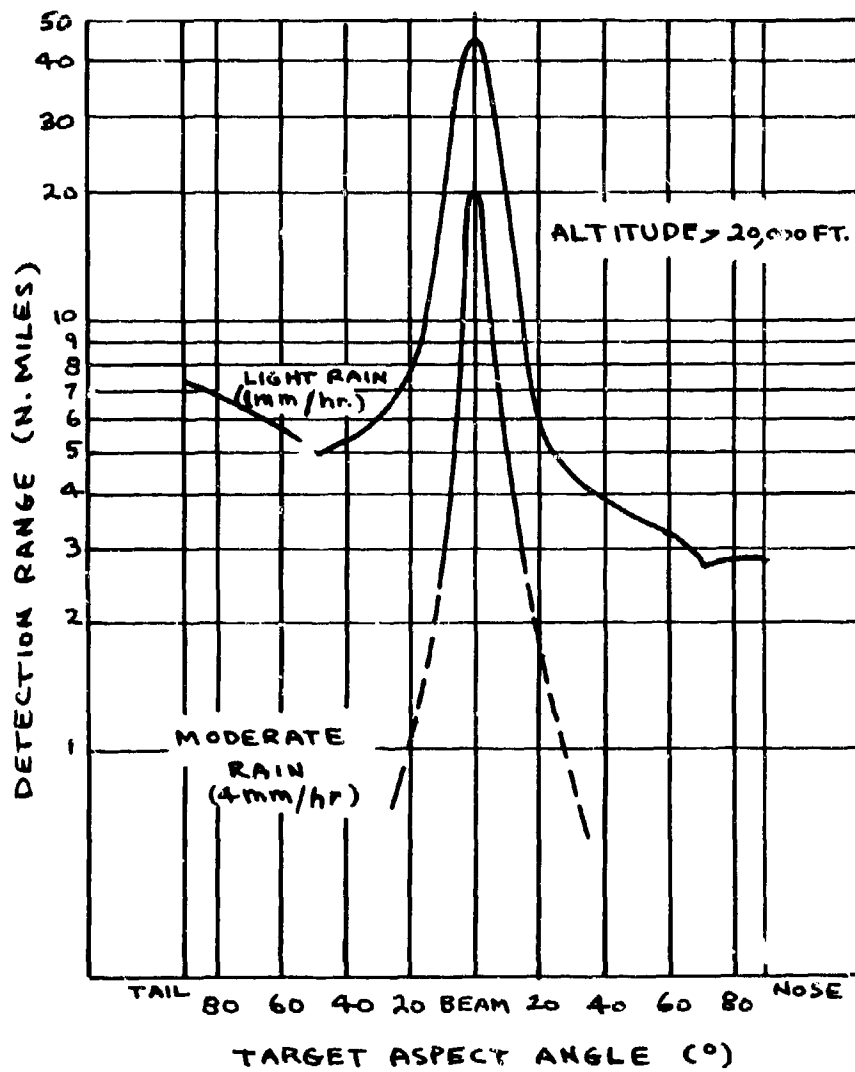
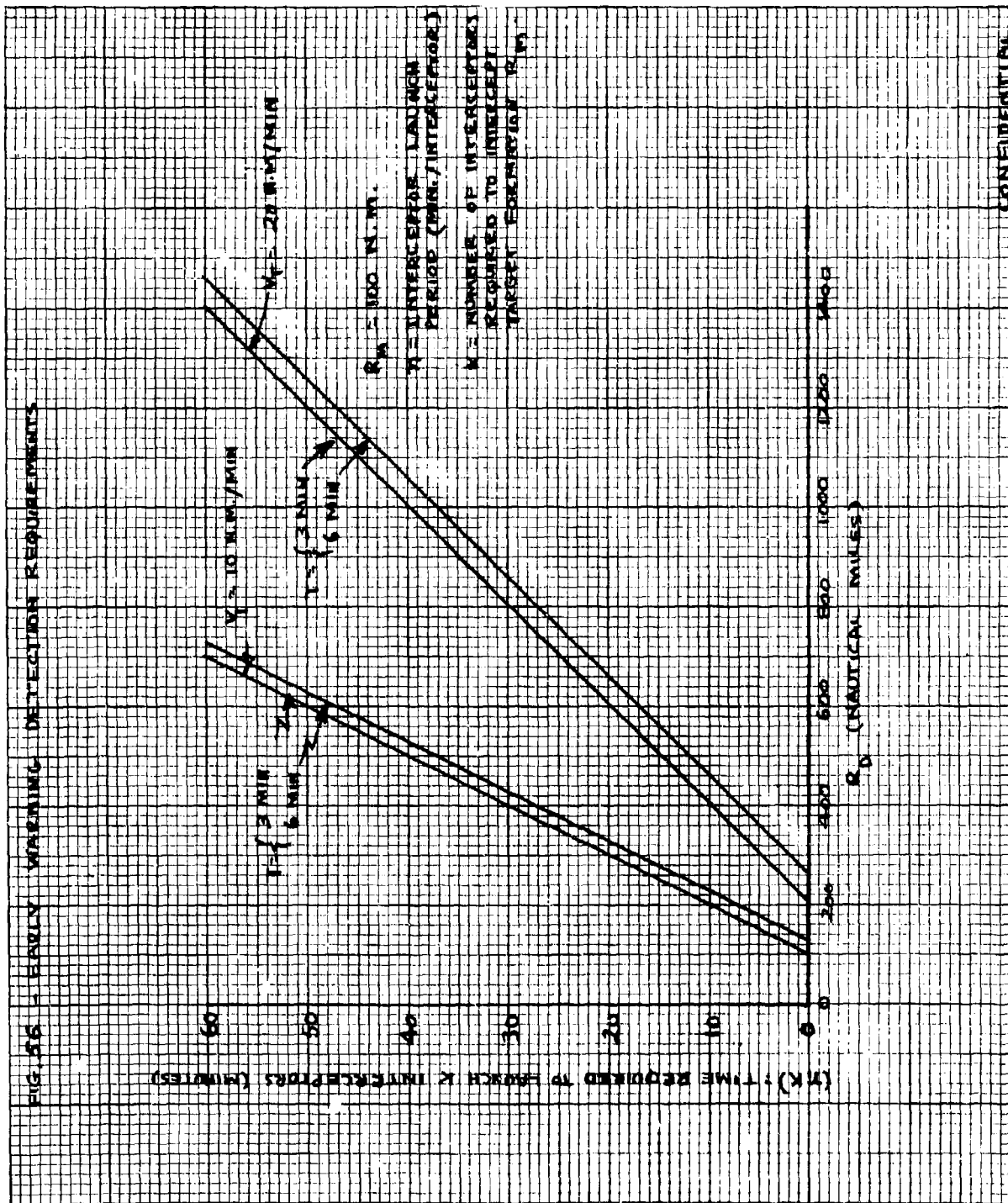


FIG. 55 - DETECTION RANGE FOR RAIN AT THE TARGET WITH VERTICAL POLARIZATION

CONFIDENTIAL



5.6.5B - AVAILABLE COMBAT TIME

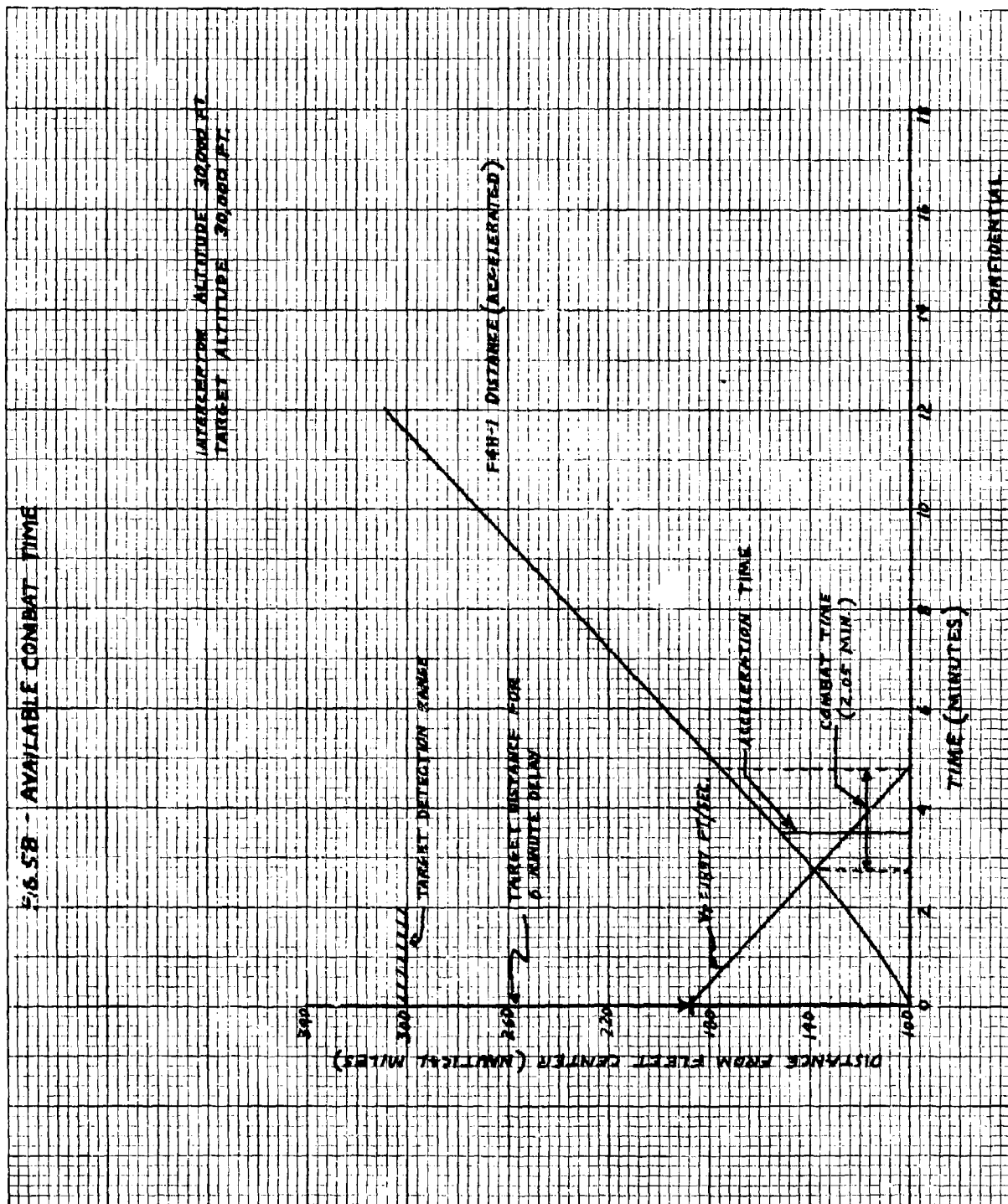
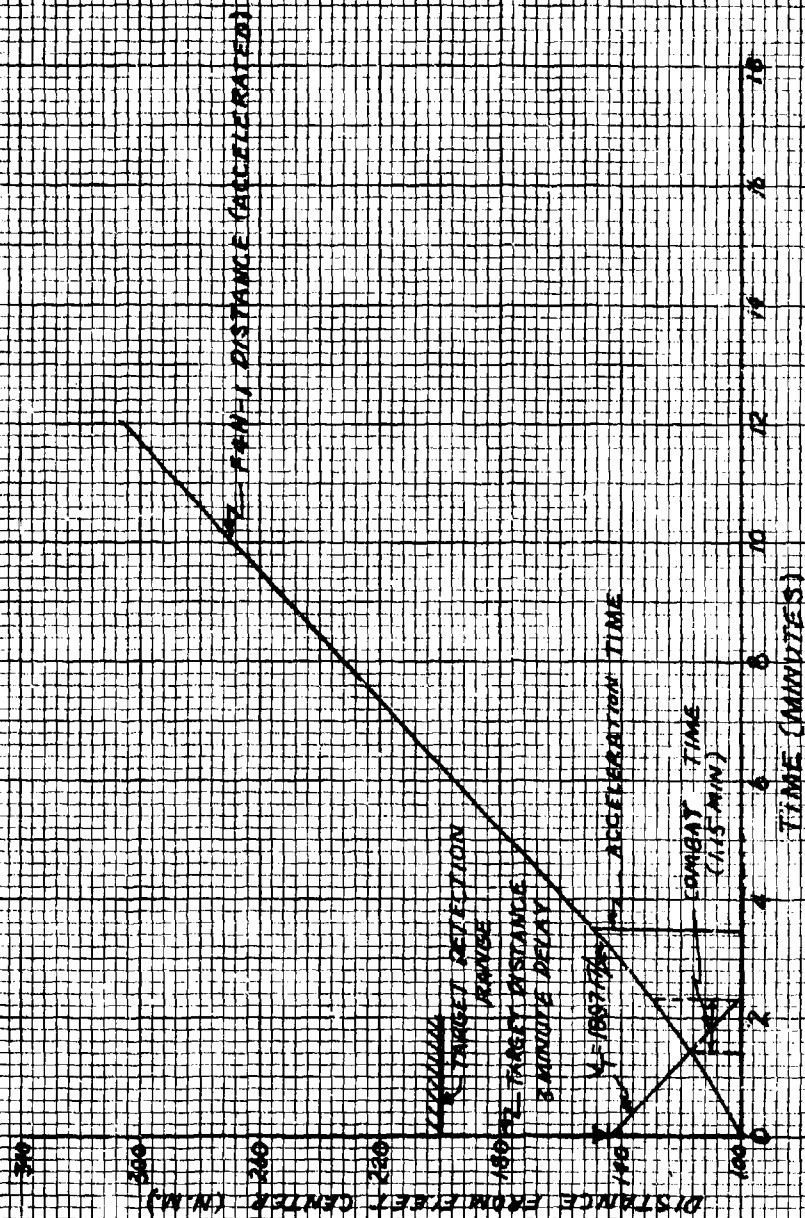
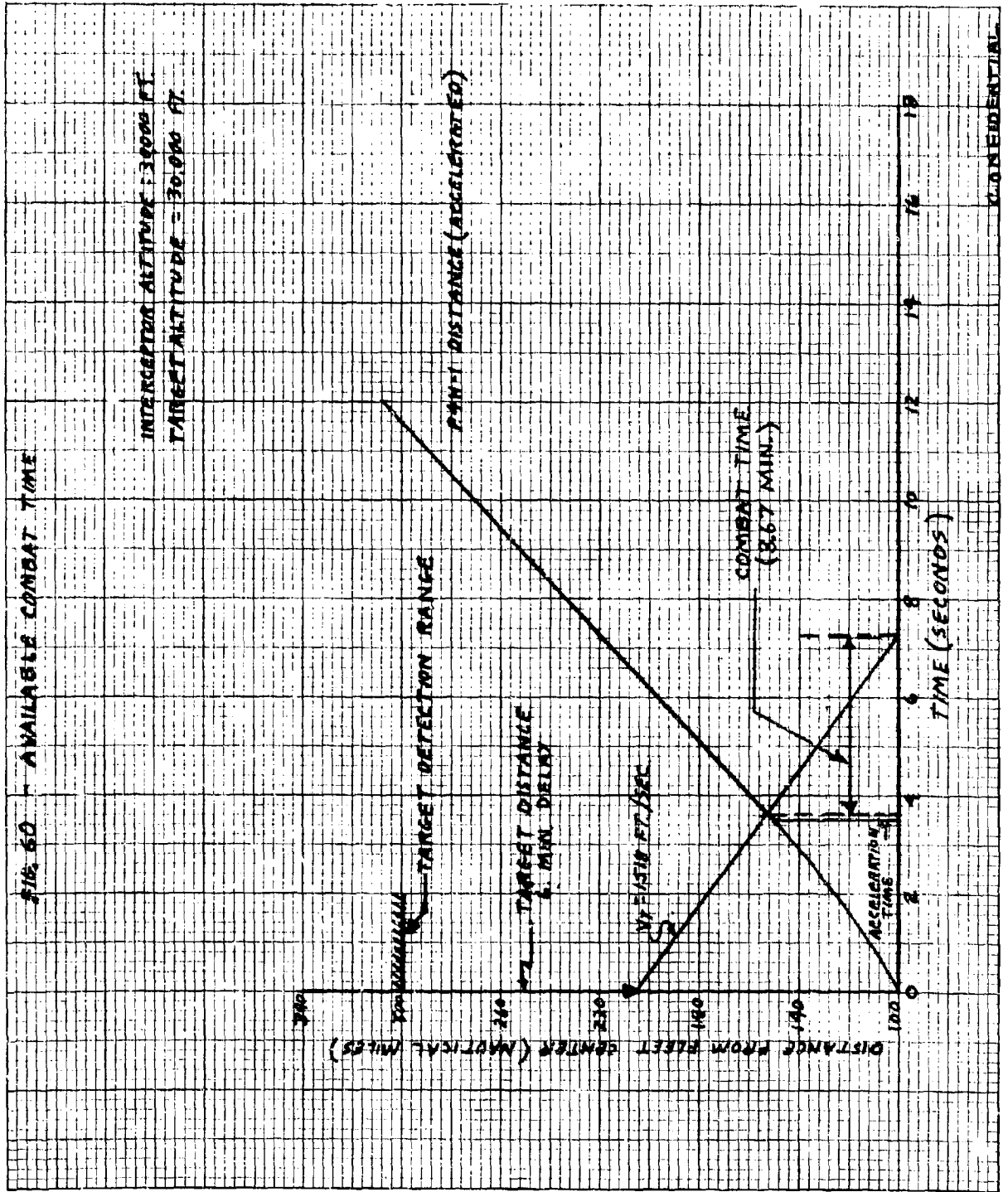


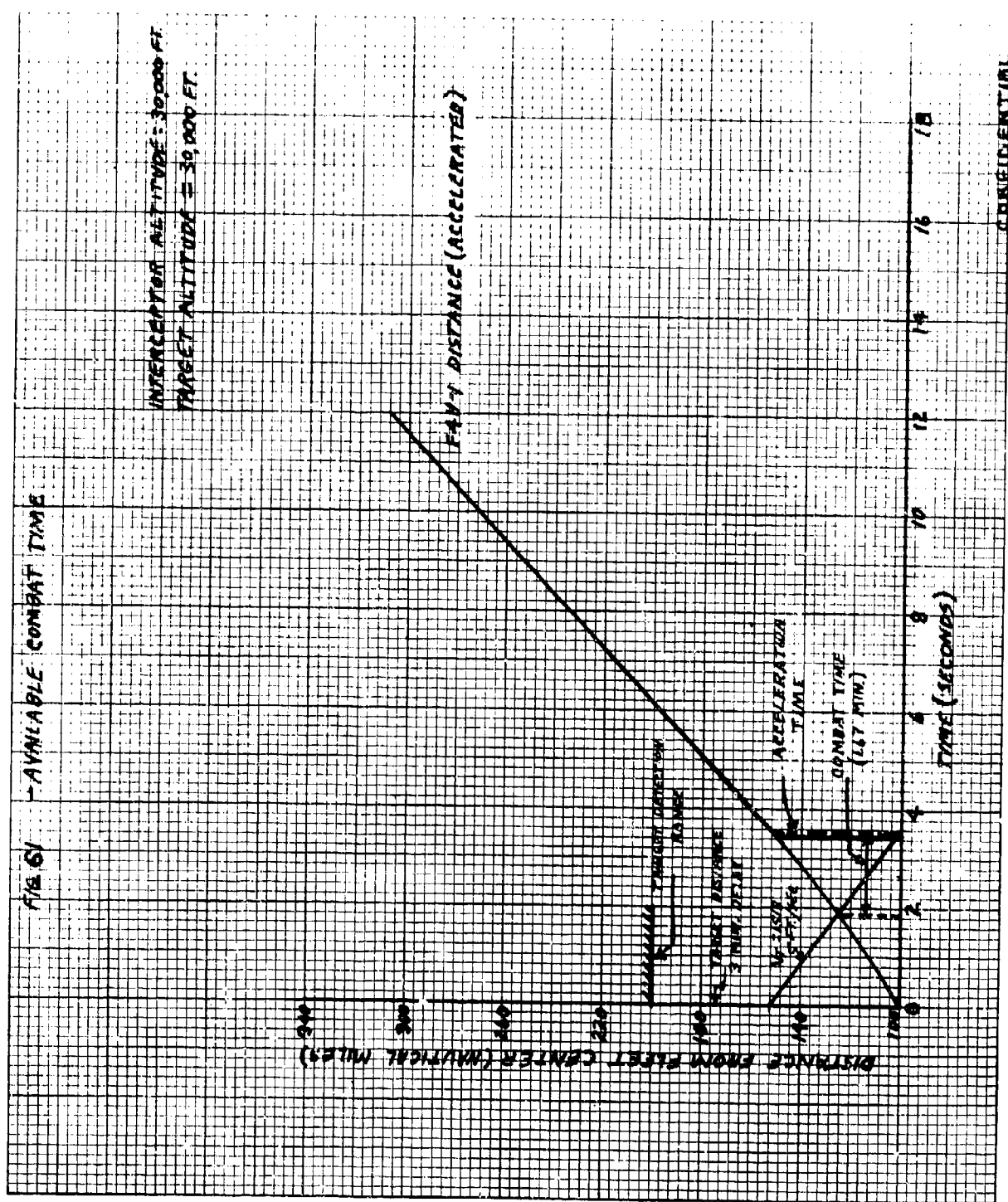
FIG. 5D - AVAILABLE COMBAT TIME

INTERCEPTOR'S ALTITUDE 30,000 FT.
 TARGET ALTITUDE 30,000 FT.



CONFIDENTIAL





CONFIDENTIAL

FIG. 60 - AVAILABLE COMBAT TIME

INTERCEPTOR ALTITUDE = 30,000 FT.

TARGET ALTITUDE = 30,000 FT.

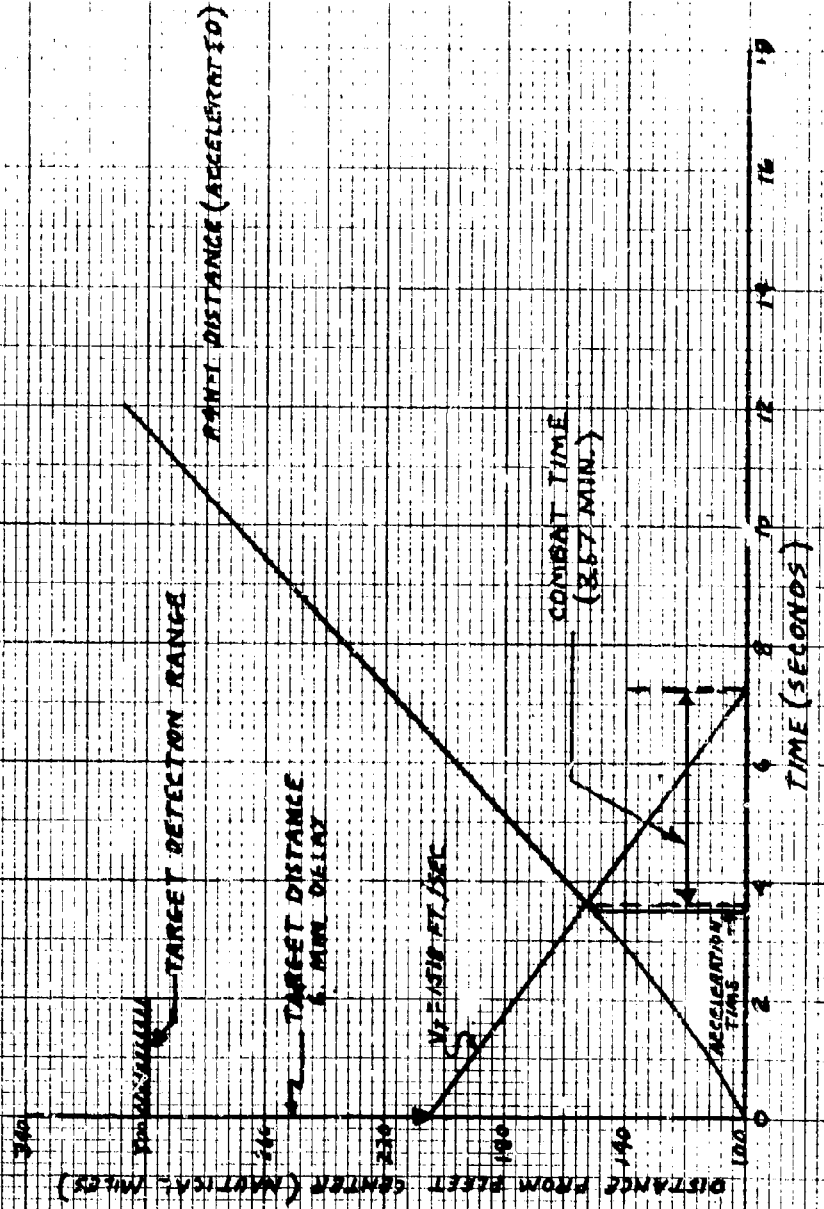


FIG 62 AVAILABLE COMBAT TIME

INTERCEPTOR'S ALTITUDE: 3,000 FT.
 TARGET ALTITUDE: 30,000 FT.

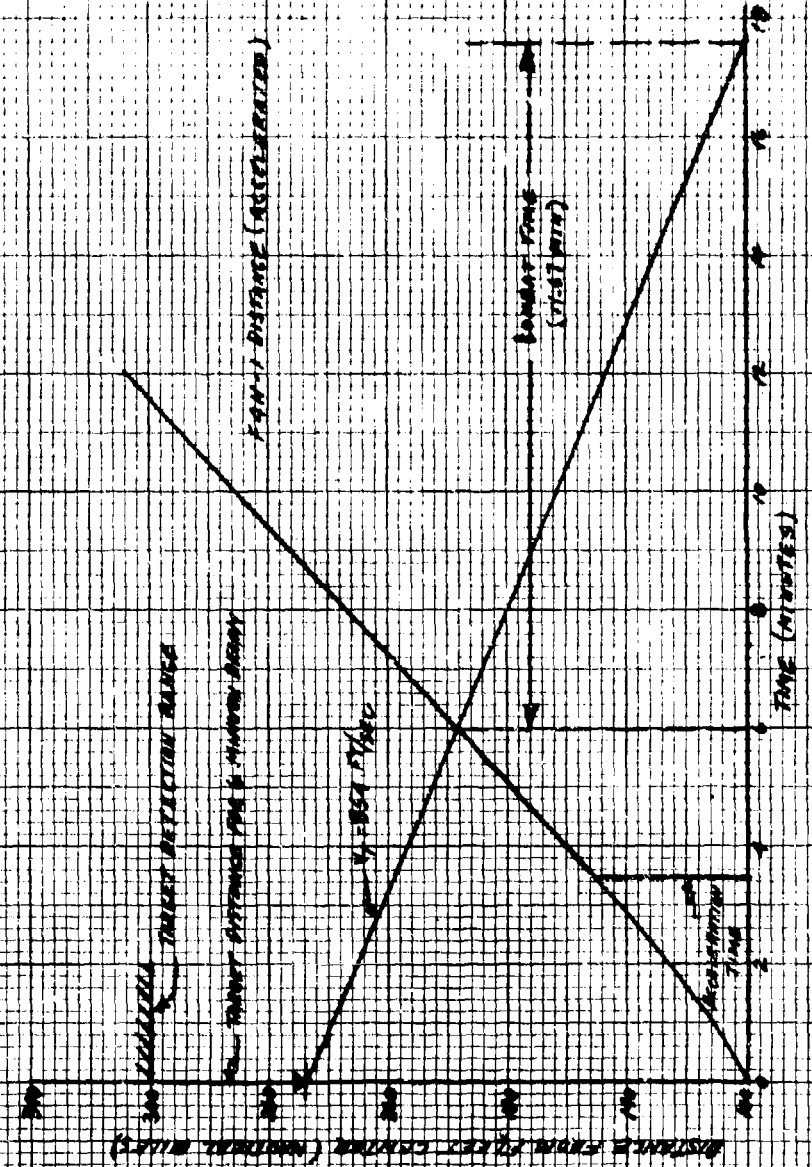
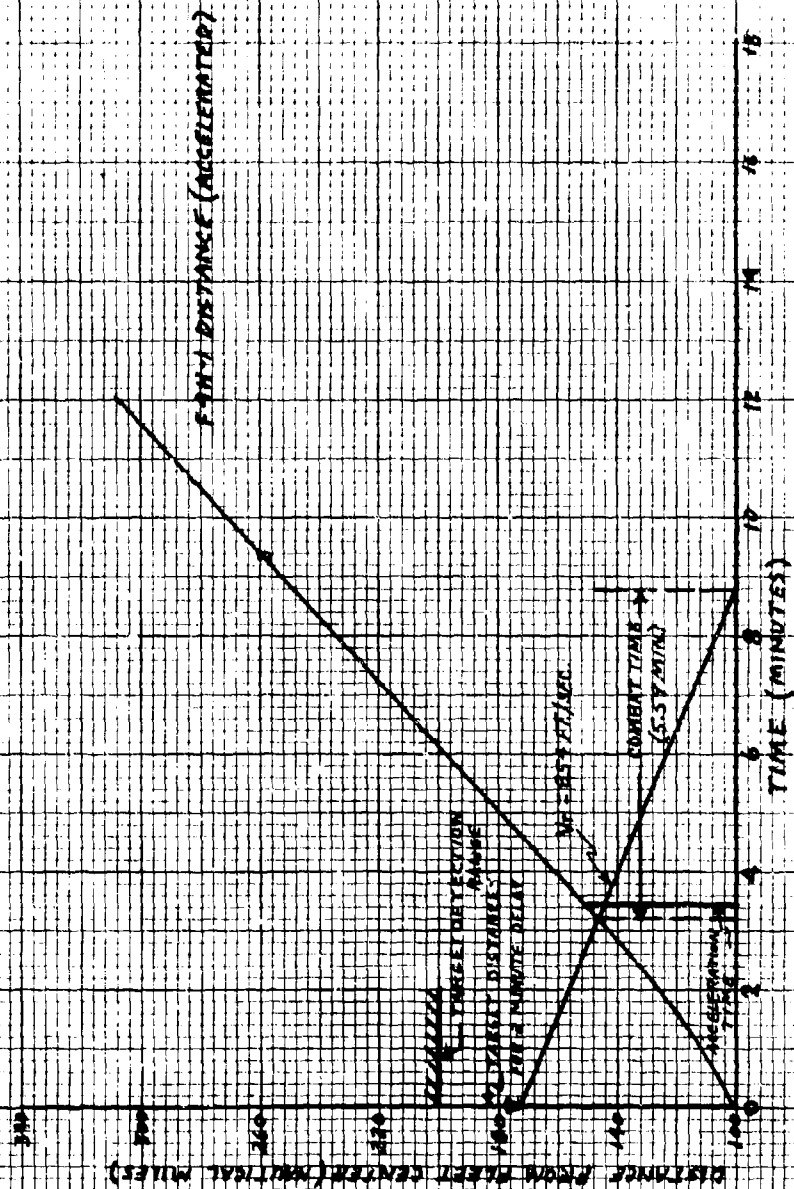


FIG. 63 AVAILABLE COMBAT TIME

INTERCEPT ALTITUDE = 30,000 FT.
 TARGET ALTITUDE = 30,000 FT.



CONFIDENTIAL

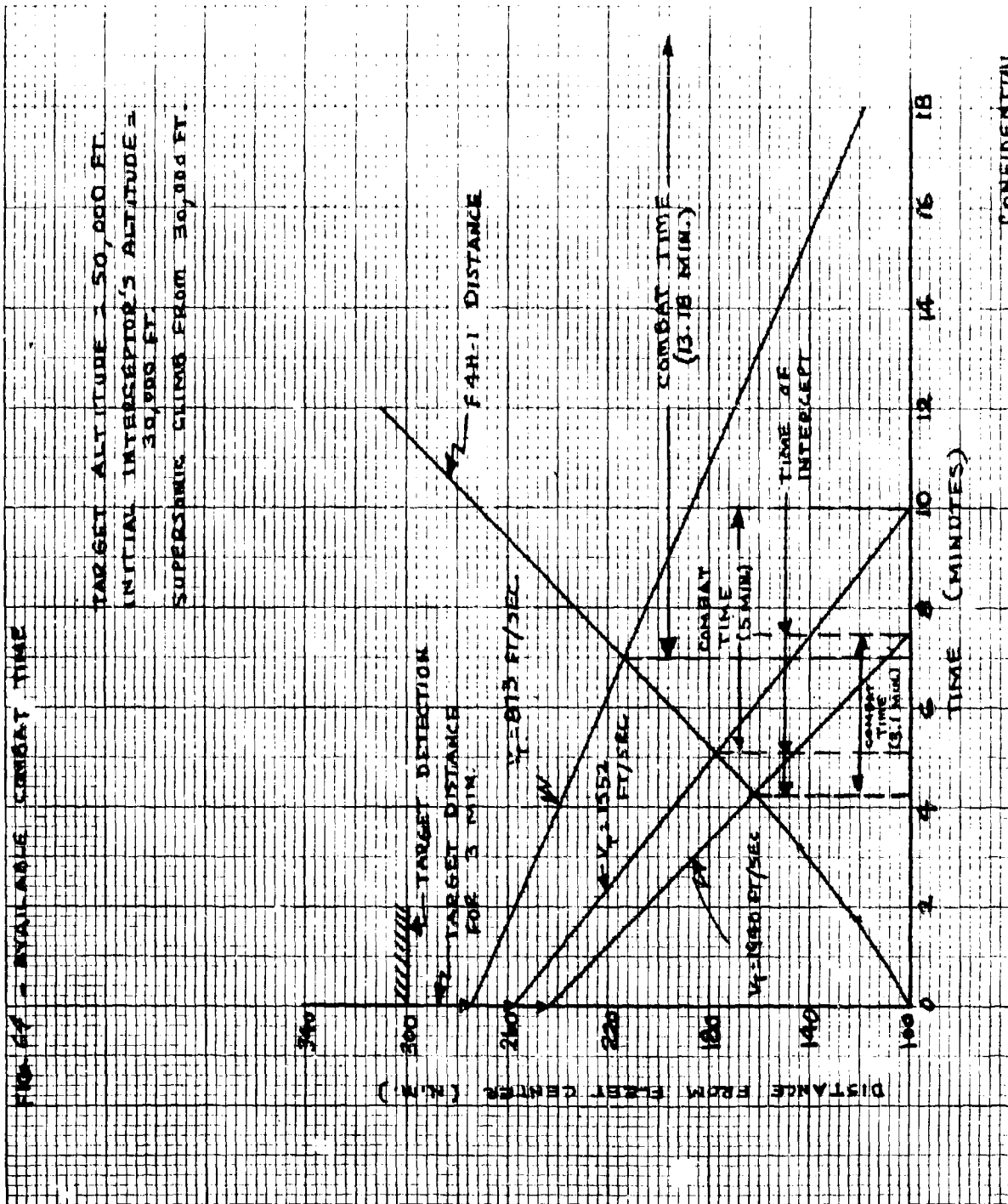
[illegible]

FIG. 27 - AVAILABLE COMBAT TIME

TARGET ALTITUDE = 50,000 FT.
INITIAL INTERCEPTOR'S ALTITUDE = 30,000 FT.
SUPERSONIC CLIMB FROM 30,000 FT.

340
300
260
220
180
140
100

0 2 4 6 8 10 12 14 16 18

DISTANCE FROM FLIGHT CENTER (N.M.)

TIME (MINUTES)

TARGET DETECTION

TARGET DISTANCE FOR 3 MIN.

$V_1 = 1900 \text{ FT/SEC}$

$V_2 = 1552 \text{ FT/SEC}$

$V_3 = 813 \text{ FT/SEC}$

COMBAT TIME (13.18 MIN.)

TIME OF INTERCEPT

FIG. 27 - AVAILABLE COMBAT TIME

TARGET ALTITUDE = 50,000 FT.
INITIAL INTERCEPTOR'S ALTITUDE = 30,000 FT.
SUPERSONIC CLIMB FROM 30,000 FT.

340
300
260
220
180
140
100

0 2 4 6 8 10 12 14 16 18

DISTANCE FROM FLIGHT CENTER (N.M.)

TIME (MINUTES)

TARGET DETECTION

TARGET DISTANCE FOR 3 MIN.

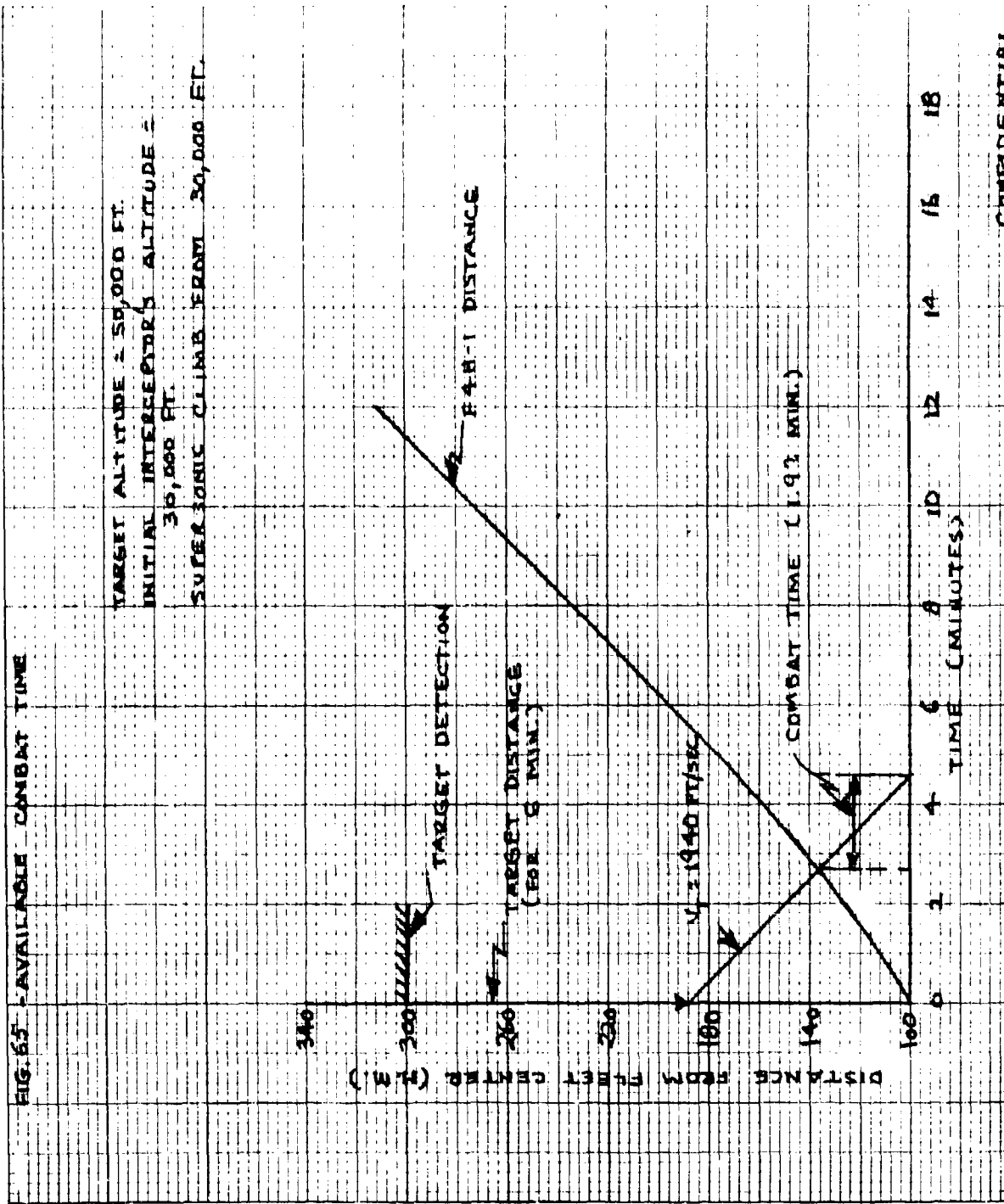
$V_1 = 1900 \text{ FT/SEC}$

$V_2 = 1552 \text{ FT/SEC}$

$V_3 = 813 \text{ FT/SEC}$

COMBAT TIME (13.18 MIN.)

TIME OF INTERCEPT



CONFIDENTIAL

FIG 166 - AVAILABLE COMBAT TIME

TARGET ALTITUDE = 50,000 FT.
 INITIAL INTERCEPTOR'S
 ALTITUDE = 30,000 FT.
 SUPERSONIC CLIMB
 FROM 30,000 FT.

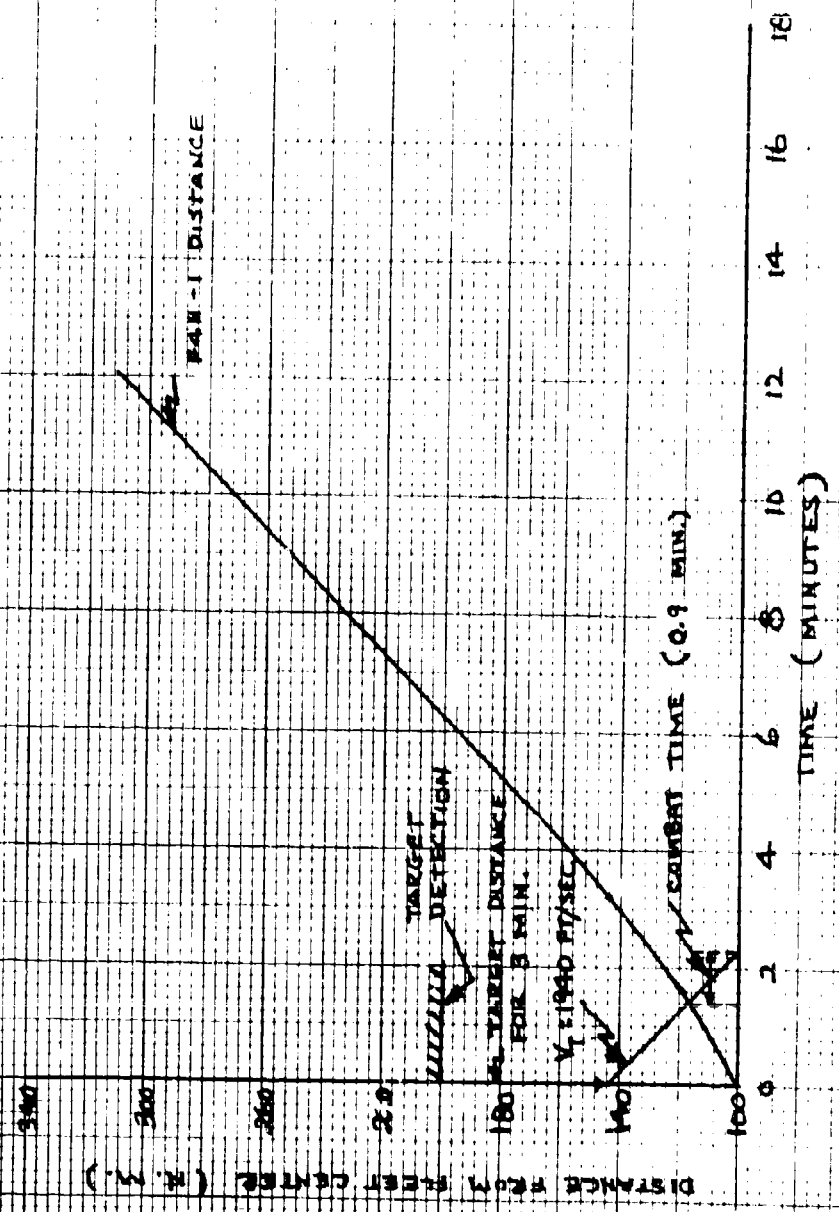
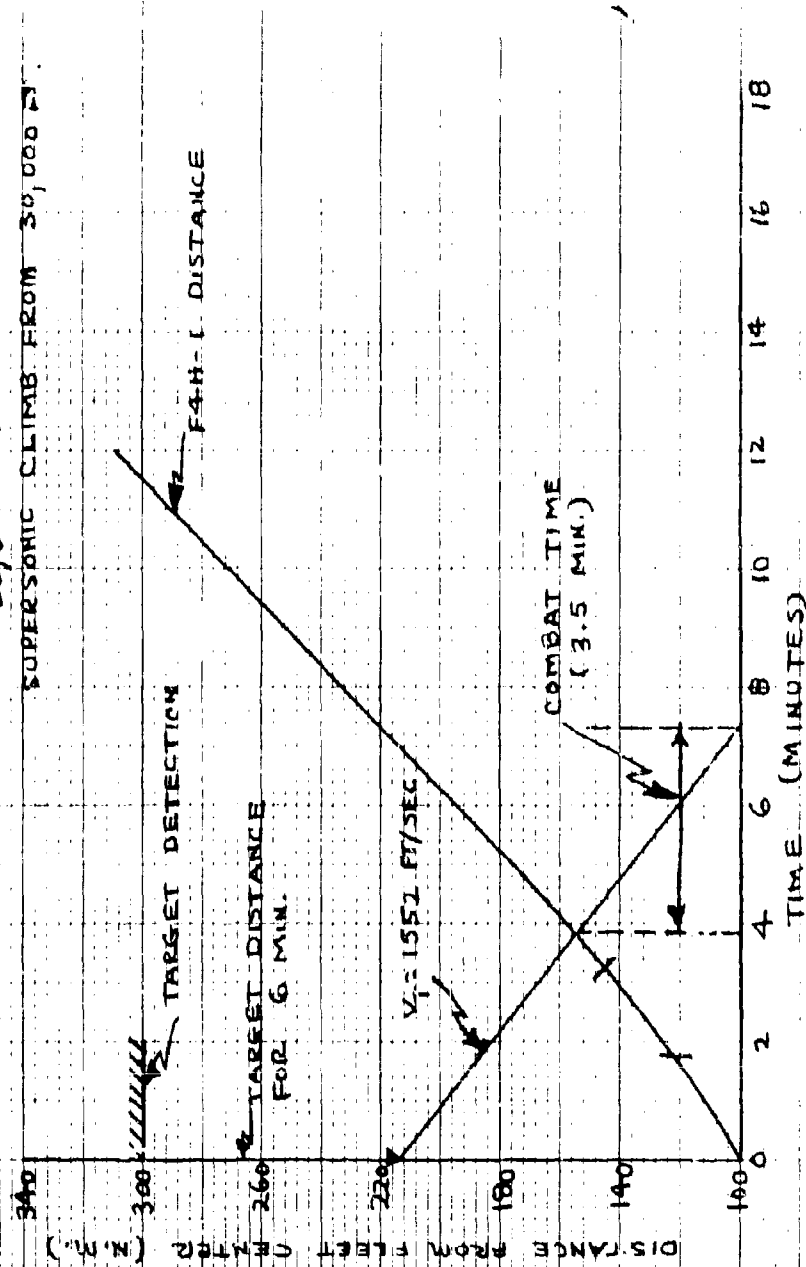
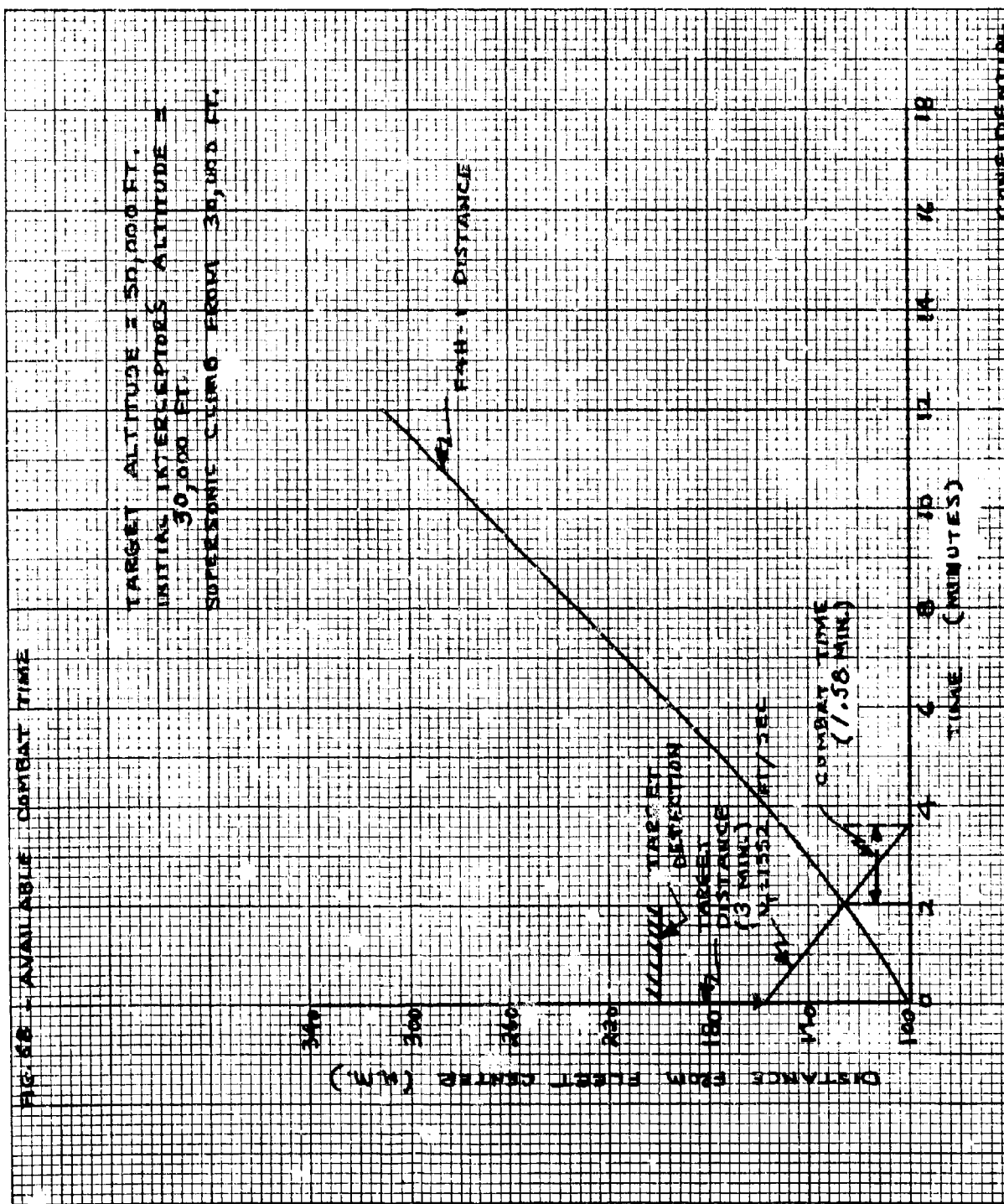


FIG. 67 AVAILABLE COMBAT TIME

TARGET ALTITUDE = 50,000 FT.
INITIAL INTERCEPTOR'S ALTITUDE =
30,000 FT.
SUPERSONIC CLIMB FROM 30,000 FT.





CONFIDENTIAL

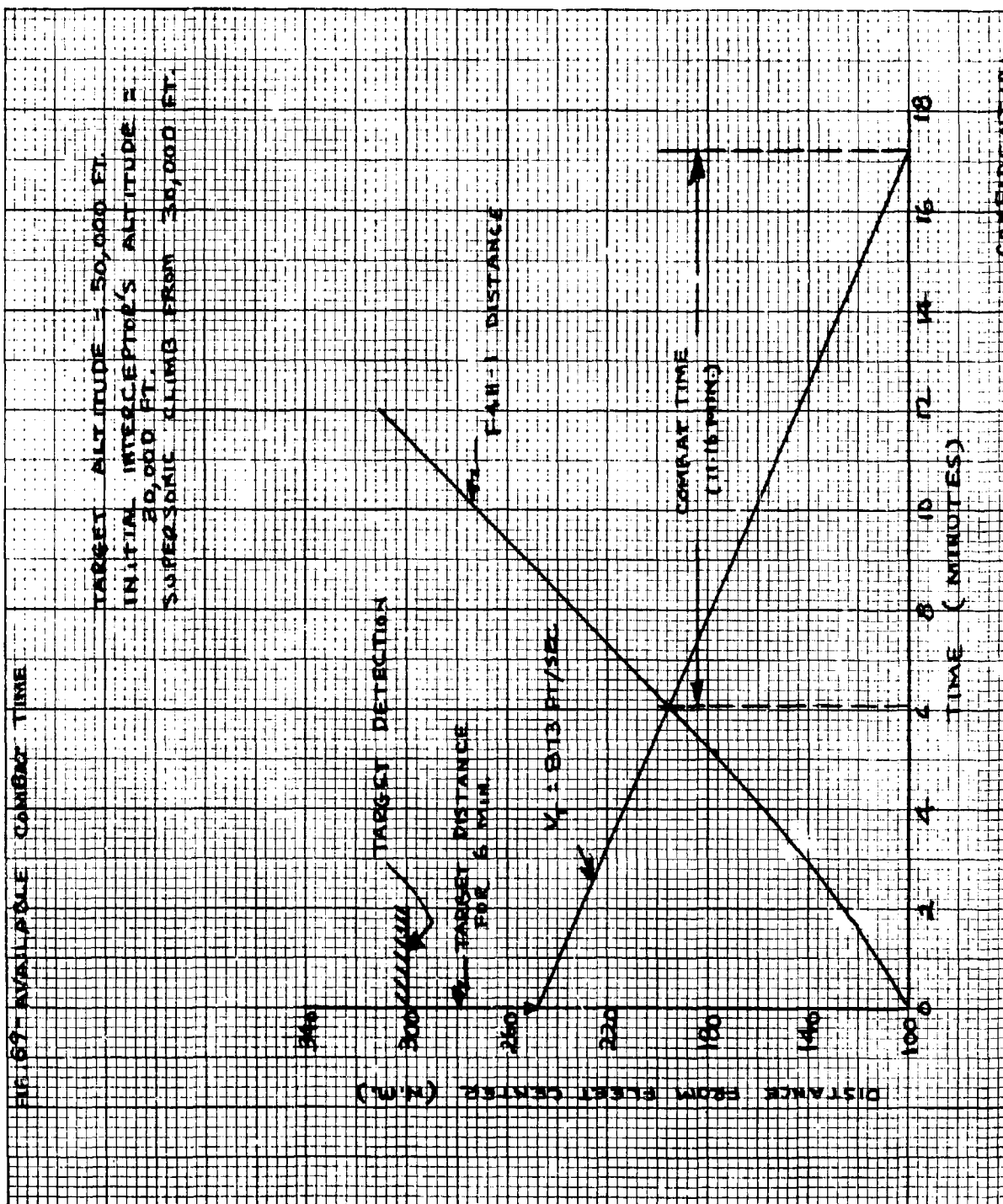


FIG. 20 - AVAILABLE COMBAT TIME

TARGET ALTITUDE = 50,000 FT.
 INITIAL INTERCEPTOR'S ALTITUDE =
 30,000 FT.
 SUPERSONIC CLIMB FROM 30,000 FT.

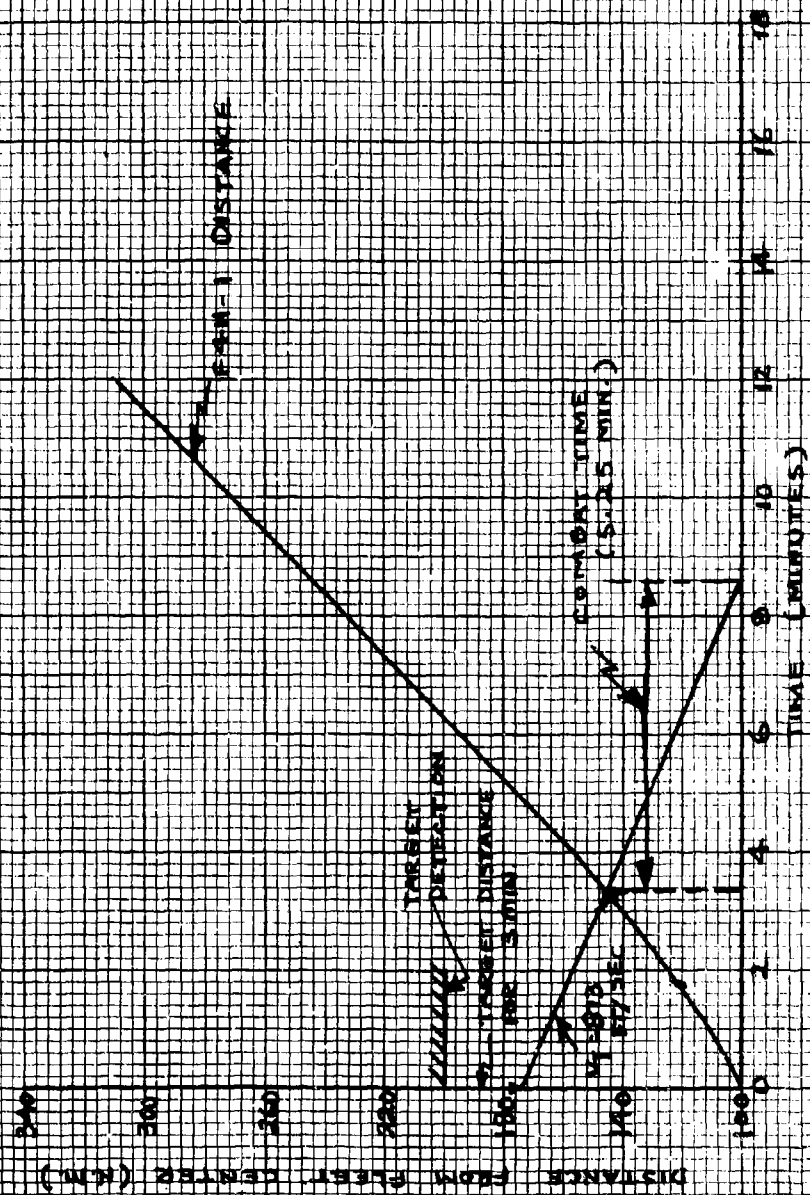
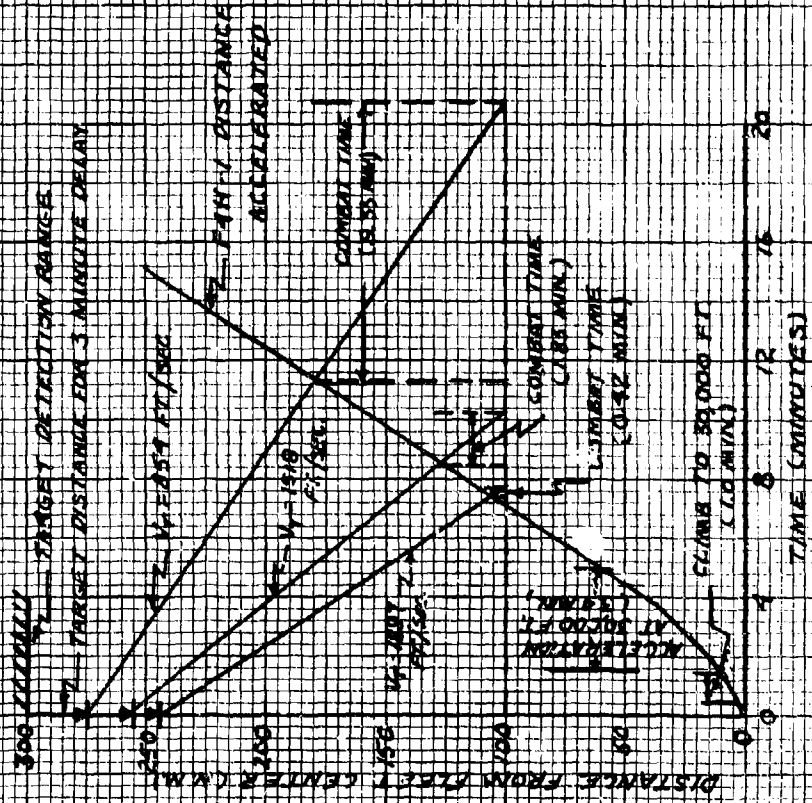


FIG. 71 - AVAILABLE COMBAT TIME

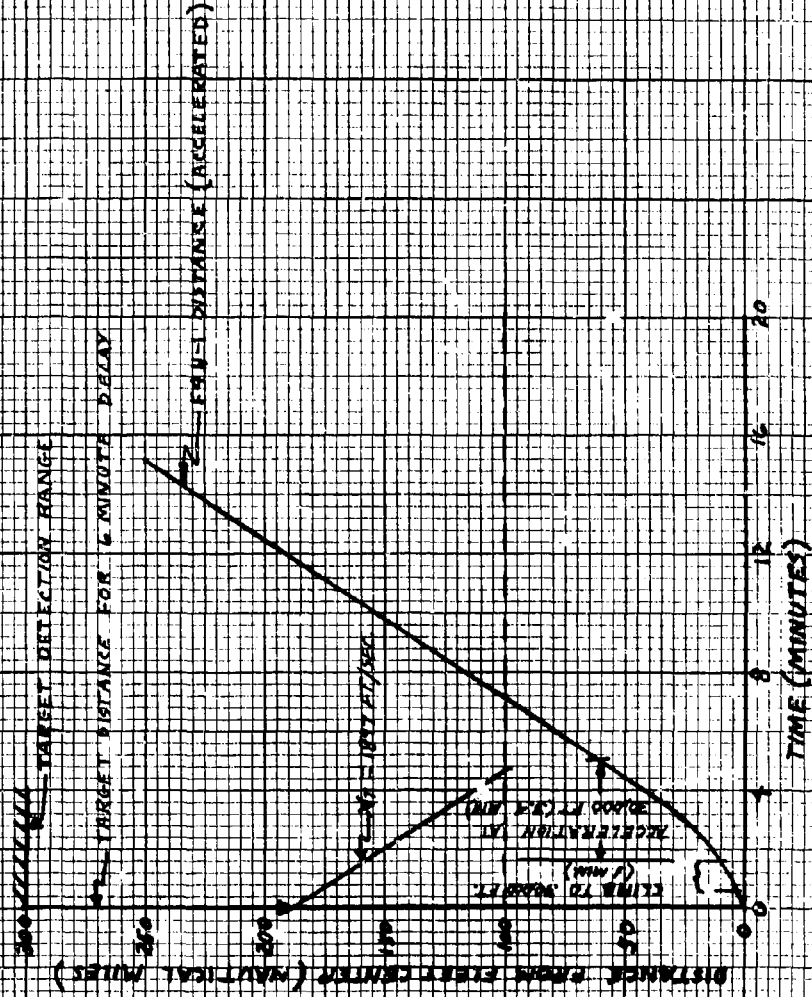
TARGET ALTITUDE = 30,000 FT
 DECA LAUNCHED IN TRAJECTORY
 CLIMB FROM 0 FT TO 30,000 FT -
 ACCELERATED



CONFIDENTIAL

FIG. 12 AVAILABLE COMBAT TIME

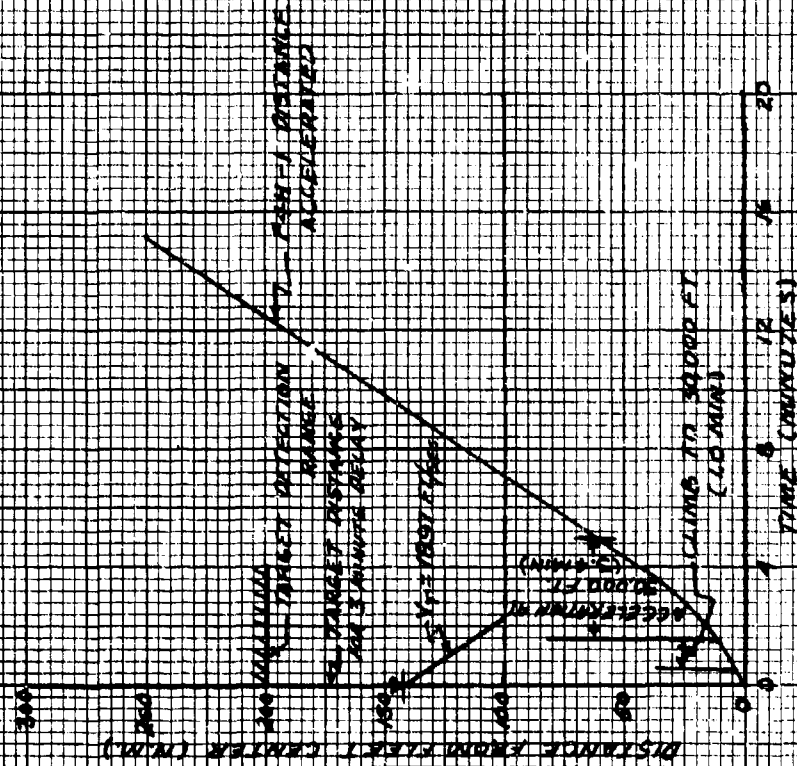
TARGET ALTITUDE: 30,000 FT.
DECK LAUNCHED INTERCEPTION
CLIMB FROM DECK TO 30,000 FT. ACCELERATED



CONFIDENTIAL

FIG. 73 - AVAILABLE CONVERT TIME

TARGET ALTITUDE 50,000 FT.
DECA LAUNCHED INTERIOR
CLIMB FROM DATA TO 50,000 FT. -
ACCELERATED



CONFIDENTIAL

FIG. 14 AVAILABLE COMBAT TIME

TARGET ALTITUDE 30,000 FT.
DECA LAUNCHED IN RECEPTION
CLIMB FROM DECK TO 30,000 FT.
ACCELERATION

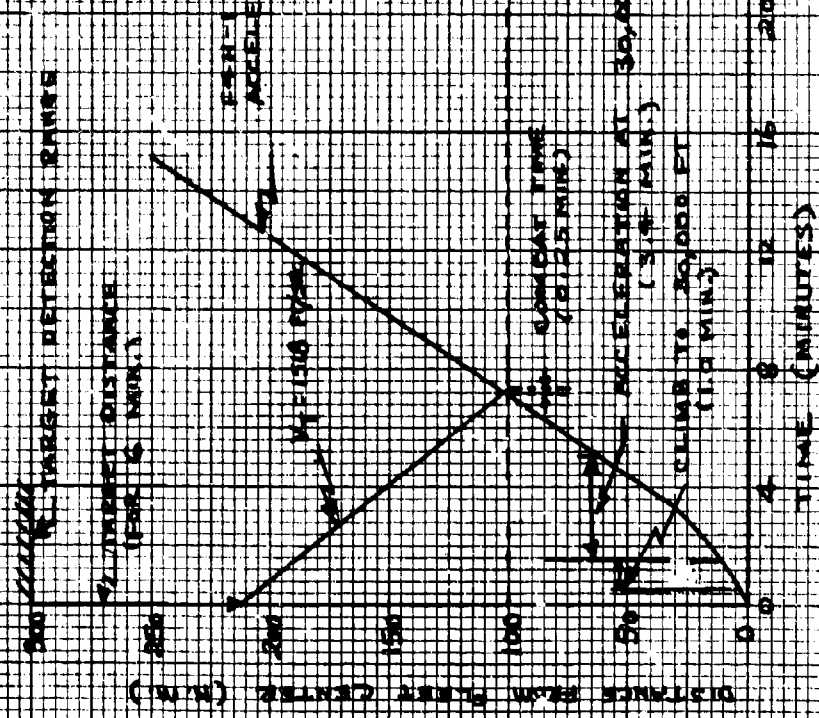
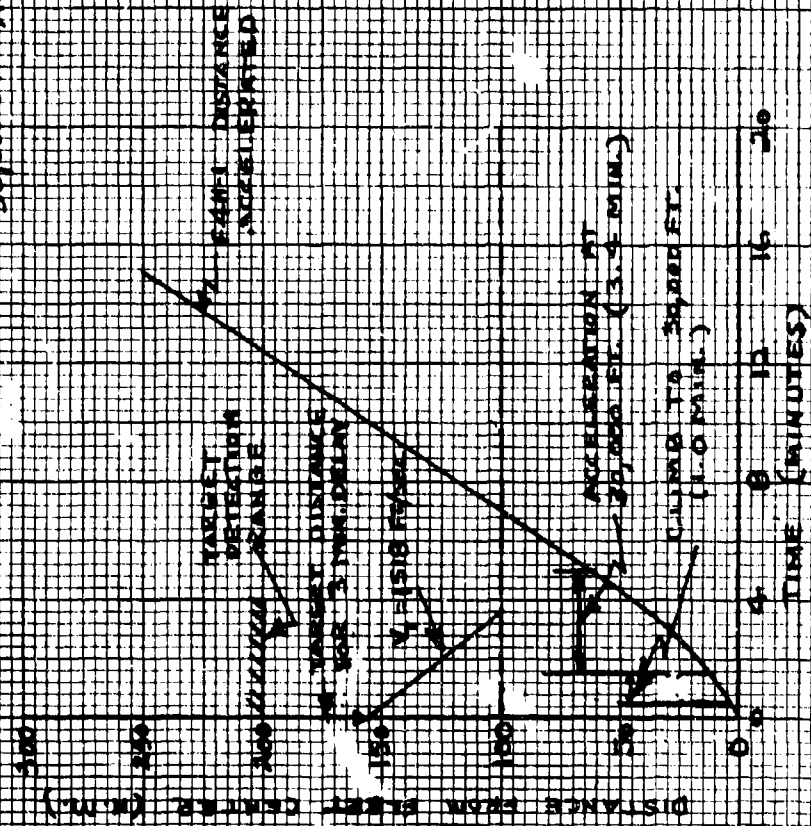


FIG. 76 AVAILABLE CONSTANT TIME

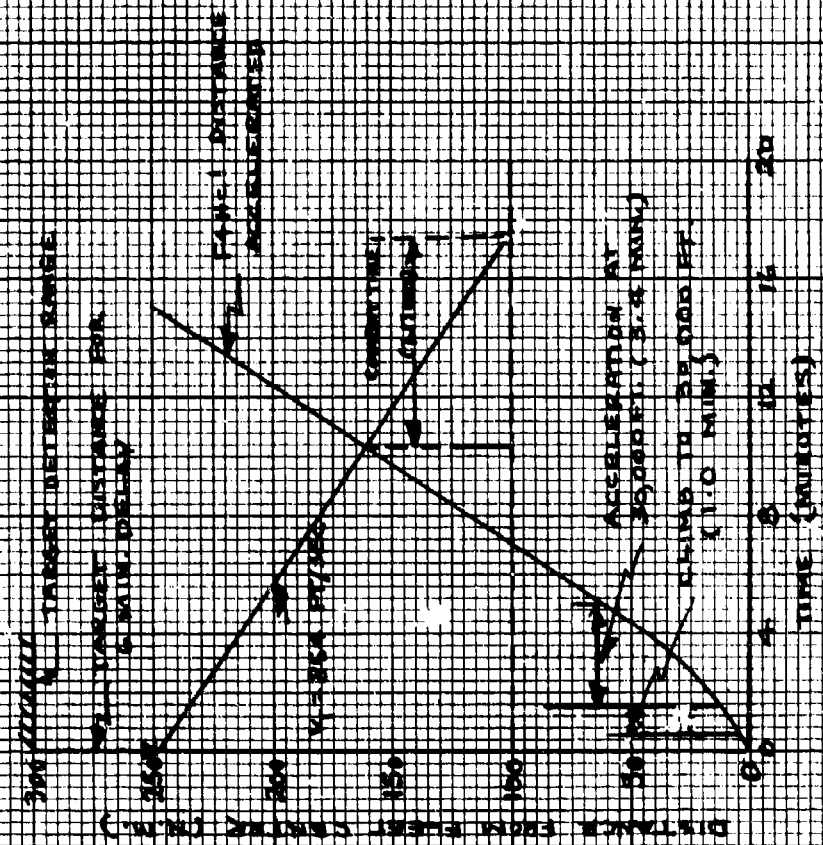
TARGET ALTITUDE 25,000 FT.
DECK LAUNCHED INTERCEPTION
CLIMB FROM DECK TO
30,000 FT. ACCELERATED



CONFIDENTIAL

FIG. 16 - AVAILABLE COMBAT TIME

TARGET ALTITUDE = 30,000 FT.
 MISSILE LAUNCHED WITH ZERO
 CLIMB FROM DECK TO 30,000 FT.
 ACCELERATION



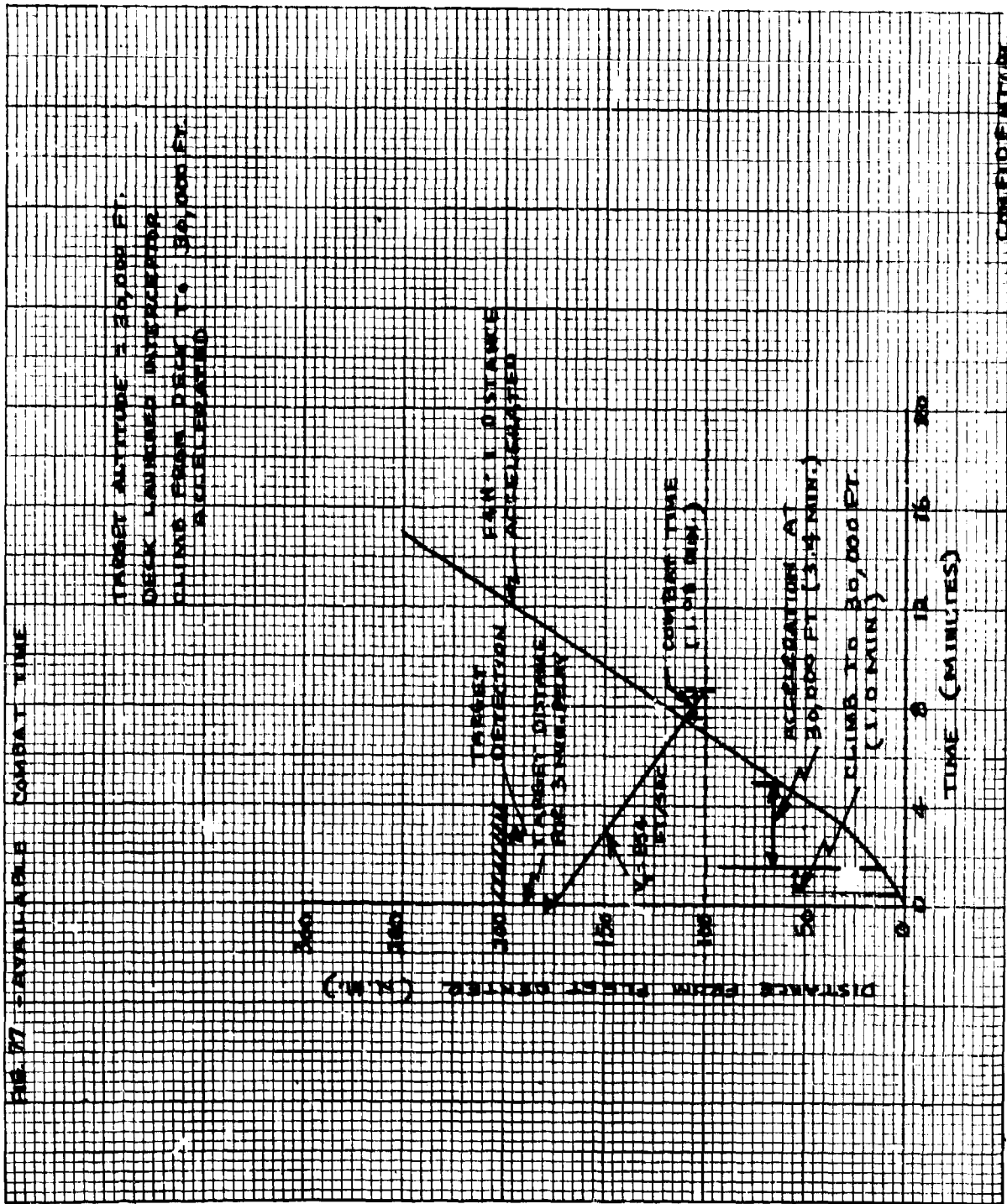
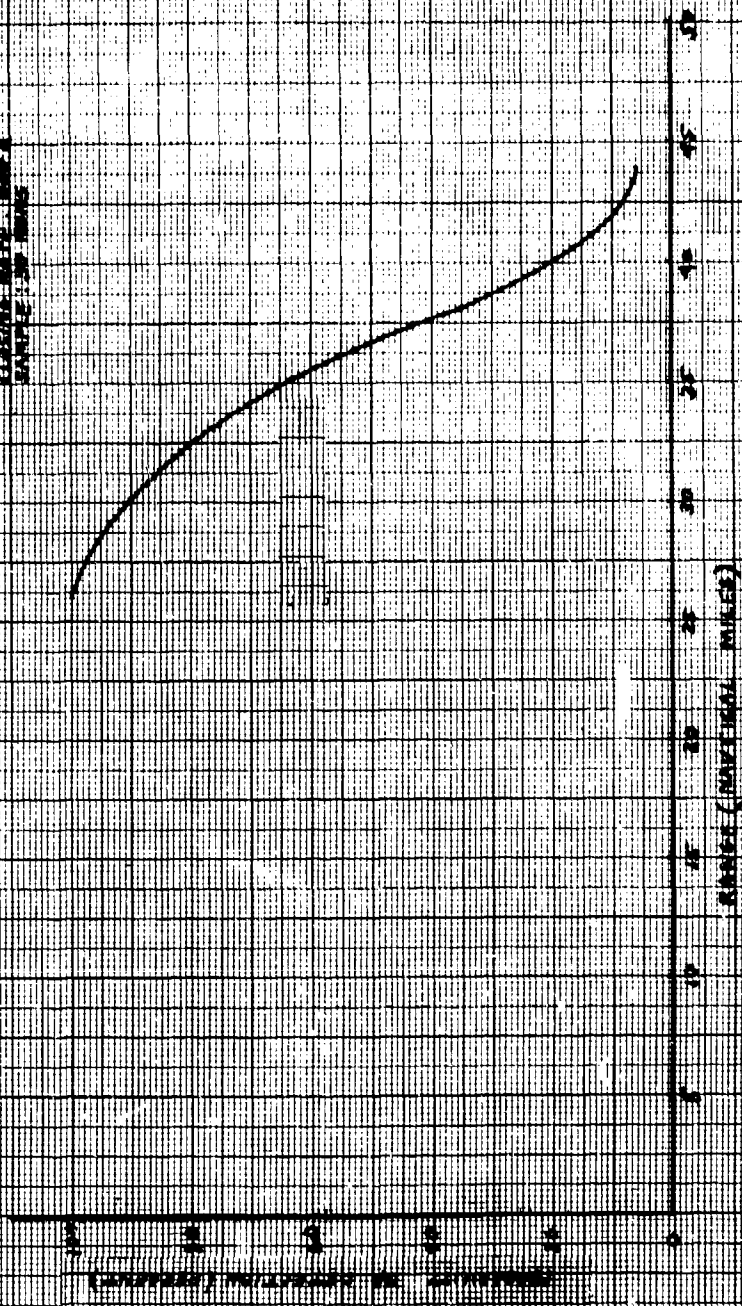


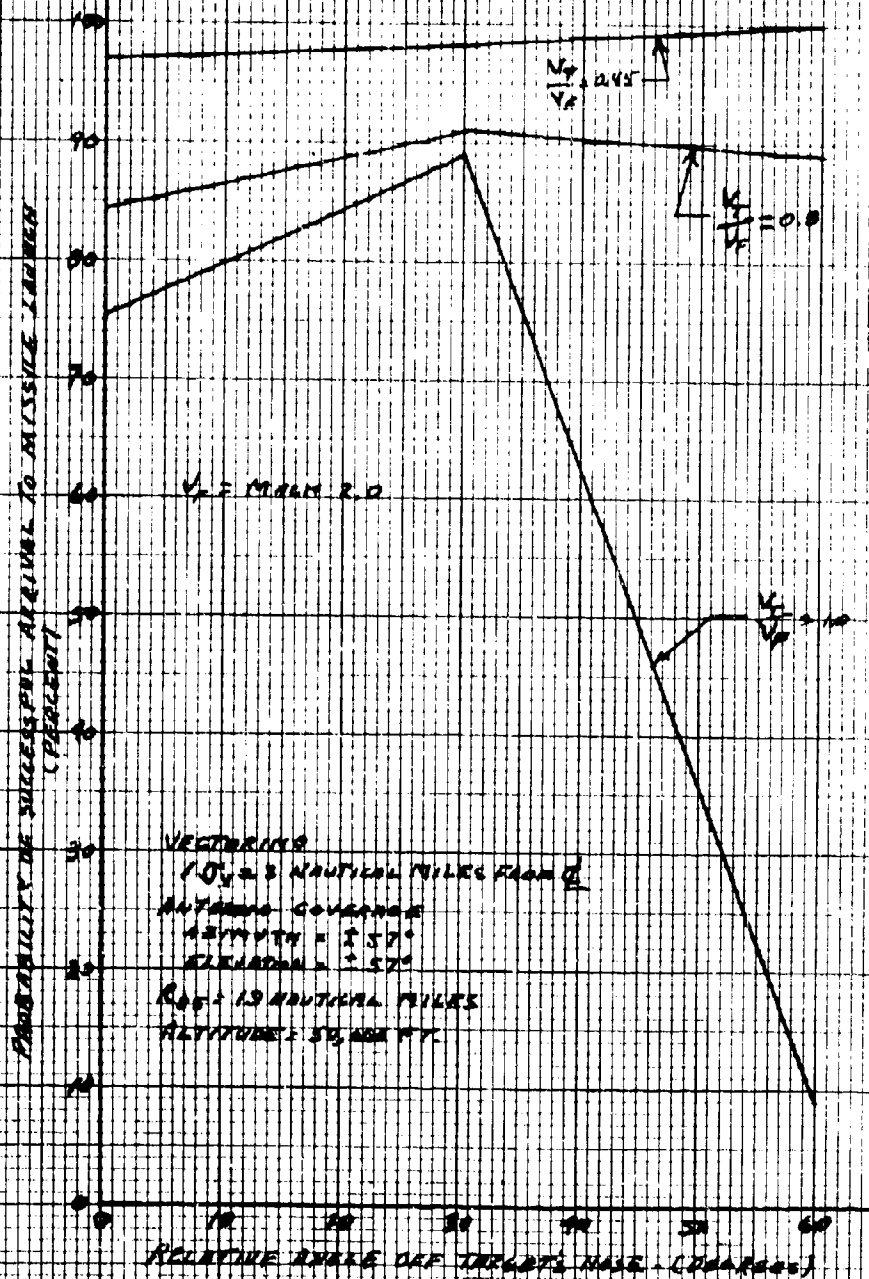
FIG. 78. EFFECT OF INCREASING RANGE -
ON THE EFFECT OF RANGE

ALTIMETER, 10000 FT
 BAROMETRIC, 29.92
 TEMPERATURE, 100°F
 WIND, 10 KNOTS
 RANGE, 100 MILES

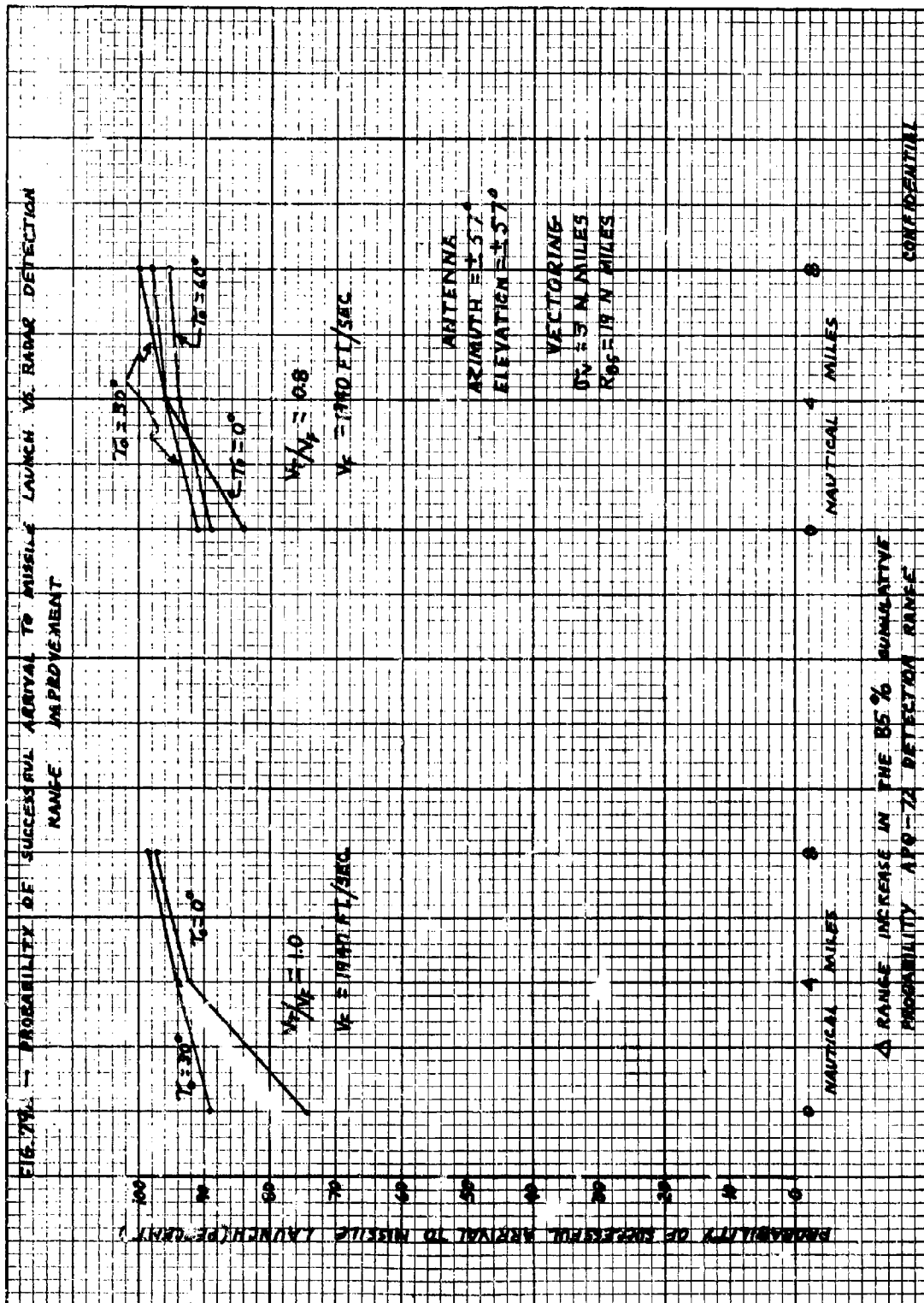


Calculated

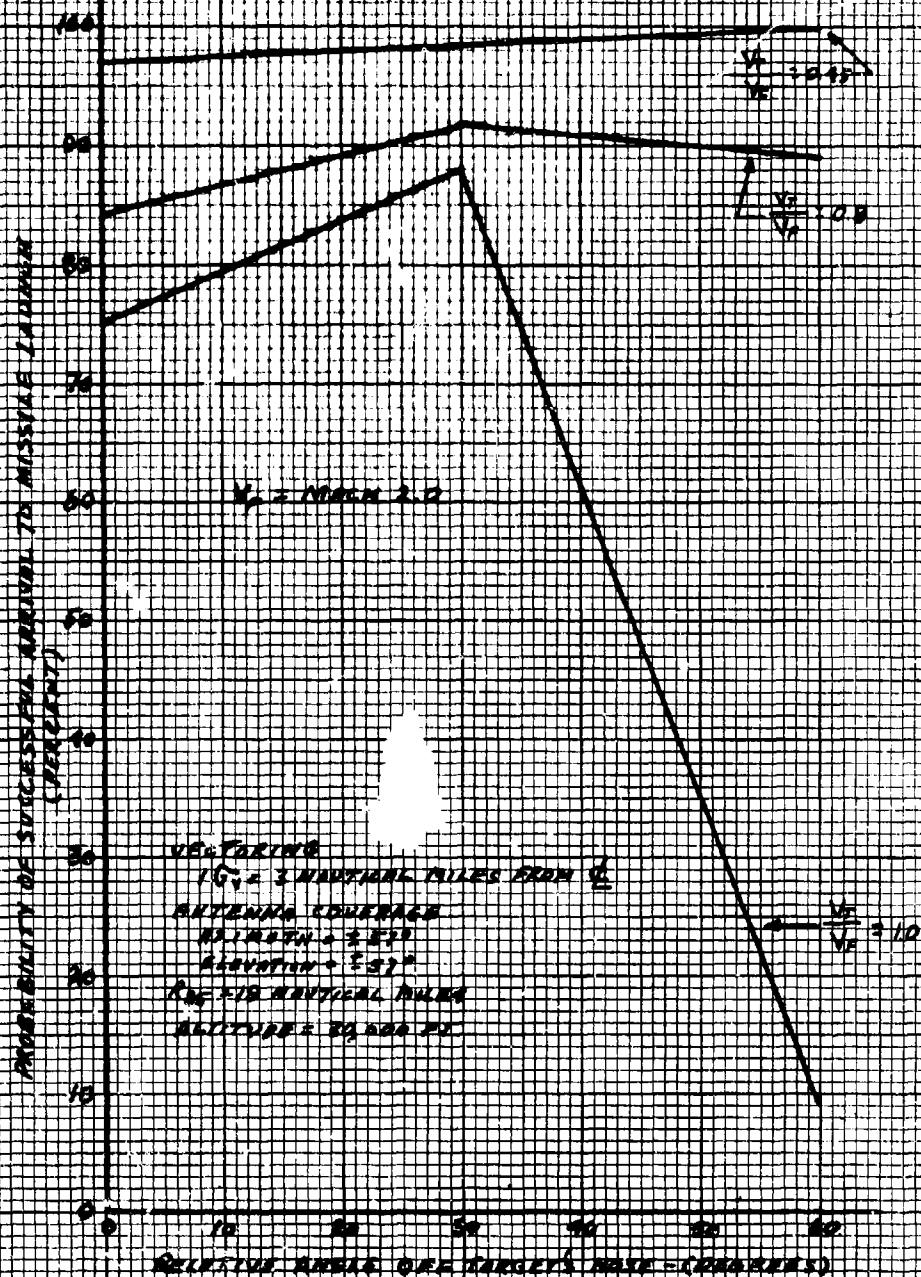
FIG 79- PROBABILITY OF SUCCESSFUL ARRIVAL TO MISSILE LAUNCH VARIOUS VELOCITY ANGLES,
IMPROVED RADAR



CONFIDENTIAL

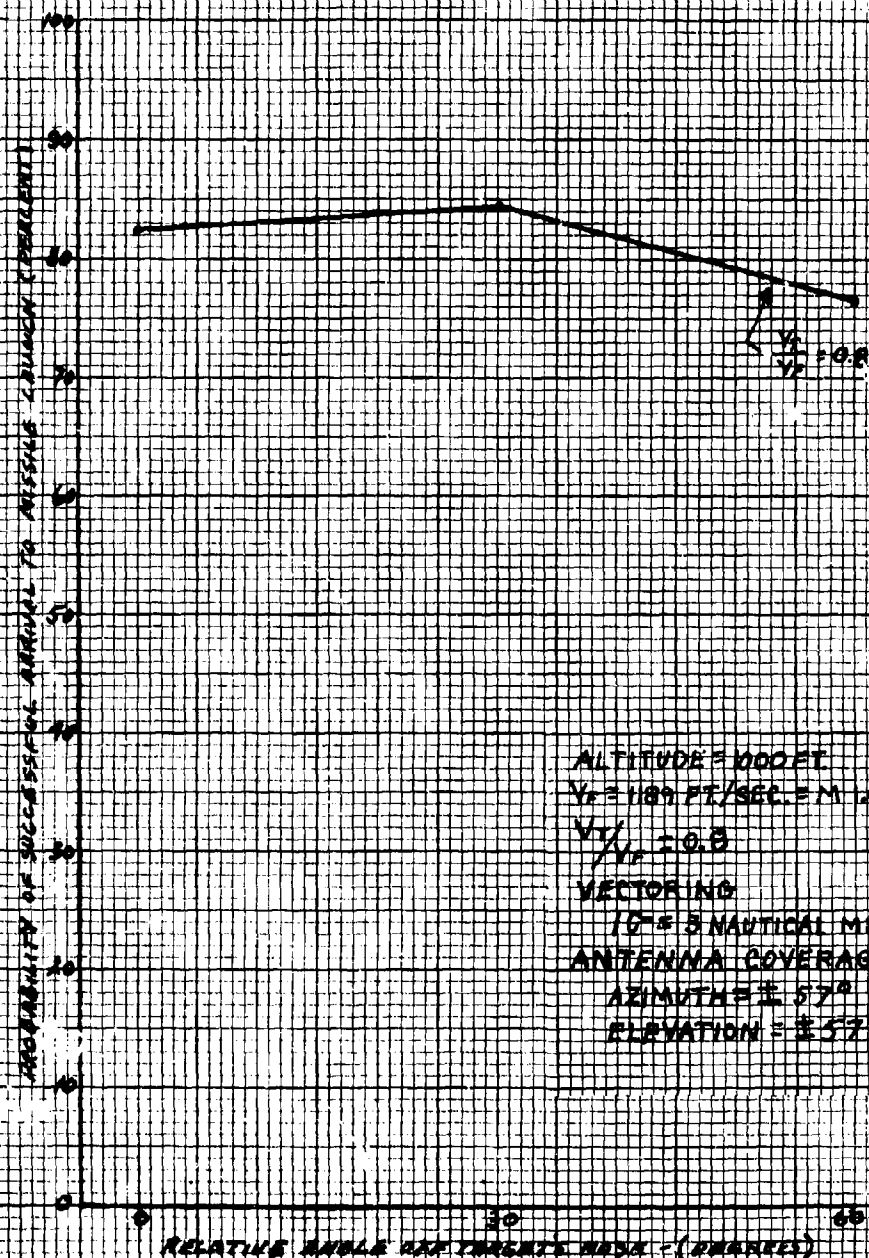


PROBABILITY OF SUCCESSFUL ARRIVAL TO MISSILE LAUNCH VERSUS VELOCITY RANGE IMPROVED RADAR



CONFIDENTIAL

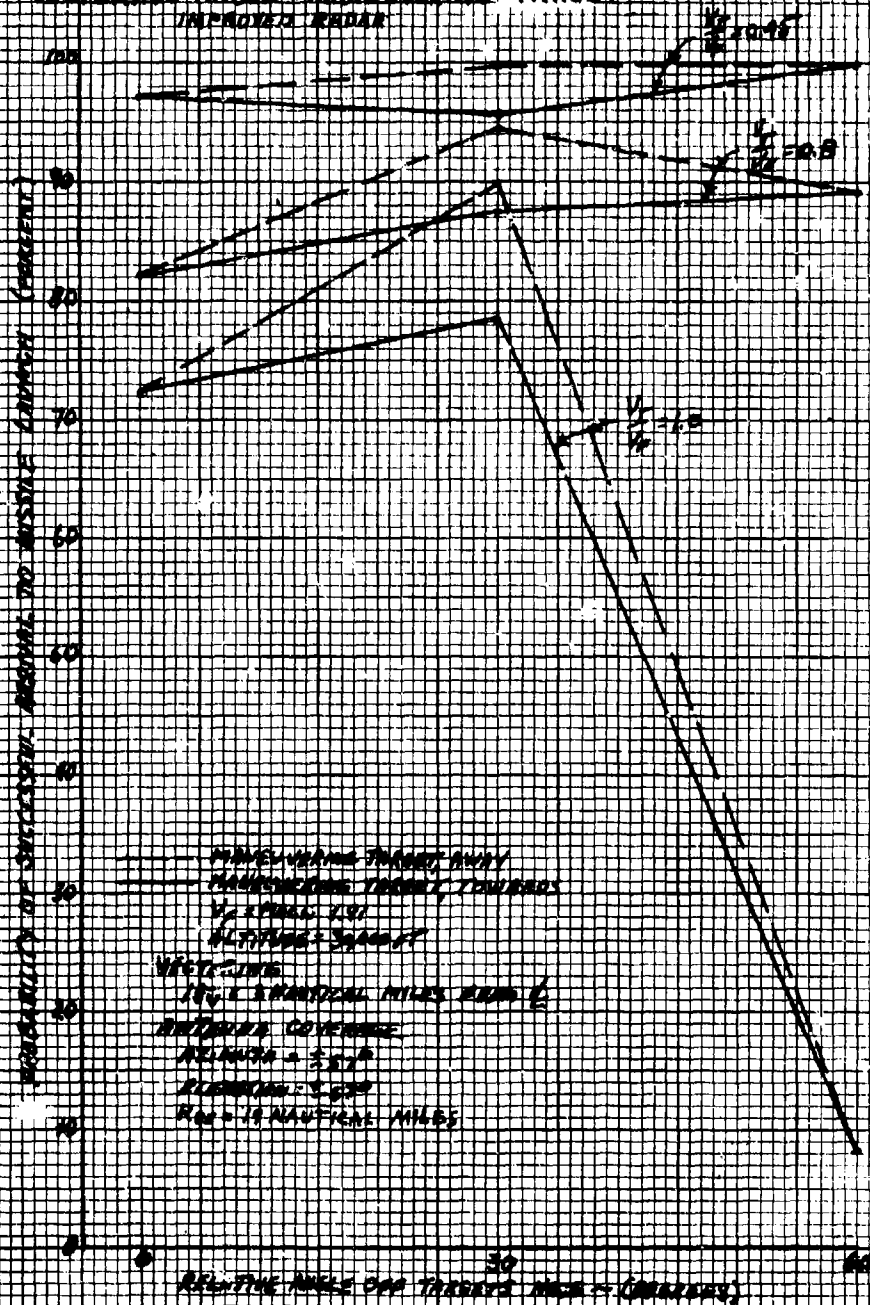
PROBABILITY OF SUCCESSFUL ARRIVAL TO MISSING CARRIER VERSUS VECTORING ANGLE IMPROVED RADAR



ALTITUDE = 1000 FT
 $V_c = 1189 \text{ FT/SEC} = M 1.07$
 $V_t/V_c = 0.8$
 VECTORING
 15° ± 3 NAUTICAL MILES FROM E
 ANTENNA COVERAGE
 AZIMUTH = ± 57°
 ELEVATION = ± 57°

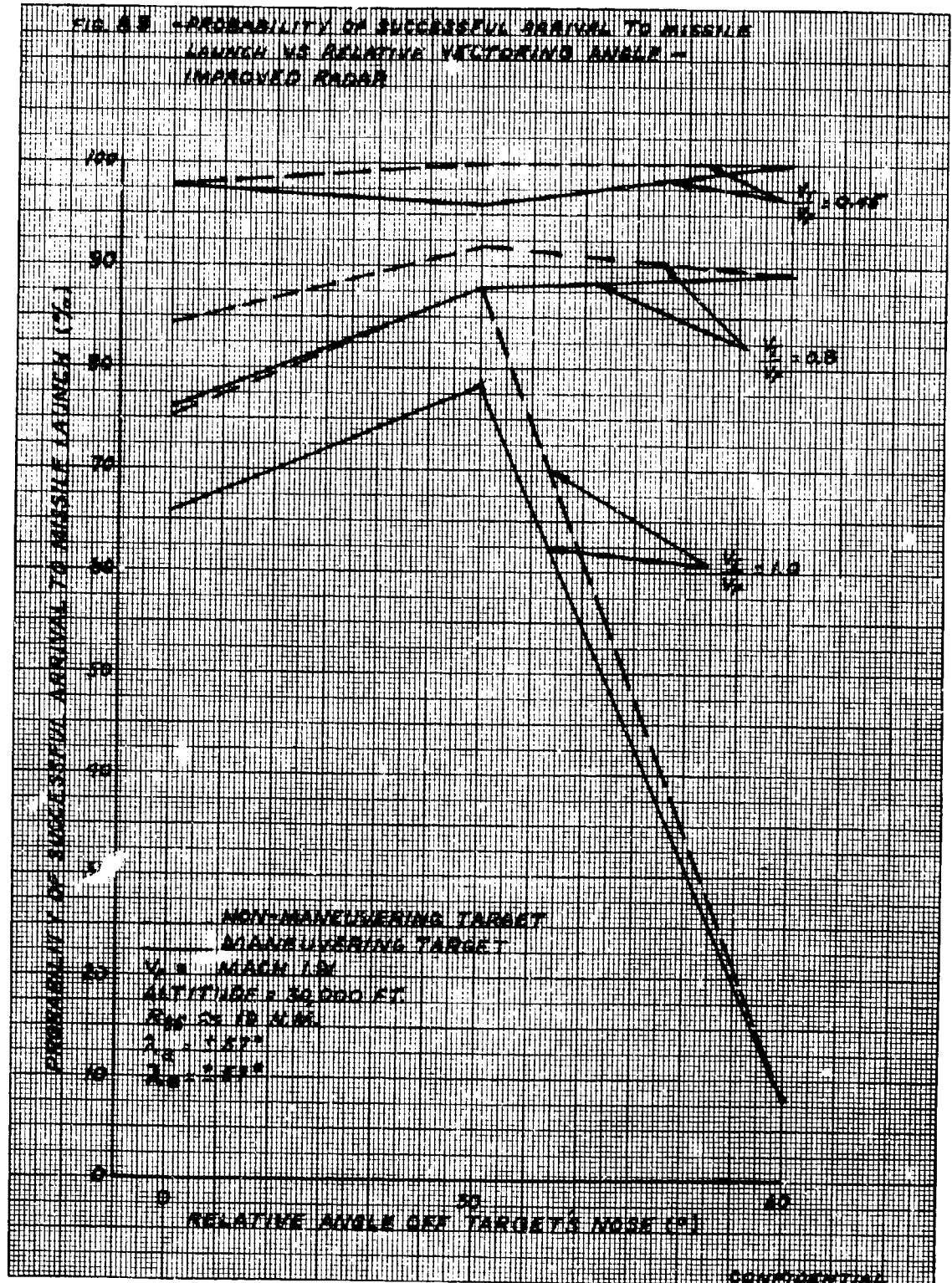
CONFIDENTIAL

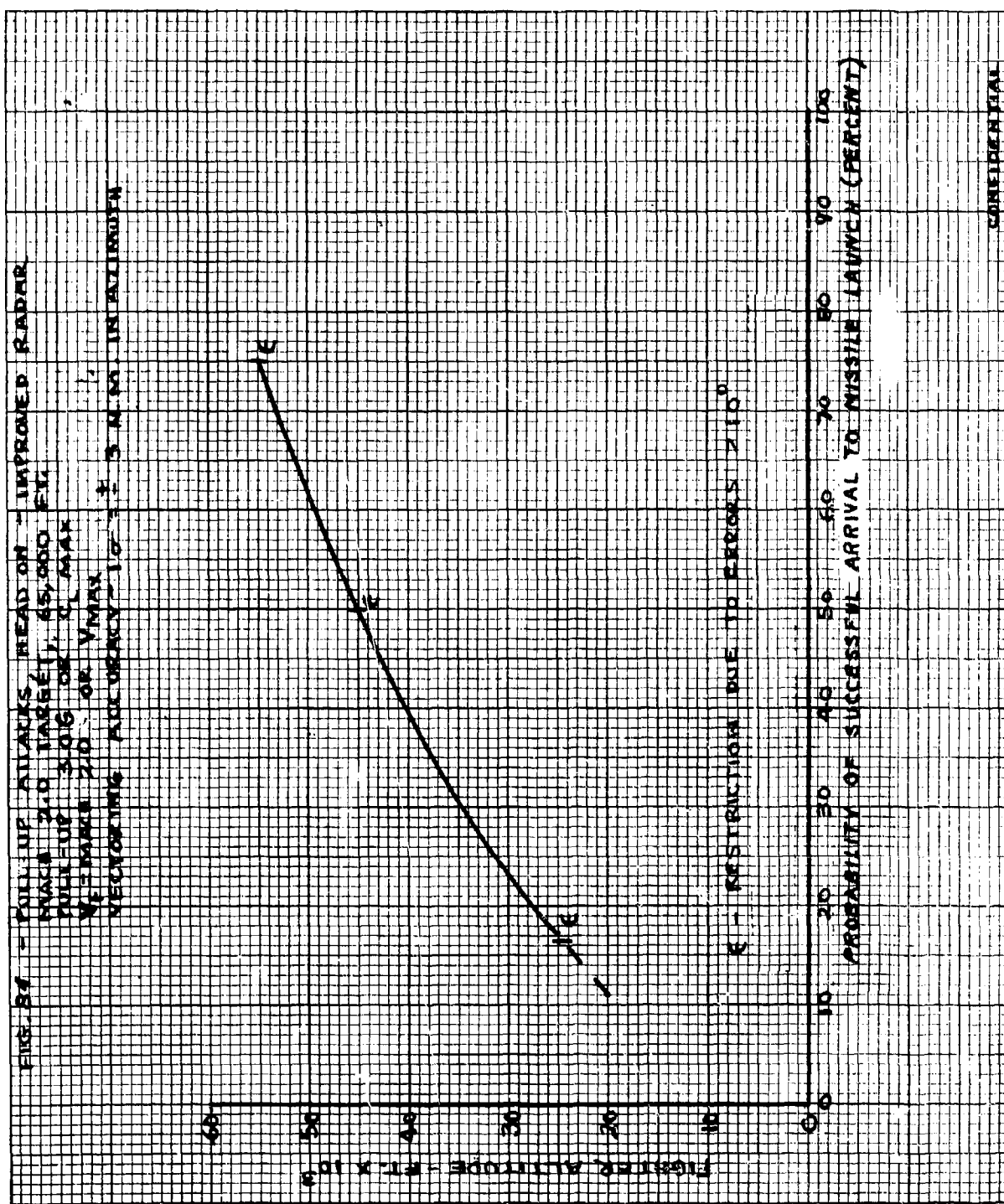
FIG. 82 - PROBABILITY OF SUCCESSFUL APPROACH TO MISSILE LAUNCH VERSUS
VECTORIZING ANGLE - HARRINGTON TARGET
IMPROVED RADAR



CONFIDENTIAL

FIG. 8.5 - PROBABILITY OF SUCCESSFUL ARRIVAL TO MISSILE LAUNCH VS RELATIVE VECTORING ANGLE - IMPROVED RADAR



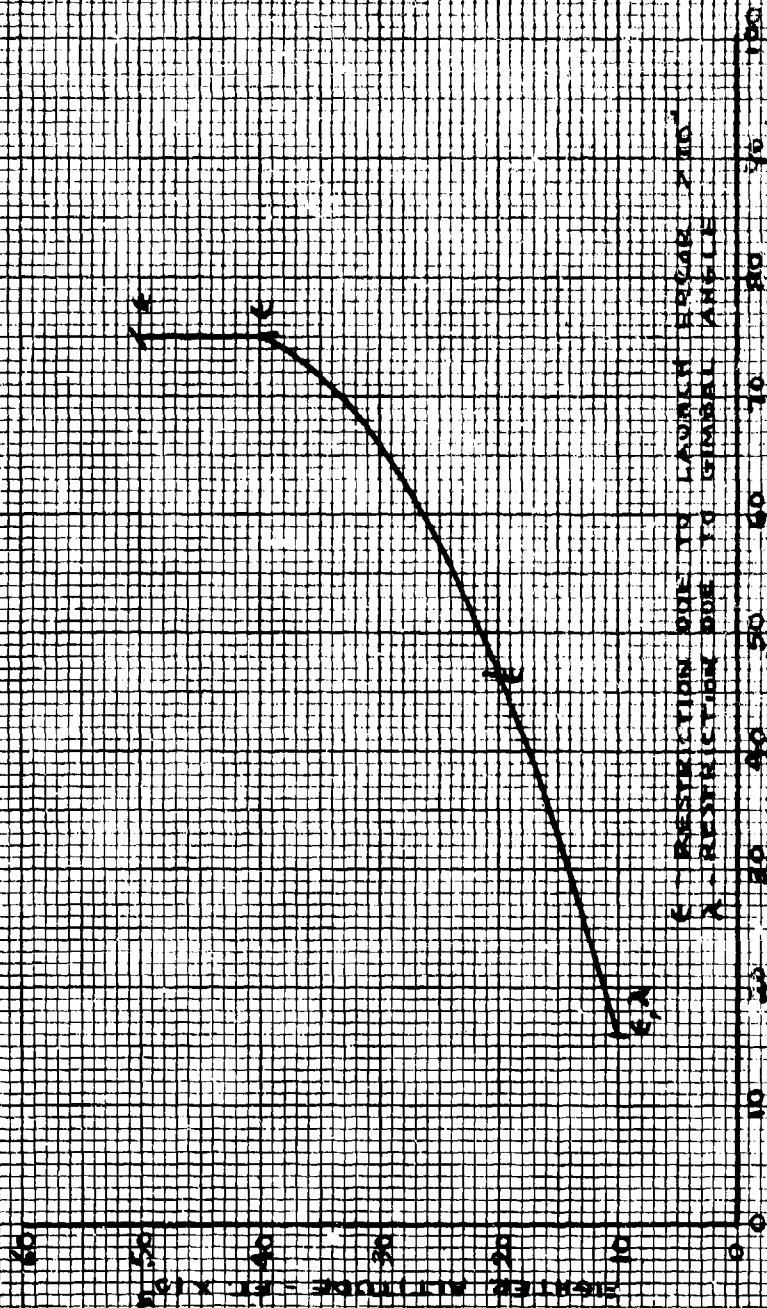


CONFIDENTIAL

FIG. 85 - PULL-UP ATTACKS. READING ON IMPROVED RADAR.
 RANGE 0.1 TARGET, 45,000 FT.
 PULL-UP 3.06 BK C-MAX
 W/ RANGE 2.0 BK V-MAX
 VECTORING ACCURACY - 10% ± 3 N.M. IN AZIMUTH



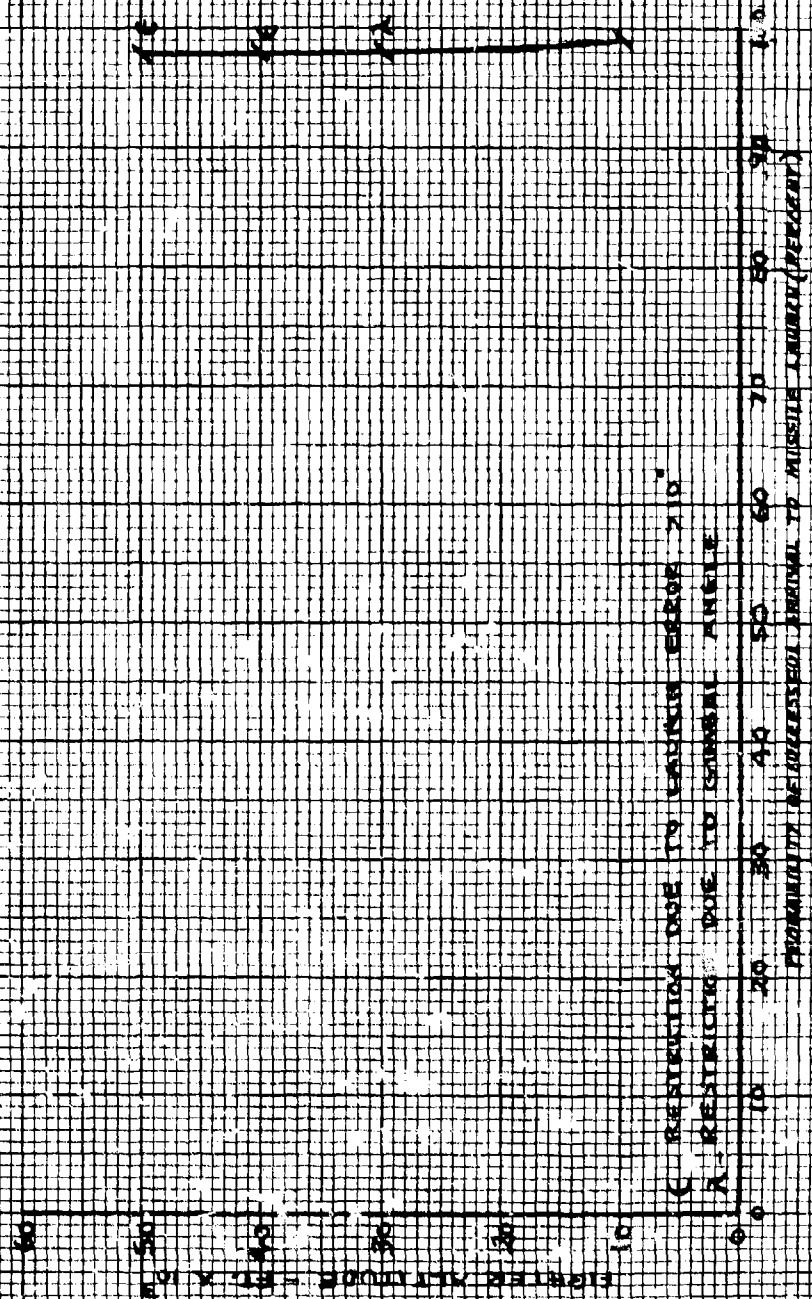
FIG. 86 - PULL-UP ATTACK, HEAD ON - IMPROVED RADAR
 MATCH 2.0 TARGET 50,000 FT.
 PULL-UP 3.0 G OR CL MAX
 VELOCITY 2.0 OR V MAX
 VECTORING ACCURACY $\pm 1.0^\circ$ ± 1.3 NM IN AZIMUTH

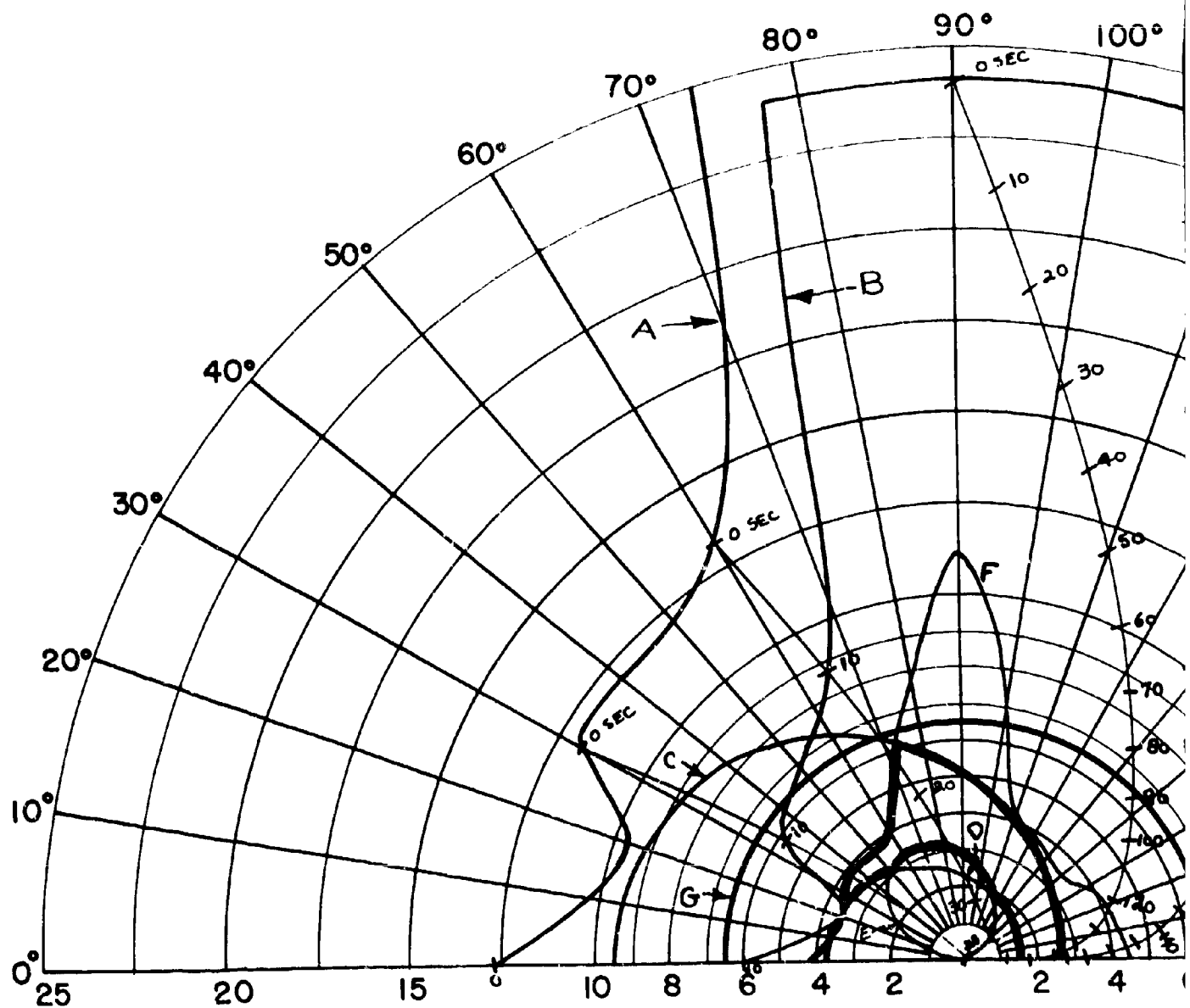


C - RESTRICTION DUE TO LAUNCH HEIGHT $> 40^\circ$
 X - RESTRICTION DUE TO GIMBAL ANGLE

PROBABILITY OF ORIENTED ARRIVAL TO MISSILE LAUNCH (PRESENT)

FIG. 87 - PULL-UP ATTACKS HEAD ON - IMPROVED RADAR
 WHICH 0.4 TARGET, 50,000 FT.
 PULL-UP 3.0 G OR 5 MAX
 VELOCITY 2.0 OR 3 MAX
 VELOCITY ACCURACY ± 1.0 - 3 NMAL IN ALTITUDE



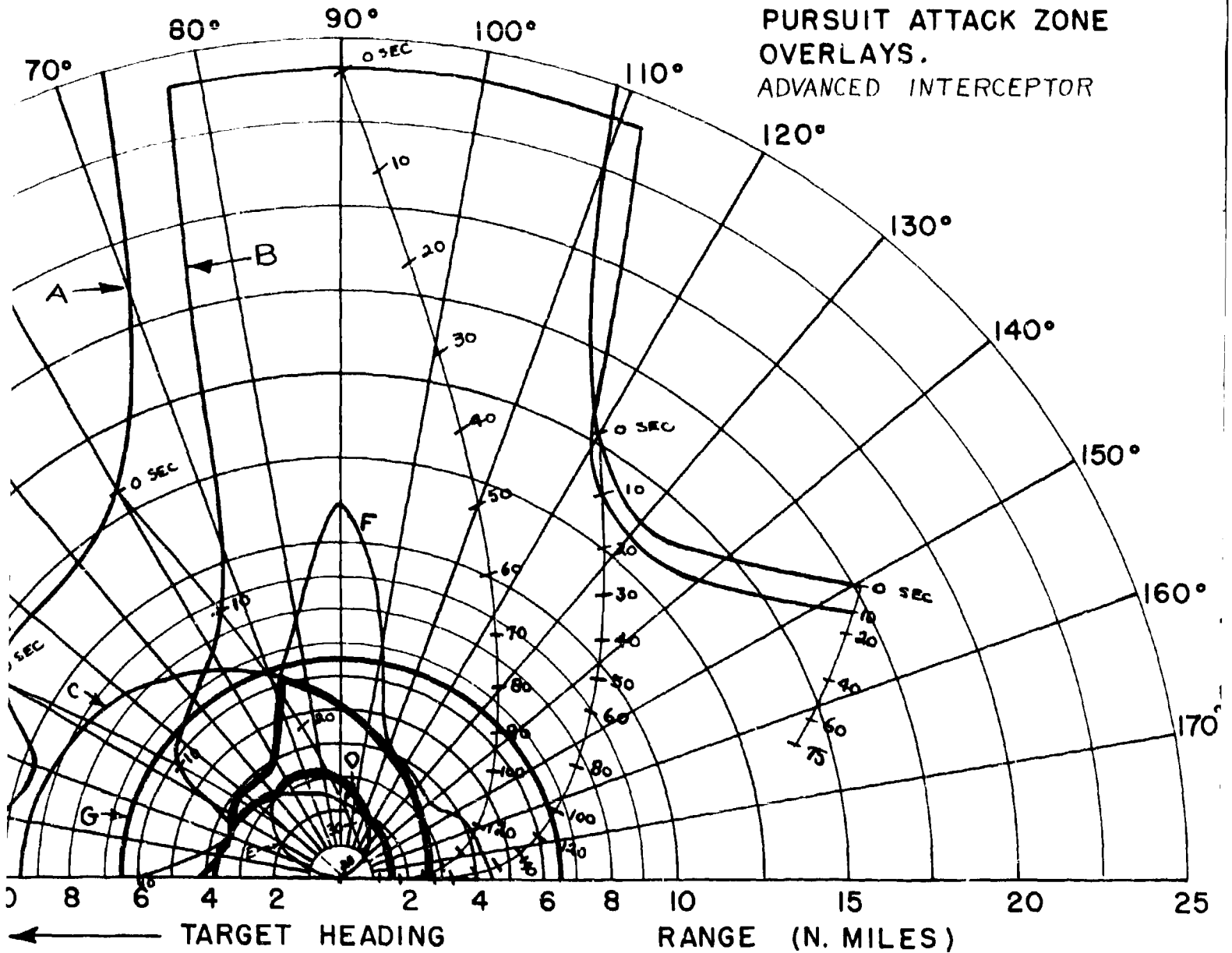


$V_F = 2134 \text{ FT/SEC}$
 $V_T = 1940 \text{ FT/SEC}$
 ALTITUDE = 50,000 FT.

← TARGET HEADING

- A - 85% DETECTION RANGE
- B - LOCK-ON RANGE (10 SEC. LOCK-ON)
- C - SPARROW III MAX. AERODYNAMIC
- D - SPARROW III MIN. AERODYNAMIC
- E - CONSTANT LOAD FACTOR LOCK-ON
- F - 90% SPARROW III SEEKER LOCK-ON
- G - 6.5 N.M. INTERLOCK

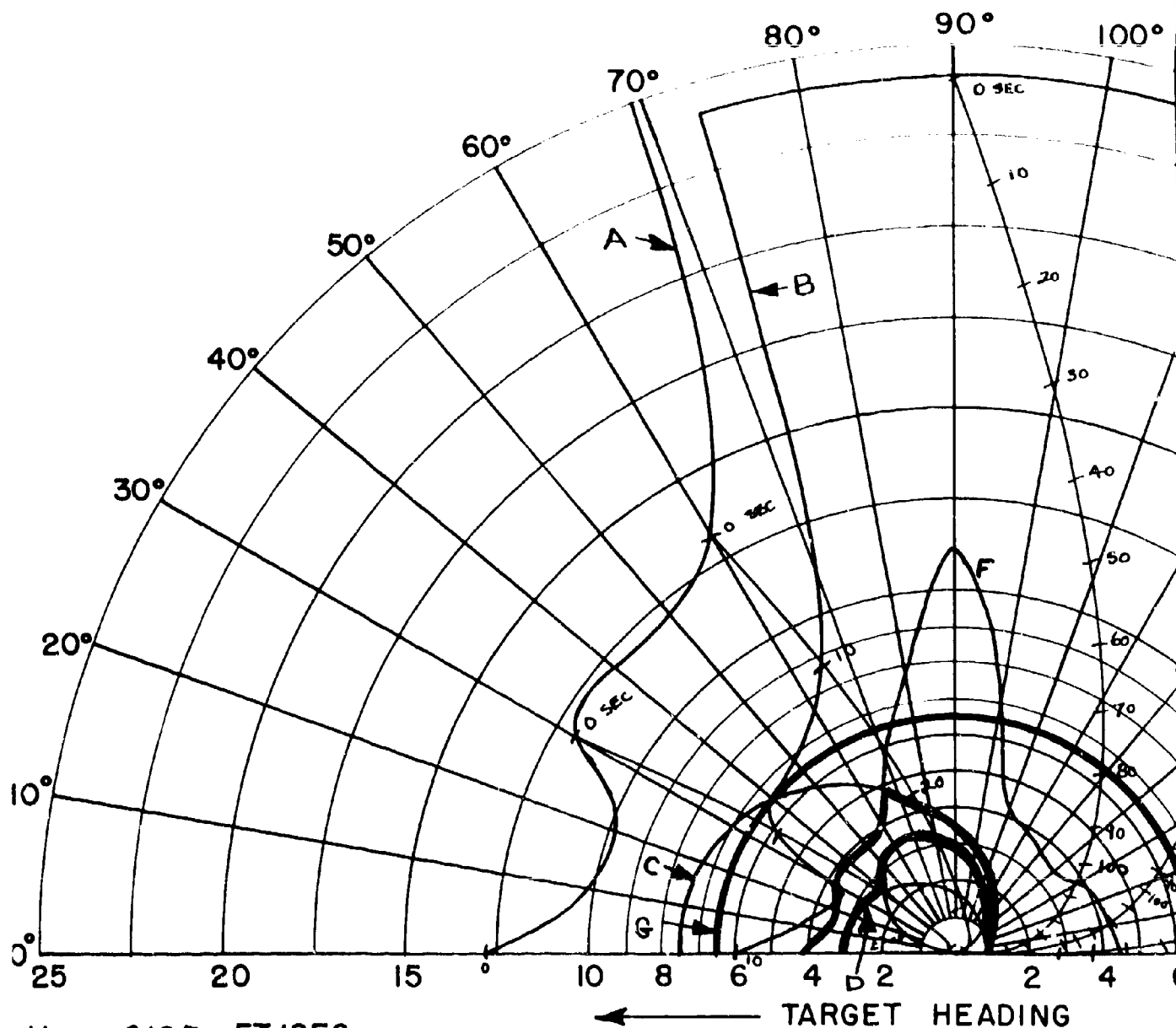
FIG. 88 - CO-ALTITUDE LEAD
PURSUIT ATTACK ZONE
OVERLAYS.
ADVANCED INTERCEPTOR



- A - 85% DETECTION RANGE
- B - LOCK-ON RANGE (10 SEC. LOCK-ON TIME)
- C - SPARROW III MAX. AERODYNAMIC RANGE
- D - SPARROW III MIN. AERODYNAMIC RANGE
- E - CONSTANT LOAD FACTOR LOCUS ($N_z = 3$)
- F - 90% SPARROW III SEEKER LOCK-ON RANGE
- G - 6.5 N.M. INTERLOCK

2

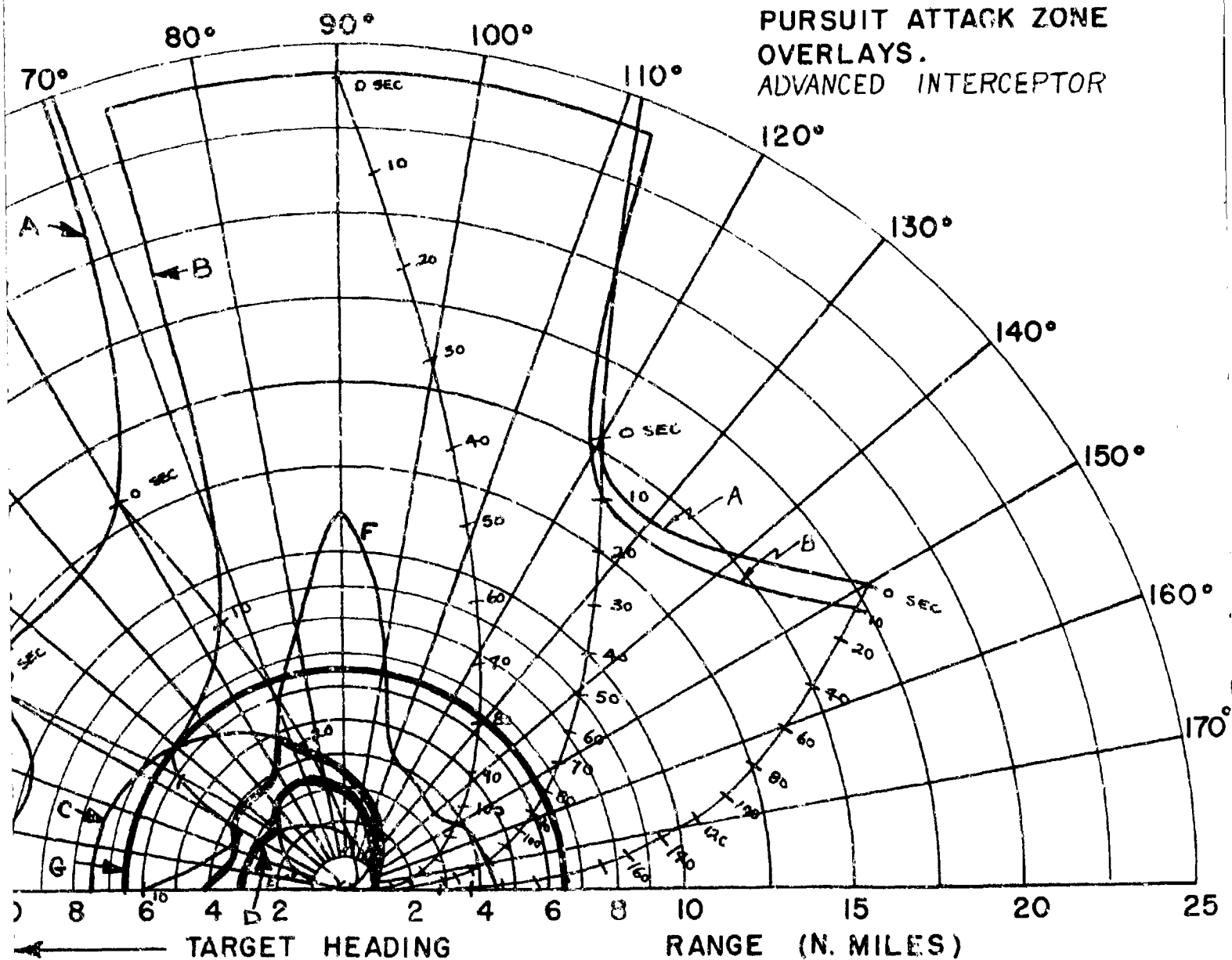
CONFIDENTIAL



$V_F = 2185 \text{ FT/SEC}$
 $V_T = 1897 \text{ FT/SEC}$
 ALTITUDE = 30,000 FT.

- A - 85% DETECTION RANGE
- B - LOCK-ON RANGE (10 SEC. LOCK-ON)
- C - SPARROW III MAX. AERODYNAMIC
- D - SPARROW III MIN. AERODYNAMIC
- E - CONSTANT LOAD FACTOR LOCUS
- F - 90% SPARROW III SEEKER LOCK
- G - 6.5 N.M. INTERLOCK

FIG. 89 - CO-ALTITUDE LEAD
PURSUIT ATTACK ZONE
OVERLAYS.
ADVANCED INTERCEPTOR



- 85% DETECTION RANGE
- LOCK-ON RANGE (10 SEC. LOCK-ON TIME)
- SPARROW III MAX. AERODYNAMIC RANGE
- SPARROW III MIN. AERODYNAMIC RANGE
- CONSTANT LOAD FACTOR LOCUS ($N_z = 3$)
- 90% SPARROW III SEEKER LOCK-ON RANGE
- 6.5 N.M. INTERLOCK

2

CONFIDENTIAL

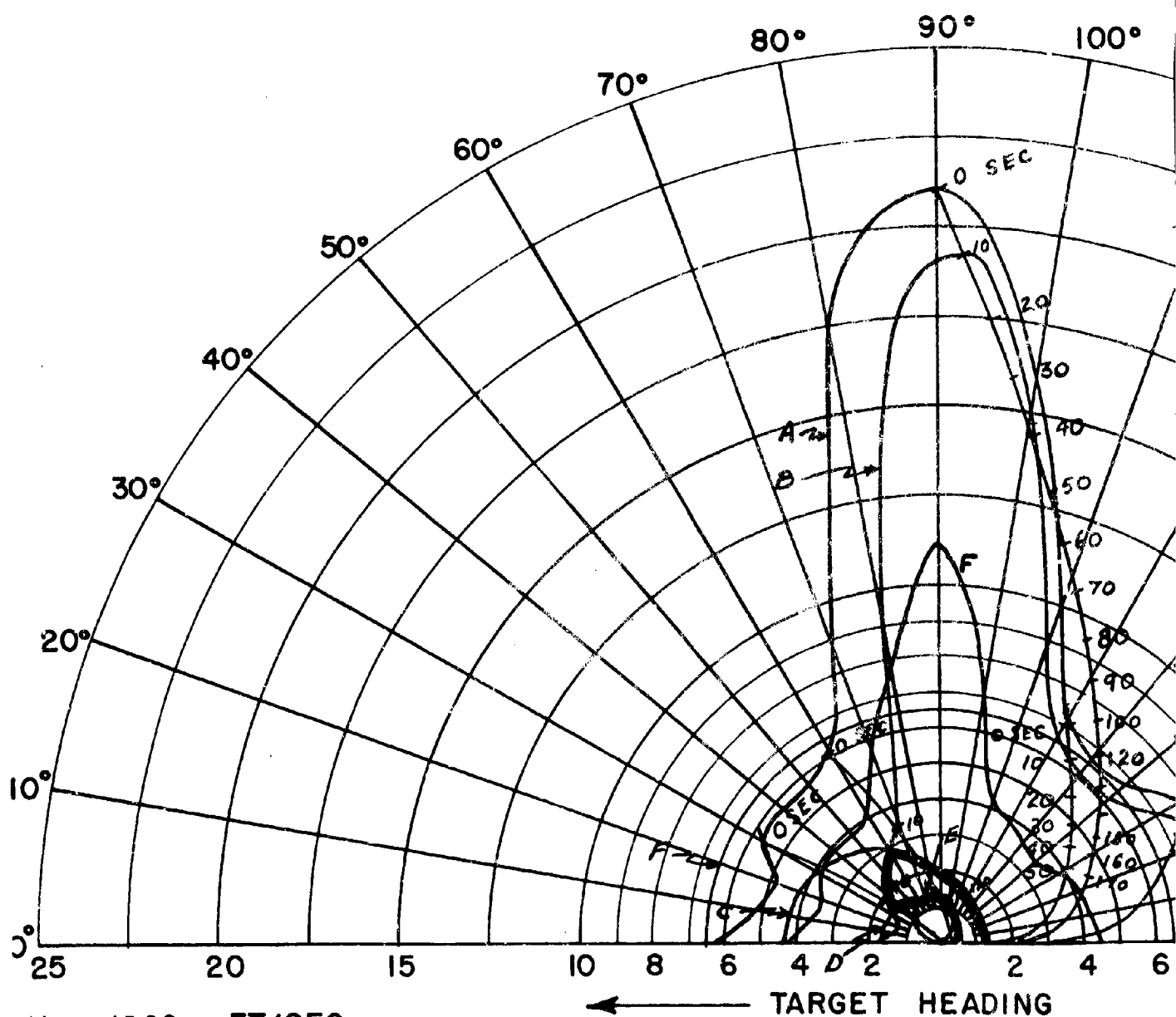
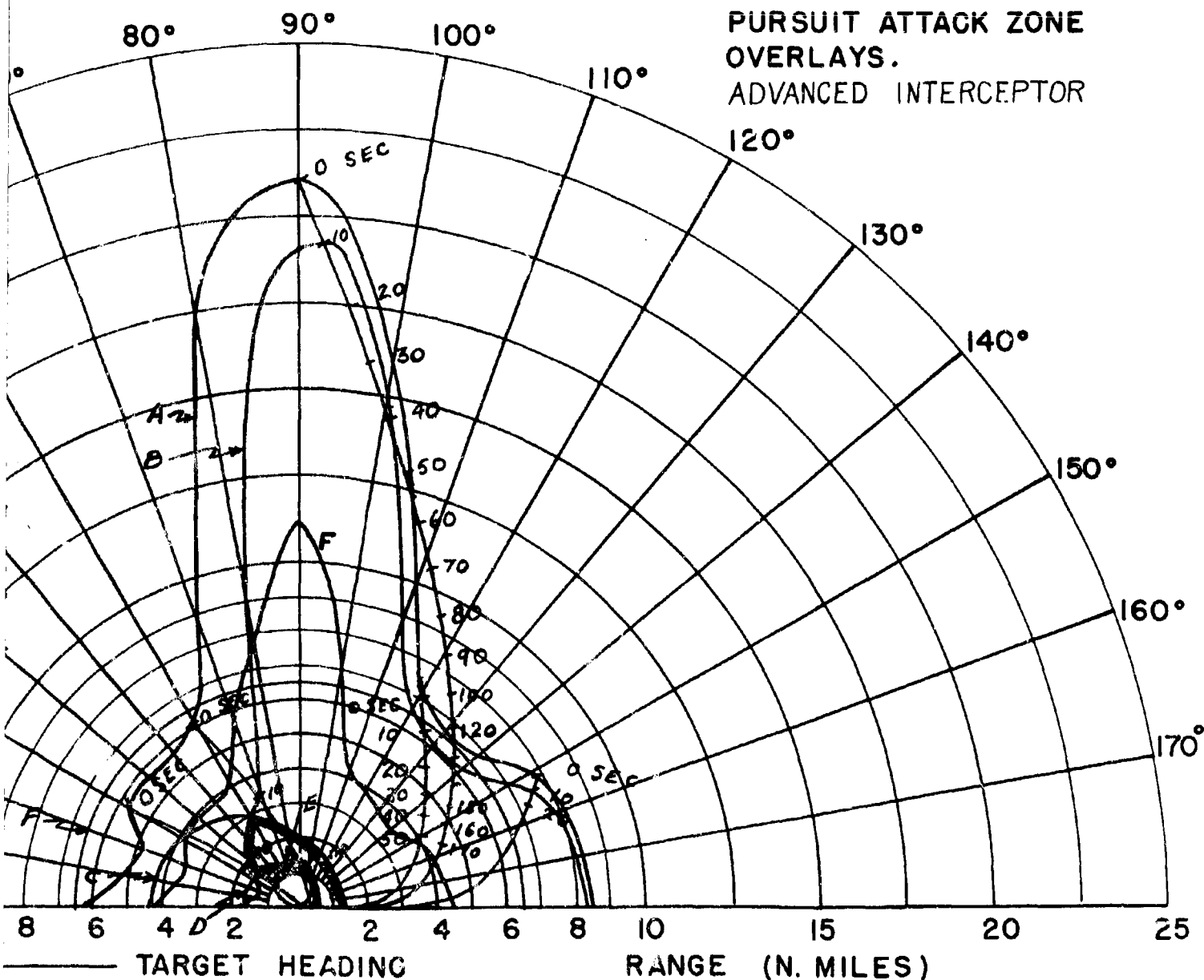


FIG. 90 - CO-ALTITUDE LEAD
PURSUIT ATTACK ZONE
OVERLAYS.
ADVANCED INTERCEPTOR



85% DETECTION RANGE
LOCK-ON RANGE (10 SEC. LOCK-ON TIME)
SPARROW III MAX. AERODYNAMIC RANGE
SPARROW III MIN. AERODYNAMIC RANGE
CONSTANT LOAD FACTOR LOCUS ($N_z = 3$)
90% SPARROW III SEEKER LOCK-ON RANGE
6.5 N.M. INTERLOCK

2

CONFIDENTIAL

$V_f = 2185 \text{ FT/SEC}$
 $V_r = 1871 \text{ FT/SEC}$
 50 LIMIT
 3 SECONDS
 REAC COARSE
 1000 COURSE

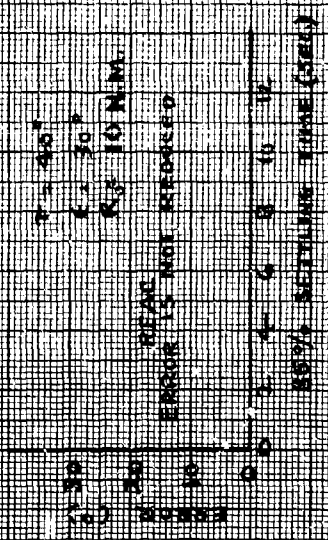
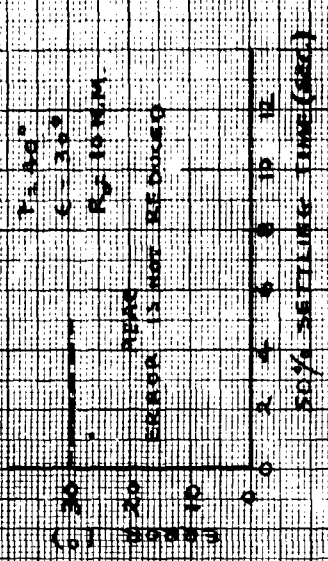
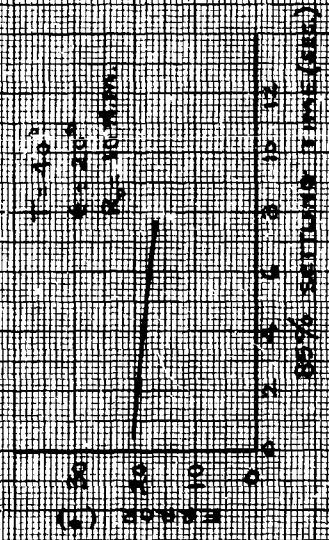
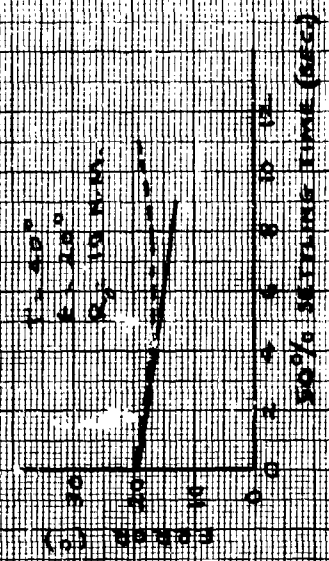


FIG. 42 - ERROR VS TIME FROM SETTLING TIME STUDY
 ADVANCED INTERCEPTOR

CONTINUED

$V_f = 2105 \text{ ft/sec}$
 $V_r = 1510 \text{ ft/sec}$

3 ft LIMIT
 3 SECONDS
 REAR COURSE
 1.8M COURSE

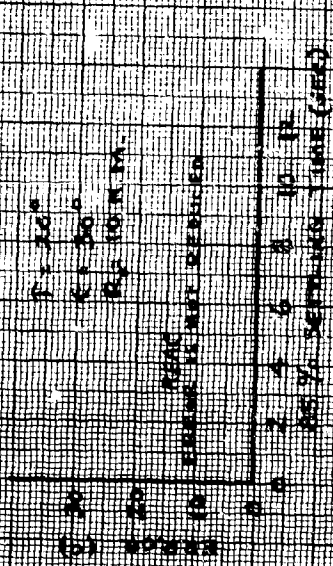
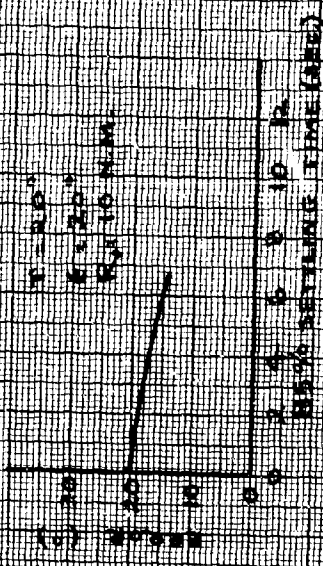
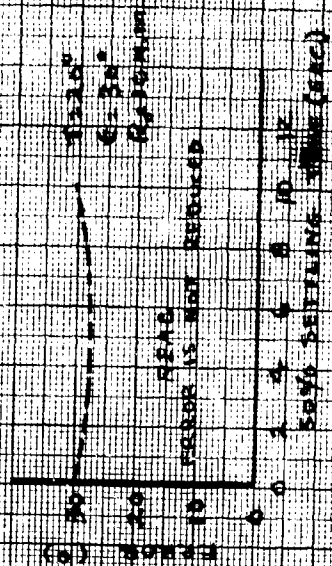
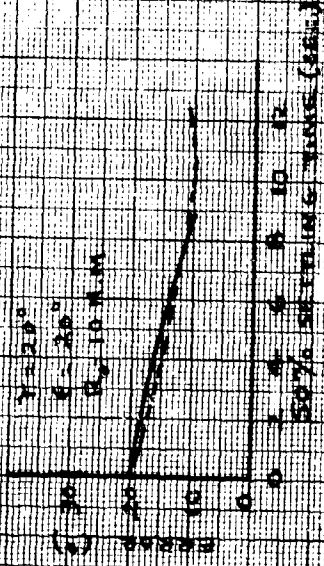


FIG. 92. PLOTS OF TIME FROM SETTLING TIME STUDY ADVANCED INTERSECTION

$V_f = 4.185 \text{ FT/SEC}$
 $V_f = 15.18 \text{ FT/SEC}$
 300 LIMIT
 300000
 300000
 300000
 300000

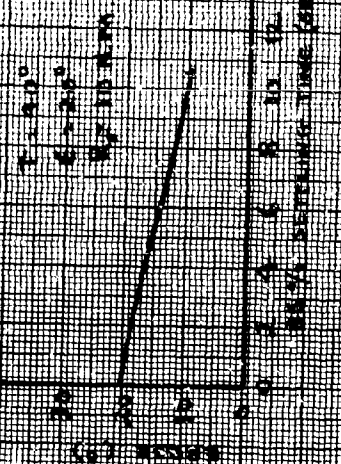
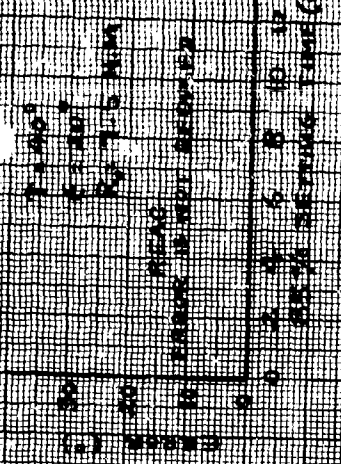
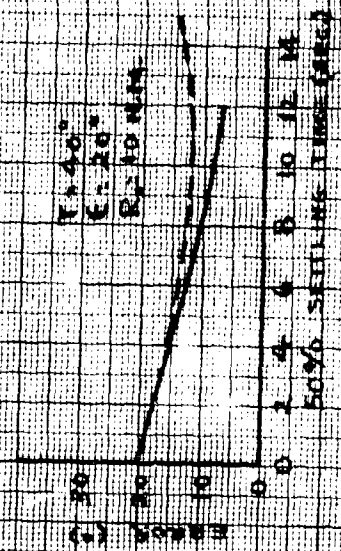
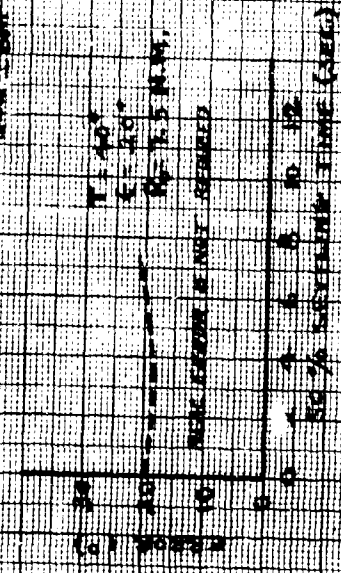
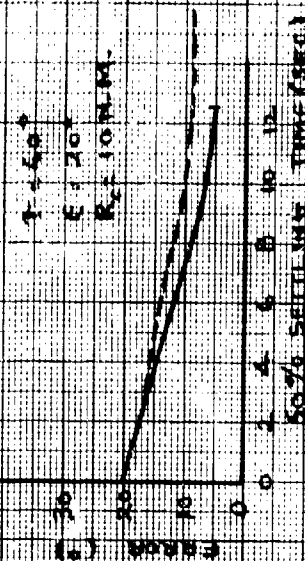
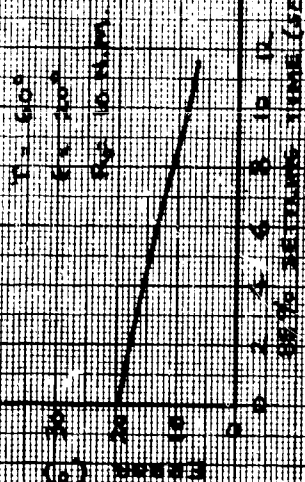
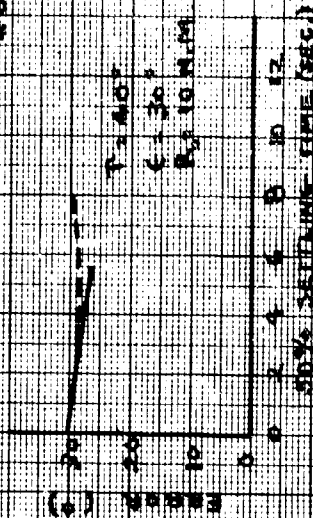
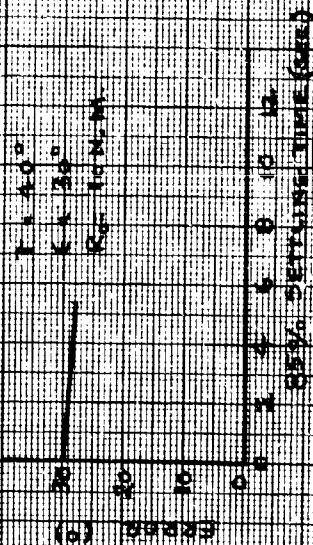


FIG. 54 - ERROR VS. TIME FROM SETTLING START ADVANCED INTERCEPT

CONSIDERATION

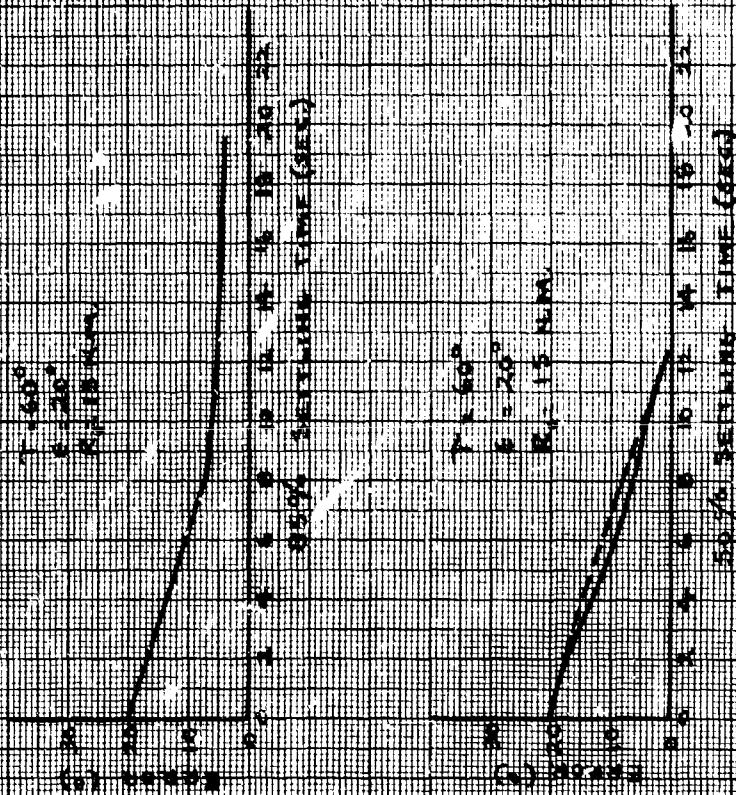
$V_r = 2105 \text{ FT/SEC}$
 $V_f = 1519 \text{ FT/SEC}$
 $3 \frac{1}{2} \text{ MIN}$
 3 SECONDS

— REAC. COURSE
 --- 1 BM. COURSE



ONE-95 ERROR VS TIME FROM SETTLING TIME STUDY
 ADVANCED INTERCEPT

Fig. 95	ENTERIC MOUNTED	ENTERIC SPLITTING	ENTERIC TUBE	ENTERIC SYRINGE
Fig. 96	ENTERIC MOUNTED	ENTERIC SPLITTING	ENTERIC TUBE	ENTERIC SYRINGE



$V_f = 2185 \text{ FT/SEC}$
 $V_T = 1518 \text{ FT/SEC}$
 50 LIMIT
 5 SECONDS
 $REAL \text{ COURSE}$
 $TBM \text{ COURSE}$

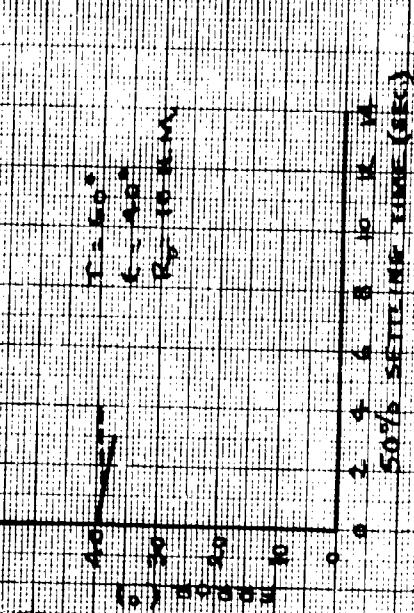
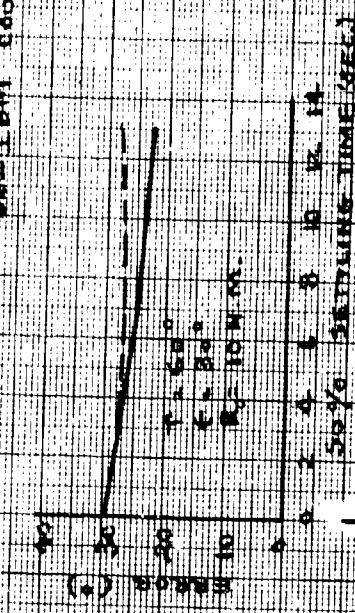
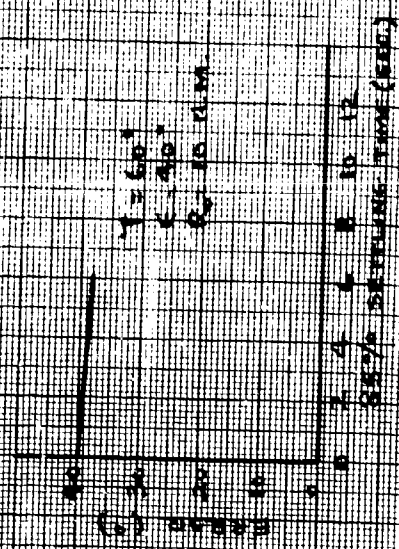
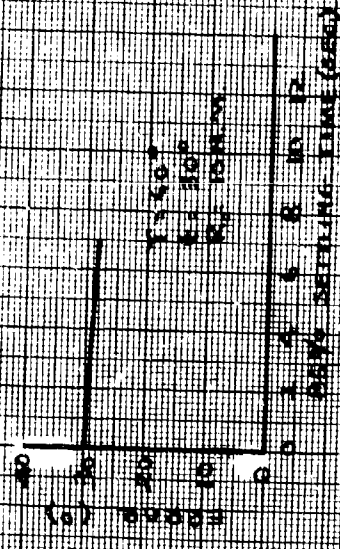


FIG. 97 - ERROR VS TIME FROM SETTING TIME STUDY
 ADVANCED INTERCEPT

SPENCER &
J.F. HUNT
RECEIVED MAR 20 1968
MAR 20 1968
MAR 20 1968

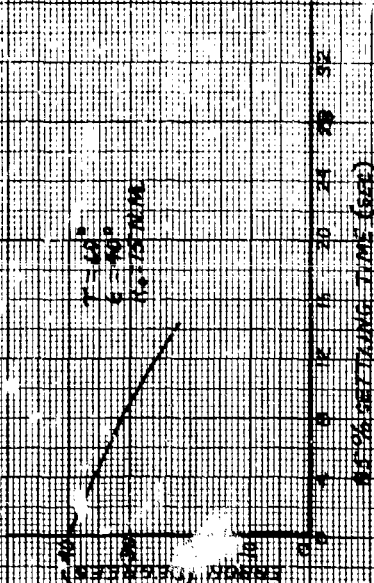
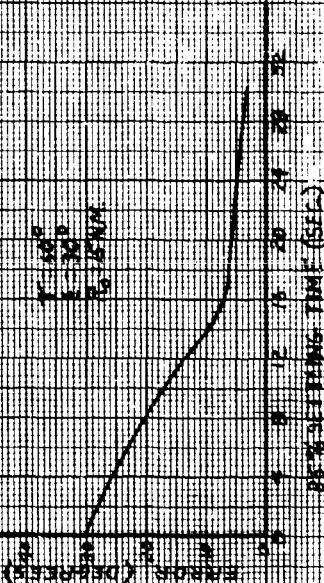
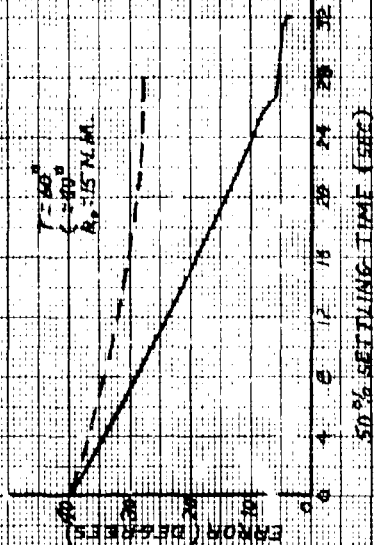
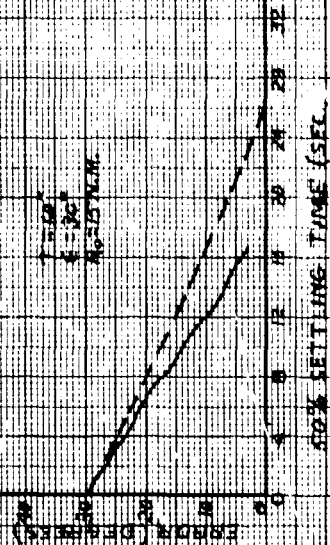


FIG 48 -- ERROR VS TIME FROM SETTLING TIME STUDY
ADVANCED INTERCEPT

NON-FUNCTIONAL

$T_f = 2185 \text{ FT/SEC}$
 $T_f = 5154 \text{ FT/SEC}$
 3% LIMIT
 3 SECONDS
 --- REAC COARSE
 --- IBM COARSE

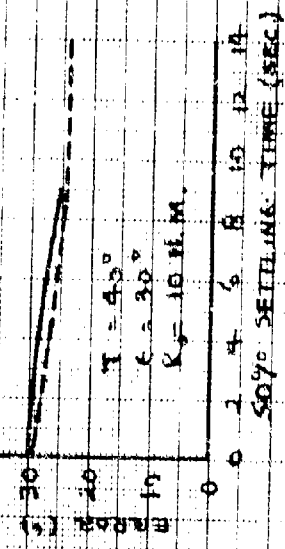
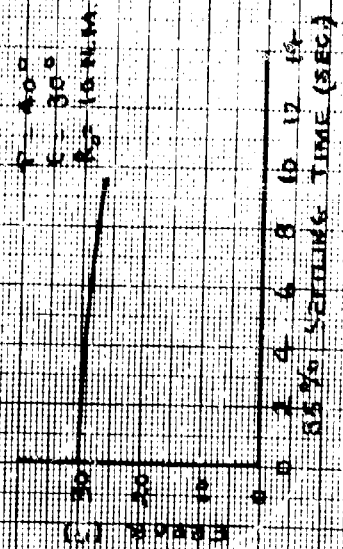
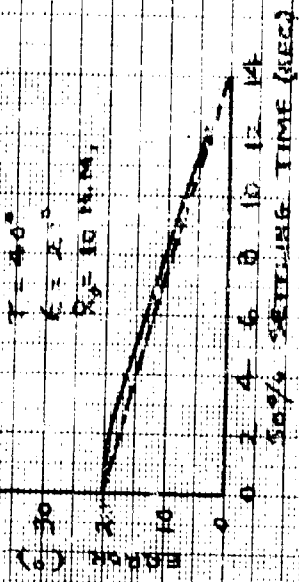
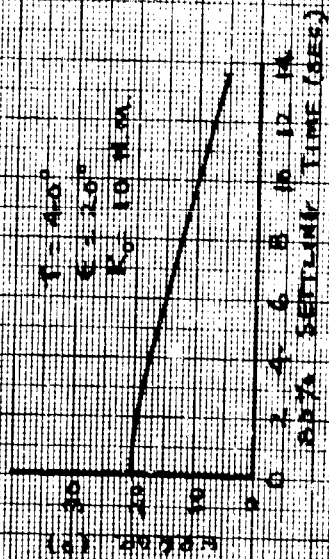
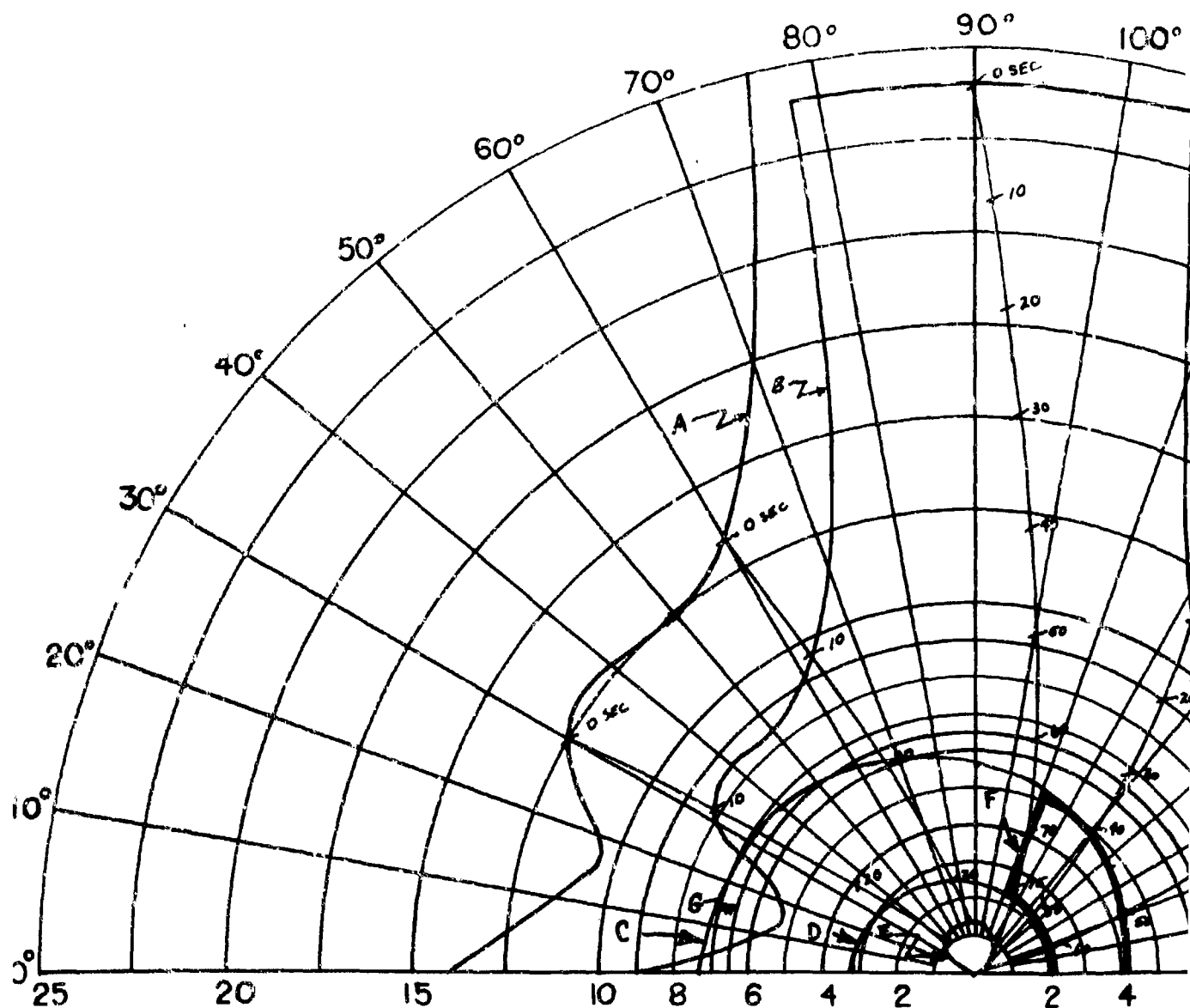


FIG. 99 - ERROR VS TIME FROM SETTLING TIME STUDY
 ADVANCED INTERCEPTOR



$V_F = 1940$ FT/SEC. (F4H-1)(F8U-3)

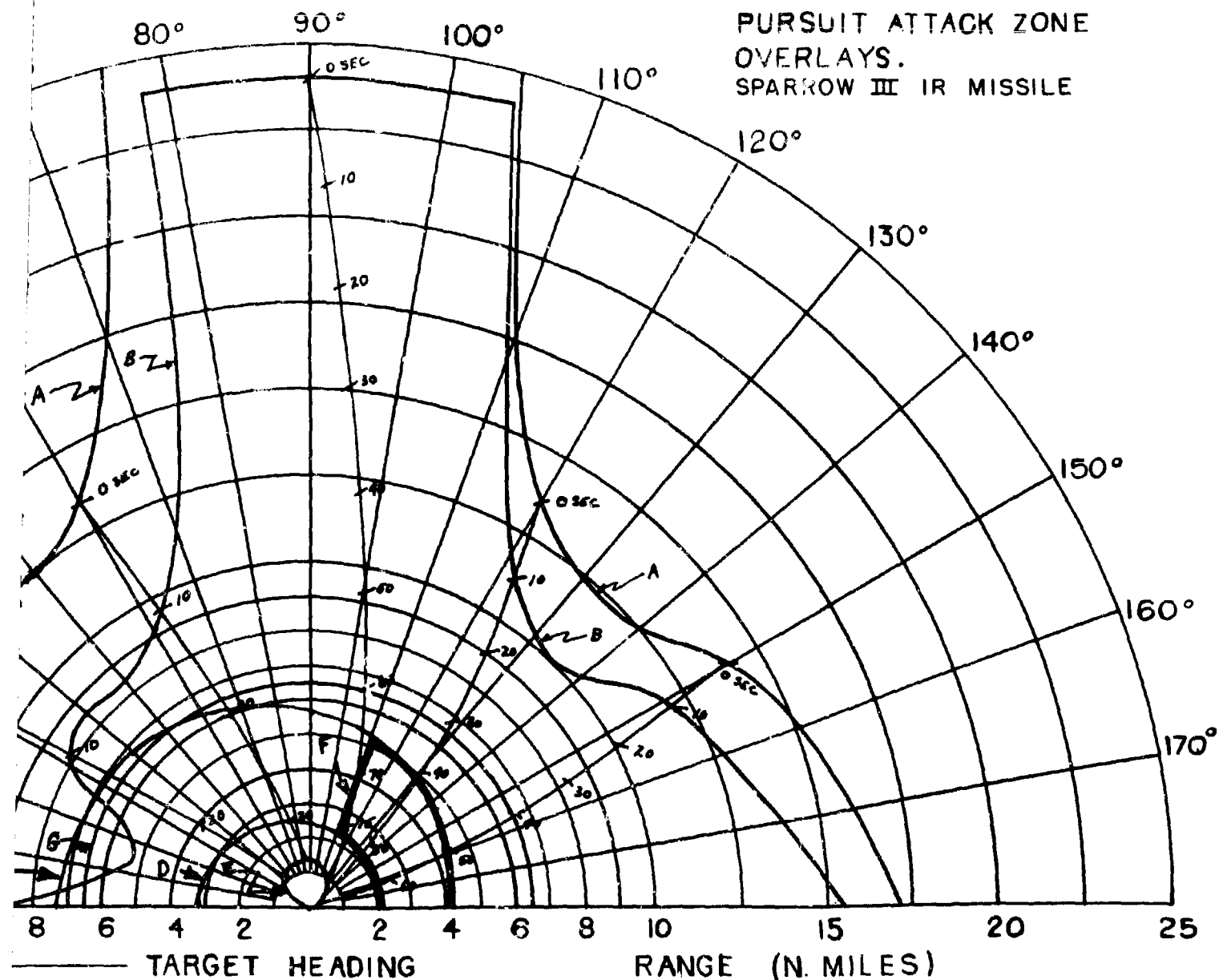
$V_T = 873$ FT/SEC.

ALTITUDE = 50,000 FT.

← TARGET HEADING

- A - 85% DETECTION RANGE
- B - LOCK-ON RANGE (10 SEC. LOCK-ON)
- C - SPARROW III MAX. AERODYNAMIC RANGE
- D - SPARROW III MIN. AERODYNAMIC RANGE
- E - CONSTANT LOAD FACTOR LOCUS ($N_z = 3$)
- F - SPARROW III IR LIMIT
- G - 6.5 N.MI. INTERLOCK

FIG. 100 - CO-ALTITUDE LEAD
PURSUIT ATTACK ZONE
OVERLAYS.
SPARROW III IR MISSILE

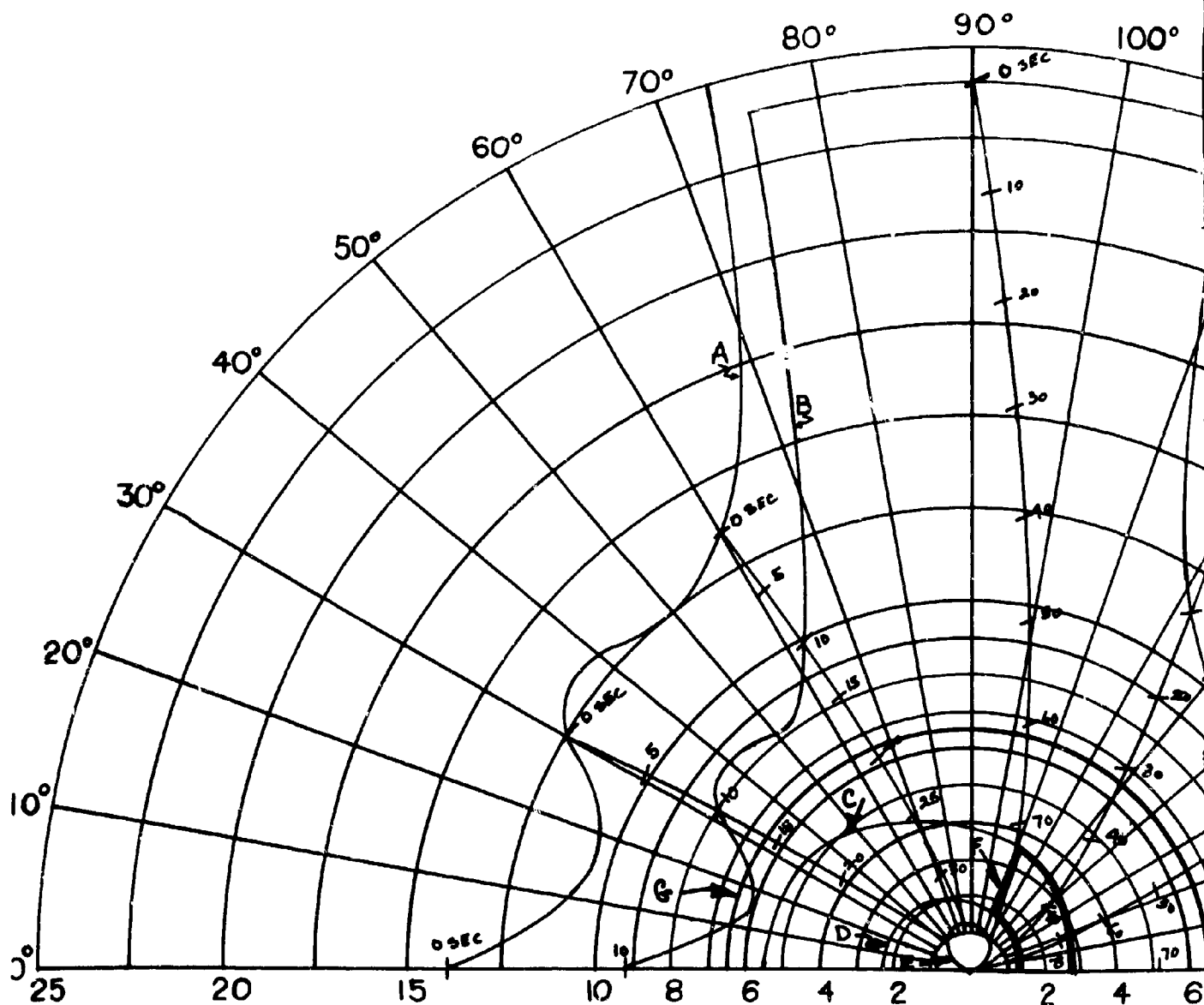


85% DETECTION RANGE
LOCK-ON RANGE (10 SEC. LOCK-ON TIME)

SPARROW III MAX. AERODYNAMIC RANGE
SPARROW III MIN. AERODYNAMIC RANGE
CONSTANT LOAD FACTOR LOCUS ($N_z = 3$)
SPARROW III IR LIMIT
6.5 N.M. INTERLOCK

2

CONFIDENTIAL



$V_F = 1897$ FT./SEC. (F 4 H-1)(F8U-3)

$V_T = 854$ FT./SEC.

ALTITUDE = 30,000 FT.

← TARGET HEADING

A - 85% DETECTION RANGE

B - LOCK-ON RANGE (10 SEC. LOCK-ON)

C - SPARROW III MAX. AERODYNAMIC RANGE

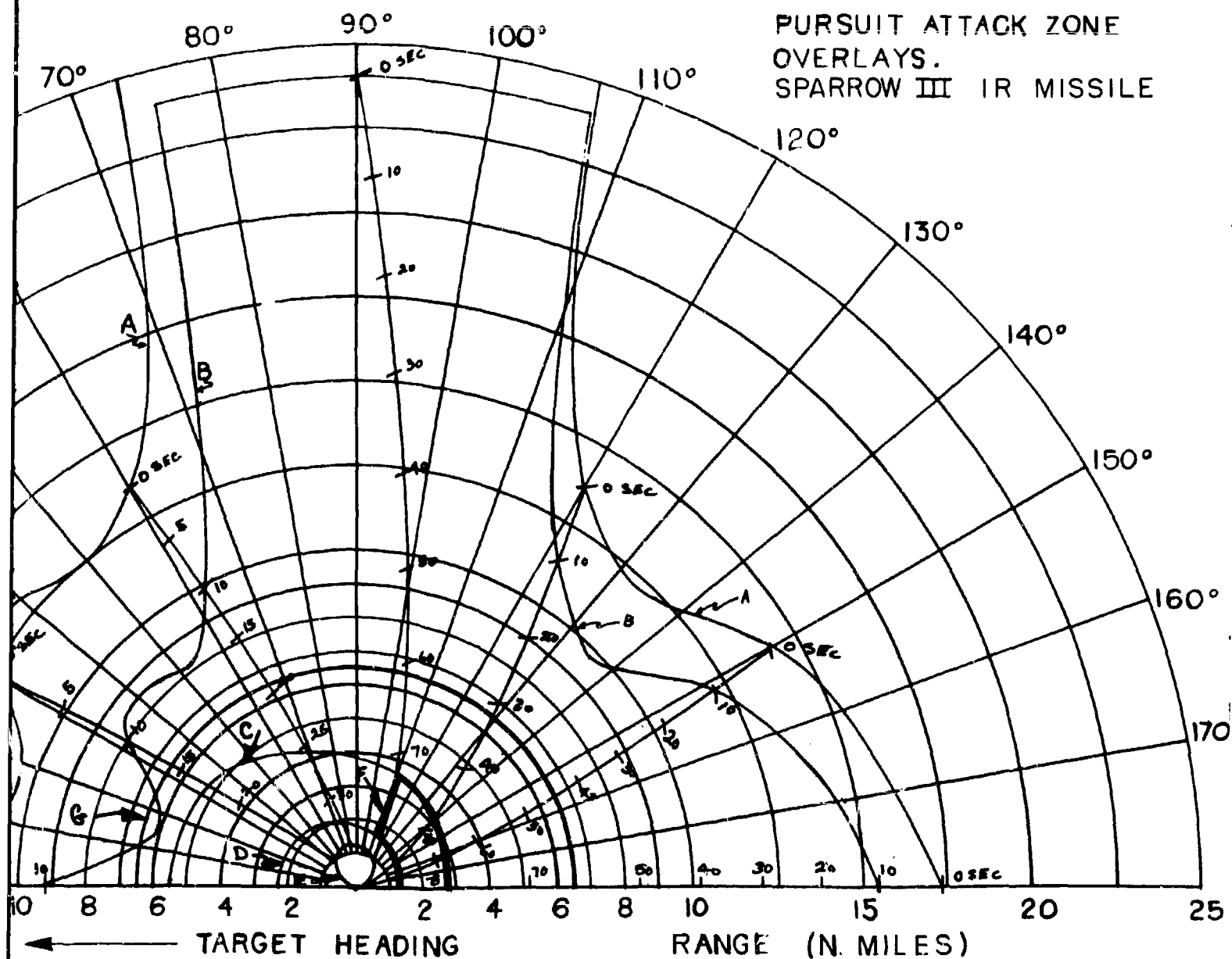
D - SPARROW III MIN. AERODYNAMIC RANGE

E - CONSTANT LOAD FACTOR LOCUS (N_Z)

F - SPARROW III IR LIMIT

G - 6.5 N.MILES INTERLOCK

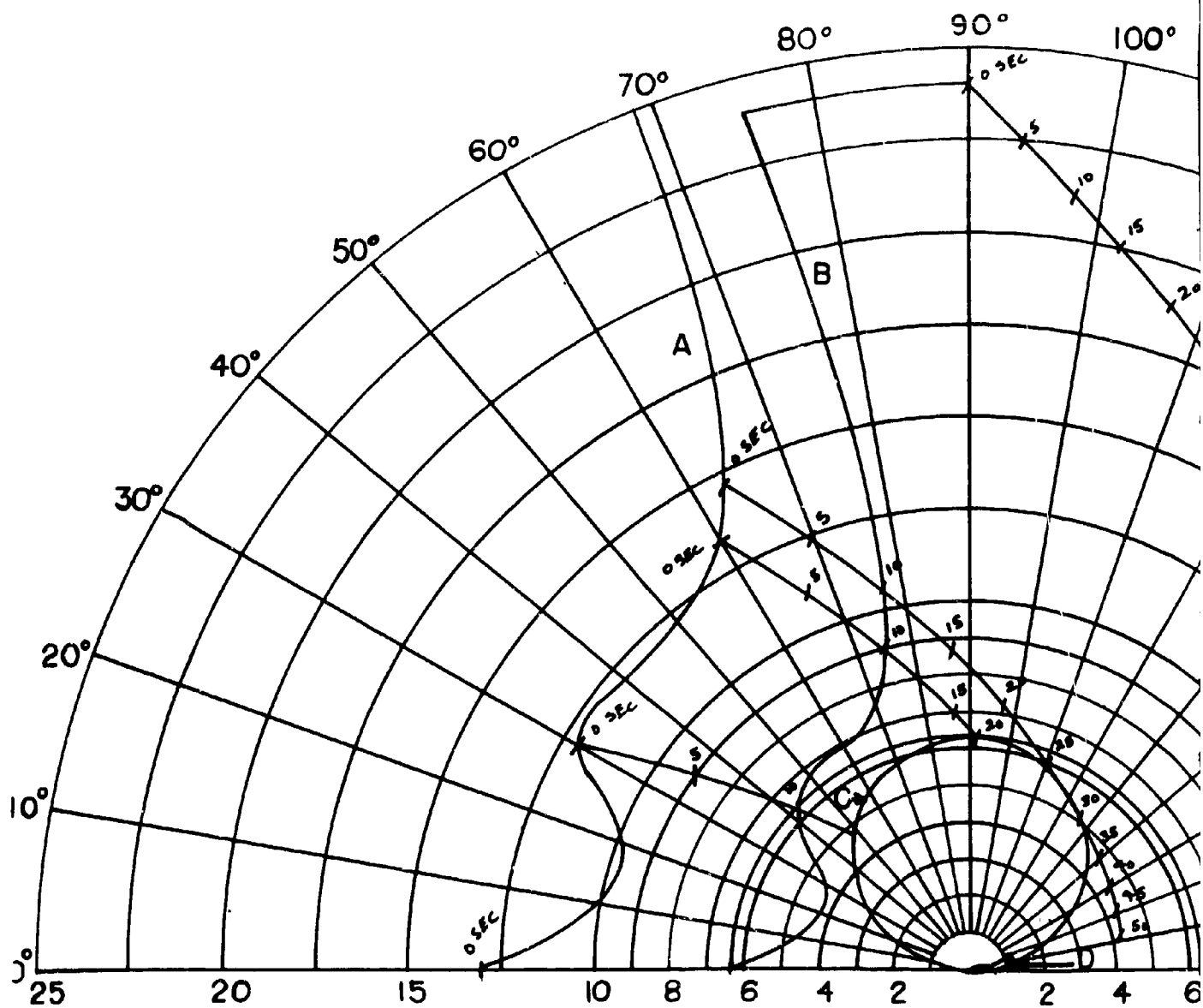
FIG. 101 - CO-ALTITUDE LEAD
PURSUIT ATTACK ZONE
OVERLAYS.
SPARROW III IR MISSILE



- A - 85% DETECTION RANGE
- B - LOCK-ON RANGE (10 SEC. LOCK-ON TIME)
- C - SPARROW III MAX. AERODYNAMIC RANGE
- D - SPARROW III MIN. AERODYNAMIC RANGE
- E - CONSTANT LOAD FACTOR LOCUS ($N_z=3$)
- F - SPARROW III IR LIMIT
- G - 6.5 N.MILES INTERLOCK

2

CONFIDENTIAL



$V_F = 1897$ FT./SEC. (F4H-1)(F8U-3)

$V_T = 1397$ FT./SEC.

ALTITUDE = 30,000 FT.

← TARGET HEADING

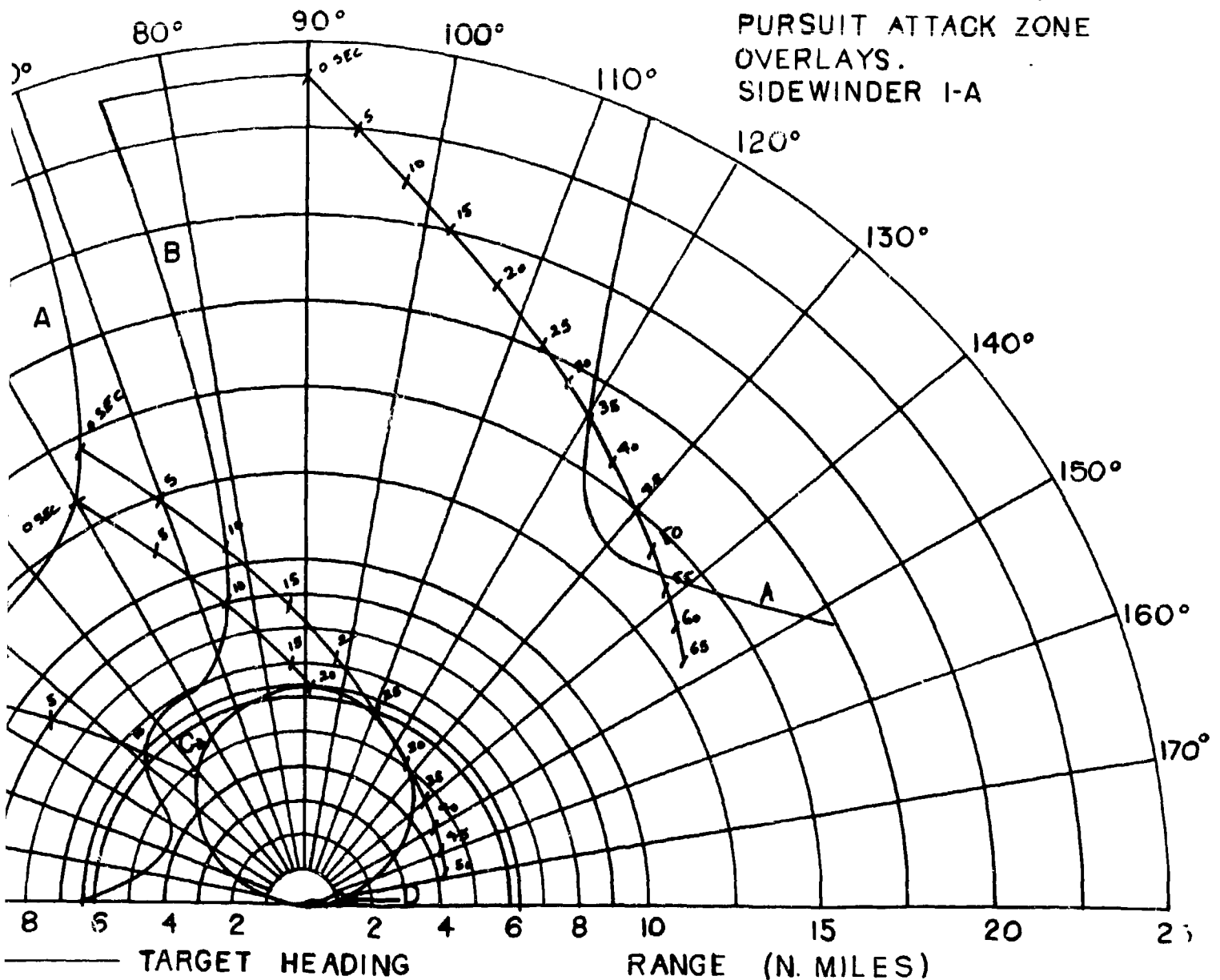
A - 85% DETECTION RANGE

B - LOCK-ON RANGE (10 SEC. LOCK-ON)

C - CONSTANT LOAD FACTOR LOCUS

D - SIDEWINDER I-A LAUNCH AREA

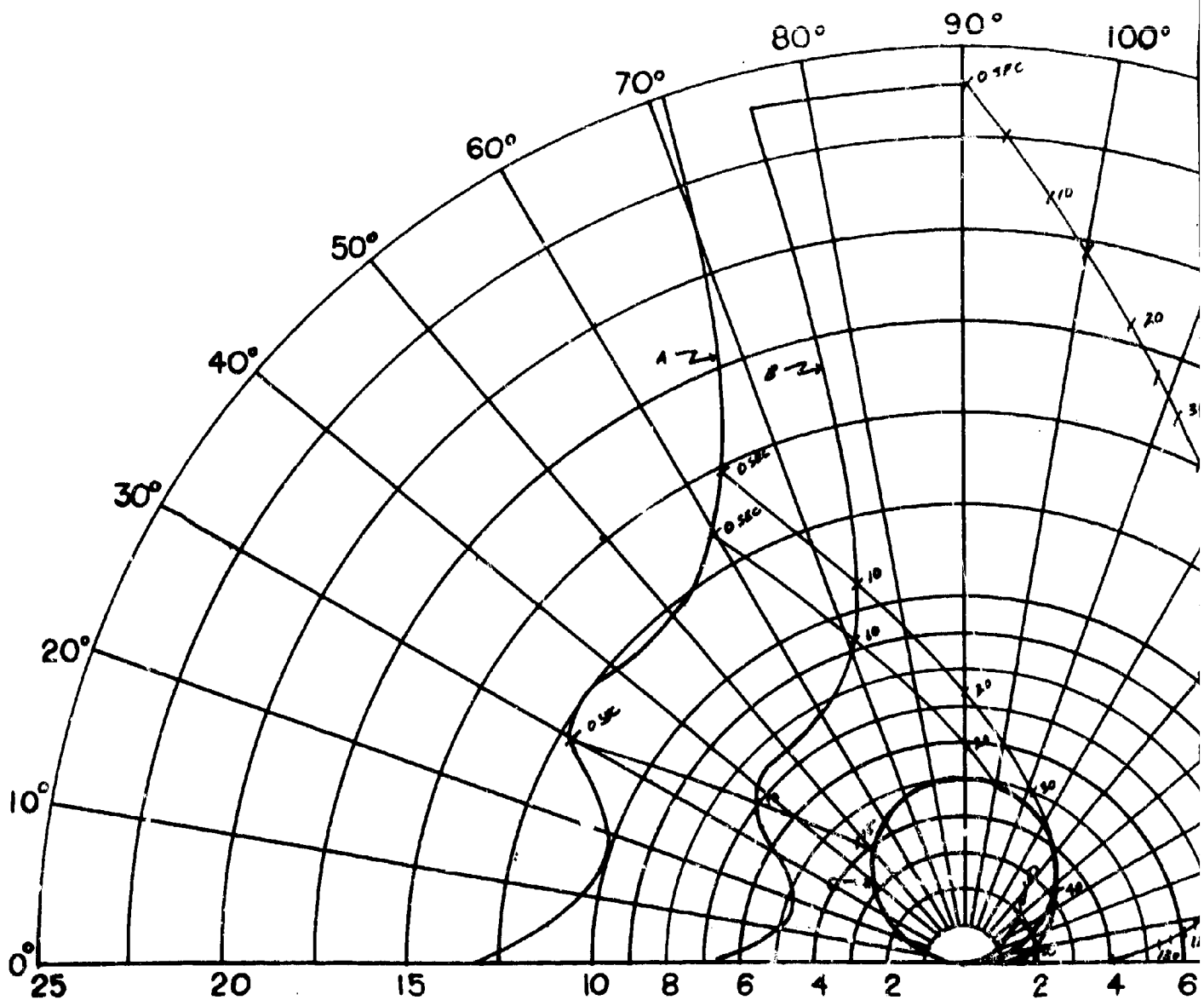
FIG. 102 - CO-ALTITUDE PURE
PURSUIT ATTACK ZONE
OVERLAYS.
SIDEWINDER I-A



85% DETECTION RANGE
LOCK-ON RANGE (10 SEC. LOCK-ON TIME)
CONSTANT LOAD FACTOR LOCUS ($N_z = 3$)
SIDEWINDER I-A LAUNCH AREA

2

CONFIDENTIAL



$V_F = 1897$ FT./SEC. (F4H-1)(F8U-3)

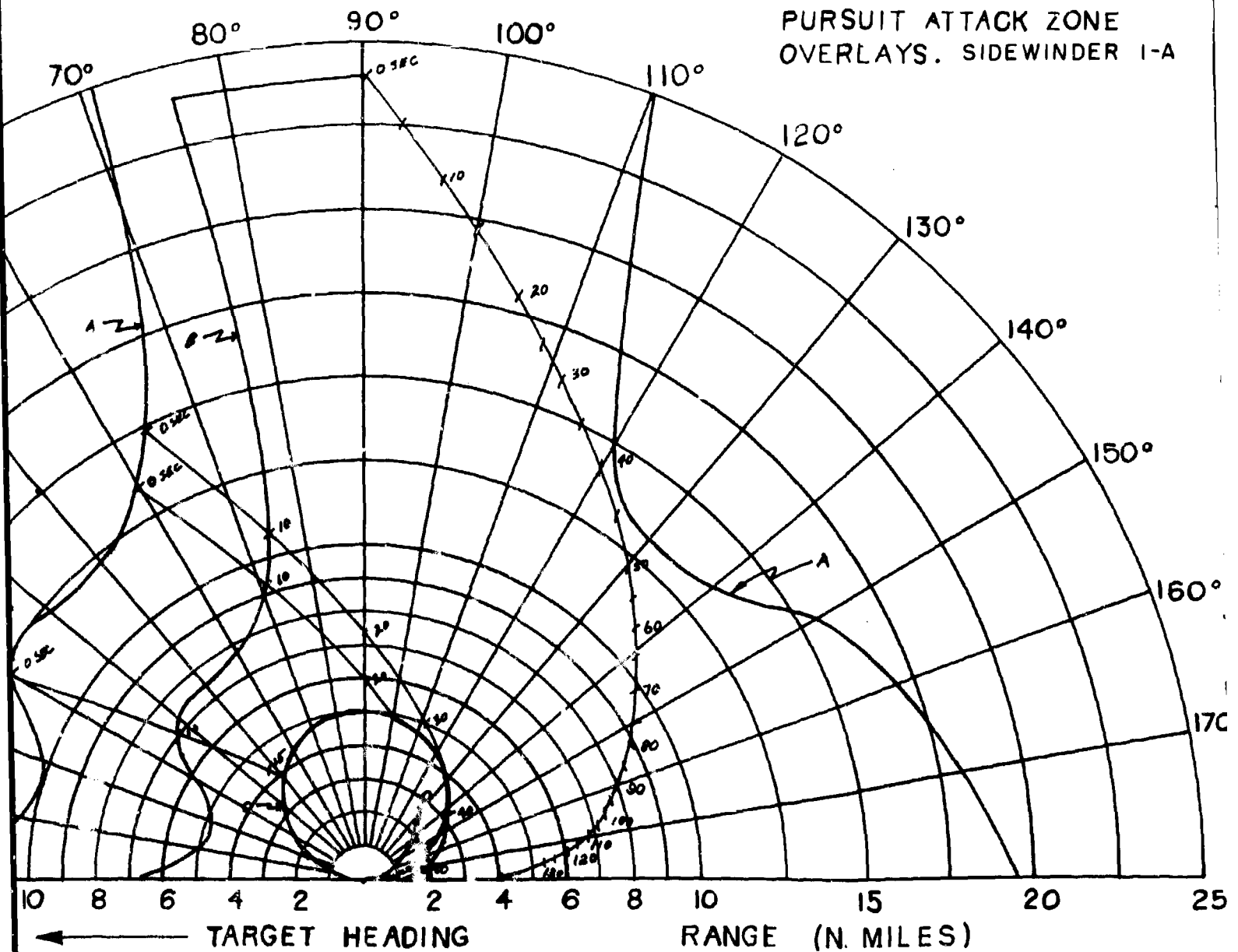
$V_T = 1518$ FT./SEC.

ALTITUDE = 30,000 FT.

TARGET HEADING

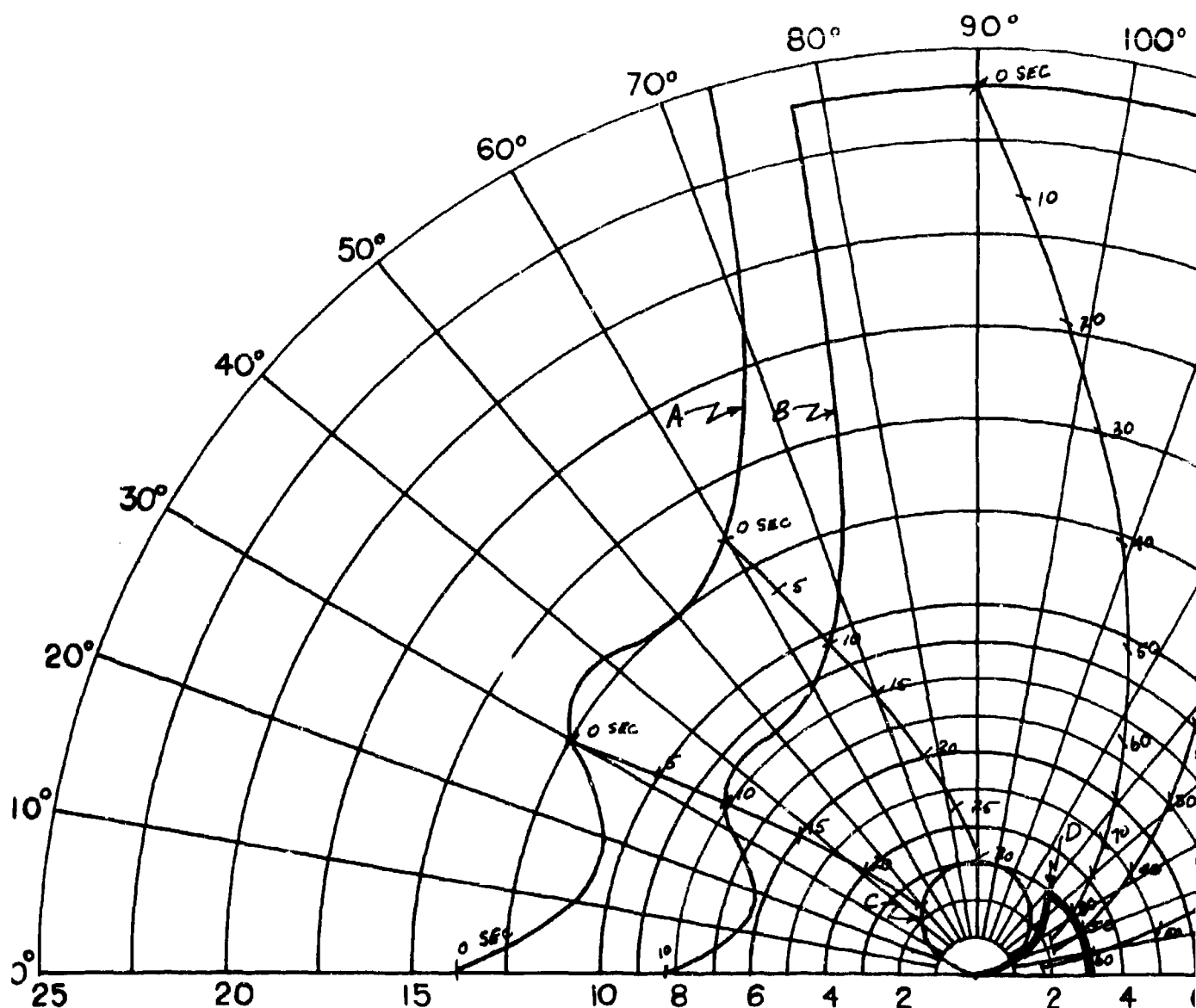
- A - 85% DETECTION RANGE
- B - LOCK-ON RANGE (10 SEC. LOCK-ON)
- C - CONSTANT LOAD FACTOR LOCUS
- D - SIDEWINDER I-A LAUNCH AREA

FIG. 103 - CO-ALTITUDE PURE
PURSUIT ATTACK ZONE
OVERLAYS. SIDEWINDER I-A



- A - 85% DETECTION RANGE
- B - LOCK-ON RANGE (10 SEC. LOCK-ON TIME)
- C - CONSTANT LOAD FACTOR LOCUS ($N_z = 3$)
- D - SIDEWINDER I-A LAUNCH AREA

2 CONFIDENTIAL



$V_F = 1897$ FT./SEC. (F 4 H-1) (F8U-3)

$V_T = 854$ FT./SEC.

ALTITUDE = 30,000 FT.

← TARGET HEADING

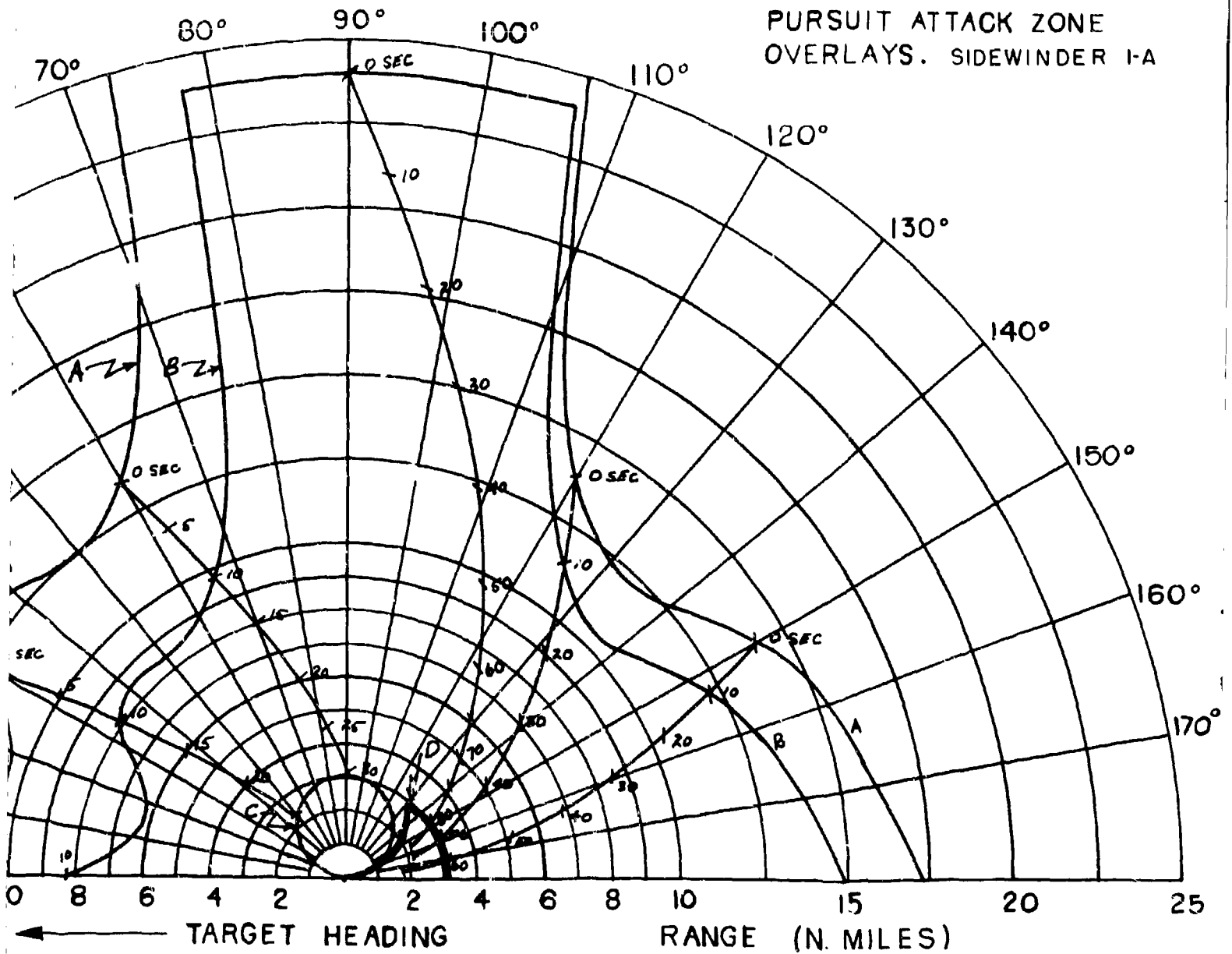
A - 85% DETECTION RANGE

B - LOCK-ON RANGE (10 SEC. LOCK-ON)

C - CONSTANT LOAD FACTOR LOCUS

D - SIDEWINDER I-A LAUNCH AREA

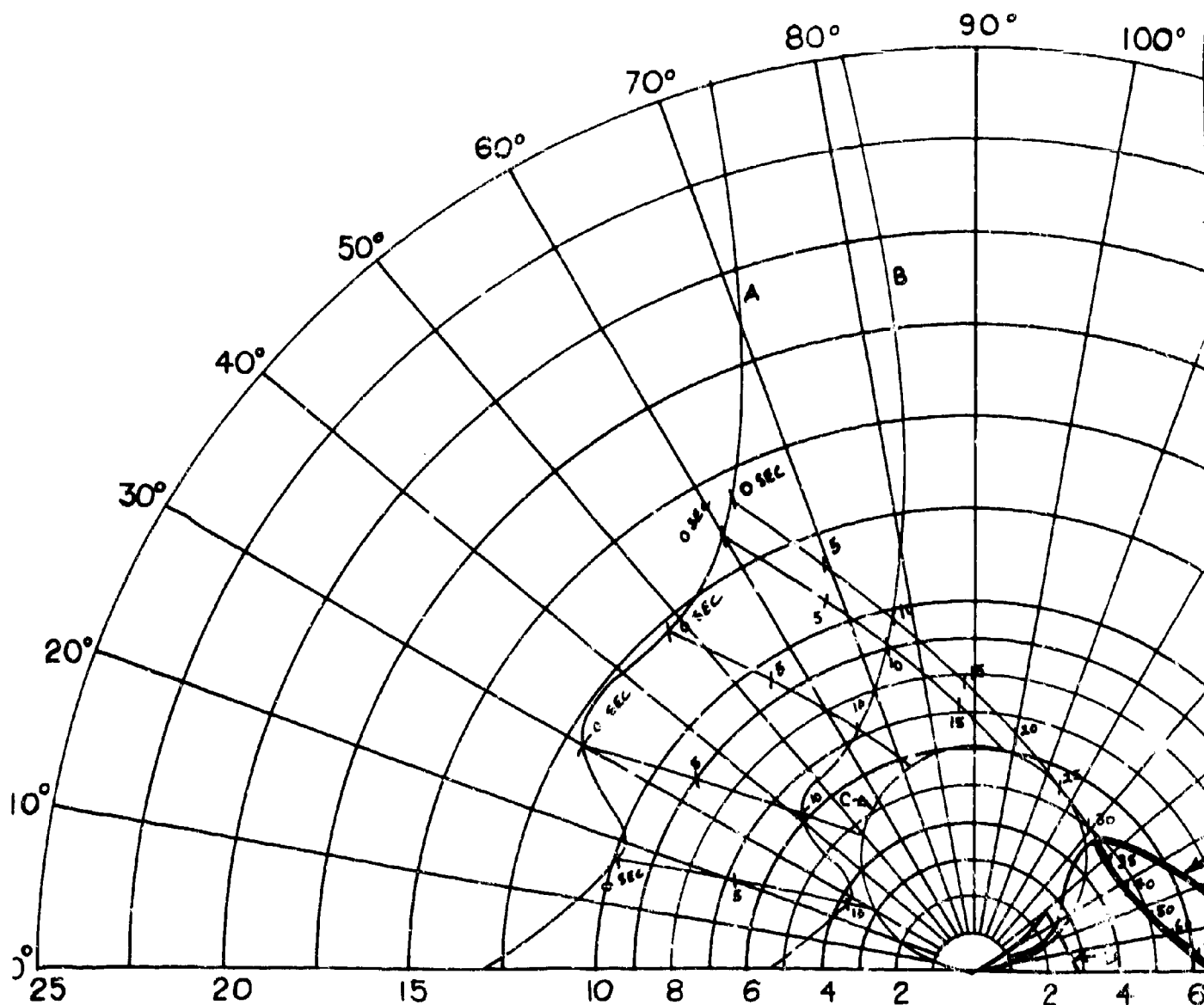
FIG. 104 - CO-ALTITUDE PURE
PURSUIT ATTACK ZONE
OVERLAYS. SIDEWINDER I-A



- A - 85% DETECTION RANGE
- B - LOCK-ON RANGE (10 SEC. LOCK-ON TIME)
- C - CONSTANT LOAD FACTOR LOCUS ($N_z = 3$)
- D - SIDEWINDER I-A LAUNCH AREA

2

CONFIDENTIAL



$V_F = 1940$ FT./SEC (F 4 H-1)(F8U-3)

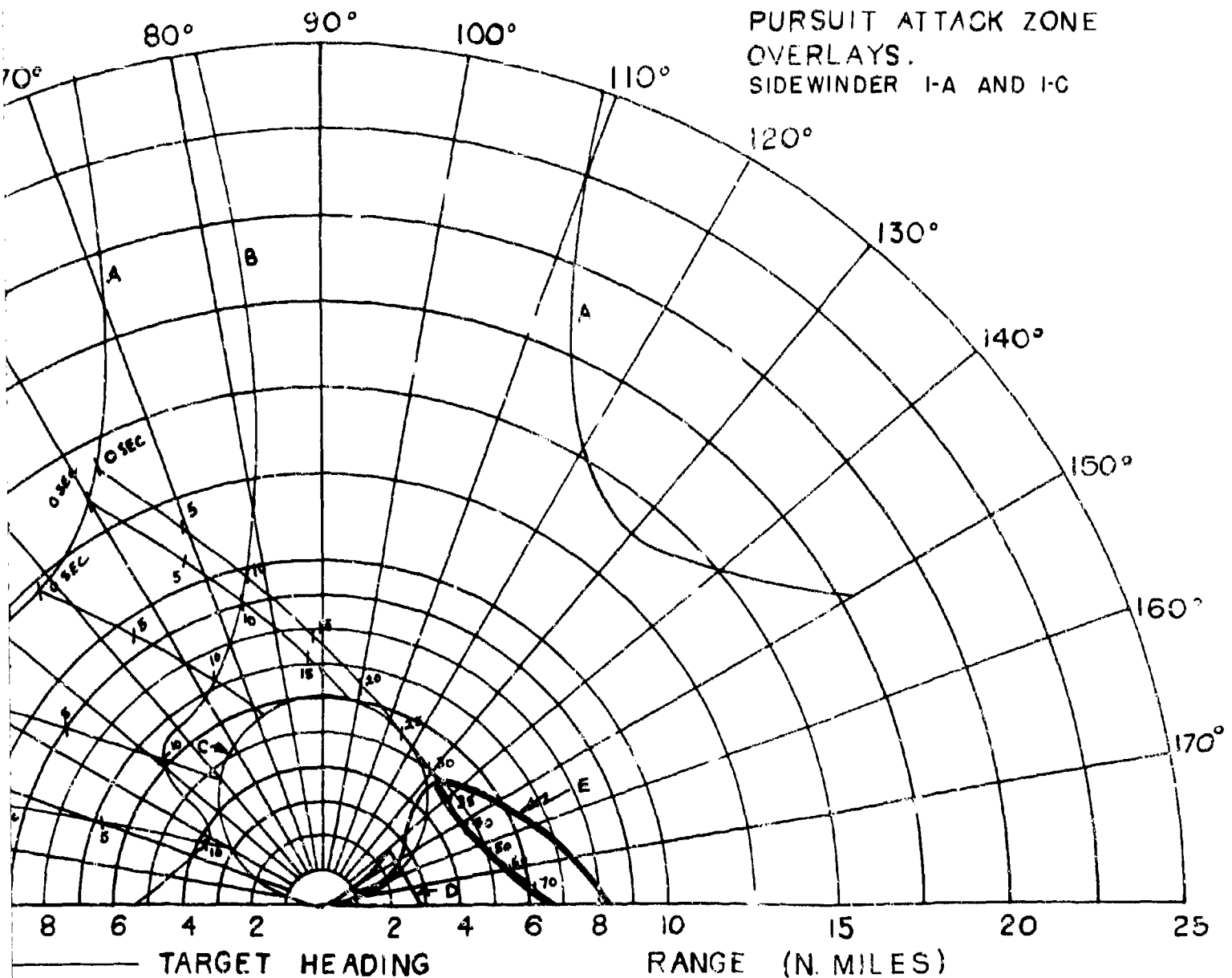
$V_T = 1940$ FT./SEC.

ALTITUDE = 50,000 FT.

← TARGET HEADING

- A - 85% DETECTION RANGE
- B - LOCK-ON RANGE (10 SEC. LOCK-O
- C - CONSTANT LOAD FACTOR LOCUS
- D - SIDEWINDER I-A LAUNCH AREA
- E - SIDEWINDER I-C LAUNCH AREA

FIG. 105 - CO-ALTITUDE PURE
PURSUIT ATTACK ZONE
OVERLAYS.
SIDEWINDER I-A AND I-C

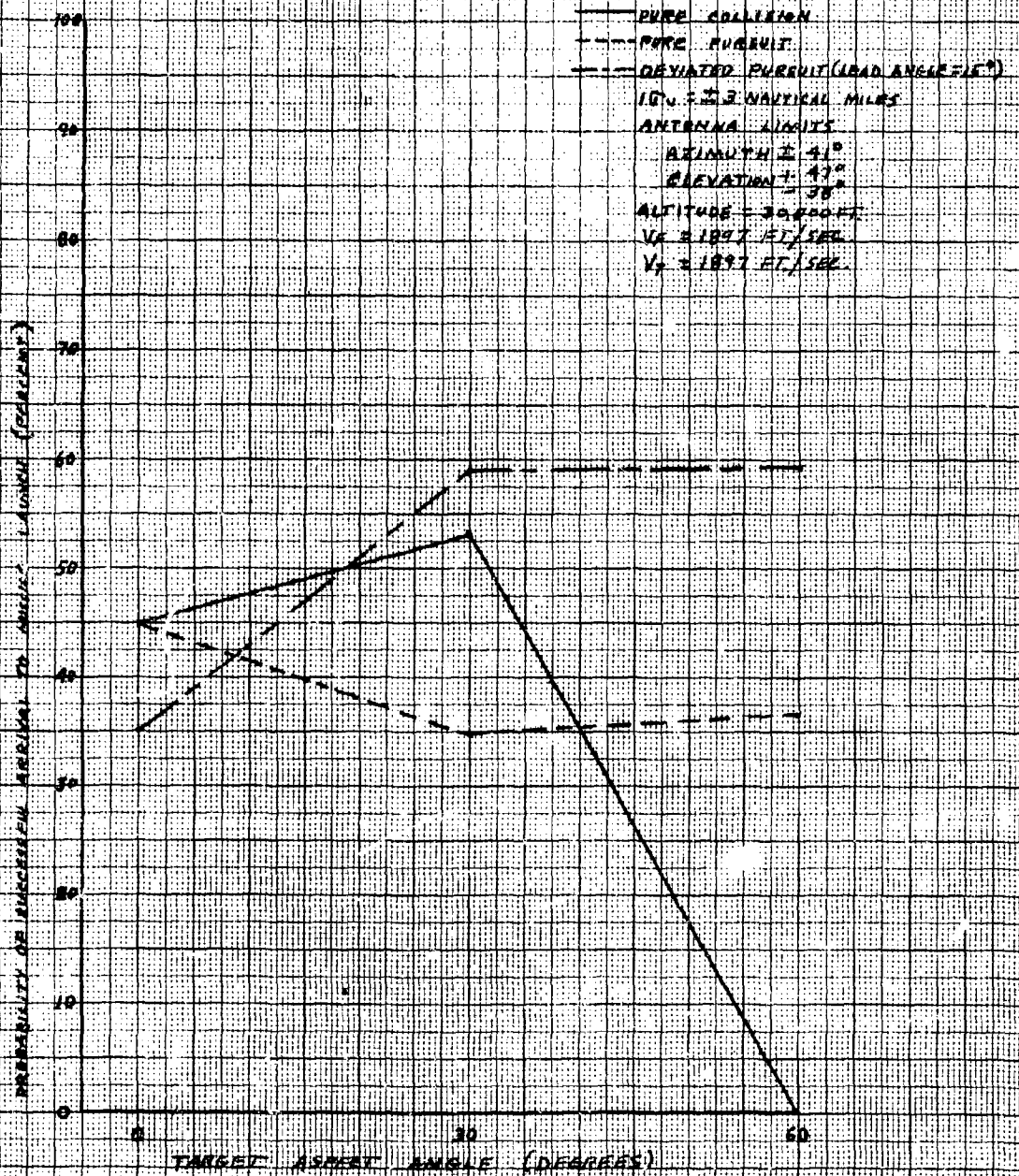


85% DETECTION RANGE
LOCK-ON RANGE (10 SEC. LOCK-ON TIME)
CONSTANT LOAD FACTOR LOCUS ($N_z = 3$)
SIDEWINDER I-A LAUNCH AREA
SIDEWINDER I-C LAUNCH AREA

2

CONFIDENTIAL

FIG 105 - PROBABILITY OF SUCCESSFUL ARRIVAL TO MISSILE LAUNCH VERSUS
ASPECT ANGLE USING VARIOUS TYPES OF INTERCEPTOR VECTORS



CONFIDENTIAL

**Naval Research Laboratory
Technical Library
Research Reports Section**

DATE: February 26, 2001
FROM: Mary Templeman, Code 5227
TO: Code 5300 Paul Hughes
CC: Tina Smallwood, Code 1221.1 *ts 3/8/01*
SUBJ: Review of NRL Reports

Dear Sir/Madam:

1. Please review NRL Report MR-754 Volumes I, II, III, IV, VII, VIII, IX, X, XI, XII, XIII, XIV, XV, MR-1372 and MR-1289 for:

- ☒ Possible Distribution Statement
☐ Possible Change in Classification

Thank you,

Mary Templeman

Mary Templeman
(202)767-3425
maryt@library.nrl.navy.mil

The subject report can be:

- ☒ Changed to Distribution A (Unlimited)
☐ Changed to Classification _____
☐ Other:

Ben H. Cantrell
Signature

3-8-01
Date

**** MAY CONTAIN EXPORT CONTROL DATA ****

Record List

03/8/101

Page 1

AN (1) AD- 368 048/XAG
FG (2) 010303
150600
160401
CI (3) (U)
CA (5) NAVAL RESEARCH LAB WASHINGTON D C
TI (6) SUMMARY OF NAVY STUDY PROGRAM FOR F4H-1 AND F8U-3 WEAPON SYSTEMS. VOLUME III.
DN (9) Memo. rept.
AU (10) Loughmiller ,C. M.
Ryon ,J. C.
Bellavin ,I. N.
Lister,R. L.
RD (11) May 1958
PG (12) 69 Pages
RS (14) NRL-MR-754-Vol-3
RC (20) Unclassified report
NO (21) See also Volume 2, AD-367 907L.
AL (22) Distribution: DoD only.
DE (23) (*TACTICAL WARFARE, NAVAL RESEARCH)
METEOROLOGICAL PHENOMENA, PERFORMANCE(ENGINEERING), DEGRADATION (U) JET
FIGHTERS, AERIAL WARFARE, RADAR, AIR TO AIR MISSILES, MANEUVERABILITY,
LAUNCHING, EARLY WARNING SYSTEMS, DETECTION, COUNTERMEASURES, AIRCRAFT FIRE
CONTROL SYSTEMS, INTERCEPTION, SEARCH RADAR, RADAR TRACKING
DC (24) (U)
ID (25) AN/APQ-72, F-4 AIRCRAFT, F-8 AIRCRAFT, SIDEWINDER, SPARROW
IC (25) (U)
DL (33) 04
CC (35) 251950

**APPROVED FOR PUBLIC
RELEASE - DISTRIBUTION
UNLIMITED**